REMOTE SENSING APPLIED TO SLOPE STABILITY IN MOUNTAINOUS ROADS IN IRAN

A thesis presented by Hassan Taherkia in accordance with the regulations governing the award of the degree of Doctor of Philosophy of the University of Aston in Birmingham.

October, 1985

A token of gratitude to my beloved country, Iran

REMOTE SENSING APPLIED TO SLOPE STABILITY IN MOUNTAINOUS ROADS IN IRAN

HASSAN TAHERKIA PhD 1985

SUMMARY

The Alborz Mountain range separates the northern part of Iran from the southern part. It also isolates a narrow coastal strip to the south of the Caspian Sea from the Central Iran plateau.

Communication between the south and north until the 1950's was via two roads and one rail link. In 1963 work was completed on a major access road via the Haraz Valley (the most physically hostile area in the region). From the begining the road was plagued by accidents resulting from unstable slopes on either side of the valley. Heavy casualties persuaded the government to undertake major engineering works to eliminate "black spots" and make the road safe. However, despite substantial and prolonged expenditure the problems were not solved and casualties increased steadily due to the increase in traffic using the road.

Another road was built to bypass the Haraz road and opened to traffic in 1983. But closure of the Haraz road was still impossible because of the growth of settlements along the route and the need for access to other installations such as the Lar Dam.

The aim of this research was to explore the possibility of applying Landsat MSS imagery to locating black spots along the road and the instability problems. Landsat data had not previously been applied to highway engineering problems in the study area. Aerial photographs are better in general than satellite images for detailed mapping, but Landsat images are superior for reconnaissance and adequate for mapping at the 1:250,000 scale. The broad overview and lack of distortion in the Landsat imagery make the images ideal for structural interpretation.

The results of Landsat digital image analysis showed that certain rock types and structural features can be delineated and mapped. The most unstable areas comprising steep slopes, free of vegetation cover can be identified using image processing techniques. Structural lineaments revealed from the image analysis led to improved results (delineation of unstable features). Damavand Quaternary volcanics were found to be the dominant rock type along a 40 km stretch of the road. These rock types are inherently unstable and partly responsible for the difficulties along the road.

For more detailed geological and morphological interpretation a sample of small subscenes was selected and analysed. A special developed image analysis package was designed at Aston for use on a non specialized computing system. Using this package a new and unique method for image classification was developed, allowing accurate delineation of the critical features of the study area.

KEY WORDS : SLOPE STABILITY, IRAN, REMOTE SENSING.

ACKNOWLEDGEMENTS

Writing an acknowledgement page is not an easy task for someone who has taken advantage of much friendship on many occasions. First of all I must thank my two supervisors Dr. W. G. Collins and Dr. J. A. Morton for their invaluable supervision. Dr. Collins in particular has devoted a considerable amount of time to assisting me in all aspects of my study.

I am also indebted to the following for their assistance : Mr. Nigel Press and his company in Edenbridge, who provided a considerable amount of practical help and computer time; Mr. J. Maden a programmer with the company who assisted me with image processing. Dr. S. Drury of the Earth Science Department at the Open University and Mr. M. Wicket of ITS company also gave me assistance and allowed me access to the DIPIX image processing system. Dr. D. A. Rothery who guided my work on the DIPIX equipment and also gave me technical advice. Mr. M. C. Patel and Mr. G. Bellavia advised me in programming and Dr. N. Rufford of Midland Environment Ltd. Aston Science Park who provided help in presenting some of the material.

I also wish to thank Mr. M. B. Golbon Deputy Secretary of Road and Transport in Iran and Mr. M. A. Assangari Minster of Road Constuction for Central and Northern Iran for allowing me to collect ground data of the study area. I should also like to thank my dear friends Mr. J. Khakshoy for providing supplementary data while I was in the U. K. and Mr. M. Zahedi Golpayegany for his assistance in obtaining fascimilies of original data. Special thanks goes to Dr. M. Amini with the Geological Survey in Iran for allowing me access to survey data, and to Mr. S. Josephnia, Head of the cartography section of the National Cartograrhic Centre of Iran for providing me with maps of the study area. I am grateful also to Mr. Homayonfar of the Regional Water Supply of Tehran for permitting me to use the Lar Dam data. I should also like to thank Mr. S. H. Razavi Head of Remote Sensing Centre of Iran for providing me with copies of two Landsat images and for general co-oporation with the work. Many other friends, all of whom it is impossible to name here, have been involved in this study. I would like to thank them all; their kindness is not forgotten.

Finally I must express my very special appreciation and gratitude to my dear wife who has given me endless encouragement throughout the preparation of this study. I could never have completed the task without her support.

CONTENTS

LIST OF FIGURES

CHAPTER 1 INTRODUCTION

CHAPTER 2 ENVIRONMENT OF THE STUDY AREA

CHAPTER 3 GEOLOGY

CHAPTER 5 REMOTE SENSING

LIST OF PLATES

CHAPTER 1 INTRODUCTION

CHAPTER 3 GEOLOGY

CHAPTER 4 SLOPE STABILITY IN THE STUDY AREA

CHAPTER 6 DIGITAL IMAGE PROCESSING

CHAPTER 7 DATA ANALYSIS CARRIED OUT WITH ASTON UNIVERSITY FACILITIES

CHAPTER 8 DISCRIMINATION OF LITHOLOGIES, UNSTABLE SLOPES AND TECTONIC FEATURES

LIST OF TABLES

CHAPTER 8 DISCRIMINATION OF LITHOLOGIES, UNSTABLE SLOPES AND TECTONINC FEATURES

APPENDIX A

CHAPTER 1

INTRODUCTION

1.1 INTRODUCTION

The primary objective of this research is to identify the problems involved in studying slope stability , by taking advantage of satellite data and geological science. In particular, the aim is to detect landslide, landslip, subsidence and other instabilities in mountainous terrain using a combination of geology, terrestrial and aerial photography and Landsat data. The area considered in the study is the Haraz Road region, North Iran.

1.1.1 The Haraz Road

The Haraz road is approximately 180 km long and connects Tehran to Amol and the Caspian Sea (Figure 1.1). It is one of four roads that connect the Capital to the north of the country.

The construction of the road began in 1937 at two sites, one in the south, and one in the north, but work was interrupted by the Second World War. Construction was finally completed in 1963, and the road was opened to traffic. However, lack of site investigation at the time of planning caused many problems when the road was subjected to traffic. After spending a large amount of money to improve the road, the Iranian government decided that it would be better to build a new road which would pass through Damavand, Firoozkuh and Zeerab, bypassing the Haraz Road. This new road was opened in late 1983, but consideration still had to be given to the villages, coalmines and an important dam (Lar Dam), which are accessible only via the Haraz Road.

Figure 1.1 Location of Iran. Showing route of Haraz Road.

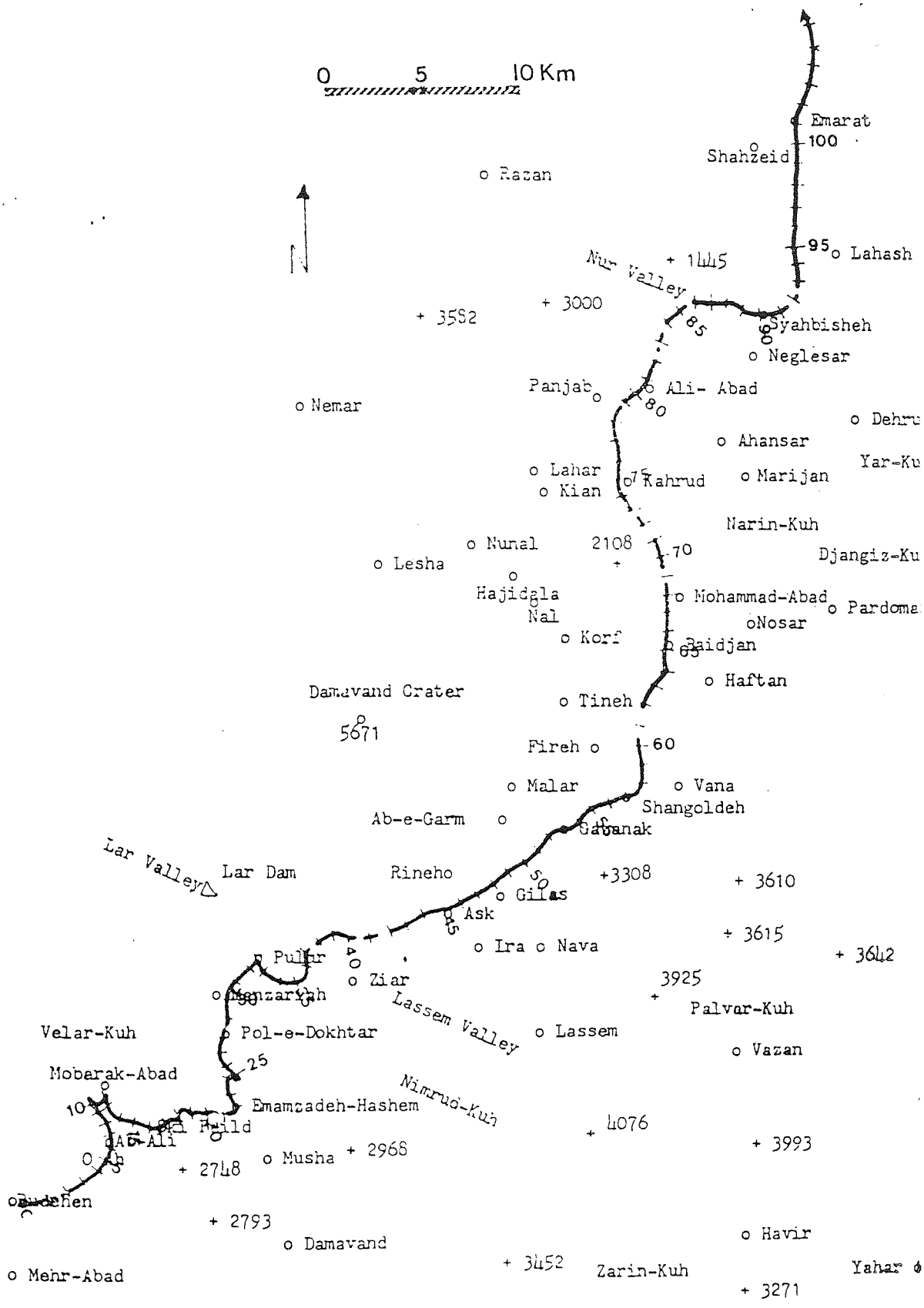

Figure 1.2 Haraz Road and surrounding villages.

It was decided that the old road was too important to close completely and would have to remain open to some traffic.

The area covered by this investigation is a section of the road which connects Ab-Ali to Emarat, approximately 90 km (Figure 1.2). This region is tectonically complex and still active. A great deal of instability is caused by the presence of the Musha-Fasham thrust fault in the south, the young Quaternary Damavand volcano in the centre and the Baidjan thrust fault towards the north, with both thrusts crossing the road at right-angles.

An evaluation of the relationship between stability and geological features can be carried out using aerial photographs and satellite images. The main purpose of the research is to correlate different sets of data and develop an appropriate method of determining stability. The value of Landsat MSS is examined for lithological stratigraphy and surface state discrimination for route planning and hazard evaluation.

1.2 DESCRIPTION OF SITE

1.2.1 Physiography

Ab-Ali, 7 km from Rudehen, is at an altitude of 2100 m with the road rising to 2700 m north of Emamzadeh-Hashim (km 21.6, Figure 1-2). The topography of this section of the road is moderate, but rock slides at Ab-Ali (km 7), subsidence and scree in the 12-15 km zone and strong winds, especially in winter, in the 18-22 km zone disturb the maintainance of the road. Development of springs in cuts (km 12-15) aggravates land movement (Plate 1.1).

The road from km 7 to km 26 is designed for speeds under 60 km/h,

and is not suitable for 95 km/h, the maximum allowed speed in Iran at the present time.

From Emamzadeh-Hashim (km 23) the gradient of the road is downward to an altitude of 2400 m at km 27.8 where the road goes to the left bank of the Haraz river, which is little more than a stream at this stage. In this area the relief is moderate but unstable. There is a sharp bend in the road at km 24.6, with a radius of less than 25 m (Plate 1.2).

Between km 27.8 and km 29 there are some overhanging rocky cuts, but after km 29 reaching Pulur, the topography of the region is subdued and there are no problems (Plate 1.3). The area between km 23 and km 29 is very dangerous in the late winter because of snow avalanches. There are two concrete galleries which protect the road from avalanches and a chute which is designed to throw the avalanches over the road into the valley (Plates 1.4).

After Pulur, km 33 to km 38, where the road transfers to the right bank of the river, it has to avoid a spur made by a young lava flow (Plate 1.5). The road is constructed on river deposits mixed with volcanic ashes and poorly cemented agglomerates, which become loose with weathering and cause landslides. Here the Haraz river used to be full and fast flowing in spring, but construction of the Lar dam (1982) has enabled the flow to be regulated.

From km 32 to Ab-Ask, km 46, at an altitude of 1900 m, the road is on the right bank of the river on a very steep slope. This part of the road consists of four tunnels with gradients sometimes steeper than 6% (Table 1.1). There are two recently built galleries for protection from avalanches. The relief of the terrain is very rough

Plate 1.1 North side of the main thrust (km 15). The water flow (→) isconsequence of a secondary fault.

Plate 1.2 Margh valley (km 25). The building is a shelter for passengers who trapped in snow in winter.

Plate 1.3 South elevation of the Damavand Mountain. Taken in end of June from km 30. Pulur village is in middle of the scene (→) at the junction of two valleys.

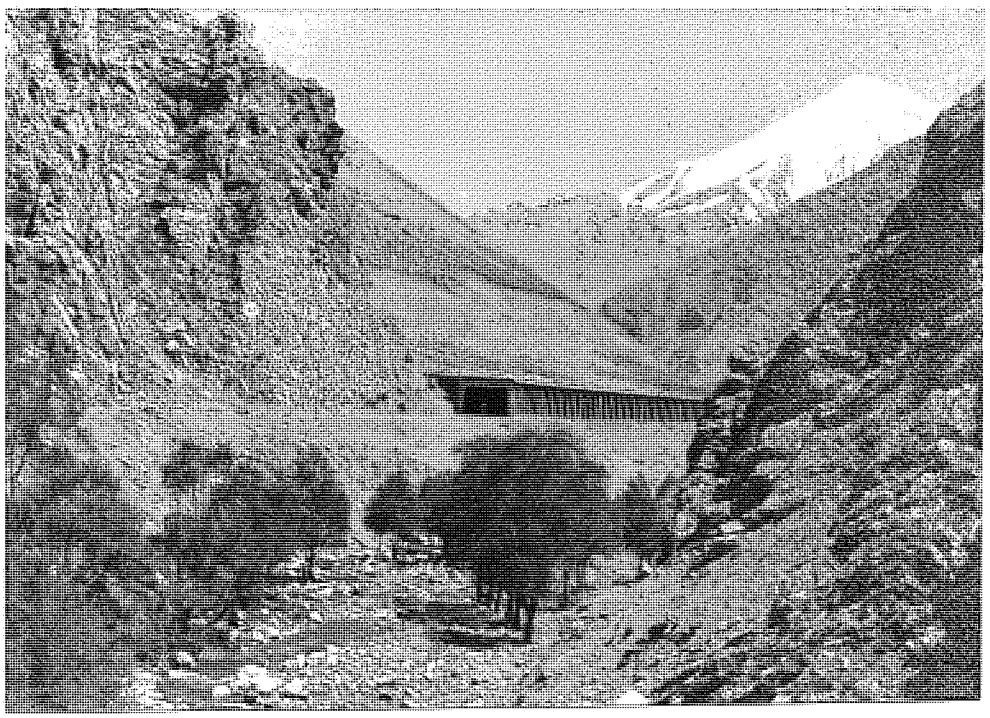

Plate 1.4 Avalanche gallery (km 28). The gallery is for protection of the road from avalanches. Top left corner rocks are Lar limestone.

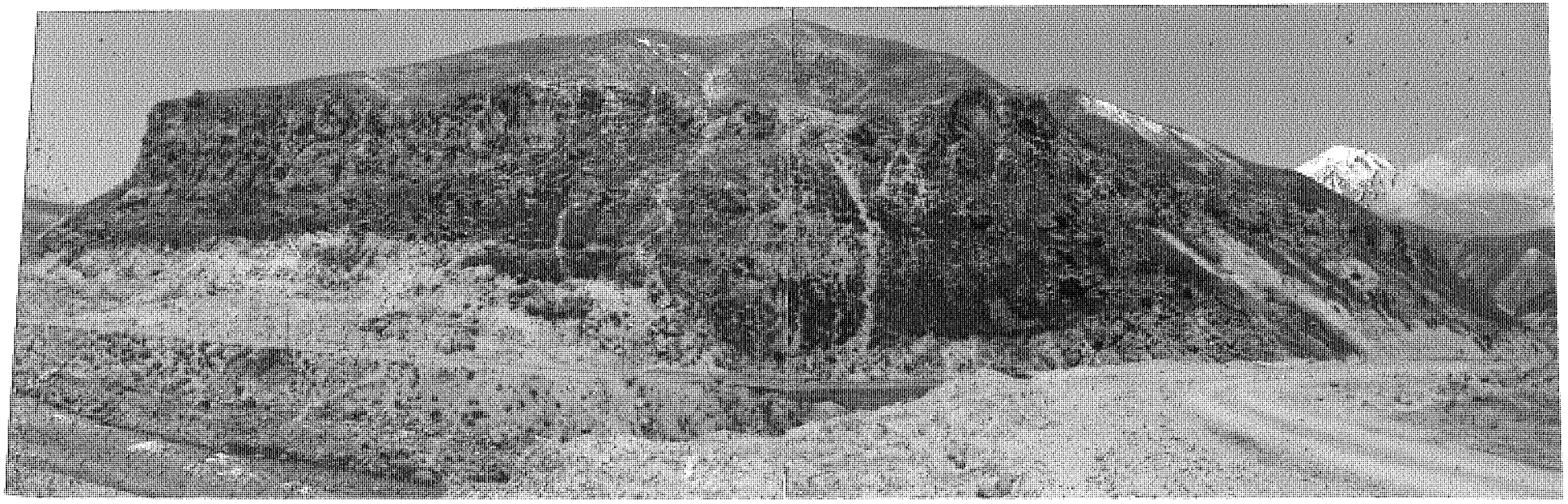

Plate 1.5 Sharp bend north of Pulur (km 34-37). Lava flow and deposits mixed with volcanic ashes. Photograph is taken from east side of the river where a new road to Lassem was under construction.

Plate 1.6 A view of volcanics (km 37). flow of trachy-basalt overlaying Lar limestone.

Plate 1.7 Unstable slope at km 56. Shangoldeh is located at the bottom right hand corner of the picture.

and the river goes through a deep valley with the road often about 200 m above the river bed. Steep slopes to the east of the road extend higher than 800 m: consequently rock fall and scree (in spring), and avalanches (in winter) are major difficulties. Quaternary lava flow from the Damavand volcano on the other side of the river terminate in a vertical bluff with exposed columns of trachy basalt (Plate 1.6). Near Ab-Ask where some warm springs exist there is a meander in the river bed which is caused by travertine sedimented from warm spring water.

The road continues on the left bank from km 46 to Vana, km 59.2, at an altitude of 1420 m. Along this section, vertical slopes on the west side of the road are often unstable, especially at km 57. In Shangoldeh the slopes are steep and very unstable and the residents have been warned to evacuate the village due to the danger of landslides (Plate 1.7).

From Vana to Baidjan-Bridge, km 66.8, at an altitude of 1150 m, the road continues on the right bank. The longest tunnel is in this section (Table 1.1). The road crosses the Baidjan thrust fault at a right-angle. The topography of the region is very rough and unstable. There is a warm spring in Ghalabon which the local people use as a medical bath.

Between km 66.8 and km 84, at an altitude of 780 m, the road runs along the left bank, while there are steep slopes on the west side and terrace deposits are located on the fractured Jurassic sandstones and rocks. The terrace deposits are eroding and being washed down over the Jurassic rocks filling the fractures and creating a smooth, oversteepened slope (Plate 1.8). This is why the relief of the area

is so rough and unstable. There are six tunnels along this section of the road (Table 1.1).

Tunnel No	Beginning km	Ending km	Length m	Max grad. %	Altitude m	Remarks
1	36+734	36+826	92	-1.5	2150	
2	37+405	37+905	500	-5.1	2125	
3	40+840	40+940	100	-6.4	2030	
4	41+330	42+030	700	-6.4	2000	
5	60+340	61+858	1518	-4.0	1320	900m with -2%
6	68+873	69+193	320	-5.3	1120	
7	71+199	71+623	424	+2.8	1060	
8	72+429	72+826	397	-4.0	1040	
9	82+397	82+496	99	-3.0	825	
10	82+473	82+799	326	-3.4	815	
11	83+525	84+106	581	-2.6	790	
12	85+395	85+508	113	-2.5	745	
13	91+552	92+102	550	-5.0	670	
14	92+322	92+448	126	+0.6	635	
Total length			5846			

Table 1.1 Existing Tunnels in the Haraz Road. Gradients are plus for altitude increase towards Amol

Between km 84 and km 90, at an altitude of 650 m, the road continues on the right bank. On the east side of the road there are massive and faulted old volcanic rocks which are very unstable. For instance, in July, 1982, there was a rock slide at km 85.6 (Plate 1.9). There is a tunnel in this part of the road (Table 1.1).

The last part of the study area ends at km 95 where the road is constructed on the left bank and has two tunnels (Table 1.1). A few km after the final tunnel the road enters a humid and forested area with gentler relief and vegetation-stabilised slopes which does not have the same problems as the mountainous region.

1.2.2 Geology

The study area has wide range of rock types from Cambrian to Quaternary, but there are three major zones, definable as follows:

a) Quaternary volcanic rocks in the middle of the study area
b) Folded post-Permian sediments in northern region
c) Deformed pre-Cambrian and Palaeozoic sediments in the southern region

These regions can be seen in Figure 3.2. Details of the geology can be found in Chapter 3.

1.3 STABILITY PROBLEMS

During its 20 years of operation, the Haraz Road has been considered the most dangerous road in the country. Casualties on this road are very high, with most being caused by the structural instability of the region; rock falls, landslides, mud flows and avalanches accounting for many deaths. At one end of the study area, km 7, on the west side of the road, which is in contact with the south edge of the Musha-Fasham main thrust, there are fractured and faulted materials: the steep slope helps make them active and this is always a danger for vehicles. A high retaining wall has been built to protect the surface, but this has not proved very effective. Between Mobarak-Abad, km 12, and a ski-slope at km 15, situated to the north of the thrust, Permian and Cambrian rocks are faulted producing substantial movement.

Where the lower Jurassic Shemshak formation (see Chapter 3) dominates, there is severe instability, which is why the road between km 22 and km 28 is unstable, especially around km 27 where water appears on the surface.

The middle Jurassic Dalichai formation is very dangerous when it is weathered, but fortunately there is very little occurrence of this formation in the Haraz valley.

Another area of instability occurs in the region of the Damavand volcanic rocks, km 33 to km 36.7, around the lava flow. The most dangerous part of the road is between km 22 and km 45, where there is a variety of rock formations and several faults. This zone is very tectonized and fractured. Water appearance at km 42 causes difficulties whilst steep and continous slopes cause rock slides and snow avalanches.

Instabilities in volcanic rocks appear again between km 46 and km 59 where the rocks are collapsing due to weathering. Severe problems can occur where volcanic rocks overlie sedimentary rock formations: the Vana and Shangoldeh landslides are two good examples of this.

The Baidjan thrust fault (see Figure 3.2), which is located in the Shemshak formation, cuts the valley at km 62; as a result severe instability problems occur in this zone. There is a big colluvial slope at km 63 which is unstable and is a great danger for vehicles.

From km 67 to km 84 where the road runs on the Shemshak formation, there are a number of dangerous points. There are several young terrace deposits located on the bed-rock higher up the slopes, which are also very unstable. These, combined with cuts made during road construction, mean that there is a great deal of rock movement on the slopes.

From km 84 to km 91.5 the road continues on Cretaceous sedimentary and volcanic rocks. The latter appear stable at first sight but they are dangerously unstable after weathering. As a result there are frequent rockslides in this area as is shown in Plate 1.9.

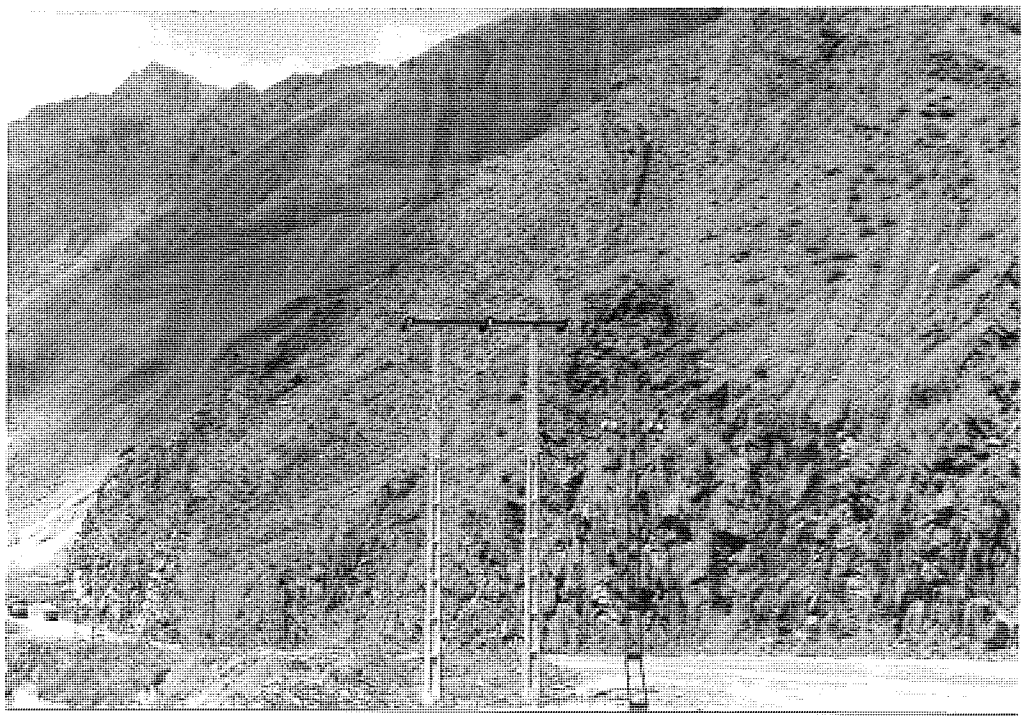

Plate 1.8 High terrace diposits (km 78). Terrace deposits overlaying lower Jurassic (Shemshak formation) rocks.

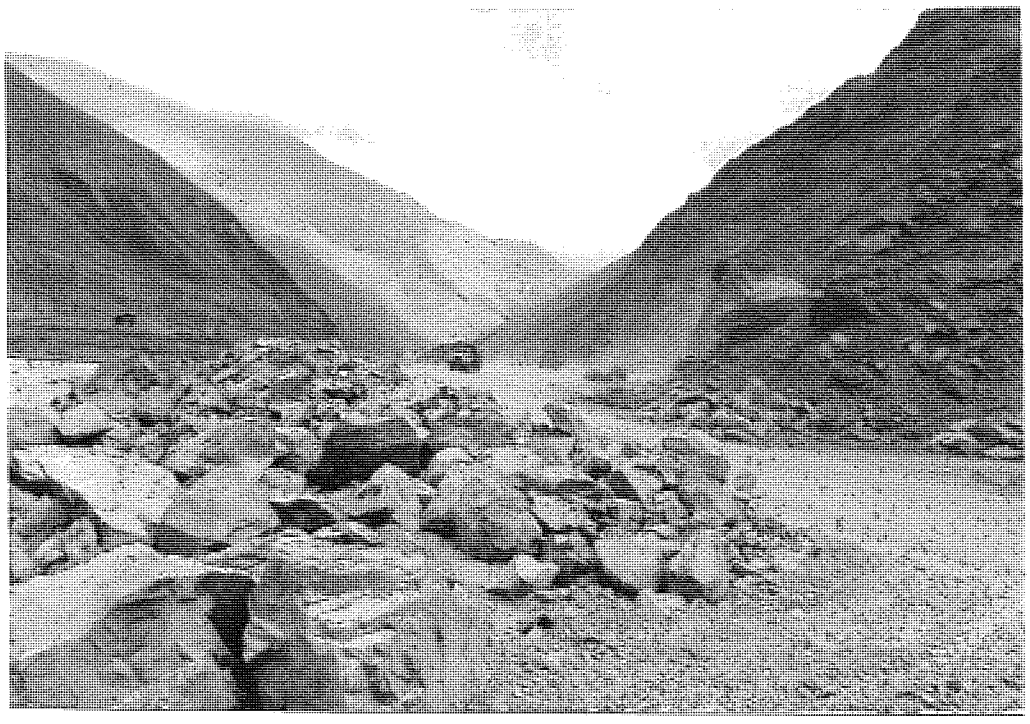

Plate 1.9 Rockslide in progress (km 86). A new rockslide on the Cretaceous rocks.

CHAPTER 2

ENVIRONMENT OF THE STUDY AREA

2.1 CLIMATE

The study area covers a part of the central Alborz mountains, and has a varied environment. The Alborz range, which trends east to west, separates the country into northern and central sections.

According to meteorological data rainfall occurs when warm moist air is forced to rise. Air currents from the northwest come across the Caspian Sea, reach the Alborz mountains and rise with resulting precipitation. Consequently the northern part of the Alborz region is very humid and covered by forest and vegetation. However, the southern part of the region is semi-arid. The climatic effects on the geology of the area: outcrops of rock in the southern region are less weathered and eroded. Discrimination of rock types is very easy in this arid zone, but is more difficult in the northern part where dense vegetation is common.

The central Alborz region reaches a peak altitude of 5671 m at the crater of the Damavand volcano, with its lowest point being at Emamzedah-Hashim, 2700 m above sea level. Central Iran, which is surrounded by the Alborz to the north and Zagros to the south and west (Figure 2.1), has a semi-arid to arid climate. This is why every weekend and on public holidays, the people of Tehran (population 8 million) and the other large cities in Central Iran want to have access to the north with its better climate and the attraction of the beaches of the Caspian Sea. This emphasises the importance of having roads giving access to the north. Details of climate are given in Tables 2.1, 2.2, 2.3 and 2.4 and shown graphically in Figures 2.1a-d and Figure 2.2.

Table 2.1 Statistics obtained from Amol Climatology Station (elevation 29m, Lat. 36.28, Long. 52.23), measurements are the average of 10 years (1965-1974). Combined of all existing data in the climatological organisations - Iran

Table 2.2 Statistics obtained from Lar-Pulur Climatology Station (elevation 2400m), (Lat. 35.50, Long. 52.05), measurements are the average of 19 years (1956-1974). Combined of all existing data in the climatological organisations - Iran

Table 2.3 Statistics obtained from Ab-Ali Climatology Station (elevation 2465m, Lat. 35.44, Long. 51.53), measurements are the average of 11 years (1962-1977). Combined of all data available in the climatological organisations - Iran

Table 2.4 Satistics obtained from Damavand Climatology Station (elevation 2077m, Lat. 35.43, Long. 52.03) measurements are the average of 7 years (1967-1973). Combined of all data available in the climatological organisations - Iran

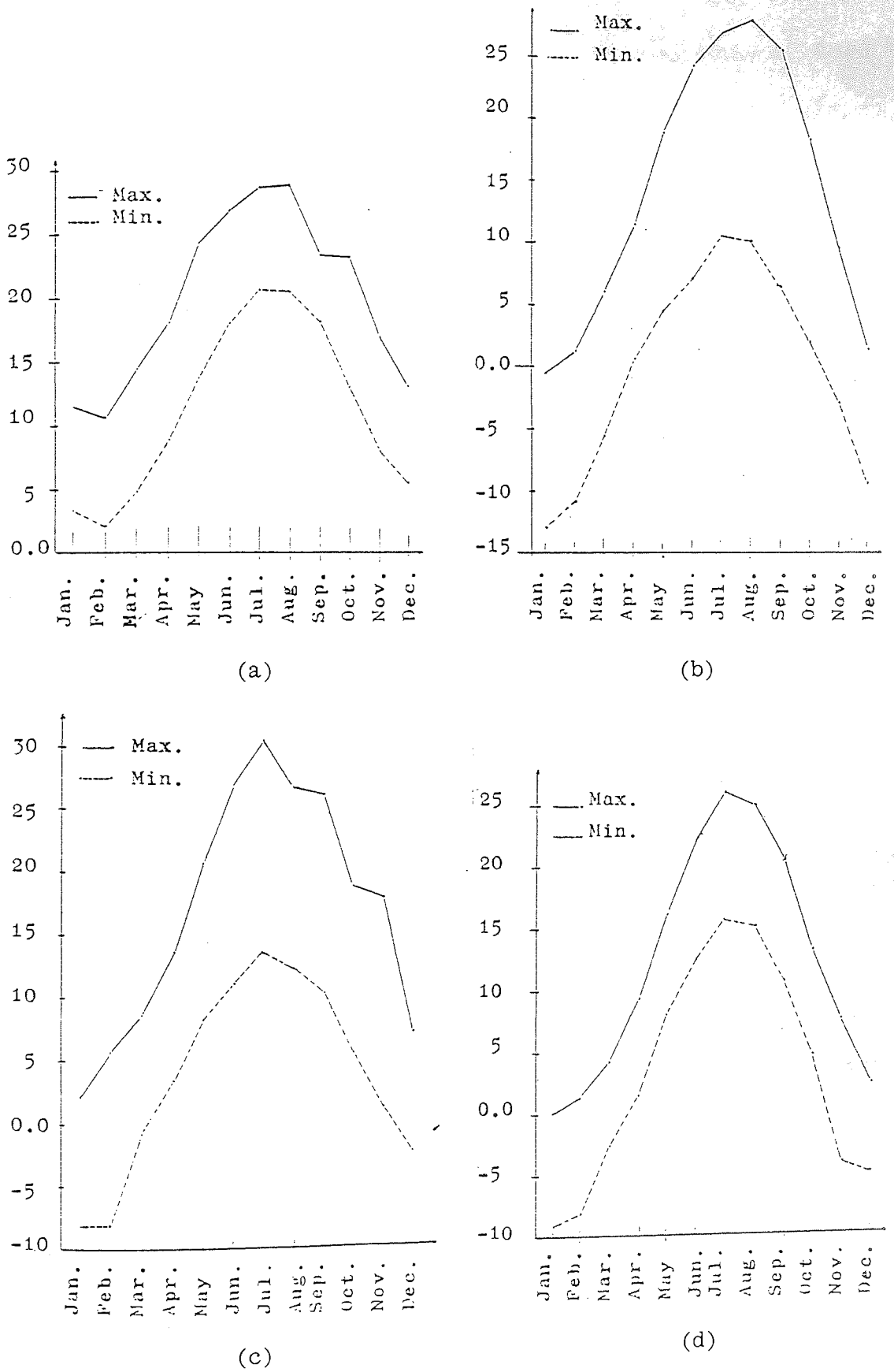

Figure 2.1 Temperature diagram. Average maximum and minimum temperature during the year in a) Amol b) Lar-Pulur c) Damavand d) Ab-Ali climatology station.

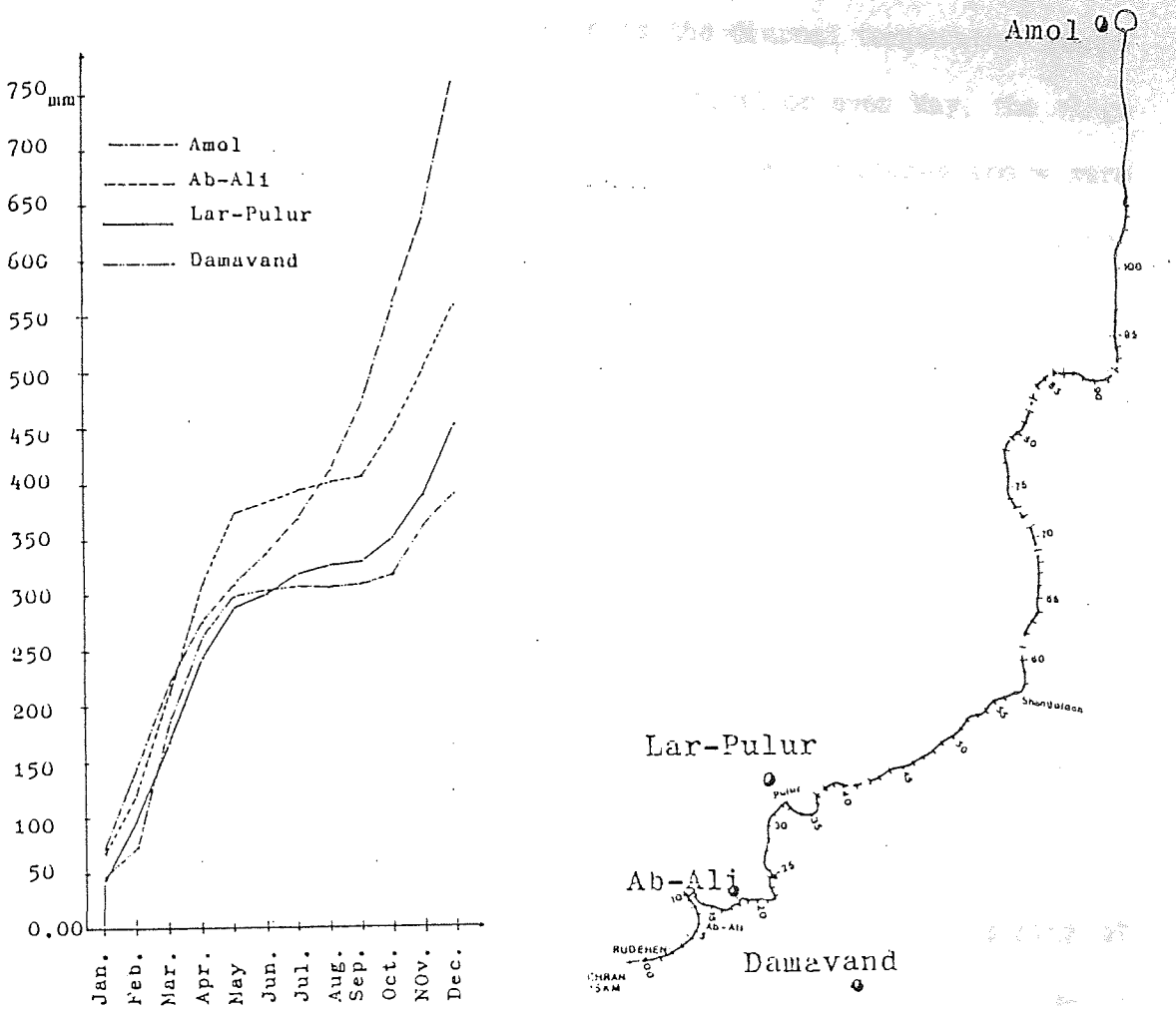

Figure 2.2 Accumulated rainfall and location of Climatologic stations. a) annual rainfall in the rigion. b) location of station where the data were collected.

The data in Tables 2.1 to 2.4 show a number of features. Firstly, the rainfall in the north (at Amol) is considerably greater than that to the south reflecting a change in climate to the north and south of the Imamzadeh-Hashia ridge(figure 2.3). To the north the higher rainfall and greater humidity are reflected in the much greater vegetative cover (the northern forests and cultivation around Amol).

Along the whole route rainfall is generally greatest in March/April which accompained by snowmelt at the same time leads to considerable surface run-off, infiltration and water table rise: all factors which contribute substantially to slop instability.

The other major climate feature is the diurnal temperature range. In the mountainous area, from November to April or even May, the range shows considerable freezing at night with temperatures above zero during the day. Frost penetration can extend 1.5m into the ground and the consequent freeze/thaw action has a profound effect on many of the rocks in the area, leading to increased fracturing and general disintegration of the rocks.

2.2 TRAFFIC

The difference in climate from the north to the south of the Alborz, results in heavy traffic on the roads to the North. The central location of Tehran means that most imported goods, including food, must be transferred from the sea ports on the Persian Gulf to Tehran and then further north. The location of the majority of factories in and around Tehran makes the situation worse and increases the amount of traffic to and from Central Iran.

As a result of increasing accidents on the Haraz road, close monitoring of traffic has become very important in recent decades. Table 2.5 shows statistics of the traffic northward on the Haraz Road. As can be seen, the peak of traffic occurred in 1978 with an average of 12411 vehicles per day, with 21 percent of these being heavy vehicles such as lorries.

There is a decrease in traffic until 1980, due to economic sanctions and a shortage of petrol and vehicle spare parts in the country. However, there is an increase in the percentage of heavy vehicles, mainly as goods transfer still has to be continued (figure 2.3). After 1980 there are no traffic data available.

Table 2.5 Traffic statistics for the road northwards per day. After Iran-Compsax reports and existing data in the Ministry of Road and Transport.

* Note: The Iranian weekend falls on only Friday, when many people travel from the Central Iran to the North for a break. Consequently on Saturday and Sunday (the begining of the week) there is little traffic going northwards. This could explain the apparent decrease in traffic in 1973 in the Table.

** Whole is automatically recorded average for whole week per day.

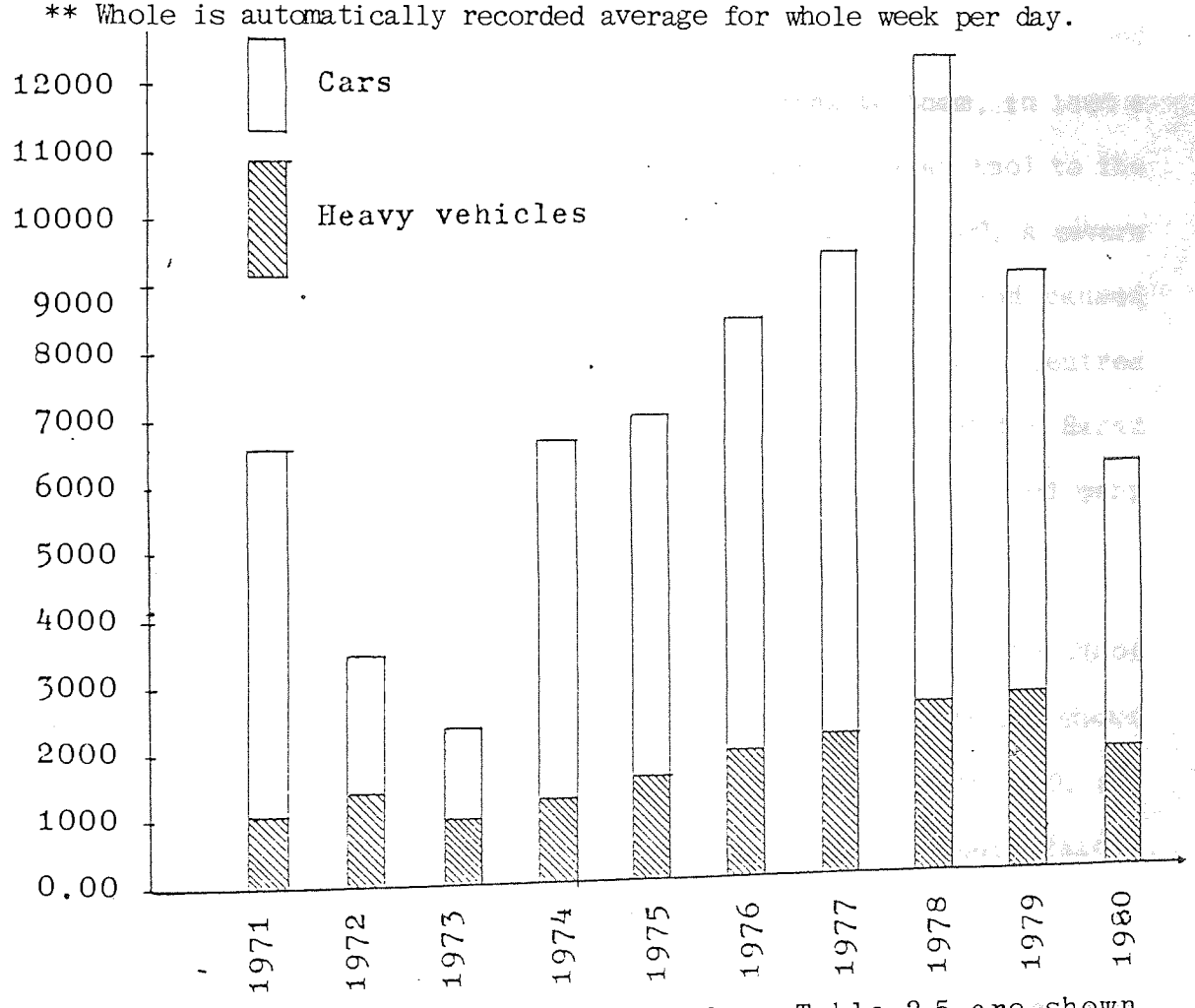

Figure 2.3 Traffic Bar chart. Data from Table 2.5 are shown graphically.

After an earthquake in March 1983, which cost several lives in the vicinity of the Baidjan thrust, the road was closed to all vehicles except lorries for several months.

2.3 SIESMOLOGICAL ACTIVITIES IN THE STUDY AREA

Iran is located on an earthquake belt running from east to west. Figure 2.4 shows the detected earthquake belts of the world. Figure 2.5 shows the areas of all recorded earthquake activity in Iran, and indicates that Central Iran is more stable than the mountainous regions. It is also seen that earthquakes are more likely in northern Iran than in any other part of the country.

The area covered by this research is very active seismologically. Ambraseys and Melville (1982) have studied the historical background of siesmological activity in Persia. According to them, in 1805 a destructive earthquake destroyed many villages between Amol to the north and Damavand to the south in the study area. In 1809, a severe earthquake hit the eastern part of the Haraz valley and caused rockfalls in the mountains. Another earthquake in 1825, centred around Kuhrud, ruined most villages in the upper part of the Haraz valley. On March 27th, 1830, a strong earthquake destroyed many villages to the north of Tehran and blocked the Haraz valley.

The events of the 20th Century are recorded in Report No. 29 of the Geological Survey of Iran, published in 1974. Table 2.6 shows earthquake activity centred on the study area from 1900 to 1970, and Table 2.7 from 1971 to 1975. Most earthquakes have been fairly destructive in this area.

In 1930 an earthquake, centred on Ah-Mobarak abad, destroyed many

villages in the region around Mobarak abad as shown in Figure 2.6 on the Musha-Fasham thrust fault. Later in 1957, the Sangichal earthquake damaged a large number of villages and caused several landslides in the region in Figure 2.7, It destroyed a newly built hotel, constructed of reinforced concrete, in Reineh.

Date	Source	Epicentre local name	Time G.M.T.	Epicentre		Magnitude M.M	Focal depth KM
				N	E		
2.10.1930	ISS	Ah-Mobarak	15 33 12	35.8	52.1	5.25-5.5	-
	CCP	abad	15 33	35.8	52.1	5	
11.5.1945	ISS	Garmsar	20 17 28	34.8	52.1	5.75	
	BCIS		20 17 38	36	52.5		
2.7.1957		Sangichal	00 42 23	36.14	52.7	average	10
	ISS		00 42 22	36.21	52.72		
	USCGS		00 42 23	36	53	7.3	
	BCIS		00 42 24	36.1	52.3		

Table 2.6 Major earthquake events from 1900-1970 recorded in the study area.

Notes: BCIS (Burea Central International de Seismologie), Strasbourg, France
CCP ACAD, SCI, USSR, 1962, Atlas of Earthquakes in the USSR
ISS International Seismological Summary, Edinburgh
USCGS United States Coast and Geodetic Survey, Primary and Monthly Determinations of Epicentres.

Date	Reference	Time G.M.T.	Epicentre		Focal depth km	Magnitude	Number of Observations
			N	E			
9.8.71	ISC	02 54 35	36.27	52.81	12	5.2B	204
"	USERL	02 54 36.7	36.2	52.7	27	5.2B	68
"	USCGS	02 54 36.7	36.2	52.7	27	5.3	68
"	MOS	02 54 36	36.2	52.8	25	5.5	
"	BCIS	02 44 42	36.2	52.6	50	6.3	
8.8.72	ISC	00 44 55.2	36.51	52.77	27	4.8	68
"	USERL	00 42 55.2	36.3	52.6	47	4.7	24
"	MOS	00 44 52	36.2	52.7		4.9	
"	MOS	00 44 52	36.2	52.7		4	
"	BCIS	00 45 01	36.3	52.5			
17.9.73	ISC	04 06 03.2	36.59	51.19	40	4.7	100
"	USERL	04 06 03.7	36.5	51.1	47	4.8	33
"	HFSI	04 05 39	35	53		4.9	
"	MOS	04 06 02	36.6	51.1		4.7	
"	MOS	04 06 02	36.6	51.1		4.5	
27.10.73	ISC	14 22 47	35.77	52.57	29		8
"	USERL	14 22 45.8	35.8	52.6	21	4.3	6
10.1.74	ISC	16 36 19.7	35.8	51.95	33		23
"	MOS	16 36 17	35.6	5.2		4.3	
5.11.74	USERL	20 02 22.3	36.2	52.8	68	4.5	13
11.4.75	USERL	14 26 44.7	35.5	50.2	50	4.7	20
6.11.75	USERL	04 09 31	35.89	53.03	38	4.9	38

Table 2.7 Major earthquakes from 1970-1976 recorded in the study area (after Nabavi, 1979)

(B) - Body wave magnitude (MB) and (S) surface wave magnitude (MS)
BCIS - See beneath Table 1
HFS - Hagfar Observatory Stockholm, Sweden
ISC - International Seismological Centre, Edinburgh, U.K.
MOS - Moscow Institute of Physics of the Earth, Moscow, U.S.S.R.
USERL - US Earthquake Research Laboratory (formerly known as USCGS)

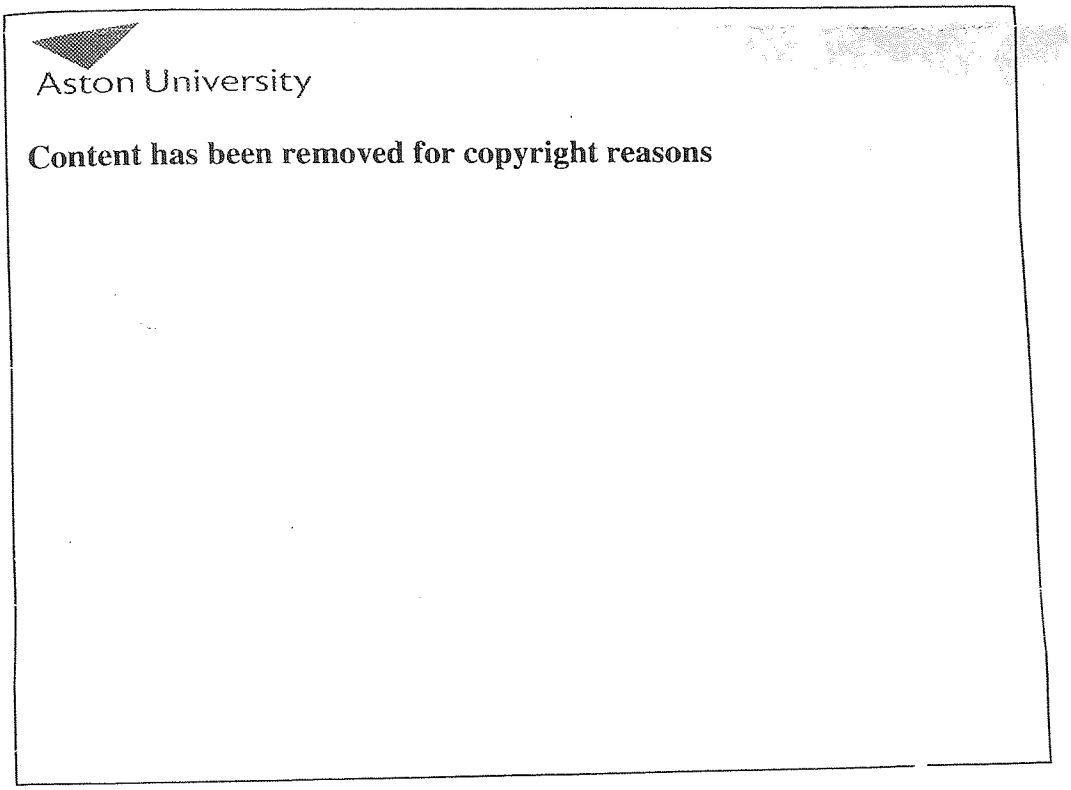

Figure 2.4 Physiographical map of Iran. (Ambraseys and Melville, 1982)

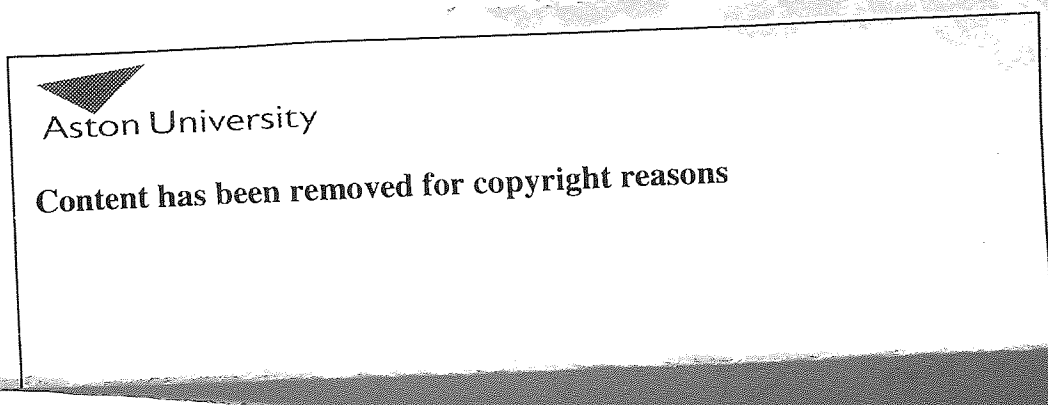

Figure 2.5 Earthquake locations. Worldwide distribution of instrumentally determined locations of earthquakes. (Ambraseys and Melville, 1982)

Figure 2.6 Areas affected by distructive earthquakes during the twentieth century. Dense areas are more severely affected and blank areas are not free of earthquake. (Ambraseys and Melville, 1982)

Figure 2.7 Areas affected by Ah-Mobarak-Abad earthquake in 1930. (Ambraseys and Melville, 1982)

Figure 2.8 Areas affected by Sangichal earthquake in 1957. (Ambraseys and Melville, 1982)

CHAPTER 3

GEOLOGY

3.1 INTRODUCTION

The geology of Iran was first effectively mapped at a small scale in 1959 by the National Oil Company of Iran. A few years later (1962) the Geological Survey of Iran was set up and more detailed mapping of the country was commenced but is still far from complete.

During the 1960's and early 1970's a number of European geologists were commissioned to prepare maps and memoirs on selected areas. In more recent years relatively little new material has been published.

The basic geology of the country consists of a southern (Zagros) and northern (Alborz) belt of fold mountains flanking an extensive central plain. The northern mountains of the Alborz contain strata of Precambrian to early Tertiary age (although there are stratigraphic gaps) complexly folded and thrust during the early Tertiary. Subsequently further Tertiary strata were deposited in the north and Quaternary volcanics and fluviatile deposits characterize the recent geological activity.

3.2 PREVIOUS WORK

The major works on the Haraz valley are those by Allenbach (1966) and Sussli (1976). The latter gives a detailed account of the lower Haraz Valley whilst the former tends to concentrate on the Quaternary volcanics of Damavand. Both works include maps at a scale of 1:100,000.

The stratigraphy of the area owes much to the work of Stocklin, et al. (1964) and the paleontology of the formations to a variety of workers, particularly Fantini Sestini (1965) with the collaboration of Assereto (1966). Cartier (1971) investigated the Cretaceous of the lower Chalus valley (to the west of the study area). The overall structure of the region has been described by Stocklin (1968).

3.3 GEOLOGICAL HISTORY OF THE CENTRAL ALBORZ (figure 3.1a and 3.1b)

3.3.1 Precambrian

Although Precambrian strata outcrop to the southeast of the study area, they are not present along the Haraz Valley.

3.3.2 Cambrian

3.3.2.1 Zaigun Formation

Stocklin et al. (1965) has measured a 450 m thickness for this formation, southeast of Zandjan. The formation consists of red, rarely dark-grey clastic limestone with micaceous siltstones.

The formation outcrops only in southeasternmost part of the study area and there are no outcrops in the Haraz Valley, thus no further details are given here.

3.3.2.2 Lalun Formation

The formation has been measured by Assereto (1966) in the Lalun valley at a thickness of 600 m, whilst Lorenz (1964) in the Karadj valley proved 730 m. The formation consists of red, thick layered sandstones and quartzites. These rocks previously were compared with the Old Red Sandstone (Devonian) of Great Britain, but Stocklin et al.

(1964) found trilobites in the overlying Mila formation proving a lower Cambrian age.

These rocks outcrop around km 17 and when weathered they alter to a red sandy soil. The upper part of the formation contains white quartzites which are quarried near km 17 and north of Mobarak-Abad (Plate 3.1). Due to the moderate slopes, outcrops of the formation do not constitute any major hazard, but minor problems appear at the time of thaw when rock falls occur in cuttings.

3.3.2.3 Mila Formation

The formation was investigated and measured by Stocklin et al. (1964) to the west of Damegan just east of the study area. It consists of pale grey, thin bedded dolomitic limestones which appear brown after weathering. Stocklin et al. (1964) and Lorenz (1964) found trilobite fossils of middle to upper Cambrian age in these rocks. The formation was laid down before earth movements in the upper Cambrian which resulted in a variable amount of erosion prior to the deposition of the overlying formation and hence a very variable thickness.

The formation outcrops at km 18 and km 43. Due to the moderate slopes around km 18 the rocks are not associated with any major hazard, but at km 43 the outcrops are located in a complex folded region which constitutes a generally unstable area.

3.3.3 Devonian

3.3.3.1 Djirud Formation

The formation has been described by Assereto (1963) from the

Djadjrud valley southwest of study area at a thickness of 750 m. The formation consists of brown, fairly strong, well bedded sandstones with grey quartzites, dark limestone and shale.

The formation outcrops sporadically around km 20 - km 23. Due to a lack of cuttings there is no instability problem in the area.

3.3.4 Carboniferous

3.3.4.1 Mobarak Formation

The 450 m thickness has been measured by Assereto (1963) to the north of Mobarak-Abad (km 12). The formation consists of massive, fossiliferous, dark grey limestone.

The formation outcrops around km 19, km 22 and km 44. These rocks are weak and weathering results in dissolution cavities. The rocks are well jointed in blocks as can be seen to the west of km 22. There are some instabilities at km 44 due to weakness of the faulted rocks, but not at km 19 and km 22.

3.3.5 Permian

3.3.5.1 Dorud Formation

The formation has been measured by Sussli (1976) to south of Amol (km 97) at 354 m thick. The formation consists of purple sandstone, siltstone and shale. Earlier, Assereto (1963) had described the formation in the Djadjrud valley.

The rocks outcop at km 13 and km 97. Due to moderate relief of the area around km 97 no instability problems occur, but at km 13

these rocks have been involved in a massive earth slide (Plate 3.1). The rocks here are made of up quartzites and sandstones, which in cuts look distinctly layered (striped).

3.3.5.2 Ruteh Formation

This formation was defined by Assereto (1963) in Ruteh valley with a thickness of 230 m, but Sussli (1976) recorded 690 m in the vicinity of km 97. The formation consists of fine-grained, dark-grey, brownish-grey well bedded limestone with some interbedded layers of dark shale.

The formation crops out near Emarat (km 100). The rocks are strong and are used as a crushed rock aggregate. Due to the strength of the rocks at outcrop the Haraz Valley cuts through them in a gorge. Despite the steep slopes involved, the formation shows no sign of instability.

3.3.5.3 Nesen Formation

The formation was recorded by Stepanov et al. (1969) with a thickness of 500 m, north of Mangol, near the Haraz road at km 102. Sussli (1976) measured both 200 m and 500 m in the same vicinity. The formation consists of thin bedded grey-yellow limestone, dark shale and claystone. The shale and claystone are very weak and susceptible to weathering and when weathered produce a highly vegetated soil.

The formation does not outcrop in the study area and is not considered further.

3.3.6 Triassic

3.3.6.1 Elikah Formation

Initially this formation was discovered by Glaus (1964), but it has been measured by Steiger (1966) in Dalichai as 500 m thick. The formation consists of two parts (t_1 and t_2), of which the lower (t_1) contains pale grey limestone, edge-wise congolomerate with occasional intercalations of marl. The upper part (t_2) is characterised by thin bedded whitish dolomite.

The formation outcrops at km 96 and km 106 and the upper layers are covered by vegetation, and no instability problems are encountered.

3.3.7 Jurassic

3.3.7.1 Shemshak Formation

The formation has been measured by Assereto (1966) in the Djadjrud valley as approximately 1000 m thick, but initially it was named by Dellenbach (1964). The formation consists of alternations of whitish quartz-sandstone, grey conglomerate, grey sandstone, grey siltstone and dark shale with thin lenses of coal.

The study area is dominated by this formation especially between km 50 and km 95. The thickness of the formation in the study area measures up to 2000 m and it contains several weak layers (amongst strong siltstones, sandstones and shales) which cause instability problems. Where the formation is overlain by volcanics, with the associated infiltration of water, instability is particularly severe. Outcrops remain unvegetated and look black because of the presence of coal.

3.3.7.2 Dalichai Formation

The formation (approximately 100 m thick) was discovered by Steiger (1966) near Dalichai village. This fossiliferous formation consists of greenish-grey, thin bedded, easily cleaved marly limestones, thinly laminated marls and more compact dark grey limestones in beds 20 - 40 cm thick.

The formation outcrops in several places along the Haraz Valley (km 27, km 64). It separates the Shemshak and Lar formations and varies from 50 - 120 m thick. It is very weak after weathering and is commonly obscured by a thick weathered profile of colluvium. Although the formation is not very thick some rock slides occur in the outcrop areas.

3.3.7.3 Lar Limestone Formation

The formation was measured by Assereto (1966) in the Lar valley as approximately 250 m thick. The formation is typically a dense, strong, pale green to cream, fine grained limestone. The lower part contains many seams and nodules of chert whilst the upper part is commonly dolomite.

The formation outcrops at a number of locations, but around km 27 and km 81 are perhaps the most typical (Plate 3.2). The outcrops are characteristically free of vegetation and often steeply sloping. These rocks are oriented east-west, dipping to the north, consequently despite open jointing and rapid infiltration there is no instability problem. Weathering and slope degradation are limited to sporadic falls of weathered rock fragments in cuts.

3.3.8 Cretaceous

The rocks of the Cretaceous age which outcrop in the Central Alborz have been subdivided by various workers into six units, namely the five members of the Chalus Formation and the Globitruncata limestone (Allenbach, 1966).

The lowest unit comprises gypsum (up to 100 m thick), with lateral transitions to freshwater marls, sandstones and limestones (k_{gy}) upon which lies a massive suite of basaltic volcanic rocks (k_m). The thickness, dominated by the basalts, reaches some 400 m but the unit rarely outcrops on the road line.

The second unit is referred to as either the Tiz-kuh Formation (Steiger, 1966) or the Orbitolina Limestone (k_1). The formation is dominated by massive bioclastic limestones which give way towards the top of the sequence to shales and sandstones. The formation is about 300 m thick. Outcrops are limited to the northern part of the road where, because of the massive and well-drained nature of the rock, they form steep stable slopes and cuttings.

Overlaying the limestone is another 200 to 300 m of basaltic volcanics, dominated by amygdaloidal flows. Occasional ashes (tuffs), agglomerates and sediments (dolomites and limestones) are present. These volcanics outcrop between km 86 and km 91 where they are dark red in colour and obviously weathered. The slopes which are extensive and deeply covered in colluvial debris are commonly unstable. The active rockslide (avalanche) at km 86 is shown in Plate (3.3).

The following formation (k2) is dominated by limestones (including dolomites) with intercalations of volcanic ashes and agglomerates as well as sandstones, shales and even conglomerates.

The latter lithologies become dominant east of the Haraz Road and the whole formation thins from almost 500 m west of the Haraz Valley to less than 100 m, east of the valley. The unit outcrops around km 29 and km 83 where despite the often thin bedded character and the presence of shales, little instability occurs.

The fifth unit (k3) or Upper Volcanic member is very similar to the basaltic volcanics of unit three, and outcrops between km 84 and km 88. Due to the sensitivity of the rocks to weathering, extensive slopes with some instability occur around km 84 to km 87.

The above five units are all correlated with the Chalus Formation of Cartier (1971), upon which lies the Globitruncata limestone. The limestone (slightly dolomitic and generally fine-grained) dominates the lower part of the 400 m thick sequence, whilst the central and upper sections are argillaceous (clayey and fissile) limestones and thick bedded sandy limestones respectively. Outcrops of the unit near the Nur valley confluence (km 84) are generally stable and give rise to few problems.

3.3.9 Eocene

3.3.9.1 Fajan Formation

The basal Tertiary sediments usually consist of conglomerate, agglomerate and marl which cover the older formations with considerable unconformity. The formation varies in thickness from zero to 200 m. The congomerate matrix is red and colours much of the formation. However, the formation does not outcrop on the road line.

3.3.9.2 Ziarat Formation

This formation was studied by Dellenbach (1964) north of Tehran. It consists of congolomerates with a red matrix and the angular nature

of some of the gravel indicates it colluvial origin.

The formation is not present in the Haraz Valley, but it crops out in Central Alborz with a thickness which varies from 0 - 200 m.

3.3.9.3 Karadj Formation

The formation was assessed by Lorenz (1964) in Karadj valley as approximately 1000 m thick. The formation consists of mainly green tuffs, basalt, andesite and lava agglomerate from Tertiary activity.

These rocks outcrop between km 1 and km 7 and around km 32-36 along the Haraz Road. The thickness of this formation here measures about 1500 m in the south and less in the north. Despite the sensitivity of the volcanics to weathering, both slopes and cuts are fairly stable.

Plate 3.1 lalun Formation (km 17). Quartzite quarries are located at the left centre of the scene.

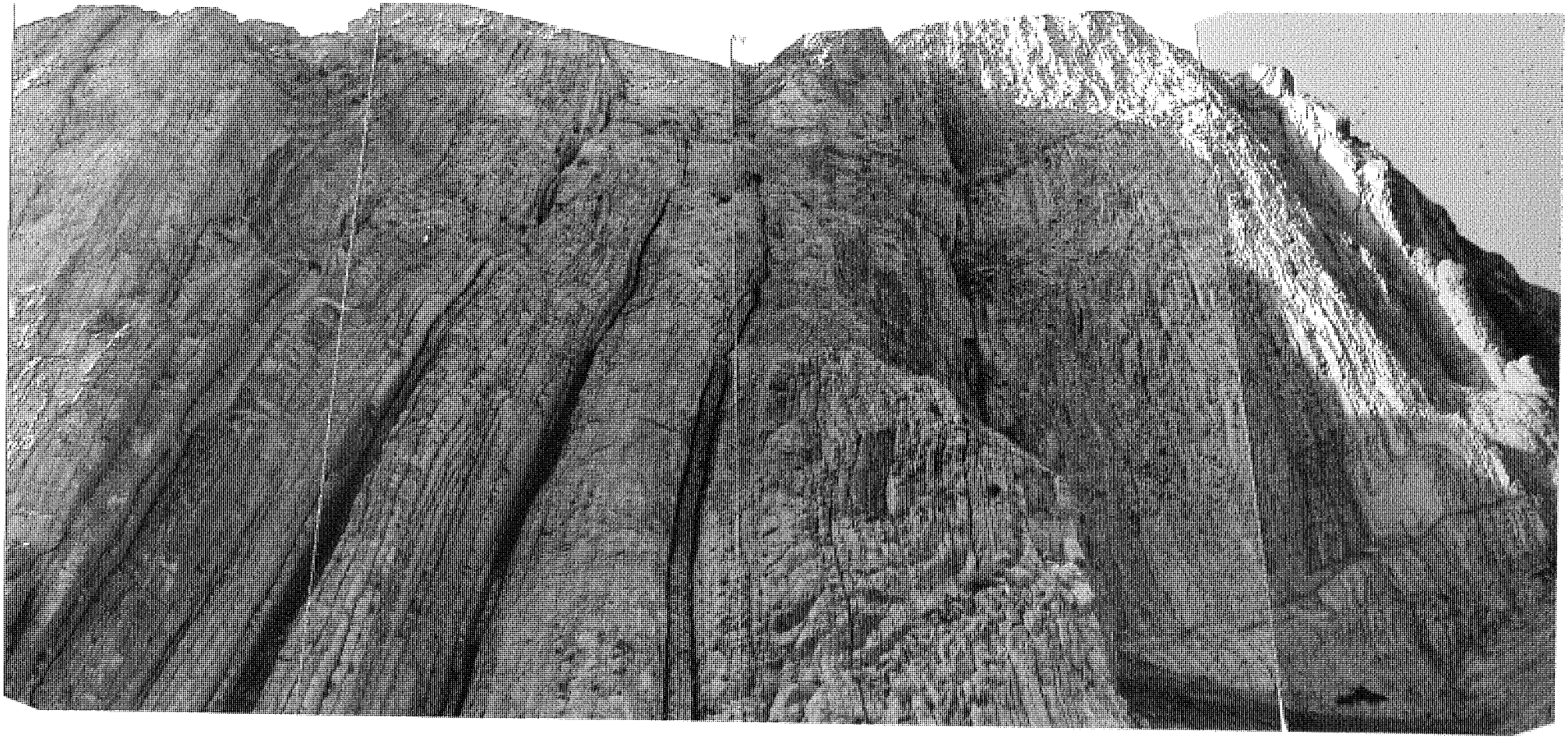

Plate 3.2 Iar limestone standing vertically beside the road (km 81). The rocks providing a vertical wall approximately 30 m high.

Plate 3.3 Cretaceous volcanics (km 86). An active rockslide can be seen at bottom right corner.

3.3.9.4 Other Formations

The other formations of Tertiary age (Figures 3.1a and 3.1b) which are all sediments, mudrocks to conglomerates and limestones do not outcrop in the study area.

3.3.10 Quaternary

The Quaternary period in the study area is dominated by the Damavand volcano. The volcano has affected the area either by flows blocking the gorges and creating lakes or the deposition of ashes. Major instabilities occur in areas where pyroclastic rocks constitute the slopes near the road.

Elsewhere along the Haraz Valley colluvial talus fans are still developing, consituting unstable regions. Other problems appear when high level terrace deposits which range up to 300 m high are located near the road.

3.3.10.1 Quaternary Sediments

The sediments have been described by Bailey et al. (1948), Derruau (1959), Bout and Derruau (1961) and Allenbach (1966).

Eruption on the south side of Damavand had blocked the Lar valley and created a lake some 30 km long. The lake then filled with sediments up to a level of 2550 m above sea level. Subsequently the Lar river re-established itself and created a deep valley through these sediments.

A similar situation has occurred at the junction of Velarud and Dalichai and at the end of the Lassem valley where the sediments (mixed with ashes) are very coarse. The alluvium of the Lassem valley is widespread and extends to a fairly high level. These alluvial deposits are present around km 28-30, associated with coarse lavas and lead to marked instability. The alluvial terrace deposits to the east are also of poor stability and are likely to cause problems on the Haraz-Lassem road (currently under construction).

Occasional travertine deposits occur in the Velarud valley, north of Damavand town and south of Ask. At the latter the deposit has disturbed the course of the river.

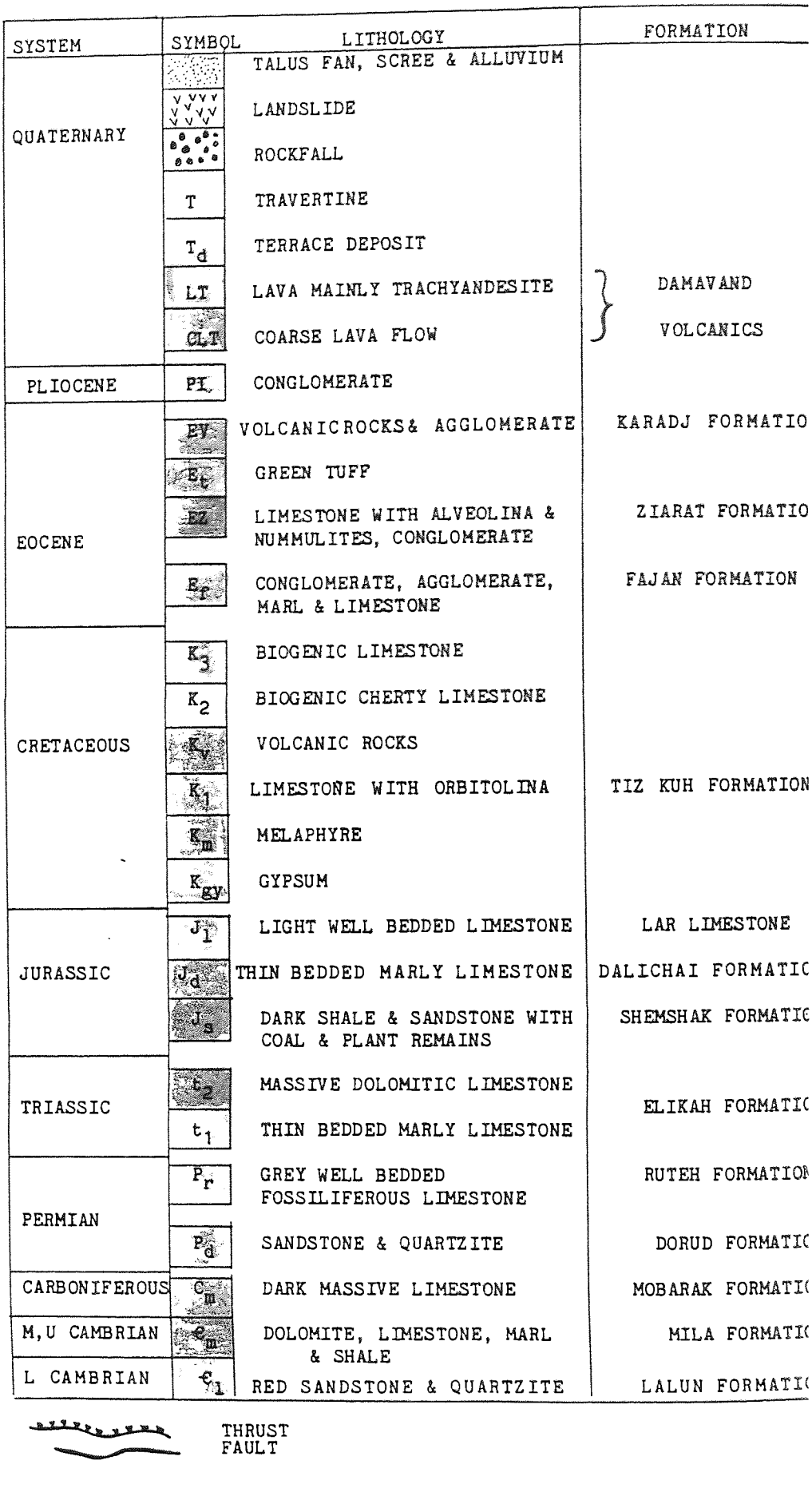

Figure 3.1a Legend of geological map (Fig. 3.1b)

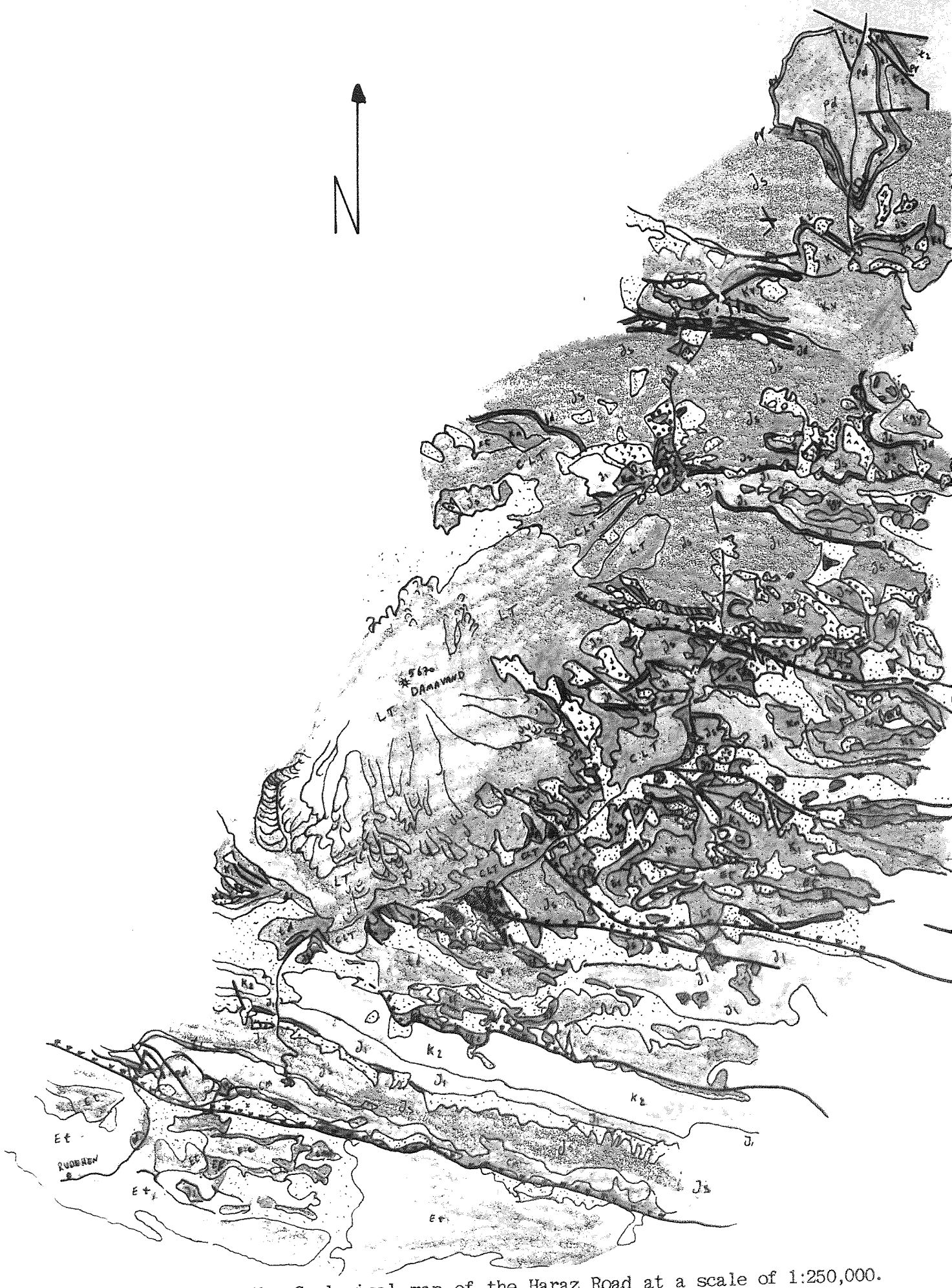

Figure 3.1b Geological map of the Haraz Road at a scale of 1:250,000.

3.3.10.2 Quaternary Volcanics

The most recent volcanics in the area are those associated with the Damavand volcano. The volcano rises to 5670 m above sea level in a classic conical morphology, and can be seen from Tehran some 70 km away. The volcano, dormant or perhaps even extinct, has attracted many scientists as well as tourists. Geological interest commenced with the work of Tietze (1878) who misguidedly hoped to find diamonds. Stahl (1897) identified basalts on the east flank of the volcano which Steiger (1966) dealt with in some detail around Pulur. Stahl (1911) was able to diagnose early volcaniclastic deposits overlain by flows of trachyte and andesite which (together with tuffs and agglomerates) make up the majority of the cone. Ovcinnikow (1930) was perhaps the first to discern that trachytes and andesites were errupted from fault controlled fissures. Various workers subsequently improved our knowledge of the petrography (Riviere, 1934; Scherillo, 1935; Christa, 1940). Jeremine (1942) investigated the chemistry of the rocks and suggested a dominance of plagioclase over alkali feldspar. Bailey and Stevens (1960) working on the south side diagnosed andesite which they considered to overlie the basalts around Pulur. Later workers improved the information and details are given by Allenbach (1966).

The Damavand volcanics dominate a substantial portion of the route (Plate 1.3). South of Pulur amygdaloidal olivine basalts are overlain by more massive olivine bearing trachybasalts at the eastern extremity of the flows (Palvar-kuh). These olivine trachybasalts contain less olivine and augite than those on the west side of the flank.

To the west of Ask columnar flow rocks of trachytic affinities

(with pyroxenes, hornblende and biotite) are present as massive grey bluffs which weather red-brown. To the far west of Baidjan the lavas overlie the Shemshak shales and mudrocks. The lavas are well jointed trachyandesites, but with porphyritic crystals of augite, hornblende and biotite. To the west of the summit are the most recent flows again of trachytic composition although augite, hypersthene and biotite are present.

Whilst dominated by lava flows, pyroclastic deposits are common and Figure (3.2) shows Allenbach's (1966) interpretation of the flows which is considered to be somewhat idealised.

The coarser pyroclastics appear in the Haraz Valley between Ask and Baidjan, where they are generally located high in the left bank of the river overlying Jurrasic strata. At higher elevations these agglomerates are overlain by flows and more pyroclastics. In the Tallow valley (above Gazanak) the tuffs can actually be seen to thin towards the cone. To the north of Malar-Fireh (Plate 3.4) the pyroclastics rest on the Shemshak and Lar formations, and there is much evidence to suggest that these pyroclastics thicken north-eastwards into the Valley. Around km 56 (Plate 3.5) the deposits consist of rounded boulders and gravel set in a reddish matrix and these may well represent a mass flow (lahar) deposit. Pyroclastics on the west side of the cone are less obvious and not of concern here.

3.4 TECTONICS

The study area is located in the Alborz range which is normally divided into five structural or tectonic units. Within the study area, three of these units only are present.

Plate 3.4 Pyroclastics (km 59). The layers are horizontal and they are not affected by techtonic activities.

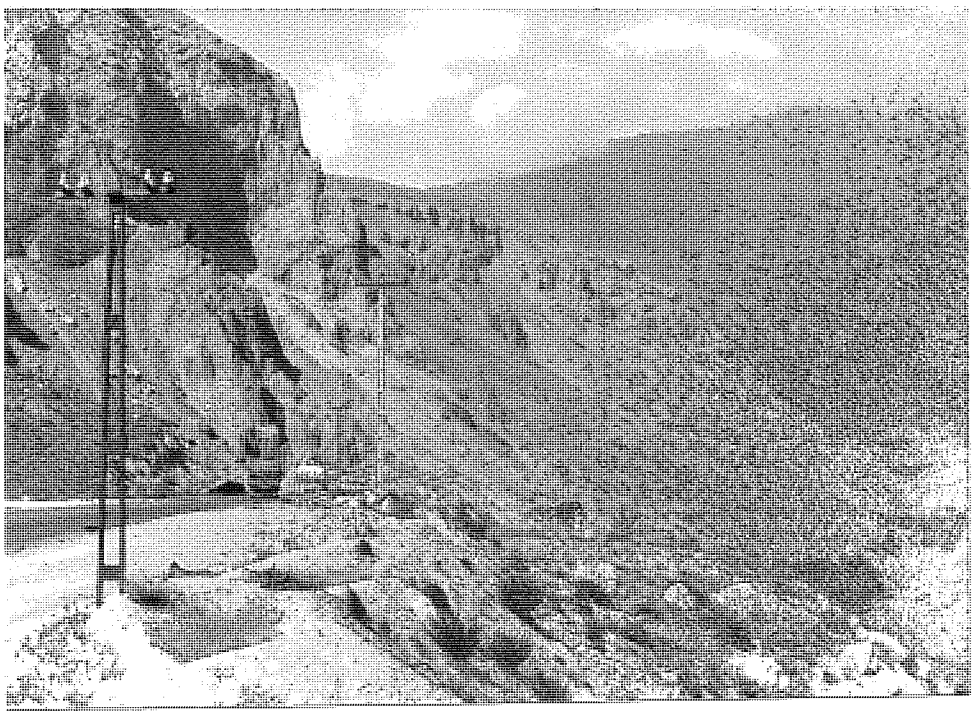

Plate 3.5 Mass flow (km 56). redish mass at centre left contains rounded boulders and gravels.

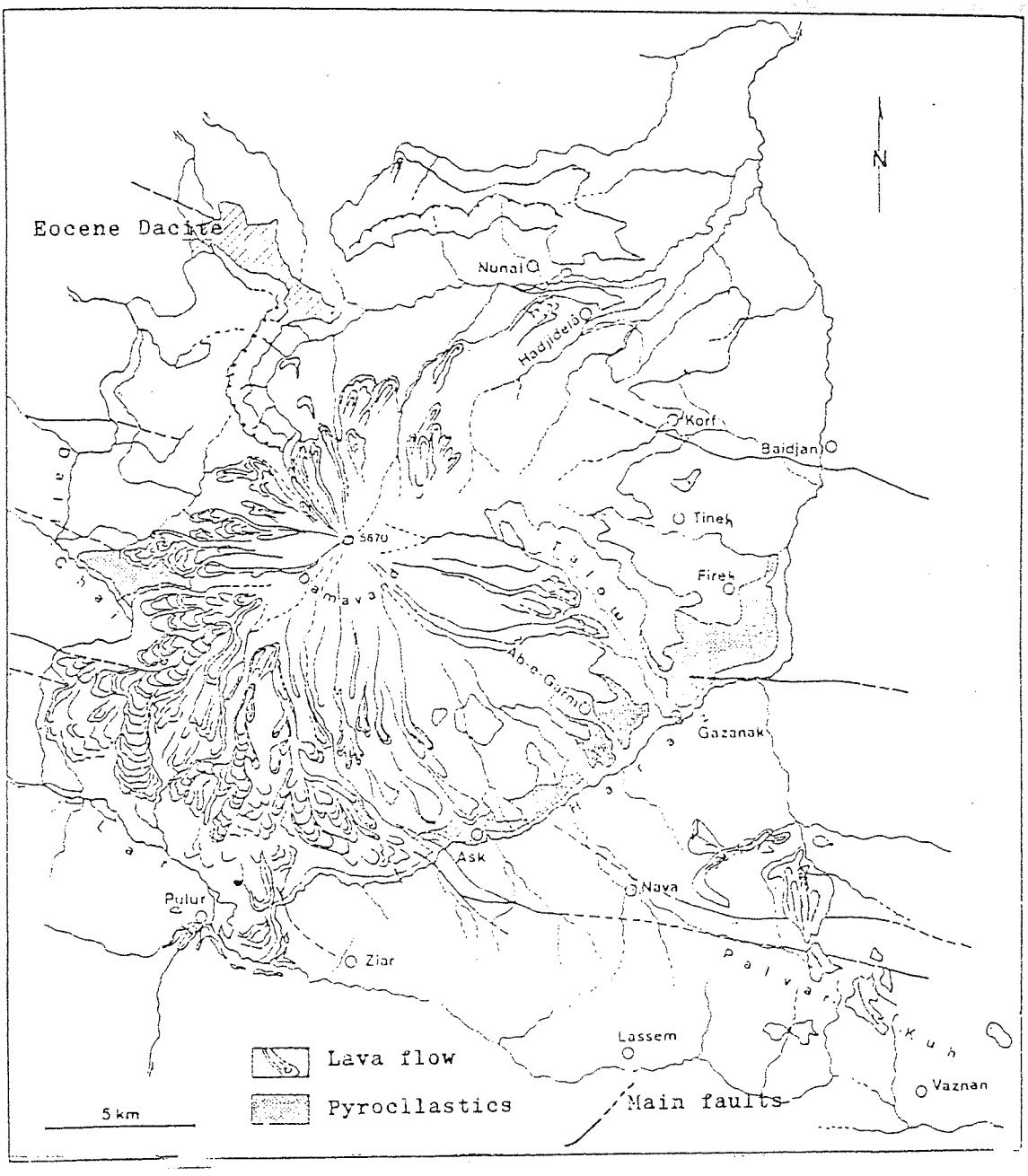

Figure 3.2 Distribution of volcanics in the study area. (after Allenbach 1966).

The general tectonic regime which is of Mesozoic to early Tertiary age consists of a series of thrust units which trend east-west. The three units in the area are bounded by major thrusts, to the north of the Baidjan thrust, to the south of the Musha-Fasham thrust and between these two. Within each unit the formations are severely folded along the same trend and thrusting is common with other faulting also present, all reflecting the general tectonic pattern of overthrusting from north to south.

The central area and a limited portion of the northern area have been extensively covered by the Quaternary volcanics of Damavand.

The major tectonic features are shown in Fig. 3.3 after Allenbach (1966) and Sussli (1976).

3.4.1 The Northern Area

To the north of the Baidjan thrust, which crosses the Haraz Valley just south of the village of Baidjan, (km 64), the formations dominantly involved are those of lower Jurassic age. In the north of the study area the Emarat anticlinorium trends across the valley and brings rocks of Triassic and Permian age to the surface. Between Emarat and Nur-rud strata of the Shemshak formation (lower Jurassic) outcrop. At Nur-rud lower Cretaceous strata appear and the valley follows the Nur fault which brings upper Cretaceous rocks to the surface. These are complexly folded around Naglesar. The sequence becomes older to the south and near Panjab-rud lower Cretaceous and Jurassic strata are present. From this location almost to the Baidjan thrust the Shemshak formation dominates. It is folded in a number of anticlines and synclines of which the Pardomand anticline is perhaps the most important. Between Baidjan village and the thrust is the

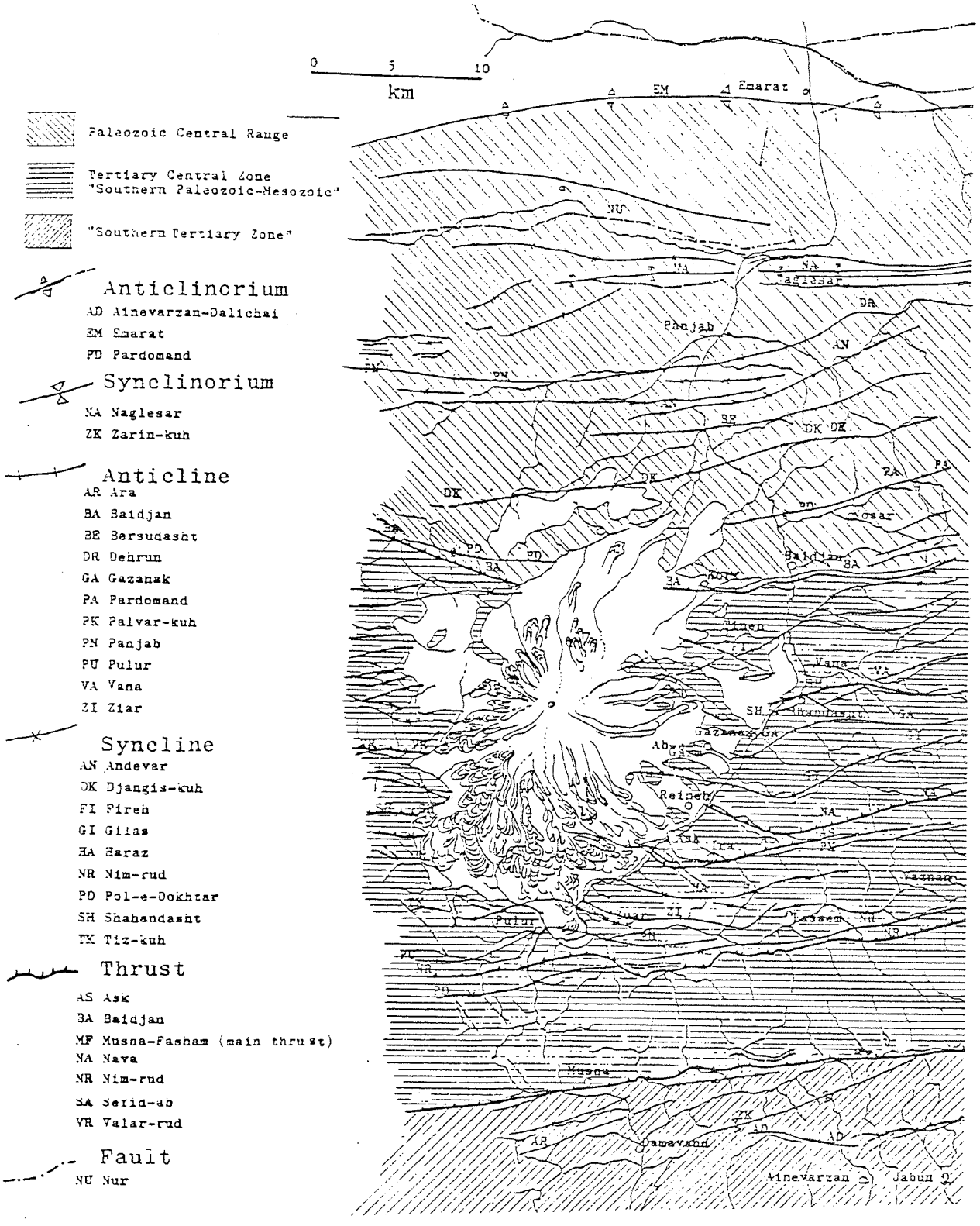

Figure 3.3 Tectonic map of the study area. Three tectonic zones are shown north to south. (after Allenbach 1966 and Sussli 1976).

Baidjan anticline which brings Triassic rocks to the surface. The thrust dips north at about 60° and trends almost east-west across the valley before dissappearing north-westwards beneath the Damavand volcanics. The thrust is still 'active' with moderate seismic activity and warm springs associated with it.

3.4.2 The Central Area

The tectonic regime in the central area is very similar with folds and minor thrusts trending sub-parallel to the Baidjan thrust in the north and the Musha-Fasham thrust in the south. Much of the area is dominated by the Shemshak formation but the Damavand volcanics obscure much of the earlier geology to the west of the Haraz Valley.

South of the Baidjan thrust the first major feature is the Fireh syncline which brings the Dalichai and Lar Limestone formations to outcrop, beyond which the Shemshak formation reappears (Vana). At Shahandasht a thrust to the south of which is a major syncline again brings younger rocks to the surface (including mid Cretaceous strata to the east of the Haraz Valley). Secondary faulting trending northwest is present in the vicintiy of Shahandasht. The Shemshak reappears again to the south of the syncline and Triassic rocks (Elikah formation) are brought to outcrop by the Gazanak anticline. The folding continues to the south with the Lar limestone appearing on the flanks of Damavand brought down by the Gilas syncline. Crossing the Nava thrust and approaching the Ask thrust the area around Ask becomes very complicated with Permian, Triassic and Carboniferous rocks at the surface associated with later faulting (trending northwest). South of the Ask thrust the Shemshak formation reappears before younger Cretaceous strata are brought to the surface by the

Haraz syncline. The Ziar anticline and other folds and the Nimrad thrust all involve Shemshak strata before the Pol-e-Dochtar syncline again brings mid Cretaceous strata to outcrop. South of Pol-e-Dochtar the sequence ages through Jurrasic, Triassic, Carboniferous and, as the Musha-Fasham thrust is approached, Cambrian strata.

The Musha-Fasham thrust is a dominant structural feature which dips north and brings the Cambrian strata to the north against Eocene strata to the south.

3.4.3 The Southern Area

To the south of the Musha-Fasham thrust the geology is dominated by Tertiary strata. These are again folded along east-west axes into synclines and anticlines of which the Ara anticline is the major feature. This anticline brings the Jurassic sequence (and some Cretaceous) back to outcrop in the vicinity of Damavand town. The southern flank of the anticline is the northern flank of the Zarin-kuh syclinorium which returns the Tertiary Eocene formations to the surface in the study area though the full effect of the synclinorium and the Ainevarzan-Dalichai anticlinorium to the south area not seen until well to the east.

3.4.4 General Tectonic Effects

The tectonics have had a profound effect on the rocks producing variations in faulting, folding, jointing and shearing at all scales. The complexity at an engineering scale is far greater than can be communicated here but in many cases the discontinuity pattern and its orientation leads to significant instabilities even though the general trend is across the Haraz Valley.

The tectonic complexity also affects the groundwater regime by bringing variable rocks to the surface and into contact with each other. This, in a number of cases, has led to groundwater conditions which aggravate the stability problems associated with the highway.

CHAPTER 4

SLOPE STABILITY IN THE STUDY AREA

4.1 INTRODUCTION

Most of the study area, particularly in the Haraz Valley, is unstable. The problem of slope stability, in both natural and in excavated cuts, has to be faced in many fields of human activity, particularly in civil engineering. Rockfalls may be caused by landslides, wedge failures, shear failures, or associated with earthquakes. A fairly sudden fall of a single wedge results in break upon impact with other rocks and would therefore, constitute a threat to anyone in the vicinity (Hoek and Bray, 1974).

The problem arises when the slope is disturbed, as in the construction of the Haraz road, and downslope movements of most varied character take place (Zaruba and Mencl, 1969). Due to the extensive and steep slopes in the Haraz Valley several areas along the road are unsafe. Debris which falls from high on the slopes, accelerates downslope and becomes a severe hazard at road level. Many of the downslope movements are triggered by seismic activity (earthquakes), freeze-thaw or meltwater infiltration.

Failure occurs when downslope forces (gravitational) exceed some form of equilibrium condition. The failures consist of three types: toppling with associated fall, roll, bounce or slide. Sliding where a distinct shear surface is involved, or particulate mass movement, similar to avalanches.

Forces due to thermal expansion, freeze-thaw cycles, vegetation growth or hydrostatic forces will all tend to move blocks away from the slope and thus towards failure. Individual blocks will then topple and move downslope in a variety of ways. For the same reason

masses of block of smaller size will move 'en mass' as a flow (avalanches). Change in body forces, notably in the hydrostatic forces, will often initiate slides, as will dynamic forces such as acceleration due to earthquakes. The presence of water may cause weathering which also alters the frictional character at the potential shear plane and reduce shear strength as well as increasing the downslope forces.

Many classifications have been proposed for downslope movements, these are mainly based on the kind of material, type of movement and causes. Wahlstrom (1974) classified the movements into two main groups, slopes in unfractured rocks and slopes in closely fractured rocks. However, Varnes (1958) has classified such movements (Table 4.1), according to the movement and material types, and this appears to be most appropriate to the Haraz road study area.

<table>
<tr><td rowspan="2">TYPE OF MOVEMENTS</td><td colspan="5">TYPE OF MATERIAL</td></tr>
<tr><td colspan="2">BEDROCK</td><td colspan="3">SOILS</td></tr>
<tr><td>FALLS</td><td colspan="2">ROCKFALL</td><td colspan="3">SOILFALL</td></tr>
<tr><td rowspan="2">few units
SLIDES</td><td>Rotational
SLUMP</td><td>Planar
BLOCK GLIDE</td><td>Planar
BLOCK GLIDE</td><td colspan="2">Rotational
BLOCK SLUMP</td></tr>
<tr><td>many units</td><td></td><td>ROCKSLIDE</td><td>DEBRIS SLIDE</td><td colspan="2">FAILURE BY LATERAL SPREADING</td></tr>
<tr><td rowspan="3">FLOWS</td><td colspan="5">ALL UNCONSOLIDATED</td></tr>
<tr><td>dry</td><td>ROCK FRAGMENTS</td><td colspan="2">SAND OR SILT</td><td>MIXED</td><td>MOSTLY PLASTIC</td></tr>
<tr><td>wet</td><td colspan="2">Rock Fragment Flow
Sand or Silt Flow</td><td>Sand Run
Loess Flow
Rapid Earthflow</td><td>Debris Avalanche
Debris Flow</td><td>Slow Earthflow
Mudflow</td></tr>
<tr><td>COMPLEX</td><td colspan="5">COMBINATIONS OF MATERIALS OR TYPE OF MOVEMENT</td></tr>
</table>

Table 4.1 Classification of the ground movements (After Varnes, 1958)

4.2 BEDROCK MOVEMENTS

4.2.1 Rockfall

Due to the long history of tectonic activity in the area (see Chapter 3), none of the exposed rocks can be called intact rocks. Additionally, the area is exposed to cold winters with freeze/thaw cycles affecting sunfacing slopes and cuts during February and March, producing further fractured rocks which become hazardous, especially when infiltration of water occurs.

In a rockfall, the moving block travels mostly through the air by free fall, leaping, bounding or rolling with little or no interaction between one moving unit and others. Release of a block can be caused by a variety of processes, but earthquake activity is a common cause. In the study are falling blocks are of three types: travelling through the air by free fall, rotating down the slope surface, and leaping and gliding. The first type rarely occurs, because there are a few overhanging cuts. However, the second and third types are very common. The extensive slopes immediately adjacent to the road (see Chapter 2), which are oversteepened frequently develop rockfalls. Rotating blockfalls involving blocks up to cubic metre in size are common and dangerous at several places along the road, (km 7, 33, 34, 50, 52, 58 ... etc). Several rock chutes have been constructed along the road at the most dangerous points to protect the road from both rockfalls and snow avalanches (see Chapter 2). The wire meshing or use of shotcrete on some fractured rock cuts may be an effective protection measure. However, the endless oversteepened slopes are impossible to control unless an artificial concrete tunnel or a chute system is constructed at the most dangerous points.

4.2.2 Rockslide

These failures come about as a result of a series of weak geological structures being disturbed, particularly at the toe of a slope (Seegmiller, 1979). That is, two sets of weak geological structures (discontinuities), one mainly faults, the other joints or bedding, exist in such a combination that wedges or slabs of rock slide into the valley. Oversteepened slopes are nonequilibrium slopes, and the persistance of such slopes with time is an excellent qualitative measure of bedrock strength. However, the competency of bedrock in most areas is not high, and the natural process of oversteepened slopes to reduce their gradient results in rockslides at several points along the valley.

Two examples of planar failures are located at km 85 and km 59. The former occurred in 1982. The latter developed several years earlier, pushing the road towards the valley bottom giving rise to an unstable slope about 100 m across by 150 m downslope. In 1975 there was an attempt to remove a block from this 35 slope by blasting, which was not very successful (Plate 4.1). Both of these rockslides are located on highly faulted areas. The former is in Cretaceous volcanics and the latter is in lower Jurassic shales and sandstones. Another rockslide, measuring approximately 200 m across by 150 m downslope occurred on a 30° slope on 25 March 1983 at km 64 (Plate 4.2). The upper Jurassic Lar limestone which dips into the valley here, failed as a consequence of a severe earthquake, and a huge mass of already fractured rock came sliding down onto the road burying vehicles. The hazard had been recognised by Iranian surveyors (Amini, 1972), and reported to the Road and Transport Secretary. After the catastrophe which cost about 200 lives, there was an attempt to

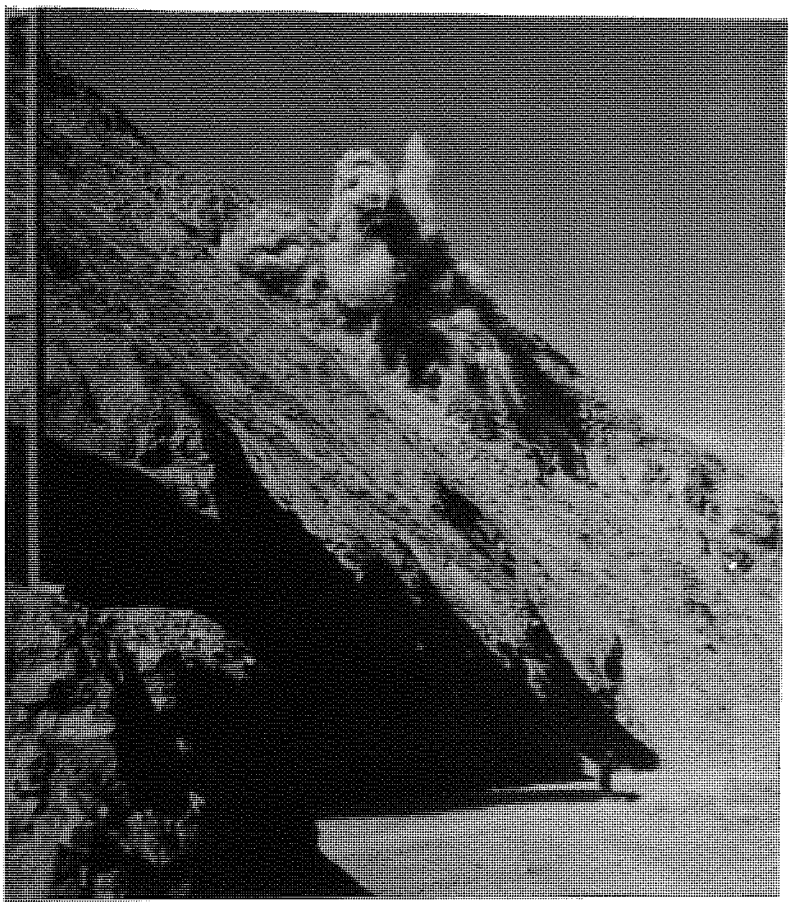

(a)

(b)

PLate 4.1 Planar failure accured in Shemshak formation (km 59). The road is pushed away by debris resulted from the movement. The photo (a) was taken in 1975 when a series of blasts have been applied to prevent the hanging blocks causing accidents. The operation was not very successful. The photo (b) was taken in July 1983 shows no improvement after eight years.

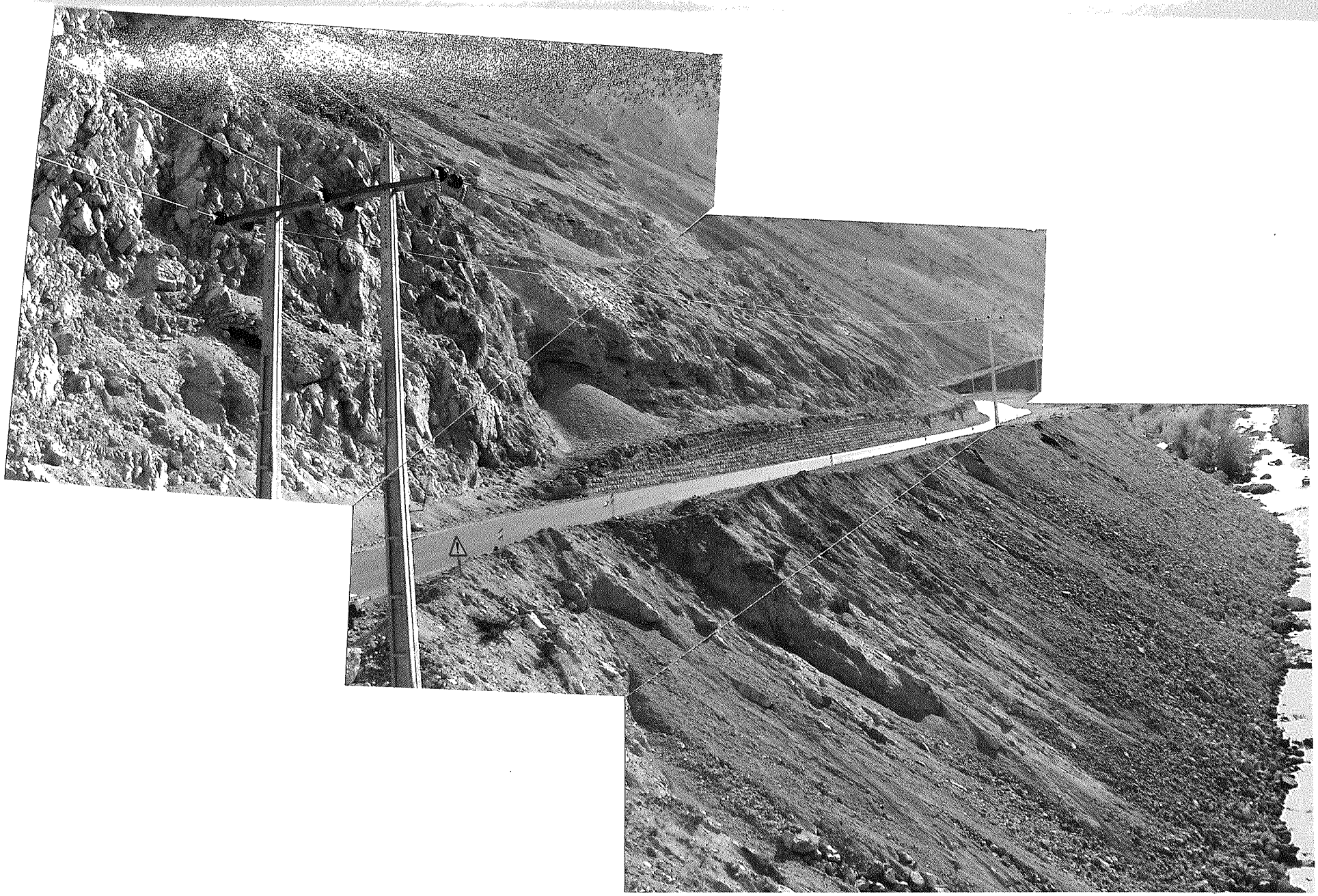

Plate 4.2 Planar failure (km 64). The debris on the right hand side of the phtograph was cleared from the road after an earthquake which caused planar failure and massive rock movement down hill.

construct a tunnel to avoid further hazards. Fortunately I drew the attention of authorities to the location of the Baidjan thrust and the associated risks and convinced them not to proceed.

4.2.3 Rotational Slides (Slumps)

In cohesive soils failure occurs along a surface approximately to a segment of a sphere. The disturbing moment involves the weight of the the slipping mass round its centre of rotation, which is resisted by the shear strength of the soil along the slip surface. A slip in cohesion soils tend to develop from a tension crack at the top of the slope, which may be occupied by water, infiltrating along the slip circle, building up a significant pore water pressure and reducing the shear strength along the slip surface.

Rotational failures in the study area have occurred at km 13 and 57 - both heavily faulted areas. From km 13 to km 15, between Mobarak-Abad and Ski-pist, the road passes a faulted region (three minor faults) in the vicinity of the Musha-Fasham thrust (Plate 4.3), where Permian rocks outcrop amongst Eocene rocks. These Permian rocks are weathered and disturbed by mining at the top of the slope, which accelerates water infiltration. Consequently an area 2 x 2 kilometres is sliding down gradually and moving the road. Several small rotational slides have developed in this area which all lie within one major slide.

To the south of Ask (km 42-45) a complex region consisting of Upper Cambrian, Permian, Triassic and Jurassic rocks. A thrust with two associated faults trends at right angles to the Haraz Valley. The overlying Eocene rocks (Karadj formation) stand fairly stable on the top of the slopes, but the other layers, Mobarak, Dorud, and

Plate 4.3 Mush Fasham thrust (km 10-17). The thrust trends east-west across the scene. The road is passing north side of the thrust where a rotational earth slide can be seen at the centre of the plate.

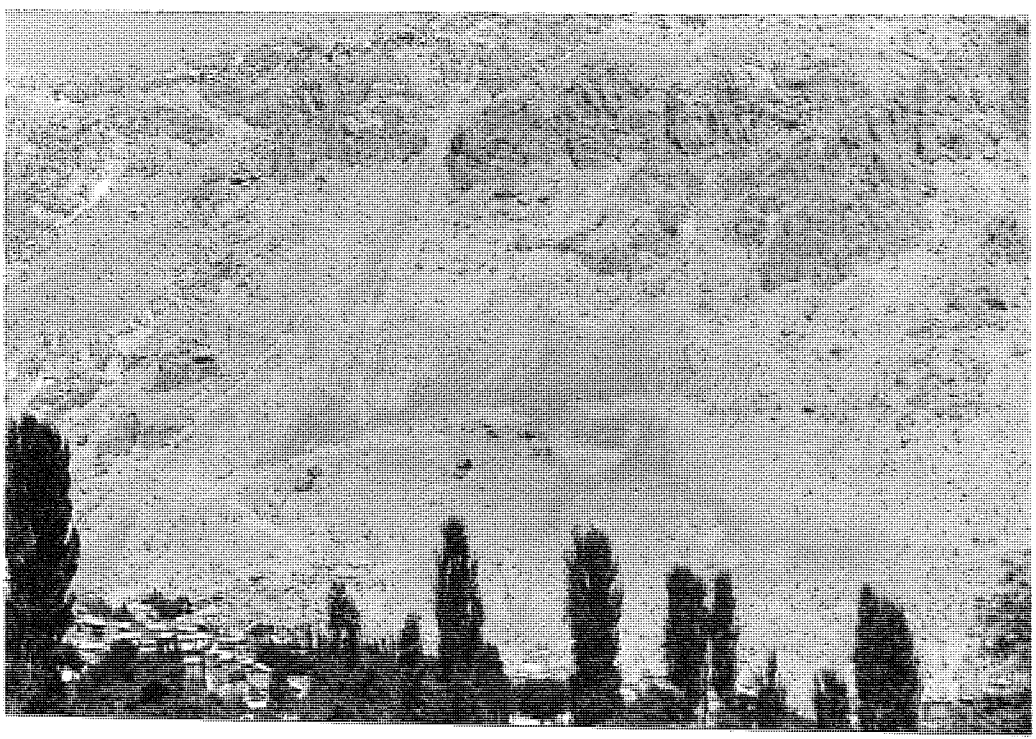

Plate 4.4 Shangoldeh (km 56). A rotational slide at lower centre of the scene measures 330 m across and 700 m downslope with 3o degree vertical angle. the village is located in bottom left corner.

Elikah formations are fractured and weathered as a result of the faulting and tend to slide down, reshaping the valley at a suitable stability angle. These movements are slow at the present time, but the signature of several well developed rotational slides is visible in the area.

Shangoldeh is located on a rotational slide which is associated with two intersecting faults in the area (see tectonic map Plate 3.2). The area is unstable as a result of the Damavand lava flows (mainly trachyandesites) overlaying the lower Jurassic (Shemshak formation). Specifically, the sandstone, shale and coal layers of the Shemshak formation are overlain by coarse highly permeable aggolomerates, measures 200 m across and 700 m downslope with 30 vertical angle (Plate 4.4). These erode as a result of weathering and frequently topple down creating a debris cover over the Jurassics (see Appendix A). Such earlier debris has consolidated in recent geological time and the fine-grained soil at the toe was cultivated, thus Shangoldeh Village was established. Infiltration of rain and snow melt have caused the gradual development of a rotational slide (slump), resulting in a downslope movement of the Village and cultivated areas (orchards). The occupants of the Village have been warned to evacuate the Village, but they have ignored the warning. Tension cracks have appeared in the buildings, and on the ground up to 500 mm wide, and a rupture is visible at the top of the slide. The road descends gradually and a distinct break in the road gradient is visible on either side of the slide. Fortunately sliding is delayed because of the direction of dip of the underlaying Jurassic rocks, which are approximately at right angles to the sliding surface. It is foreseeable that the further development of this slump in the Shemshak formation followed by further infiltration of water may result in a

rapid slide to the river bed.

4.2.4 Rock Fragment Flow

Apart from exposed rock slopes, the study area is dominated by rock fragment slopes (colluvial) which can be considered coarse grained soils. In the Haraz Valley these constitute large, extensive colluvial fans. The fans are currently developing vary from a few metres to a bigger size approximately 300 m across by 500 m downslope with rapid angles and their thickness varies from one to several metres. Where the fans are associated with cuts, and their toes are disturbed, rock fragment flows develop and may activate the whole fan to flow. An example of rock fragment flow is located at km 63 (Plate 4.5) where the road traverses the toe of such a fan. These fans cause several instability problems including rockfall, where rotating rocks roll on the smooth surface slope of the fans together with sliding of the fans 'en mass', which carry or push the road away. The fans along the Haraz valley are free of fine soil, consequently they are also free of vegetation, and most of the year they are bare and susceptible to rapid water infiltration.

4.2.5 Debris Flow

Due to the faulted and fractured nature of the rocks in the Haraz Valley the presence of debris is observed everywhere. The thickness of the debris varies from a few centimetres to several metres. Every depression or change in slope surfaces are filled by debris, making it smooth. This is especially common between km 70 and km 80, the area shown on Plate (4.6).

Plate 4.5 Rock fragment flow (km 63). The flow measures approximately 300 m across and 300 m downslope with rapid angle (45 degree) in the toe.

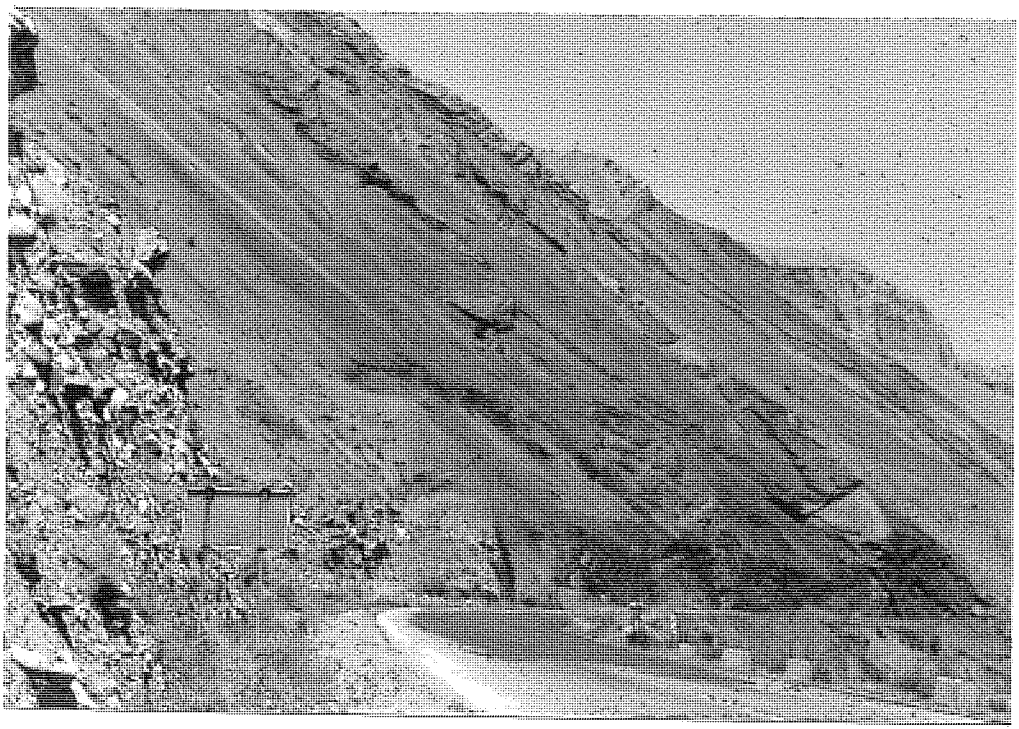

Plate 4.6 Debris flow (km 70-80). As a result of erosion of pyroclastics on the top the debris flow downslope filling any rough surface constructing a smooth and steep slope.

4.2.6 Sand Flow

Extensive slopes composed of sand grade material are rare in the area. However, a sand flow at km 87 has developed in the Cretaceous volcanics associated with faulting. Plate 4.7 shows the area where a retaining wall has been constructed to prevent the sand reaching the road. The flow measures approximately 250 m across by 200 m downslope with a vertical angle of 35°.

4.2.7 Mud Flow

Mud flows occur when fine-grained soils, with or without coarser debris, becomes mobilised by an excess of water. Most of them behave like wet concrete in a chute with differences due to variations in water content. The flow of some wet silts and fine sand may be triggered by earthquake shocks. Wet flows are generally characterised by elongated, tongue-shaped mass of fine-grained material usually with darker photographic tones than their surroundings (Burton, 1970).

To the north of the Baidjan thrust on the west side of the valley a mud flow is in progress in a size of approximately 50 m across by 500 m downslope with 20° vertical angle (Plate 4.8). This mud flow has developed on the Shemshak formation and appears very dark because of coal seams and grey shales in the formation. The mud flow is on the opposite side of the valley and thus no effect on the road.

Another mud flow is located at km 39, which becomes active due to melt water and rain. However, it is not on a large enough scale to constitute a major hazard to the road approximately 100 m by 200 m and the construction of an arcuate retaining wall and periodic clearance give adequate protection to the road.

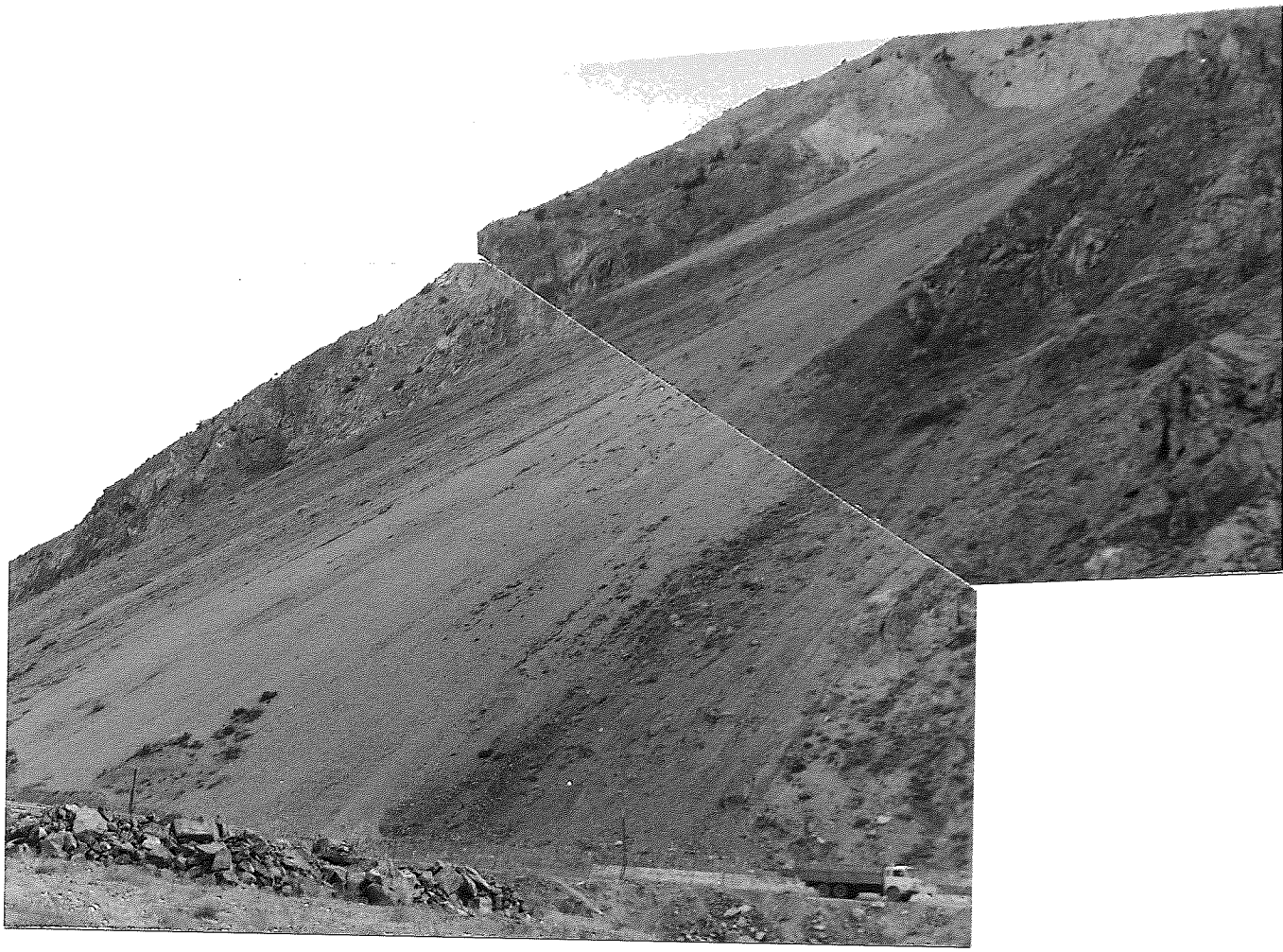

Plate 4.7 Sand flow (km 87). Located in Cretaceous volcanics.

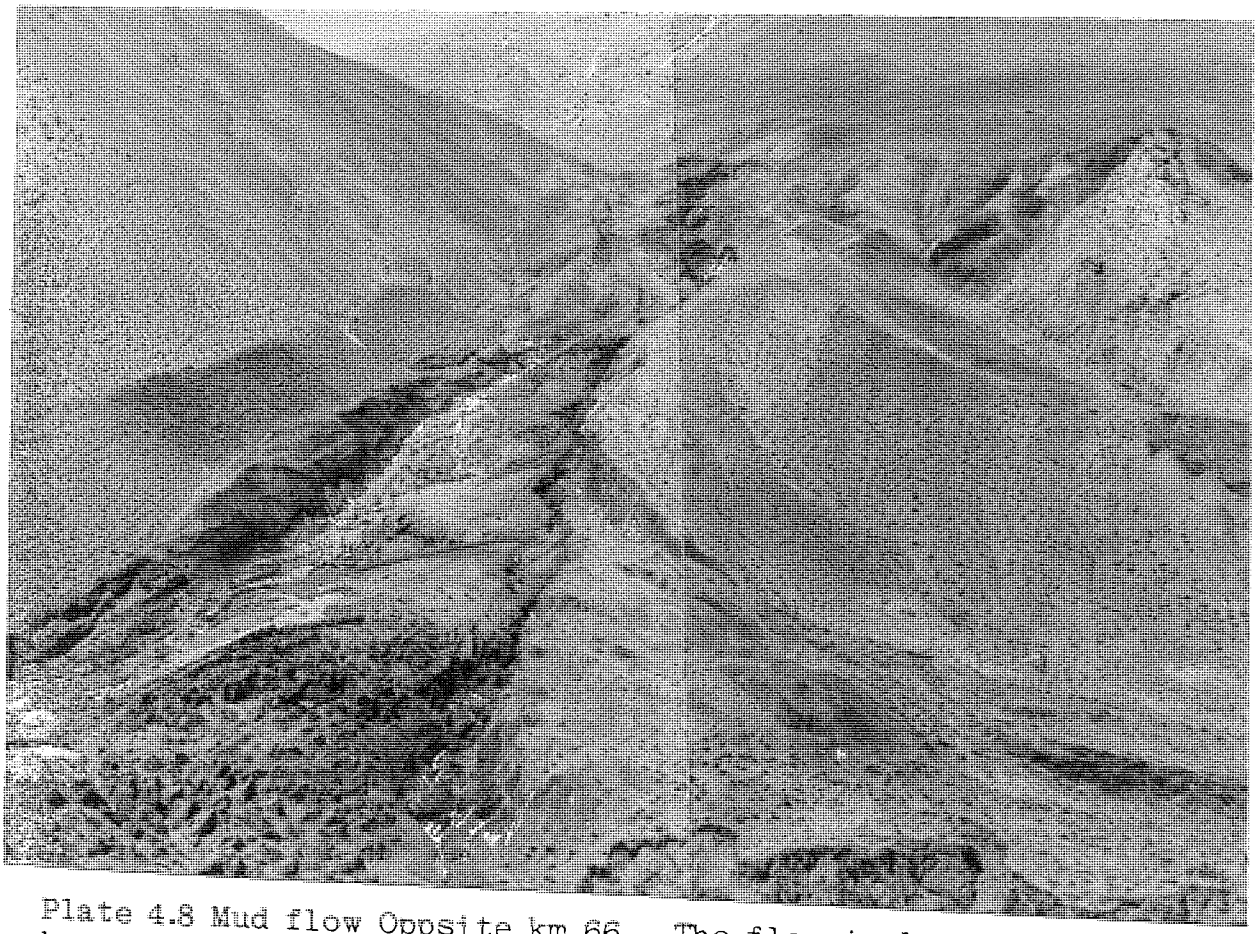

Plate 4.8 Mud flow Oppsite km 66. The flow is located in left bank and the road is passing from right bank.

CHAPTER 5

REMOTE SENSING

5.1 BACKGROUND

5.1.1 Historical Aspects

The first reference to the application of photography in making topographic maps was about 1840, when Arago, Director of the Paris Observatory, advocated the use of photography for topographic purposes (Fischer et al, 1975). In 1849, Colonel Aime Laussedat, an officer in the French Corps of Engineers, embarked upon an exhaustive programme to prove the advantage of photography in the preparation of topographic maps. In 1858, Laussedat experimented with a glass plate camera carried aloft by balloon over Paris and finally developed a mathematical method to convert overlapping perspective views to topographic projections on any plane, on which he reported in 1898.

On October 13th, 1860 James Wallace Blake, accompanied by Professor Sam King, ascended to an altitude of 630 metres in King's balloon and successfully photographed part of the city of Boston.

The first recorded photographs were taken from an aeroplane piloted by Wilbur Wright in April, 1909, when he took motion pictures over Centocelli, Italy. The Orel-Zeiss stereoautograph was developed about 1910, but it could not be applied to vertical aerial photographs. A later instrument, the Hugershoff Aerocartograph developed in the early 1920's was used in the United States. The Zeiss Stereoplanigraph was manufactured in 1923 and is still in use throughout the world today.

Extensive and practical use of aerial photography for military purposes dates from the early days of World War I (August 1914). Aerial photographs were taken of German-held territory by Lieutenant Laws, of the Royal Air Force (RAF); he was also involved in aerial photography in World War II.

5.1.2 Development of Photointerpretation Techniques for the Earth Sciences.

The first official recognition of the photograph as a scientific record of geological data led, in 1890, to the formation of a Committee on Photographs within the Geological Society of America. From that committee came the reference to a new activity called "Photogeology". The object of the new movement was to make a photogeologic survey, and to secure for the Society a national collection of photographs illustrating the geology of the country. The next development in about 1920 was the use of aerial photography by petroleum geologists in the USA.

5.1.3 Multispectral Black-and-White Photography

The main concept of this method is the taking and viewing of simultaneously exposed black-and-white photographs, having identical formats, through filters which divide the light, reflected from the terrain, into several wavelength intervals. Additive colour can be considered to be the superimposed projection of positive photographs made from the spectral negative through selected filters to produce "true" or "false" colour representations of the scene.

On May 17th, 1861, James Maxwell gave his famous lecture at the Royal Institution. During the lecture his experimental image was

projected in blue-violet, green and red separately and then finally with the colours superimposed. However, it was another 20 years before this became commercially feasible to produce.

The first multispectral photographs from space were taken by Apollo 9 in 1968. These were obtained in three distinct spectral bands, covering the visible and near infrared part of the electromagnetic spectrum. Four Hasselblad cameras equipped with green, red and infrared filters were boresighted and synchronized. Three of the cameras were loaded with black-and-white film and the fourth with colour infrared film.

5.1.4 Radar Systems

The Radio Detection And Ranging System (RADAR), operating in the microwave region and at longer wavelengths, was known as early as 1889, when Heinrich Hertz showed that solid objects reflected radio waves. However, serious development of systems began only about 60 years ago in both the UK and USA, primarily for detection of military ships and aircraft. Side Looking Airborne Radar (SLAR) which operates in high altitude aircraft and at relatively long ranges, had been developed by 1960. In 1964 it was used by American geologists to generate radar imagery for earth resource survey purposes. Flight data were collected over specified test sites as well as at numerous locations in North and Central America and these data were turned over to investigators at a variety of institutions, including the US Geological Survey. The results showed that the data, despite their relatively coarse resolution, were a useful tool for Earth Resources studies.

5.1.5 Space Era

In October 1957, a new concept of human observation began. The Russian's first artificial satellite, named Sputnik 1, was launched and surprised the scientific world. Sputnik was football-sized and carried only a radio transmitter sending signals. It completed an orbit of the Earth every 96 minutes at a height varying between 215 and 930 km. It had been launched by a three-stage vehicle mounted one on top of the other. It came to the end of its life during the first week of 1958.

In February 1958, American Von Braun's team launched the Explorer 1,a successful pioneer satellite 6 inches in diameter. As well as a radio transmitter it was equipped with a "Geiger Counter", used to detect electrically charged particles, such as cosmic rays. Sputnik and Explorer showed that satellites had come to stay, and during the next four years there were many launchings, both in the USA and USSR.

On 12th April 1961, man entered space for the first time, the pioneer being Major Yuri Gagarin, a USSR air force officer, in the spacecraft Vostok 1. He was aloft only 108 minutes, but his flight was a significant start in this branch of the science. The first American manned space flight took place for only 15 minutes, on 5th May 1961. Alan Shepard hopped up and down reaching a peak altitude of 187 km. It would have been difficult then to believe that less than ten years later Shepard would be able to step from Apollo 14 onto the surface of the Moon.

Due to its proximity the Moon was the first target in the Space Exploration Programme. This began in 1959 when the USSR launched the three "Lunas". The first Lunik ,in January 1959, passed within 750 km of the Moon and sent back some valuable data. The second crash-landed

on the Moon's surface the following September, but Luna 3 really stole the limelight; it sent back pictures of a region previously absolutely unknown - the Moon's far side which is always facing away from the earth (Markhov, 1962).

By interpretation of ground based images, Shoemaker and Hackman prepared Lunar stratigraphical maps in 1962 (Shoemaker and Hackman, 1962). It was thus shown that geological maps could be compiled if imagery of good quality was available.

On 31st July 1964, after the failure of 6 Rangers, the seventh impacted on the Moon's surface after sending more than 4000 pictures back to the earth. The USA followed this programme with Rangers 8 and 9 early in 1965. An important question posed was that of the Lunar surface bearing strengths which was answered by the controlled landing the Russian Luna 9 in 1965. The Russian success was followed soon afterwards by America's first Surveyor, which came down about 800 km from Luna 9 and transmitted more than 11000 pictures.

In July 1969 Armstrong and Aldrin landed the "Eagle" on the Moon and at 2.55 GMT on 21st July 1969, Neil Armstrong became the first man to step onto the Moon.

Besides the Lunar programme, Earth Orbital Observatories were launched, beginning in 1960 with the launch of Tiros 1, the first Meteorological satellite. This was followed by the Mercury mission in 1961 when M4-9 stimulated interest in the use of orbital photography for natural resources evaluation, as well as geological research (Moore, 1982). The manned Gemini mission provided several 70 mm colour photographs of the Earth's surface, and the special unmanned Apollo 6 mission produced a series of overlapping vertical photographs

across North America, the Atlantic and West Africa. In addition several hundred colour photographs were taken from Apollos 7 and 9. The Apollo programme shifted in 1968 from Earth-orbital flights to the Lunar missions.

5.2 EARTH RESOURCES SATELLITES

The greatest advance to date in Earth-orbital photography undoubtedly began in 1967 when NASA initiated a study of the feasibility of a series of Earth Resources Technology Satellites (ERTS). ERTS-1 was launched in July 23rd 1972 and operated until January 6th 1978. ERTS-1 was the first unmanned satellite specifically designed to acquire data about Earth resources on a systematic, repetitive and multispectral basis. Just before the launch of ERTS-2 in January 22nd 1975, the ERTS program was officially renamed as the "Landsat" programme. Hence ERTS-1 was renamed Landsat-1 and ERTS-2 became Landsat-2. The third satellite of this series, Landsat-3 was launched on March 5th 1978, the fourth on July 16th 1982, and the fifth on March 2nd 1984.

Landsats 1-3 were placed in nominally circular orbits at an altitude of 919 km (variations of 880-940 km have been noted) with an orbital inclination of 82^{o} and circling the earth once every 103 minutes: resulting in 14 orbits per day. The successive orbits of Landsat satellites are about 2760 km apart at the equator. On each pass the satellite images a 185 km swath, hence there are large gaps in image coverage between successive orbits on a given day. However, the satellite orbit progresses slightly westward with each day, just overshooting the orbit pattern of the previous day. This results in images that overlap those of the previous day; the overlap at the

equator is about 14 percent and at 80° latitudes the overlap is 85 percent. It takes 18 days for the Landsat orbit pattern to progress westward before it reaches total coverage of the earth. Thus the satellite has the capability of covering the globe, (except parts of the polar regions) once every 18 days, or about 20 times per year. The orbit of the Landsat satellites is sun-synchronous i.e. the satellite keeps pace with the sun's westward progress as the earth rotates. Therefore, the satellite crosses the equator at the same local sun time (9.42 a.m.) on each pass. The significance of the sun-synchronous orbit is that a specific area can be imaged under similar sun illumination conditions during specific seasons. Figure 5.1 and shows the configurations of the Landsats 1-3.

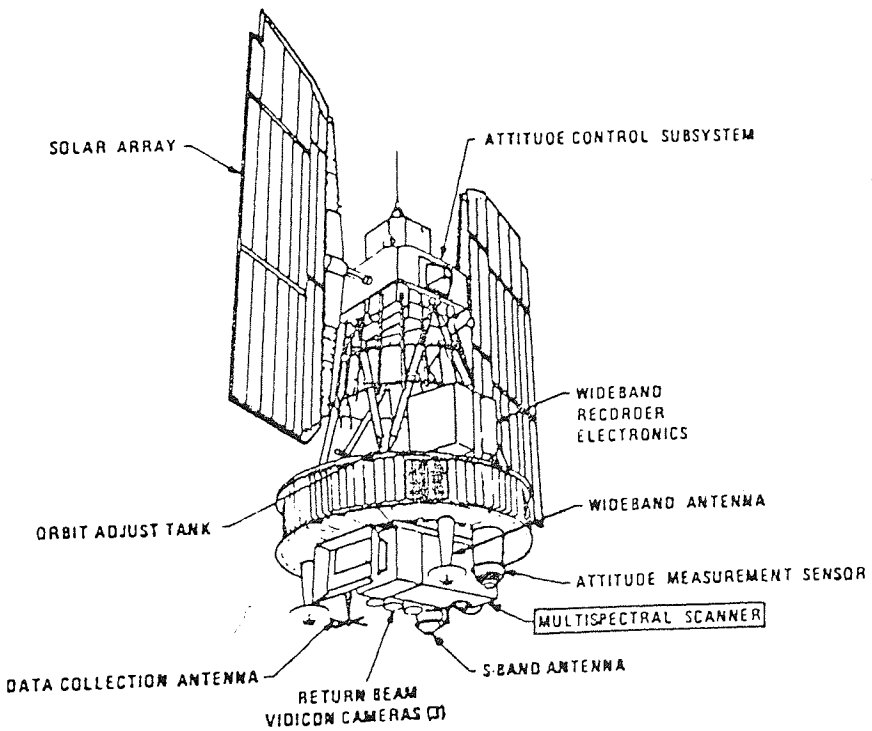

Figure 5.1 Diagram of Landsat 1-3. (after Rothery 1982)

Landsat-1 and 2 had two types of remote sensing systems onboard:

1) Three Channel Return Beam Vidicon System (RBV)

This system consists of three television type cameras which view the same 185 x 185 km ground area simultaneously. The nominal ground resolution of the cameras is 79 m. The spectral range of each camera is similar to that of colour infrared film.

Channel (band)	Wavelength (nm)	Colour
1	475 - 575	Green
2	580 - 680	Red
3	690 - 830	Reflected infrared

RBV system images were stored on a photosensitive surface within each camera. This surface is then scanned by an electron beam to produce a video signal which is transmitted to ground receiving stations.

2) Four Channel Multispectral Scanner (MSS)

MSS are the primary data source onboard Landsat-1 and 2. As with the RBV the MSS images a 185 km swath but in four wavebands rather than 3.

Channel (band)	Wavelength (nm)	Colour
4	500 - 600	Green
5	600 - 700	Red
6	700 - 800	Reflected infrared
7	800 - 1100	Reflected infrared

The MSS scans each line from west to east during the southward motion of the satellite. Each Landsat MSS scene covers an area of 185 x 185 km with 10 percent endlap between scenes. As with RBV the nominal ground resolution cell of MSS is 79 m (Figure 5.2).

Two major changes were introduced in the payload of Landsat-3. A thermal (10400 - 12600 nm) channel was added to MSS and the spatial resolution of the RBV system was improved by using three broad-band cameras rather than a multispectral system. The thermal channel of the Landsat-3 MSS failed shortly after launch. The other four channels, identical to those on board Landsat-1 and 2, continue to provide data at a 79 m nominal resolution.

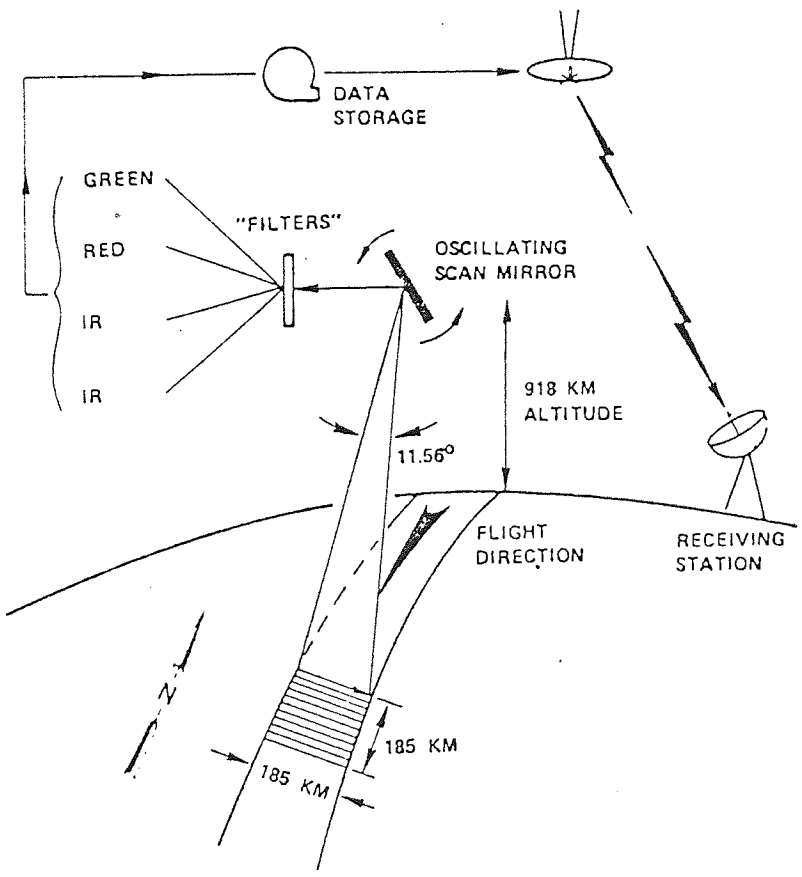

Figure 5.2 Schematic diagram of the Landsat 1-3 operating procedure. (after Rothery 1982).

The RBV onboard Landsat-3 gives a nominal ground resolution cell of 30 m, with a spectral reflectivity range of 505 nm to 750 nm. The two cameras view adjacent 98 km square ground scenes with 13 km

sidelap, resulting in 183 x 98 km scene pair. Therefore four RBV scenes fill each MSS scene.

Landsat-4: the first of a new generation of earth resources satellites, was launched in July 1982. These satellites are the continuation of the Landsat programme. This new generation of satellites has both on improved spatial resolution and a wider spectral range.

Besides a four channel MSS (similar to those onboard Landsat-1, 2 and 3) Landsat-4 carries an advanced multispectral scanner called the Thematic Mapper, (TM). The Thematic Mapper is a seven channel scanner which is designed to maximise vegetation and rock type discrimination. Bands 1 to 5 and band 7 of the Thematic Mapper have a ground resolution cell of approximately 30 m and Band 6 has a spatial resolution of 120 m. This represents a substantial improvement in spatial resolution over the previous Landsat systems. Wavelengths of the different channels in the TM are given in Table 5.1.

Table 5.1 Landsat TM Channels

Channel (band)	Wavelength (nanometre: nm)	Colour
1	450 - 520	Blue
2	520 - 600	Green
3	630 - 690	Red
4	790 - 900	Reflected infrared
5	1550 - 1750	Near infrared
6	10460 - 12500	Thermal infrared
7	2080 - 2350	Near infrared

Landsat-4 was inserted into a different orbit from Landsats 1-3. It circles the earth every 99 minutes at an altitude of about 705 km, resulting in 14.50 orbits per day. The Landsat orbit cover the neighbouring swath occurs seven days later. The overlap of neighbouring swaths at the equator is 7.6 percent. It takes 16 days for the Landsat-4 orbit pattern to give a total coverage of the Earth.

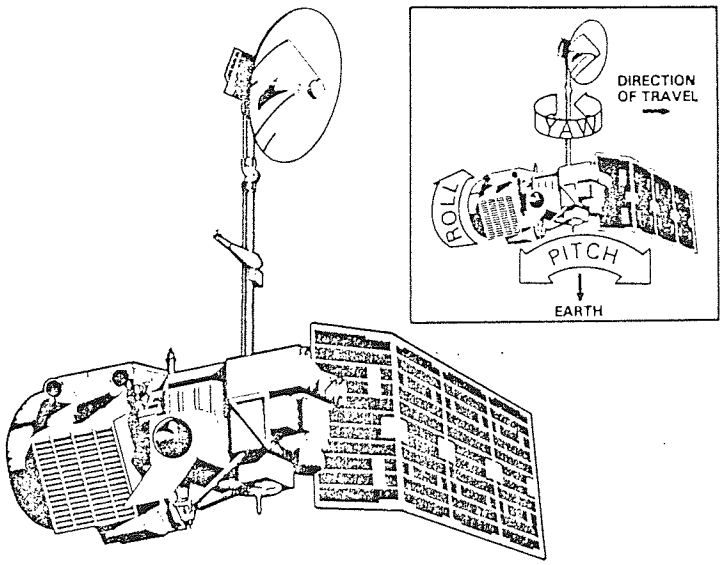

Figure 5.3 Configuration of Landsat 4 and 5. The travel direction and three movement causing instability of the satellite are shown. (after Landsat 4 Data User Book).

Landsat-5 was successfully launched on March 1, 1984, and is currently supplying both MSS and TM with all systems functioning nominally. All characteristics of this satellite are similar to Landsat-4, but its cycle is offset 8 days from that of Landsat-4. Figures 5.3 and 5.4 show the diagram of Landsat 4 and 5 and modular design of them.

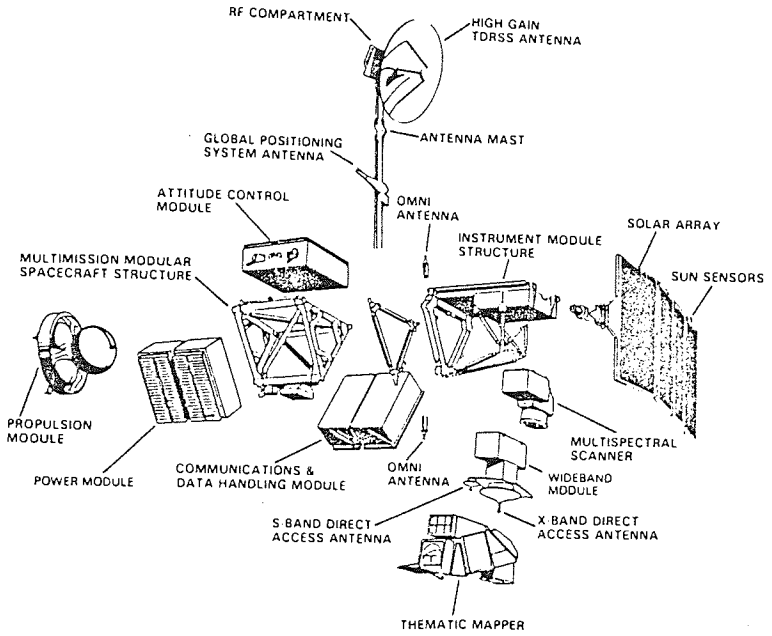

Figure 5.4 Modular design of the Landsat 4 and 5. (after Land sat 4 Data User Book)

5.3 APPLICATION OF SATELLITE IMAGERY

5.3.1 Agriculture

The intense worldwide preoccupation with food supply has focussed much attention upon the contribution of spaceborne remote sensing to improved management of agriculture. The accuracy of the satellite based data is influenced by numerous factors associated with the quality of the integrated spectral response. Integrated response from the crop and background, in addition to the resolution level, imposes severe requirements on training and prediction with regard to data comparability.

Accuracy of crop identification with present Landsat data has reached 90% or higher in studies of areas where there are large,

homogenous, rectilinear fields with little variation in crop type (Price, 1982). In developing countries cropland is frequently interspersed with non-cropland, fields are small and irregularly shaped, therefore crop identification is unreliable. In such complex environments a single Landsat image may not provide enough data to be useful for the purposes of crop discrimination. Misclassifications may also occur when individual pixels contain mixed reflectance values from two adjacent surface types, such as cropland bordering a lake.

Satellite data, especially from Landsat, are capable of being used for certain types of crop identification, and boundary delineation. Field size, crop assemblage and time of year all play some part in influencing crop identification. Identifying crops and measuring acreage is only one step in the process of forecasting crop production. The other step is forecasting yields. To date U.S. studies indicate that for wheat yield forecasting, Landsat MSS data alone are not likely to replace existing methods. For various crops, TM data promise significant improvement in yield estimation. Satellite data may be combined with other data from various sources in an appropriate computer modelling system (Imhoff et al., 1982).

Considerable interest has arisen in the agricultural community concerning the possible application of MSS data (derived from Landsat) to monitor the spread of blights of major crops, such as wheat stem rust. A variety of explanations have been suggested for the marked reduction of infra-red reflectance associated with higher incidence of disease and insect attack. One explanation is the collapse of the spongy mesophyll structure causing changes of the internal refractive indexes in the leaves. However, a number of investigators have found that there may be no change in infra-red reflectance when measuring

the plant close-up using hand-held radiometers. The explanation in these cases appears to be a general reduction in crop extent and a corresponding greater area of exposed soil.

5.3.2 Rangeland Management

Any attempt, using traditional methods, to map land use over large areas has not only been costly but has usually necessitated the piecing together of data from many sources, scales and dates. Airphoto interpretation from one area may, by necessity have been combined with data derived from field work in another area in order to provide complete regional coverage. The data from Landsat represent a significant advance in providing a relatively uniform data set which does not vary greatly in terms of scale and resolution from area to area and is not intentionally biased towards a particular category of land use information.

The present sensor Instantaneous Field of View is adequate for the identification of only broad categories of grassland types. In developing countries where the distribution of these broad categories is not widely known or mapped, Landsat data can make a useful contribution to rangeland management.

Comparison of successive sets of satellite data, rather than interpretation of only one set, gives more precise boundaries and helps to avoid misclassifications. Combining data from microwave sensors on meteorological satellites with TM images can detect low soil moisture and severe removal of pasture, permitting an assessment of the extent of overgrazing (Ulaby et al., 1982).

One interesting case occurred when the European farming area was revealed on the rainy season imagery, particularly on MSS bands 4 and

5. Lighter tones revealed excessive grazing leading to a breakdownin grazing potential in succeeding years. By superimposing a scaled map onto the image it was possible to identify the farms where excessive grazing existed. Clearly, where there is some form of control on the intensity of usage of land, imagery can be used to locate these over-exploited areas.

Operating on a few days frequency of satellite cover, and using also meteorological satellite data, an effective system of rangeland condition can be established. These data can be used to monitor trends, and can be stored in a bank to assist forecasting. A system of rangeland monitoring from space can help in assisting a number of important decisions particularly relevant in developing countries:

i) timing of introduction and removal of livestock in grazing areas

ii) preparation of plans to prevent overgrazing and to open up new areas for grazing

iii) additional investment in range improvements by draining, irrigating, seeding or fertilising.

5.3.3 Forestry

Indications are that Landsat data could contribute to forest management and help to reduce forestry inventory costs. The data have proved useful with respect to:

a) sampling procedures for estimating volume of timber

b) monitoring of commercial forest cutting.

Developing countries are increasingly aware of the need to manage their forest resources - not only to meet their timber and energy

needs, but also to preserve the ecological balance. Mapping of forest vegetation, estimation of timber volume and measurement of the rate of depletion, are essential steps in the planning of control measures to which satellite data can make an important contribution.

In most of the developing world data on forest resources are crude and incomplete. Landsat data may be of significant benefit providing basic information on the location and extent of forest resources and various changes occurring in the woodlands (Ochanda and Hepp, 1982).

Another difficulty inherent in the mapping of diverse vegetation with low resolution scanner data, relates to pixel averaging. Multi-temporal scanned data obtained during subsequent annual seasons may help to correct this spectral distortion. Forest discrimination with Landsat data is poorest during the summer season but yields better results during the spring, autumn, and winter (Smit, 1980). Therefore, it would seem that a more accurate classification of vegetational species will require data acquired over two or more seasons. Landsat TM data promise improvement in forest inventories and associated maps through the ability of the thematic mapper to identify small variations in forested zones.

5.3.4 Groundwater

Groundwater is an important water resource in many countries but more especially in the third world countries where thousands of people die each day because of inadequate water supplies. A large proportion of the world's water resources is made up of groundwater. If water tables of depths up to 5 m could be detected this would go a long way towards reducing human suffering and saving life.

Landsat data can provide information on surface lithology, fracture patterns, vegetation and geomorphic indicators of shallow aquifers. This can serve as strategy for groundwater prospecting if the information is correctly interpreted.

5.3.5 Surface Water

At present, use of satellite imagery lies mainly in making inventories of surface water bodies such as rivers, lakes and marshes. The area covered by surface water is delineated by various techniques using the particular reflectance characteristics of water. For example the decreased reflectivity of high soil moisture at the surface enables the delineation of recently flooded area. Appearance and disappearance of land features around lakes and reservoirs can be used to evaluate water levels and the volume of water stored (Krinsley, 1976, Benny, 1980).

Characteristics of river channels such as width, depth and turbulence are very difficult to distinguish since the resolution of Landsat images is 79 x 79 m. However, Landsat imagery in the near infrared bands can be used with success to identify water bodies and for detecting temporal variation of large rivers and lakes by visual examination of photographic images/hard copy or by digital processing of computer compatible tapes.

5.3.6 Frozen Surfaces

A substantial proportion of the world's freshwater resources is stored temporarily in the form of snow, especially in high mountain regions. Knowledge of the distribution of snow fields and their

volumes in terms of water equivalent is required so that forecasts of stream flow and water storage can be improved.

Under optimum (cloud free) conditions, elevations of snowlines have been estimated to the nearest 60 m from Landsat images. In some regions the extent of snow cover has been estimated to a proven accuracy of 96 percent. In other areas greater detail was obtained from Landsat snowline mapping than is commonly obtained by aircraft surveys. Melt rates and runoff volumes can be assessed even in quite inaccesible regions by sediment plumes extending away from glaciers (Bagchi, 1983).

5.3.7 Water Quality

The detection, from satellite imagery, of pollutants in rivers and estuaries would have significant benefits. Current measurement techniques consist essentially of manual sampling and analysis and these are very expensive to operate.

Changes in quality of water caused by suspended sediments, concentration of pollutants and biological activity of various kinds can be assessed from Landsat images by reflectance variations. It must be realised that the use of LANDSAT images in this application is only a pointer towards further detailed study.

5.3.8 Geology

Satellite acquired remote sensing data are extremely useful for geological mapping and exploration, because they are a very cost effective means of delineating many types of geological features over large areas. The broadest use of satellite imagery in geological mapping lies in the construction of regional structural (tectonic)

maps (Rothery, 1982). Major geological features, contacts between different rock units, and landform types can be effectively mapped from images. Detail of the mapping is comparable to, and sometimes superior to, mapping by conventional aerial photos or ground methods. Providing training set data (ground control) and other supervised methods are applied, computer produced geological maps at scales of up to 1:250,000 can be made from images with suprisingly good accuracy. Repetitive coverage of images acquired at different seasons enhances different geological features. This also enables the geologist to monitor altered or transient geological features - such as changes in the courses of streams and rivers, and the position of sand dunes.

Satellite data provides geologist with a completely new perspective from which to view the earth. For the first time geologists have a tool that enables them to study entire mountain ranges or continents as a whole. A mountain range can be imaged by a single MSS scene or completely encompassed by small number of scenes. Entire continents can be covered by a few hundred MSS scenes or by only a few Meteosat or Tiros scenes. This enables the geologist to inter-relate the features across an entire fold belt without having to deal with thousands of aerial photographs of several different scales, light angles, exposure quality and print quality. The unique ability of satellite imagery, which portrays large portions of the earth's surface, enables the geologist to characterise large, widely separated regions and to compare known mineralised areas with regions as yet unexplored. This is particularly important in inhospitable and inaccesible terrains. The unique characteristics of Landsat images (of particular use in geology) are spatially registered multispectral imagery, and multi-seasoned images of the same area.

When coupled with interpretation of aircraft acquired data and fieldwork, satellite imagery is particularly effective and, while maintaining accuracy, can greatly reduce the time required to map or assess an area. It is a powerful cost saving tool used for locating and eliminating areas which, on the basis of the image, appear to have unfavourable geological settings. Thus limiting detailed geological mapping, sampling and geophysical surveys to the areas of greatest promise.

There is evidence that satellite imagery can lead to direct detection of certain geological features that are strongly correlated with oil and gas production. It is also suggested that dealing on a pixel by pixel basis may make it possible to detect the vegetation anomolies associated with certain types of metal deposits (Carr and Gloss, 1983).

5.3.9 Cartography

Considerable potential exists for utilising Landsat imagery in preparing new, or updating existing maps. Although applications of imagery for cartographic use are restricted to small scales it still has a signficant role in this application. Even with the present understanding of the subject and available technology, planimetric maps of scales 1:500,000 are not uncommon. In some cases certain features on maps of 1:250,000 can be corrected or updated using Landsat imagery.

More than half of the areas of Asia, Africa and South America are not yet mapped geographically at scales larger than 1:1,000,000, and base maps for many other areas are outdated. These uncharted areas can be mapped quickly and cheaply, and existing maps updated by using

Landsat data. The time required to produce maps of scales of 1:500,000 can be reduced to less than one quarter of that required if conventional techniques were employed. For maps of smaller scale (1:1,000,000) production costs are reduced even further (Imhoff et al, 1982).

Satellite (MSS) imagery has several characteristics that enable it to contribute significantly to cartography. It has the potential to become one of the most efficient means of depicting geographical features of the earth's surface. These characteristics include:

i) uniform view over a wide area
ii) near orthogonal (vertical) view
iii) superior definition of certain features
iv) capacity to produce a finished map in very near 'real time' of the data acquisition
v) geometric and radiometric fidelity.

5.3.10 Soil Survey

Studies to determine whether Landsat data could provide useful soil surveys have been encouraging. Variations in soil characteristics can be identified in computer enhanced Landsat imagery. Delineation of these patterns, confirmed by ground observation, can yield soil association maps which provide a good indication of probable soil characteristics (Shih and Schowengerdt, 1983). Using a spectral map of a country, prior to field sampling and measurements, a soil surveyor can determine quickly the location and areal extent of soils with significant differences. Such information can greatly reduce the number of observations and time required in the field. The areas where this can not be achieved are those where dense

tropical vegetation prevents any observation of the soil, although some information can be gained by mapping vegetation types which have an affinity for particular soil types. Different rock types produce soils of specific chemical composition and physical properties, and frequently give rise to particular relief and drainage features, and they may also carry distinctive plant communities.

5.4 CHANGES MEASURED BY SATELLITE BASED DATA

The rate of change perceived on LANDSAT data is an important factor in determining the usefulness of multidate analysis. Although satellite repetitive coverage is every 18 days, the combination of weather conditions, specifically cloud cover, often results in no more than two or three high quality images being obtained per year. The actual number depending mainly on geographical location, and the atmospheric conditions.

5.4.1 Seasonal Change

a) Movement of ice in rivers, lakes and coastal waters, particularly in Arctic and Antarctic regions
   - Useful knowledge for shipping, knowing when and where to send shipping traffic can save time and thus money. The frequency of poor weather conditions, especially of poor light in winter, has hindered this potential use (Maruyasu et al., 1982).
   - Mapping of common iceberg locations (N.R.S.C. and Macauley Institute, 1983) can aid in determining safe areas for oil platforms.

b) Snow coverage - approximations of water held (flood determination) or change in water held from each image.

5.4.2 Long Term Changes

a) Changes in river courses - useful in the planning and design of river borne structures.

b) Oceanographic and coastal changes - aid in the planning and design of erosion barrier systems and the mapping of potentially unstable areas. The monitoring of coastal waters and the changing depths in navigational channels.

c) Landslides - aid in the post-event analysis.

d) Glacial advances and retreats - long term analysis (cartographic).

5.4.3 Induced Changes

a) After the construction of new reservoirs satellites can be used to monitor the extent and condition of water during filling of the reservoir.

b) Environmental changes e.g. major hydrological disruption occurred downstream from the Latian dam on Djadjrud river basin to the southwest of study area. The hydrological disruption affected the vegetation cover and was thus exposed on the satellite image. Another use is the monitoring of surface mining operations and land deterioration in arid areas.

c) Changes in water sedimentation qualities due to, for example, the construction of a harbour.

d) Land use changes

   1) Intensity of land use in urban areas - urban growth patterns can be determined

   2) Vegetative vigour.

e) Agricultural change. Change in agricultural intensity

   1) Forestry crops

2) Dry land farming, irrigated cropping

3) Range utilisation

4) Crop rotation - considered for potential contributions to predicting soil erosion qualities.

5.4.4 Disasters

Frequent occurrence of various types of disasters leave tens of thousands of people homeless and cause damage to property and agricultural land. This has considerable impact on the social and economic standards of the affected area. This is particularly true in the case of third world countries where the occurrence of such events is more frequent than elsewhere. If a system of warning or assessment of these disasters can be developed then necessary precautionary measures can be taken towards eliminating, or at least minimising, the extent of the damage associated with the disaster. Even in the western hemisphere there is a substantial demand for developing and utilising such techniques.

Experiments have shown that there are varying degrees of feasibility for utilising Landsat data for warning and/or assessment. Use of Landsat data for the assessment of floods, droughts and bush/forest fires has shown a considerable amount of promise. Use of satellite imagery as a means of warning has proved successful in tracking hurricanes. There is also considerable potential for the assessment of crop disasters, hailstorms, earthquakes, volcanic eruptions, landslides, glacial movement and water pollution.

A most promising area of application is in the assessment of floods which are amongst the most widespread, frequent and damaging of disasters that occur in the world. Remotely sensed data (satellite

imagery) can be used in combination with land use maps to identify most flood prone areas, thus permitting an estimation of the economic consequences of flooding. However, the use of Landsat images to capture short lived events such as floods or forest/bush fires is a hit or miss proposition. If a satellite passes over such an area on a clear day then excellent images of the event can be obtained. On the other hand such an event can be missed if no images are taken or the earth's surface is obscured by extensive cloud cover, as is often true during flooding. In such cases, lingering effects can be used to assess the impact of the disaster. For example the soil in a flood plain remains wet for several days after flood waters have receded thus making it possible to record the data even after the event. In the case of bush/forest fires the affected area will have dark image tones for a considerable time after the fire has ceased.

Methods of assessing each disaster type vary, but all require a sound understanding of reflectance properties of specific features and related subjects. In some cases assessments can be made inferentially. For example, in the case of assessing droughts, comparative analysis of Landsat images (taken at different times) will indicate the changes that point to impending drought. This is inferred from such changes as decreases in surface water, decrease in vigour of vegetation and in some areas, desertification through the movements of sand dunes. In other disaster categories Landsat imagery can be particularly useful, especially in conjunction with data from ground based data collection platforms. The use of SPOT imagery with its higher resolution and more frequent observation of the site will be invaluable for observing disasters.

CHAPTER 6

DIGITAL IMAGE PROCESSING

6.1 INTRODUCTION

Landsat data provide a very useful source of information for engineering and the natural sciences. For generalised regional studies simple hard copy of Landsat images (e.g. photographic prints in black and white or colour composites) is an adequate source of information. However, for more detailed interpretation of smaller areas and for specialised purposes, digital image processing is needed to extract the detail required. (Beaven 1984, Rothery 1984). A digital image consists of arrays of discrete values called data numbers (DN), at discrete spatial coordinates; each element of these arrays is known as a pixel or picture element. In the case of Landsat MSS data, each pixel is described by seven bits of data (2^7) in bands 4, 5 and 6, and by six bits of data (2^6) in band 7. Digital image processing involves handling data in a multiband digital image. This incudes radiometric and geometric corrections, contrast stretching in a range of eight bits (2^8), arithmetic manipulation, principal components analysis and transformation. The image processing systems which were employed in this research were:

i) an IDP3000 at the U.K. National Remote Sensing Centre (NRSC), RAE, Farnborough;

ii) a DIPIX ARIES-II at the Open University and ITS Company (both at Milton Keynes);

iii) a DIAD of the Nigel Press Company, Edenbridge, Kent;

iv) a HARRIS H500 at Aston University (see Chapter 7), and

v) a GEMS at Silsoe College, Bedfordshire.

6.2 MSS IMAGE PROCESSING PROCEDURES

MSS data released by the Goddard Space Flight Center from 1979 onwards was pre-processed on a Master Data Processor (MDP) a procedure which resulted in a number of distinct improvements over earlier data. There was improvement in the performance of radiometric and geometric corrections including correction for band-to-band offset, line length, earth rotation, and detector-to-detector sampling delay. For still greater clarity the image data were mapped to the Hottine Oblique Mercator projection, (HOM) using a geometrical model based on ground control points (GCP's), or systematic data if GCP's were not available (NASA 1979).

The satellite data used for the research described in this thesis were pre-1979 because the ground receiving station in Iran was not active after 1978, and (due to restrictions in data acquisition from Landsat 1, 2 and 3) only a few single bands were recorded for the region after 1978. No data was received by the ground station in Iran from Landsats 4 and 5, and neither of these satellites carried a recording system on board. (In future after the launching of the Eastern Tracking Data Relay Satellite (TDRS) Landsat 5 will be able to collect data almost worldwide.)*

The digital data used here, being pre-1979, were only partly pre-processed for radiometric calibration and scan line length adjustment. Images from 4 dates were used; 4th September 1972, 7th April 1975, 13th July 1977 and 28th April 1978. Several processing techniques were carried out to correct and enhance these data and finally further

*TDRS consists of two geostationary satellites which are to be launched at two sides of the earth. Both can be seen from the Goddard station and at any time one of them can see Landsat, and relay data to the ground receiving station.

manipulation was applied to find correlations between Landsat data and ground truth.

6.2.1 Radiometric Correction of MSS Data

6.2.1.1 Line Replacement

This task consists of replacements of dropped scan lines by interpolation. Each line, or part of a line which was missed was replaced by the average of the preceeding and following lines. The resulting image was cosmetically improved, removing the visual distraction of bad lines.

6.2.1.2 Destriping

There are six detectors assigned to each of the four bands (giving a total of 24), which receive light during each MSS mirror scan. Although an extensive effort was made before launch to match these detectors to a uniform gain and offset response, their behaviour in operation is invariably non-uniform. Thus one or more lines in each array of six may have higher or lower average radiance values over the entire line length, giving rise to an often noticeable striping (lighter or darker than neighbours) in individual images (NASA 1982).

Almost every digital image processing system has software to remove striping; on the DIPIX the task "DS" was used for this purpose. The process works by equalising the shapes of the histograms from each of the six sensors in each individual band. An option was selected to increase the dynamic range of the data to fill unoccupied levels of histograms by interpolation in order to improve the fit of the histogram equalisation. This procedure is a necessary precursor to

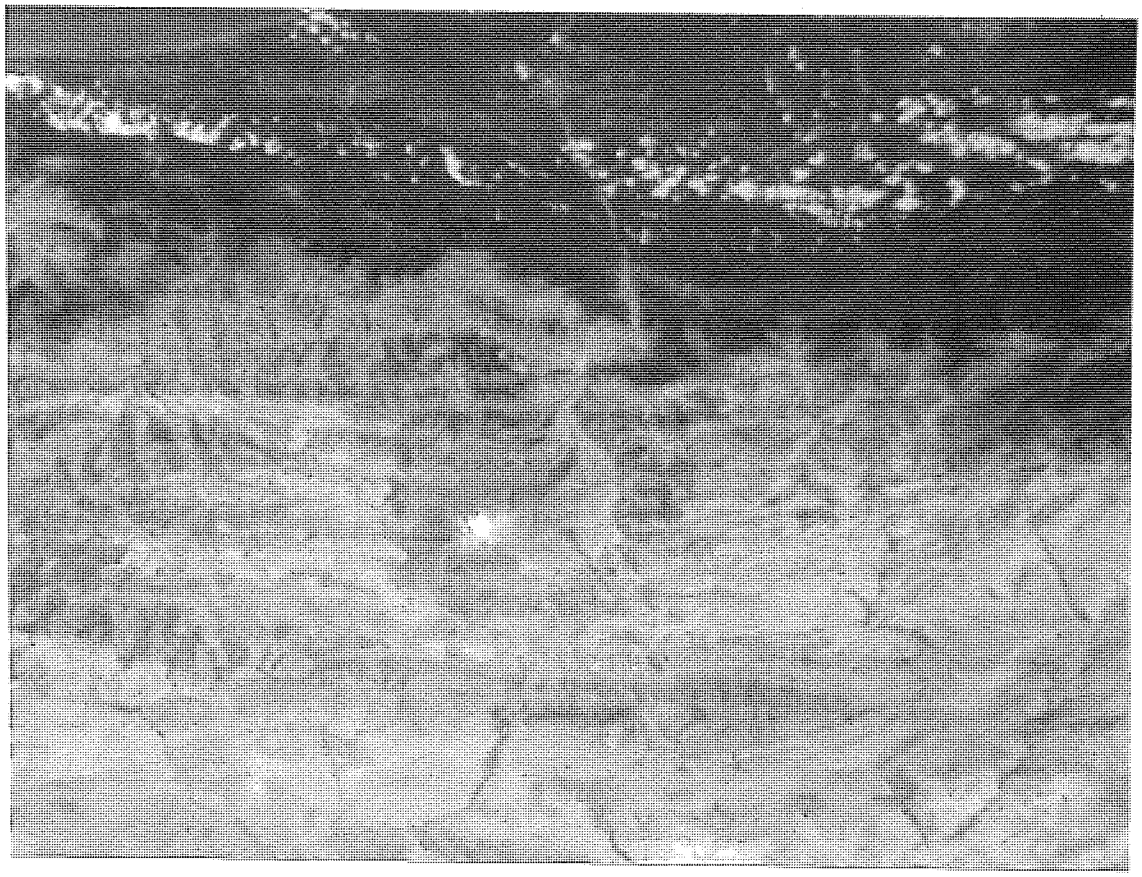

(a)

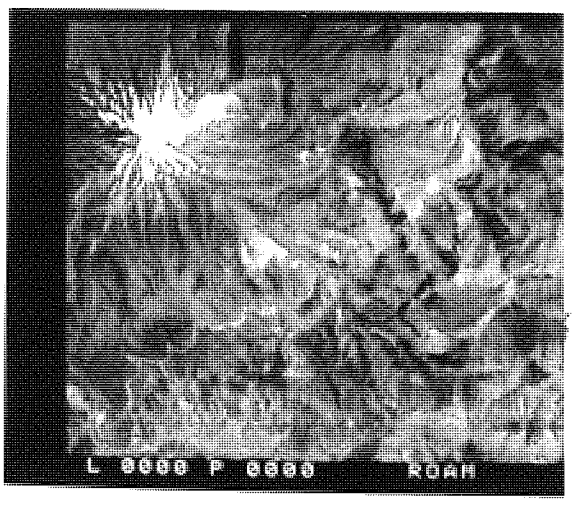

(b)

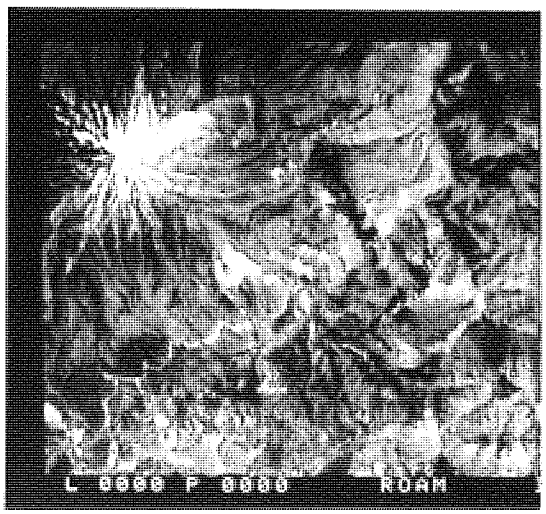

(c)

Plate 6.1 Destriping the raw data. a) Band 4 of July image before applying any correction showing poor quality and striping. b) The same scene after geometric correction and resampling. Two horizontal lines on the top and bottom of the plate appeared after registration to ground control points because of over stretching the rubber sheet. c) The two lines were replaced and more stretch was applied.

classification and principal components transformation, and it also improves the visual quality of False Colour Composites.

Plate 6.1 shows a subscene in the study area before and after destriping and geometric correction. As can be seen Plate 6.1a which is combined from raw data is uniformly striped at every 12 lines. By applying the "DS" software the whole subscene was equalised and the resultant image is more acceptable for visual interpretation.

6.2.1.3 Haze Removal

The atmospheric affects of attenuation and scattering, which are particularly noticeable at shorter wavelengths (bands 4 and 5), cause an artificial brightening of the histograms. This tends to make a false colour composite appear too blue. This systematic error in the image can be largely removed by setting dark shadow value to zero (task "LT" or "SC" on the DIPIX). Until haze has been removed, the application of statistics is misleading. Removing haze by this method can lose some data as a result of cutting the tail of the histogram. However, it is helpful for visual intepretation (Plate 6.2).

6.2.2 Geometric Correction

In the absence of a reliable base map, the image was geometrically corrected on the DIPIX using a hard copy of band 5 produced at a scale of 1:1,000,000 by NASA data processing facility (NDPF) at the Goddard Space Flight Centre. Forty five ground control points were recognised and were transferred to the image. On the basis of a fit with a trial 2nd order polynomial transform, 12 were rejected and the remaining 33 (with better than 100 m accuracy in both east-west and north-south directions) were used to define the 2nd

order transform which was actually used. Resampling to 50 m x 50 m square pixels was then performed using cubic convolution.

An example of this method is given on plate 6.3, showing a single subscene. Plate 6.3a shows a row image whereas Plate 6.3b demonstrates the same area after applying radiometric and geometric corrections.

6.2.2.1 Registration of Multitemporal MSS Images

After geometric correction of one scene (4th September 1972), images of the same scene from the three other dates were registered using tie points to the corrected image. Due to the extensive relief of the area and seasonal sun azimuth and altitude variations, the shadows were mismatched in all four images. By registering all four images together, there was effectively one image with 16 different bands ready for further processing. Considering the huge amount of data and the cost of computer time it was decided to select a subscene containing 1100 lines by 640 pixels which covered the mountainous areas of the Haraz Road (Plate 6.4). All further processing was applied only to this subscene rather than on the whole scene.

An example of deformation of imagery to match with ground control points is shown in Plate 6.5. The neighbouring image (28th April 1978) can be seen before geometric correction (Plate 6.5a) and after registeration with the control points.

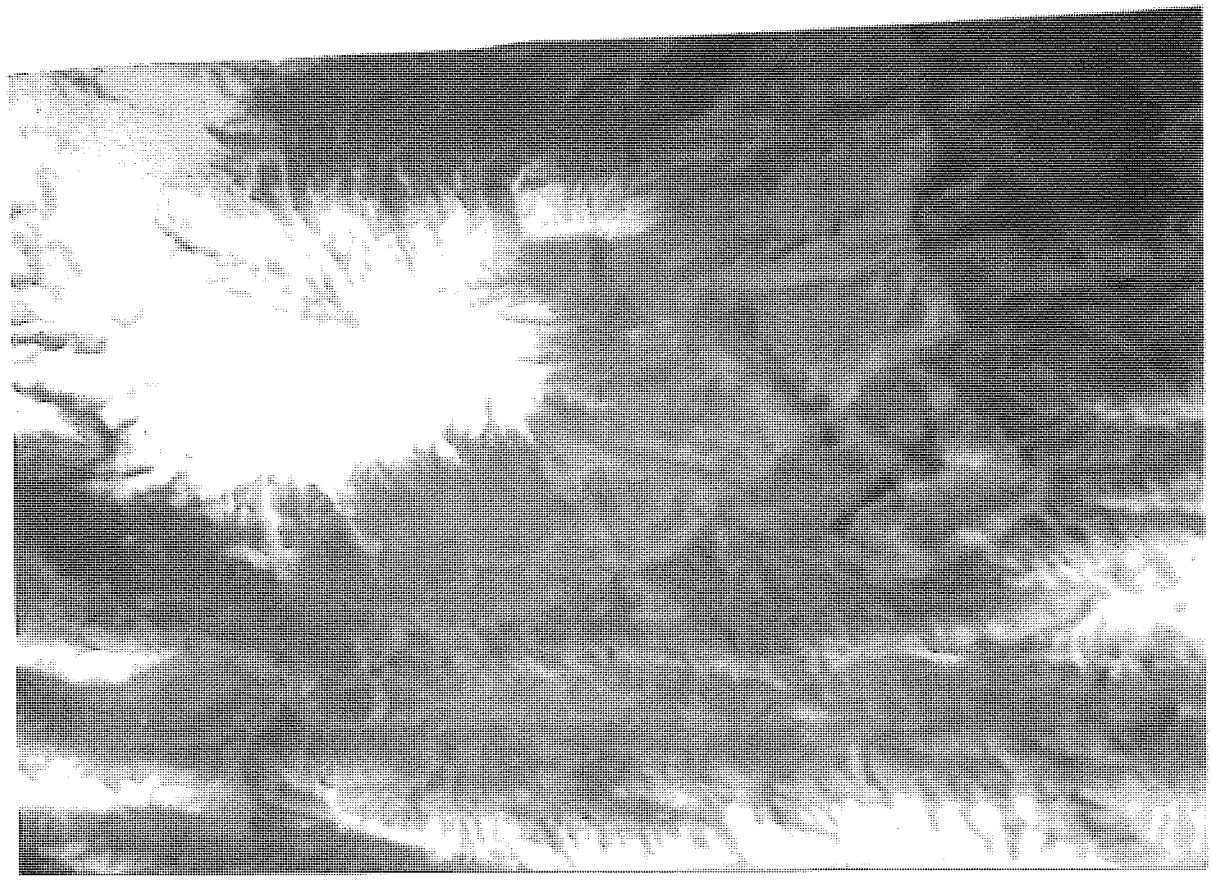

(a)

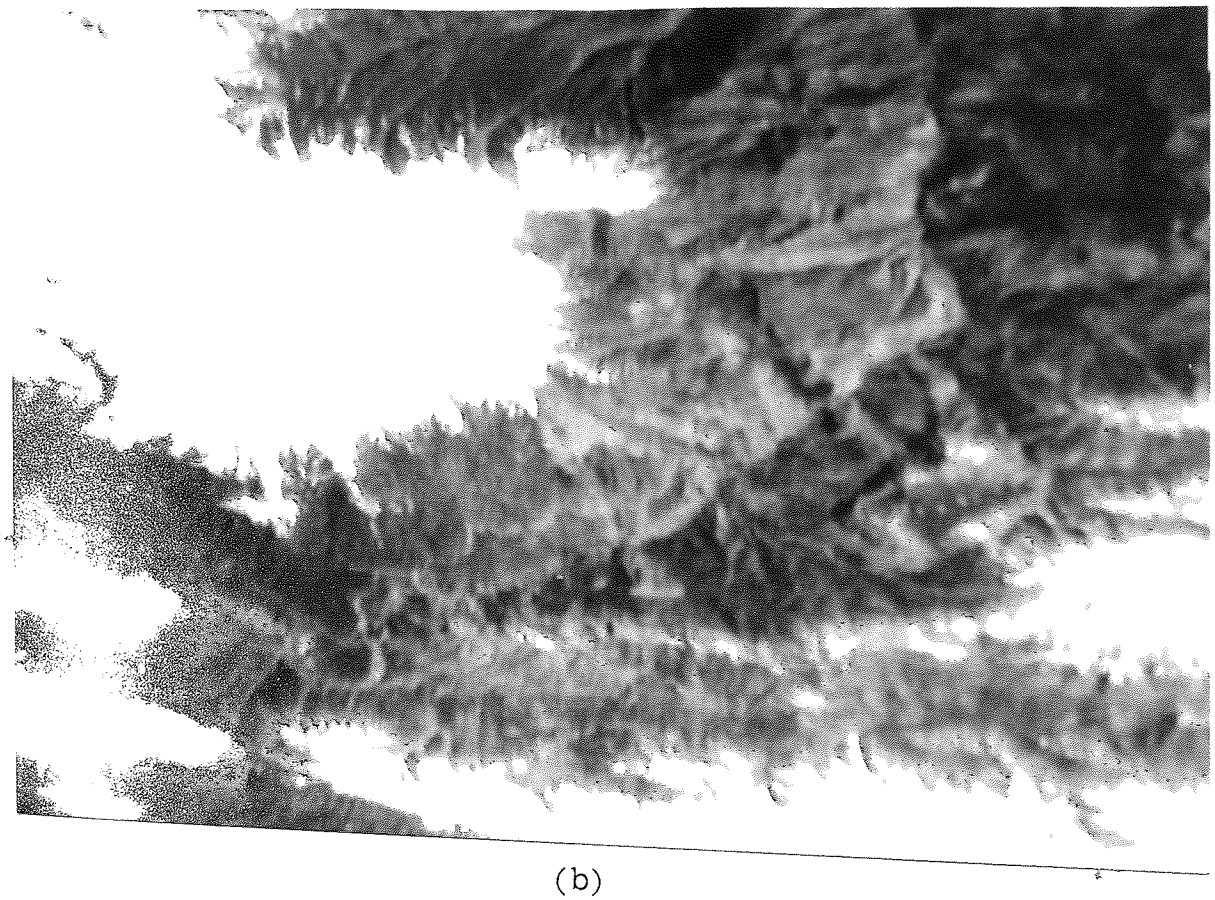

(b)

Plate 6.2 Demonstration of haze removal. a) This plate shows a subscene of 28th April image before removing haze with histogram stretched 0-255. b) The same subcene when histogram was correctly stretched by cutting off its tail and upper part which contains noise, then assigning 10 to zero and 100 to 255.

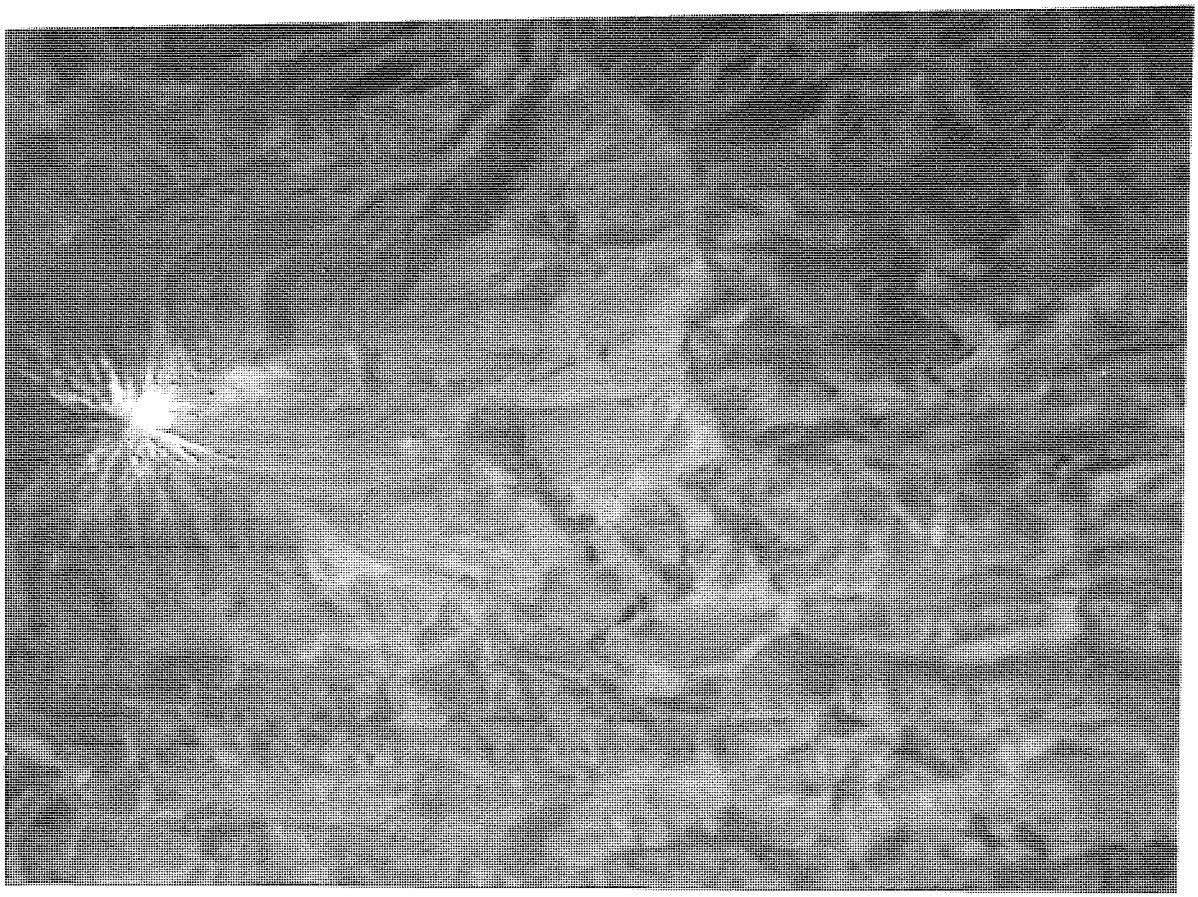

(a)

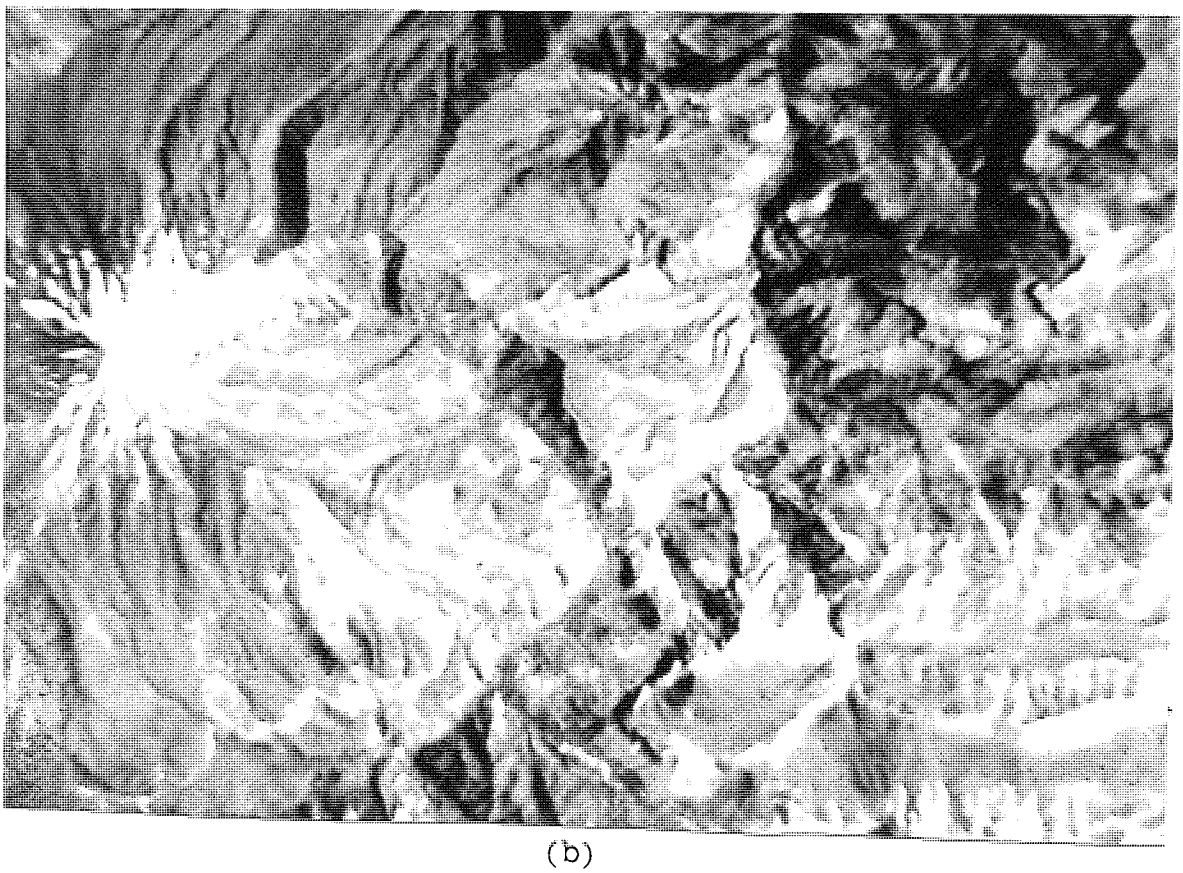

(b)

Plate 6.3 Geometric and radiometric correction. a) This single band of July image is linearly stretched (0-81). b) The same area after applying radiometric and geometric correction. As can be seen all the edges are enhanced and distortion of features are removed, consequently the image is more acceptable for visual interperetation.

Plate 6.4 The study area (sub image). The picture shows some of the most hostile terrain along the Haraz Road.

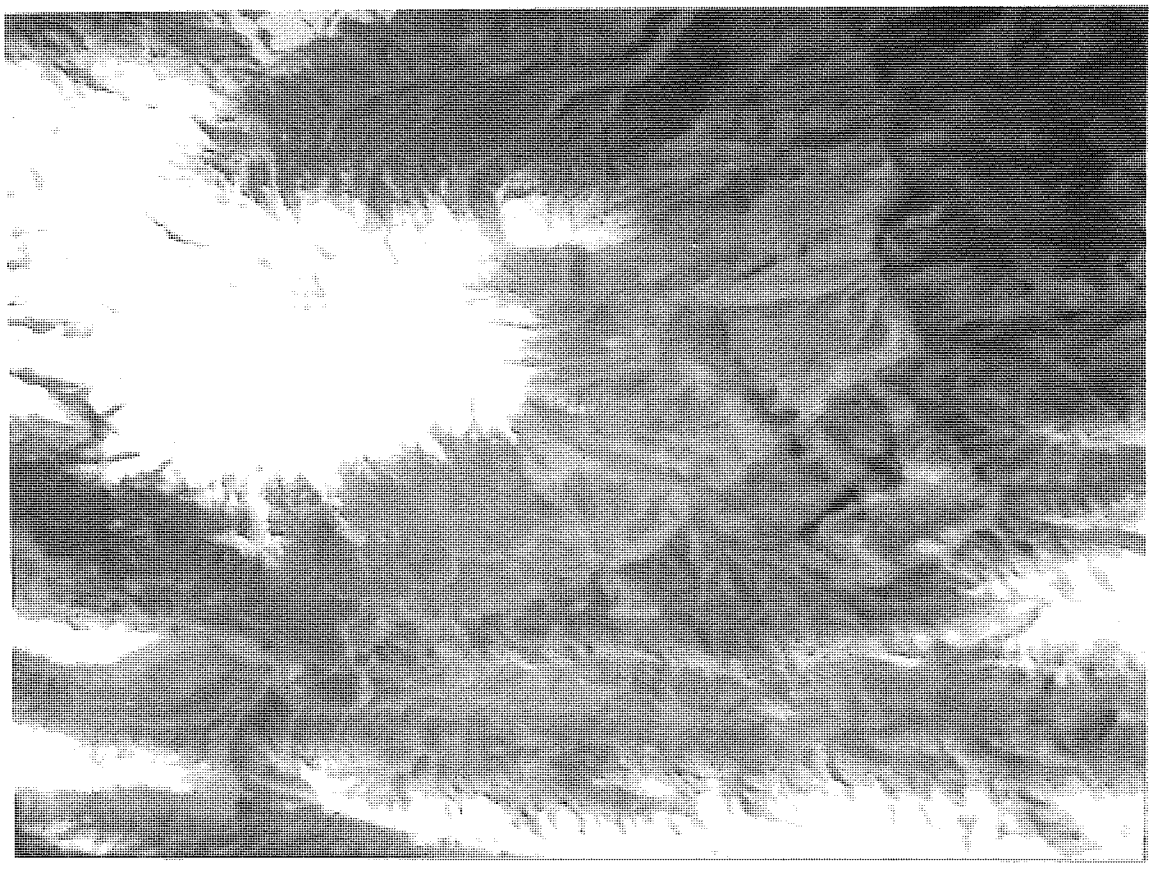

(a)

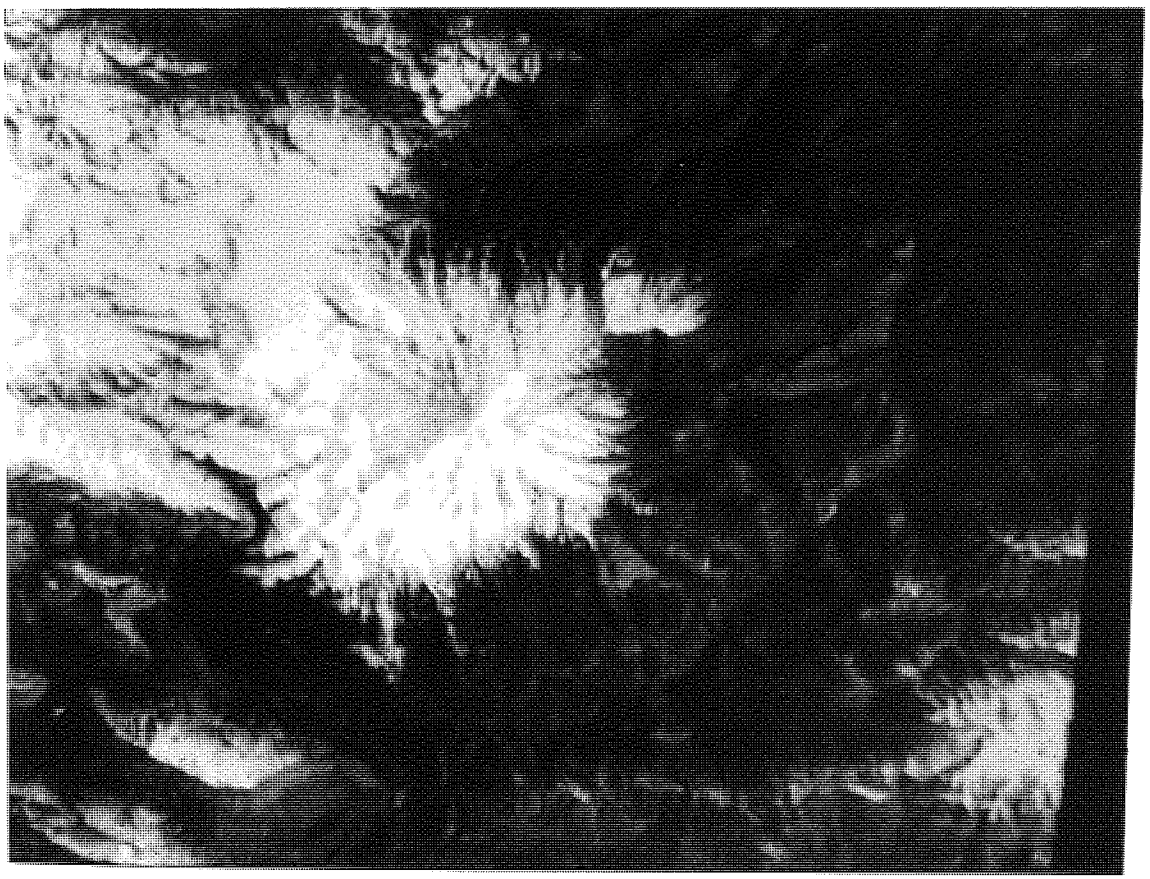

(b)

Plate 6.5 Geometric transformation. a) Band 4 of 28th April image radiometrically corrected. b) Colour composite of the same image constructed with band 4 in blue, band 5 in green and band 7 in red after geometric correction. The right hand edge of the subscene which corresponds to the eastern edge of the 28th April image is skewed south west after geometric correction.

6.2.3 Enhancement of the MSS Data

Enhancement is the modification of an image to facilitate visual extraction of information. Spatial filtering (e.g. edge enhancement) and multispectral manipulation (e.g. contrast stretching and principal components transformation) are two major aspects of image enhancement, the aim of which is to increase the aesthetic appeal of an image and the amount of information which can be perceived. Several enhancement techniques are described below.

6.2.3.1 Edge Enhancement

Edge enhancement consists of emphasising the high spatial frequency information in an image, and supressing the low frequency information. This enhances the subtle variations of brightness defining the edges and textures of regions of terrain. Plate 6.6 shows the image improvement after edge enhancement was applied to a geometrically corrected image.

6.2.3.2 Contrast Stretching

The main aim of contrast stretching is to produce an image using the full dynamic range of the display device. Without contrast stretching the displayed image usually appears very dark and unappealing. When this task is applied interactively on the computer, the user is the final judge of how well a particular arrangement works. One method is to make the decision by looking at the histograms for each individual band. An input-to-output mapping exercise is performed, so that the grey level (DN) distribution is improved This task, which is particularly appropriate when the

histogram is not unimodal, can be applied to an image linearly or non-linearly. If a scene or subscene contains dominant reflectance types (for example forest and farmlands) the histogram distribution will tend to be Gaussian, but if there is also a large clear water surface it will produce a spike in the histogram at low values. In this situation it may be best to stretch the histogram in non-linear or saturated linear fashion rather than linear (Figure 6.1).

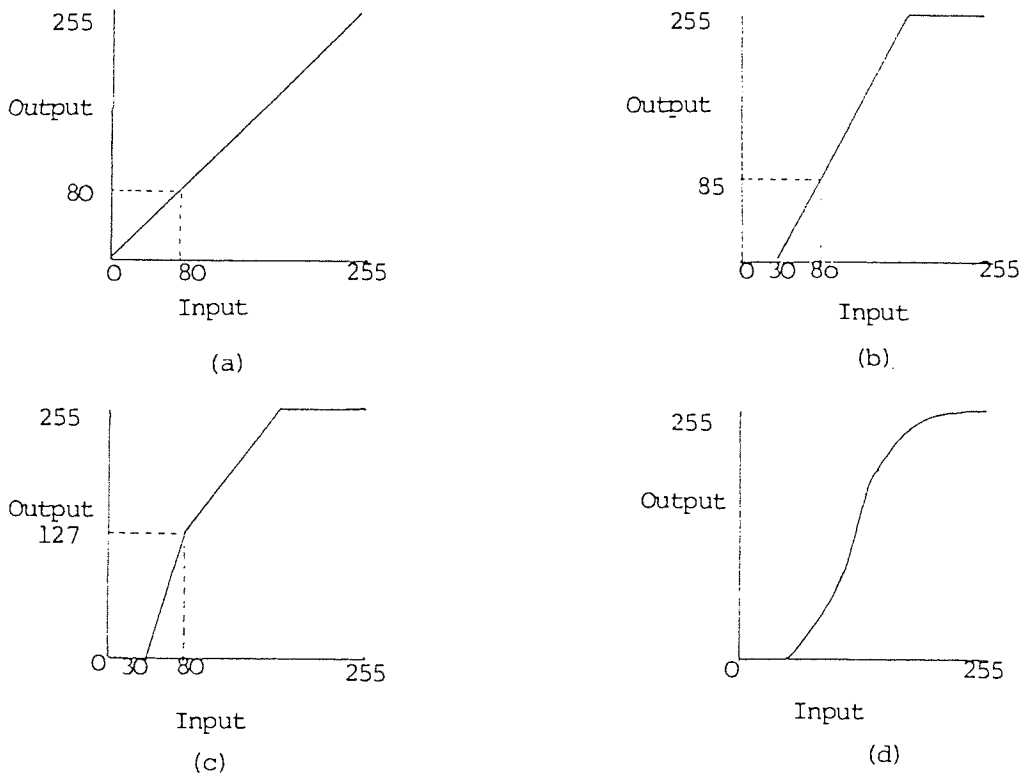

Figure 6.1 Different stretching procedure diagrams. a) Raw data before stretch. b) Simple linear stretch is apllied with a cut off 30 and saturation of 180 consequently input of 80 became 85. c) Two step linear stretching which put input of 80 at 127 (mid range). d) Non-linear stretch to search for the best enhancement of a particular features.

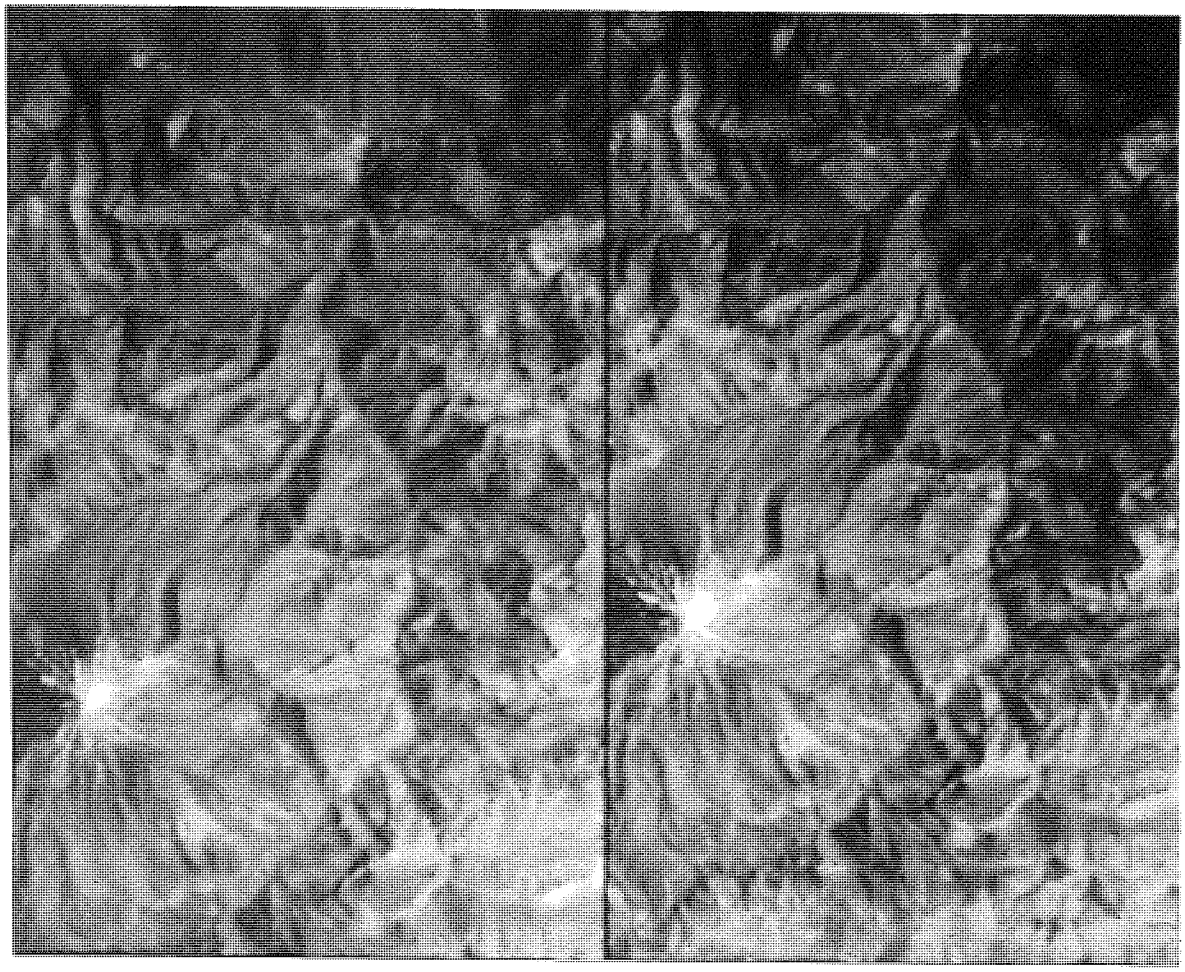

Plate 6.6 Edge enhancement. A comparison of an image before edge enhancement (left) and after edge enhancement (right).

6.2.3.3 Principal Components Transformation

This task locates the direction in multispectral space along which the image data has greatest variance; the first principal component axis. Other components are orthogonal to this axis and contain successively less variance. The first principal component in these images contained about 85 percent of the variance. The second principal component contained 10 percent and the two others contained the remaining few percent, mainly noise. Principal components 1, 2 and 3 of all sub-images were extracted and proved to be of great value, particularly the first and second. The first principal component was good for discrimination of topographic features, whereas the second was good for discrimination of surface reflectances. The third and others were dominated by noise (Plates 6.7 and 6.8).

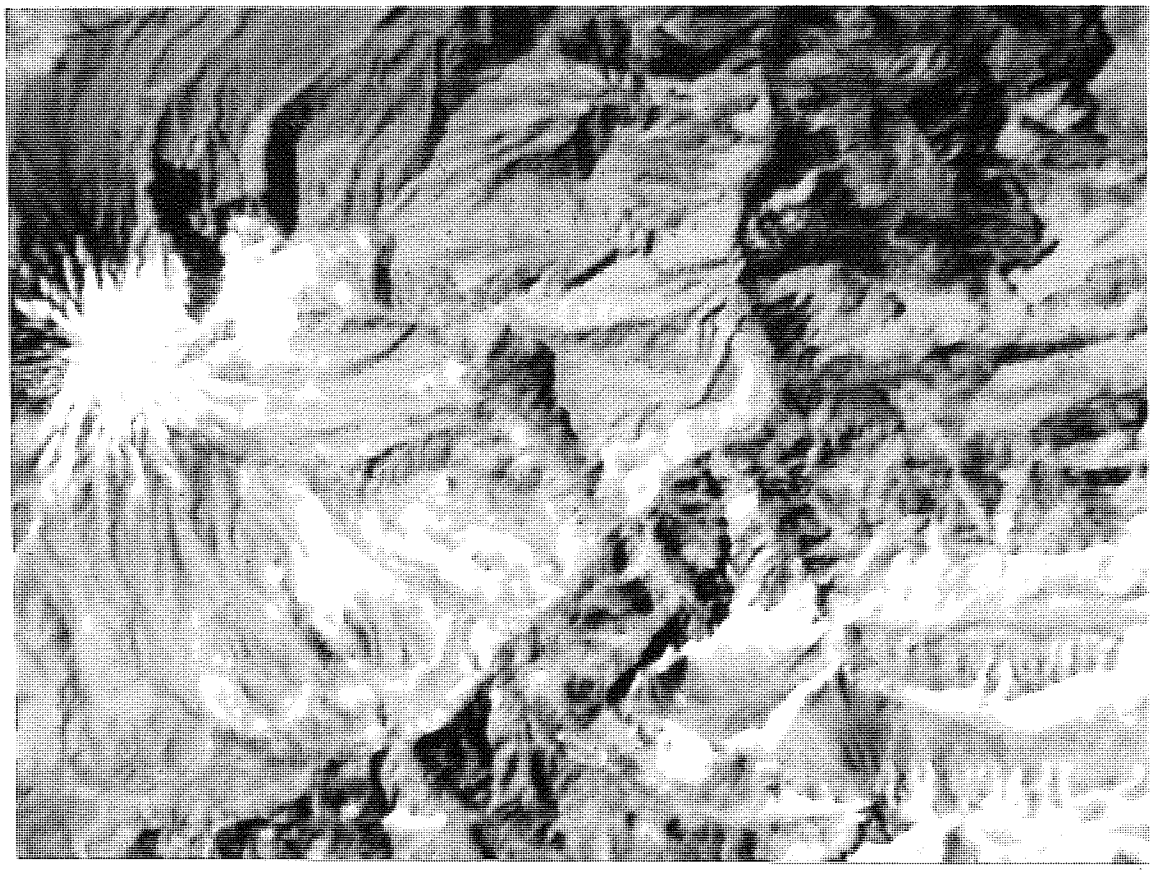

(a)

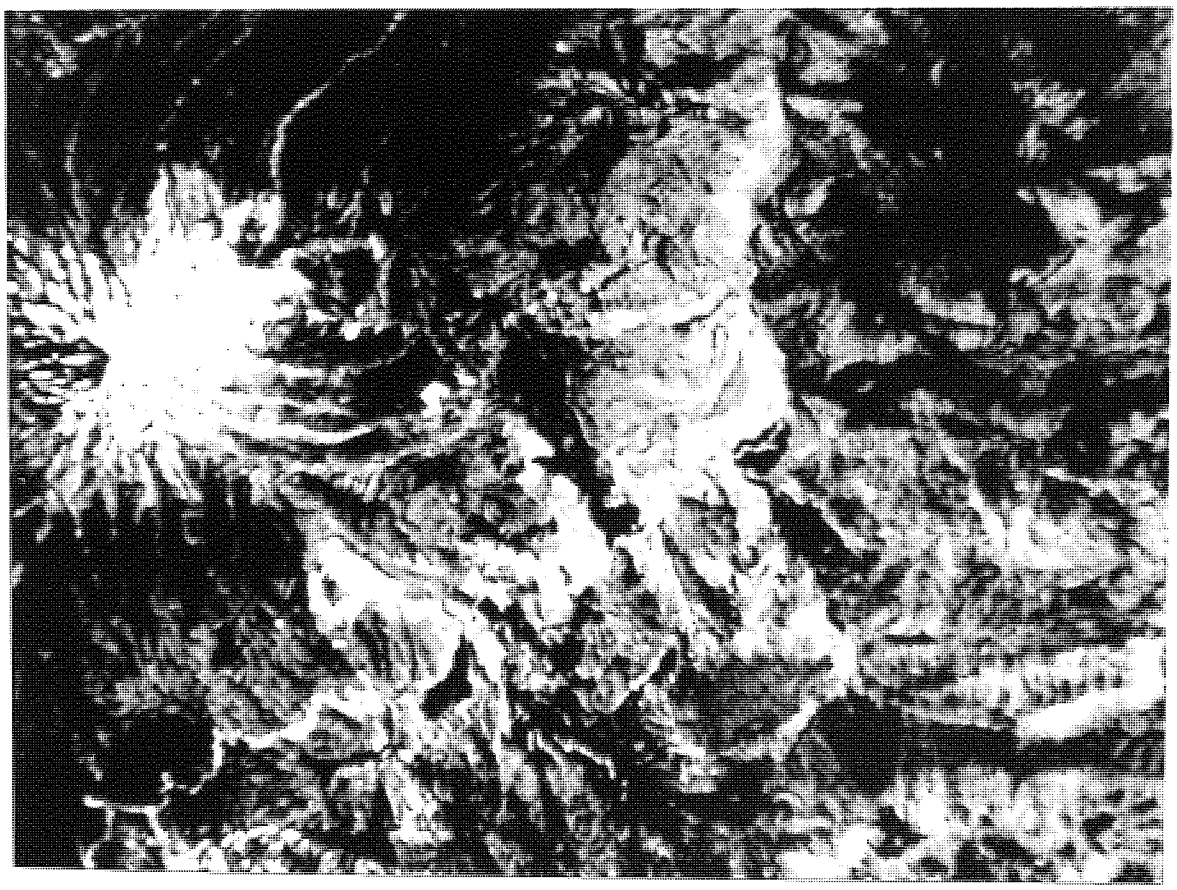

(b)

Plate 6.7 First and second principal components. a) First principal component of all eight bands of both July and September images which shows mainly topography free from vegetation cover. b) Second principal component of the eight bands showing low values for vegetation and also revealing some tectonic features.

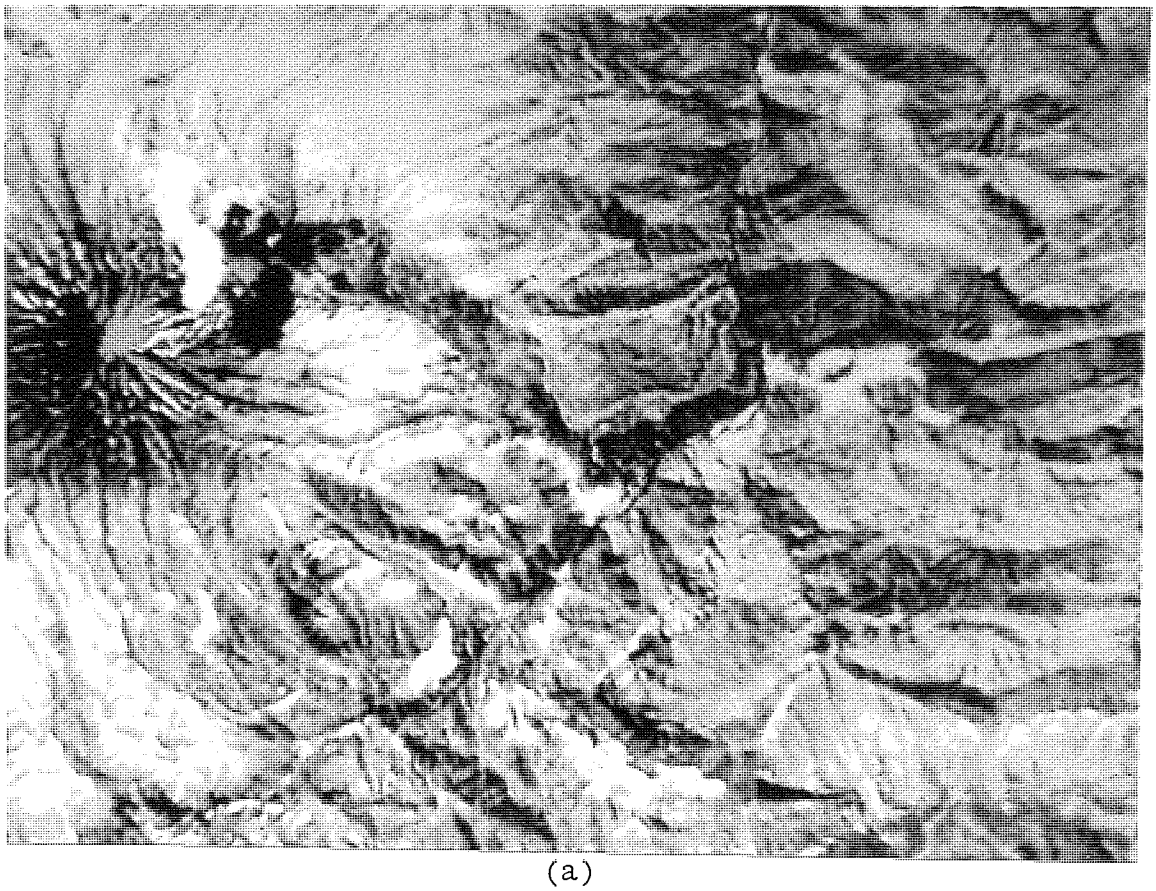

(a)

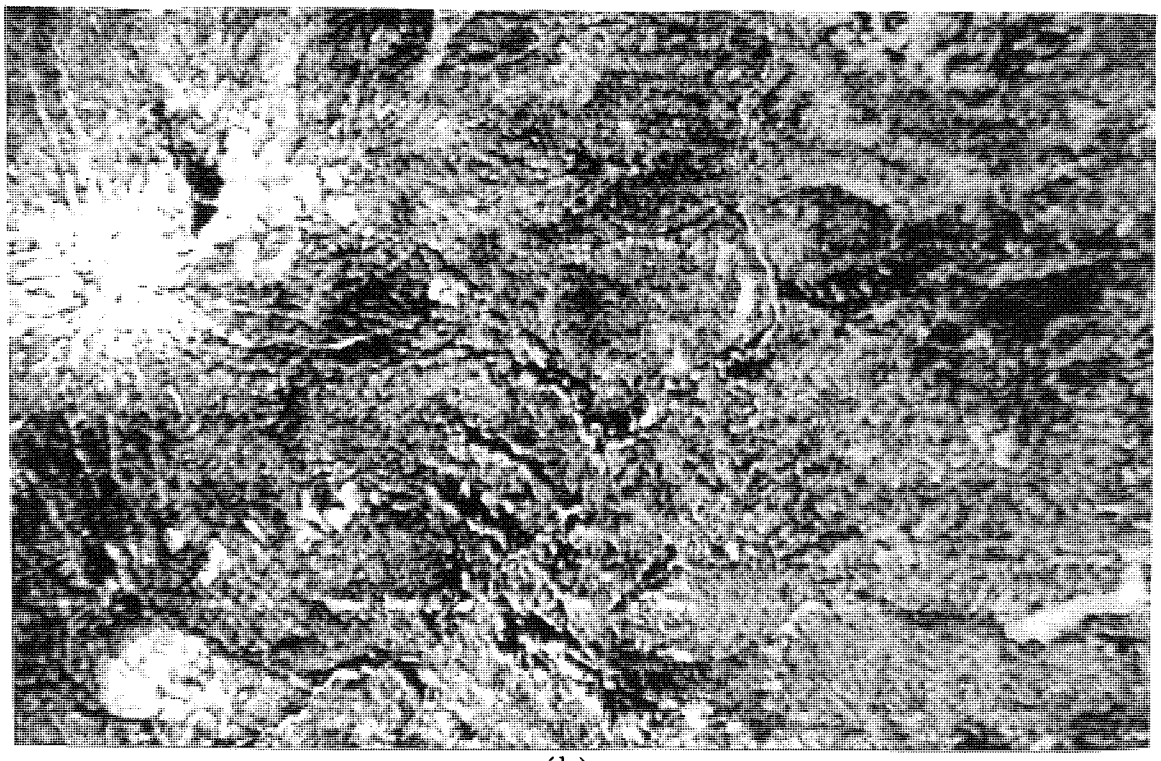

(b)

Plate 6.8 Third and fourth principal components. a) The third principal component shows shadows clearly whilst allocating low values to highly illuminated ares; thus this component can be used to extract information from shadowed areas. Gravels on the river bed also appear dark whereas vegetated areas gain high data numbers. This also reveals some tectonic features. b) This component contains mainly noise but it is also useful for interpreting structural features. For example the Baidjan thrust can be more easily distinguished from this component than from the others.

6.2.4 Arithmetic Functions

Arithmetic functions are a method of enhancement involving simple addition, subtraction, multiplication and division of data from different spectral bands.

6.2.4.1 Addition

Addition of two MSS bands together combines the contents of both bands and enables the interpreter to treat them together. By using this method the user must realize that it is possible for the summation of two bands to give some pixel values in excess of 255 which is the maximum value that the computer can display. Two methods can be applied to avoid this inconvenience, the first where the user can decide to set any outlying numbers to 255, and the second method, called scaling, where the user can multiply all data numbers by a gain to set them in the range of 0-255.

This process was applied to combine bands 5 and 7 of the September image, bands 5 and 7 of the July image and bands 5 and 7 of the April image. To enhance soil or rock and vegetation reflectance characteristics the results were displayed as a false colour composite. The resultant image was much better than the usual image. In particular the principal component of this image revealed more detail. The only difficulty was snow cover in the April image which affected the principal component (Plate 6.9).

6.2.4.2 Subtraction

This task is applicable to all four MSS bands particularly band 7 minus band 4, band 6 minus band 5, and band 7 minus band 5, where the

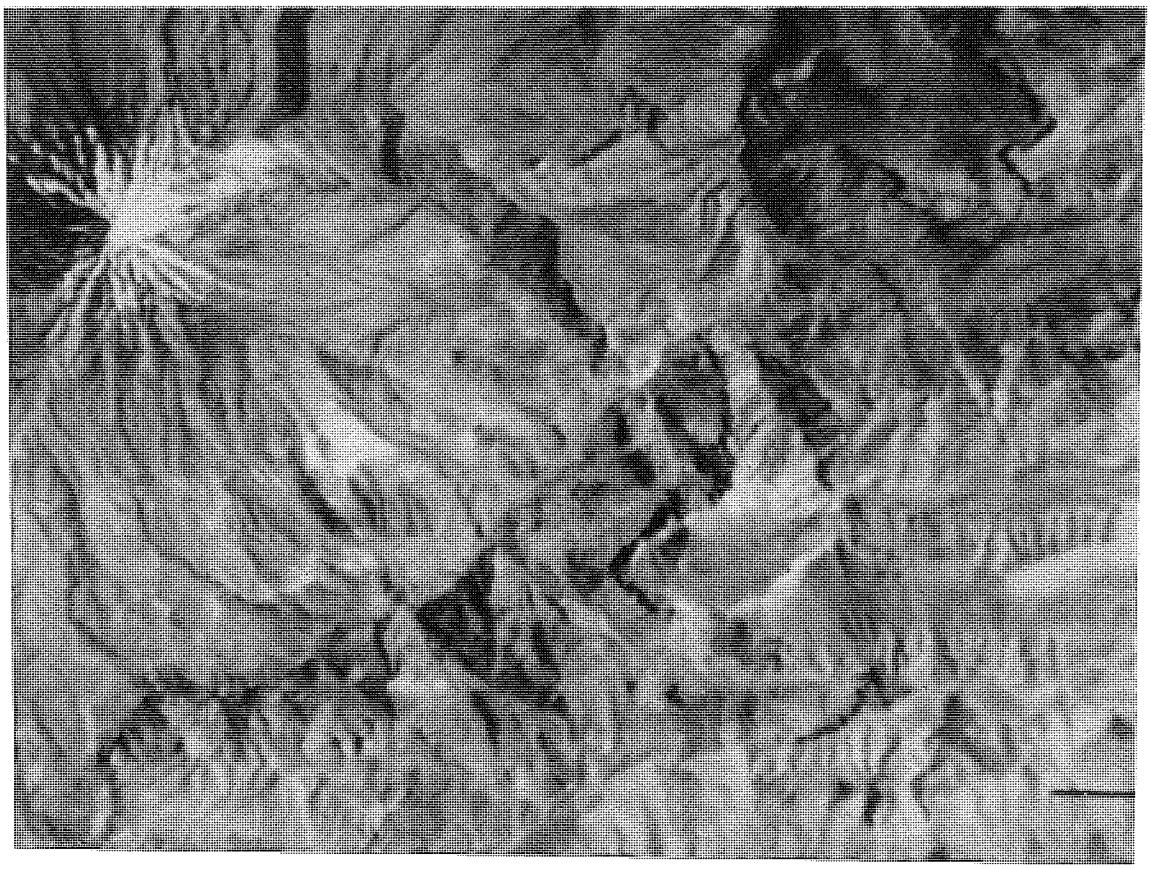

Plate 6.9 Addition of band 7 and band 5 of July image.

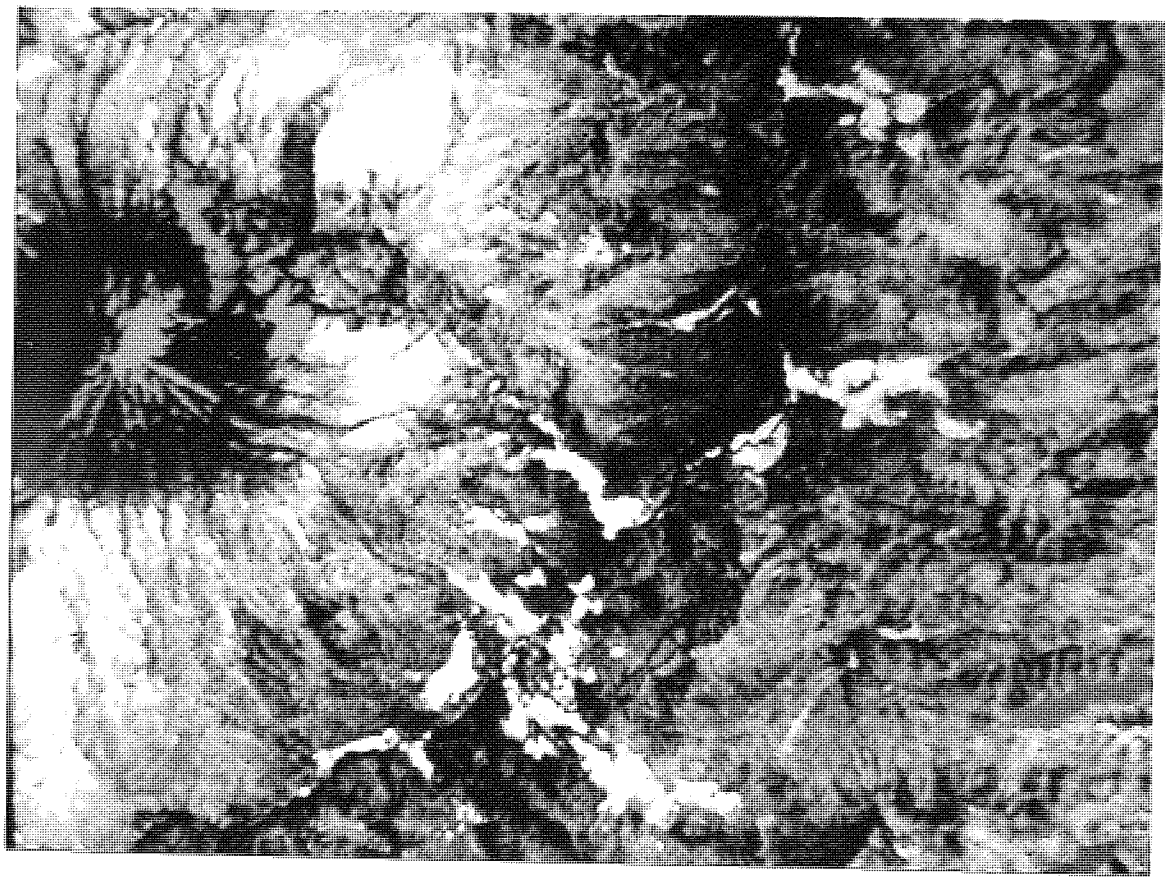

Plate 6.10 Subtraction image of band 5 from band 7 (B7-B5). As can be clearly seen, vegetation in this image appears highly reflective and shadows have gained high values. Consequently linear features such as the Haraz Valley bottom are highlighted.

resultant image is very good for vegetation discrimination and forest inventory (see Appendix A). To overcome subzero data values the investigator can either set any minus values to zero, or add an offset to raise the lowest value up to zero, then the gain can be modified to stretch all DNs between zero and 255. Plate 6.10 shows the resultant images in which linear features are revealed very well .

6.2.4.3 Ratioing

This task is very common in image processing and the method is especially useful for vegetation analysis. The division of data values in two bands typically results in ratios in the range 0 to 4. These are then multiplied by an appropriate gain factor for presentation.

Several ratios were generated for all four images separately and the results were evaluated. Had this investigation involved the study of a large area, this method could have been helpful, but in this context, where the targets were very small areas associated with slope instabilities, ratioing of the bands was found not to be very useful (plate 6.11).

6.2.4.4 Vegetation Index

A simple vegetation index can be obtained by the transform of (band 7 - band 5): (band 7 + band 5). The vegetation index can be written as [band 7: (band7 + band 5)] - [band 5: (band 7 + band 5)]. In this, the first part is called the sum normal of band 7 representing vegetation characteristics, and the second part is called the sum normal of band 5 which represents bare soil. A generalized vegetation index can be defined as the sum normal difference between a

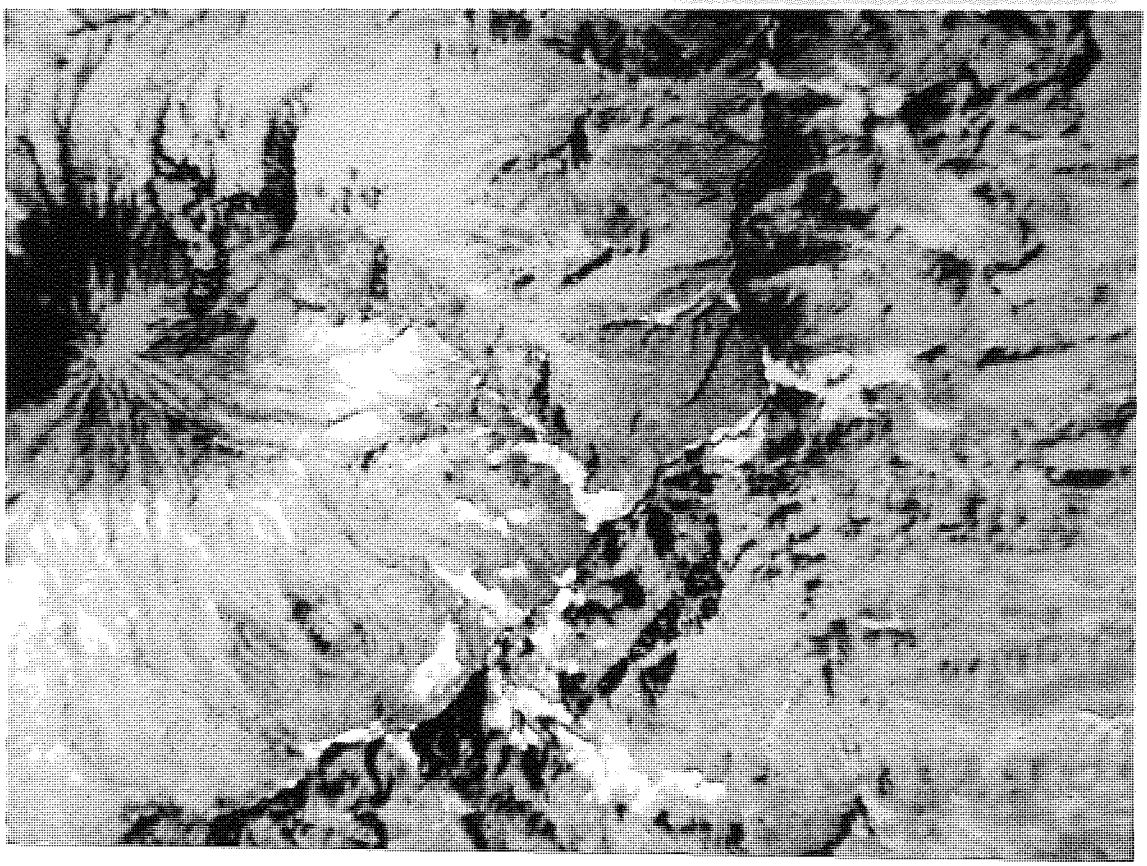

(a)

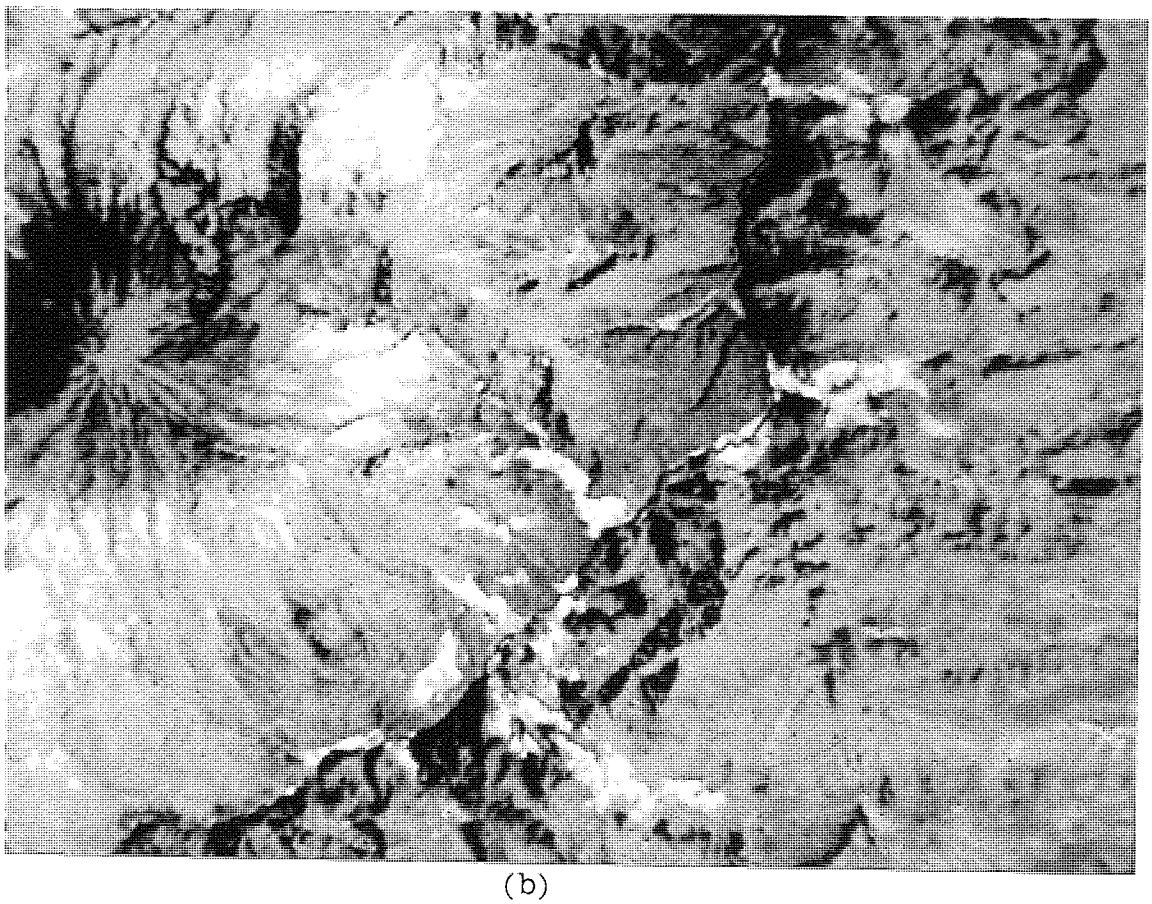

(b)

Plate 6.11 Ratio images of September image. a) Band 7/band 5 highlights vegetation but shadows remains black. b) Band 7/band 4 also highlights vegetation and dark shadows appear grey because of noise in band 4. For the vegetation inventory it seems better to use the 7/4 ratio.

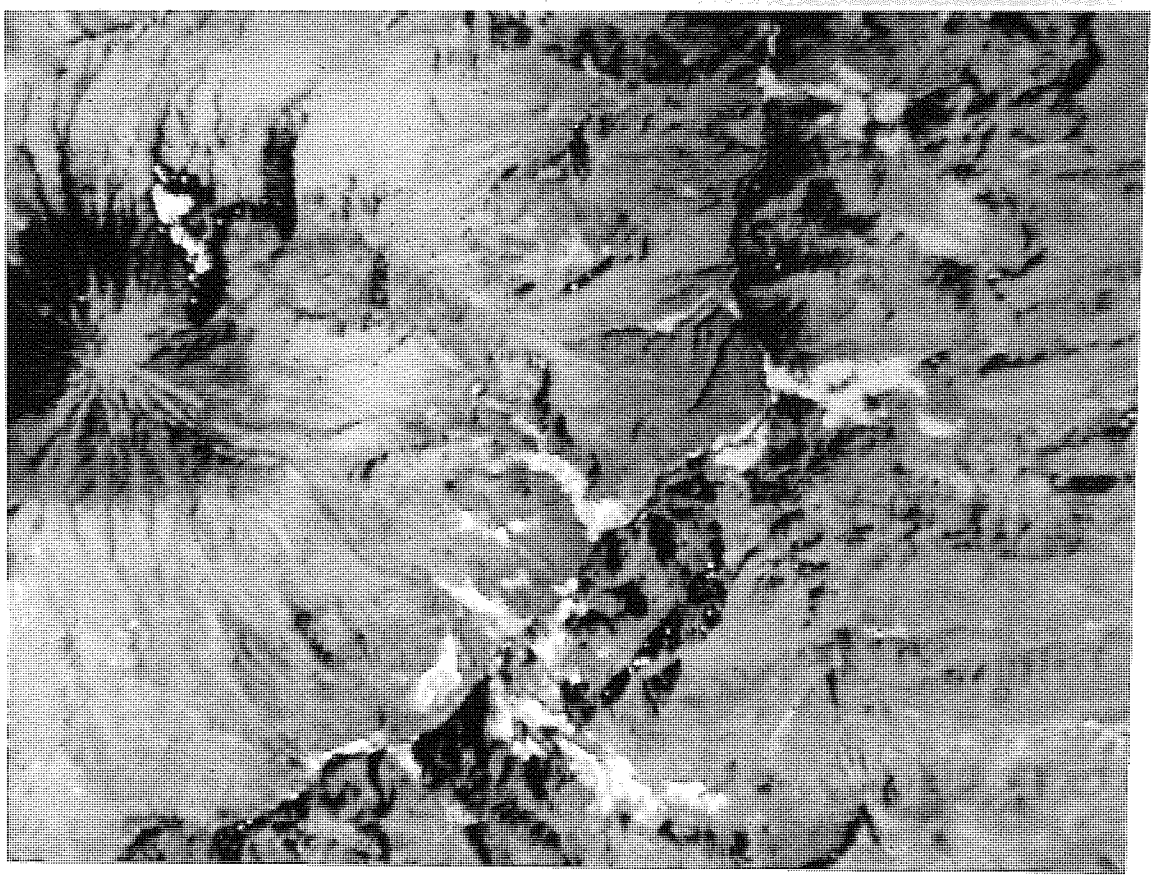

(a)

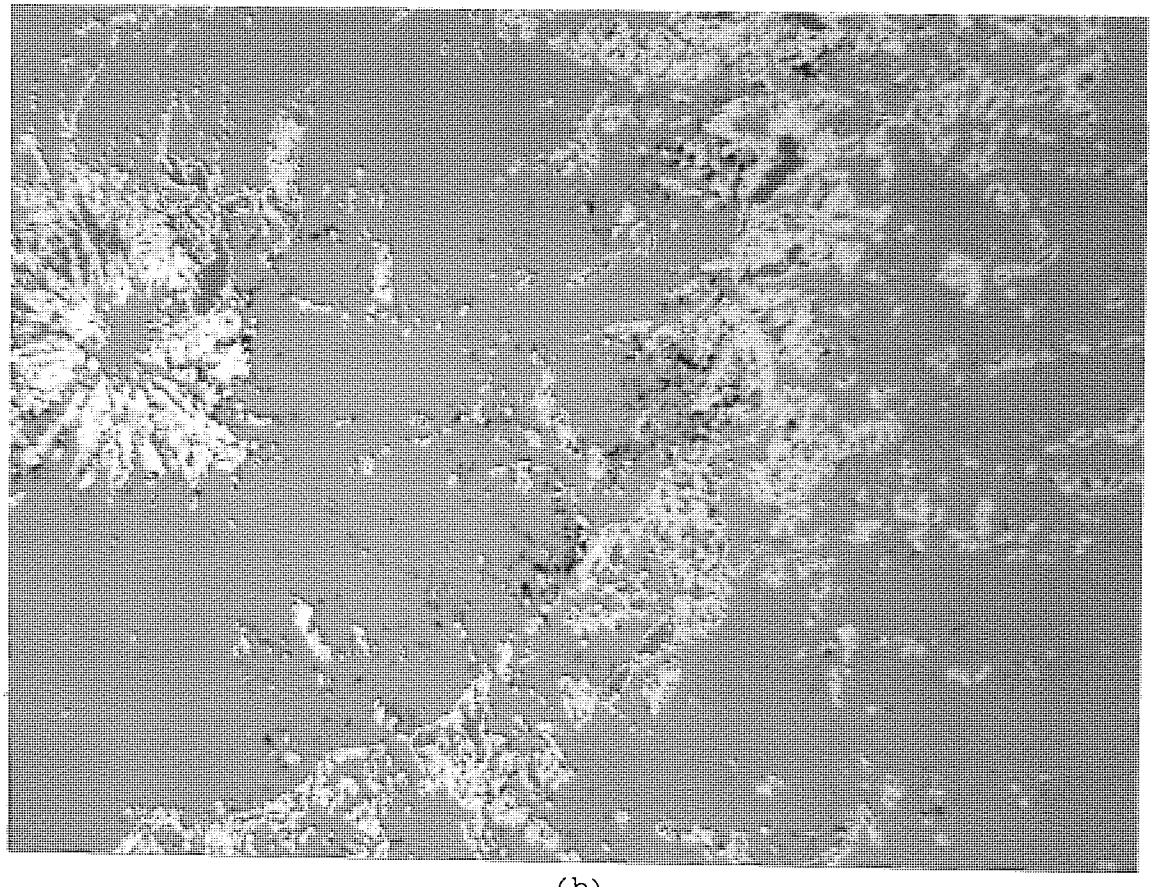

(b)

Plate 6.12 Vegetation Index of September image. a) Vegetation index (B7-B5)/(B7+B5) which was stretched (27-226). Cloud shadow at the top of Damavand Mountain is also classified as vegetation. b) Colour slice of the lower part of the histogram of plate (a) which shows disturbed dotty areas in dark blue representing unstable areas along the valley.

characteristic vegetation vector and a characteristic soil vector (NASA 1982).

The process was applied to the subscenes and with the exception of the snow covered areas, the results were very good in generating a vegetation inventory. However, due to the many unvegetated and well exposed rock surfaces of the study area this result was not of great help for unstable areas (Plate 6.12). A detailed study of this method on small subscenes showed better results to locate unstable slopes (see Chapter 7).

6.2.4.5 Normalization

This task provides a normalized black and white image by dividing one band by the sum of several bands. Dipix users can apply division of any band by the sum of up to eight other bands. The resulting image is free of noise and appears sharper than before. The user can alter the contrast of the image by changing the offset and gain.

This was applied to several bands of the subscenes and the resulting images were very good. Plate 6.13 is an example of this enhancement.

6.3 IMAGE CLASSIFICATION

Classification of images can reveal more information to help the analyst to match particular areas and reflectance. There are two major methods for classification of an image and the investigator must decide which method is apropriate for his particular study. Using the Dipix it is possible to have up to 32 classes defined automatically in feature space (unsupervised classification), which ideally correspond to different types of land cover. Sometimes several of the 32 classes

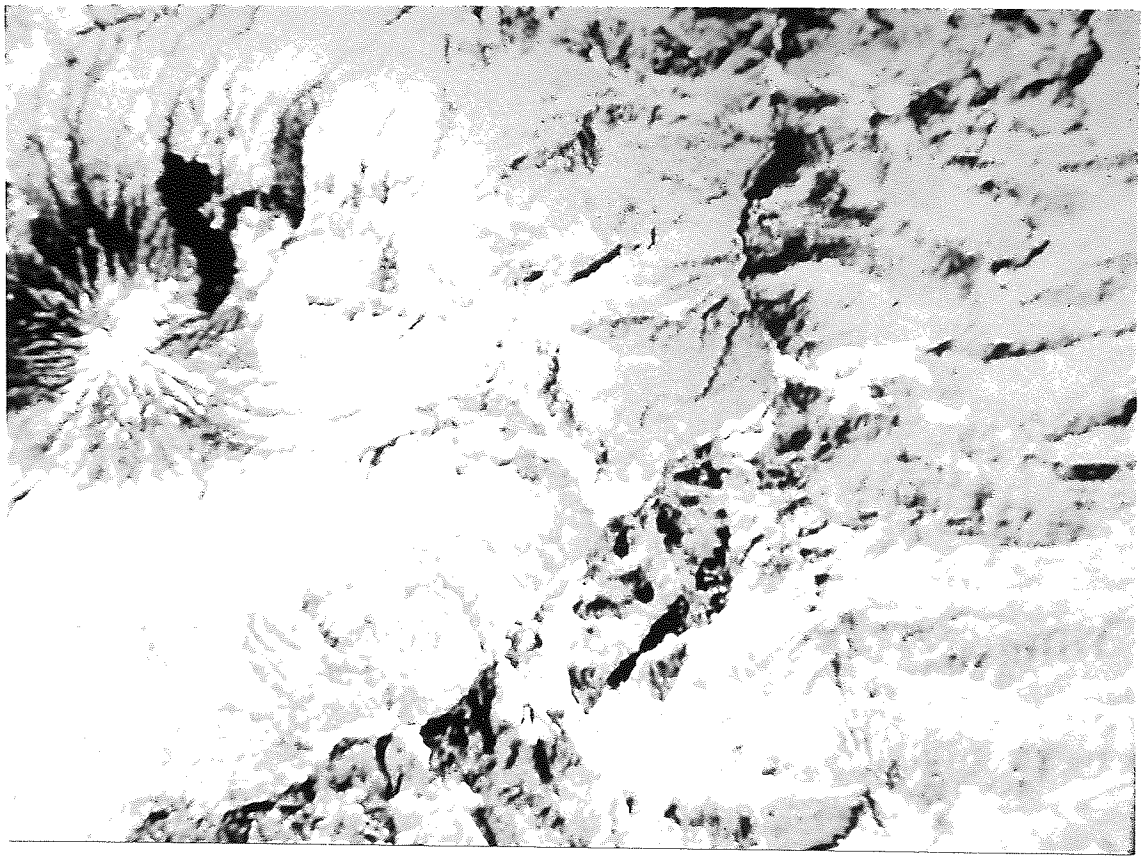

Plate 6.13 Normalised image. This image is the result of dividing band 7 of the September image by bands 6,5,4 of that image, and 7 and 5 of the July image.

correspond to a single land cover category. An alternative method is supervised classification, where the operator defines training areas belonging to known land cover types. The statistics from these training areas form training sets which are used to drive the classification. These two techniques are discussed more fully below. For best results it is recommended to classify an image by unsupervised classification to find out primary classes, then supervised classification can be applied to improve the resultant classes.

There are two major and popular classifiers: the maximum likelihood classifier and the parallelepiped classifier. Both classifiers implemented on the DIPIX can classify from one to sixteen bands (or feature files), separating from 2 to 32 classes. Of these two methods the maximum likelihood classifier is the more flexible and

is particularly appropriate for areas where classes overlap in feature space. The reason for this is that in the maximum likelihood classifier an n-dimensional ellipson is employed for each class, whereas in the alternative technique an n-dimensional parallelepiped is used which cannot allow for overlaps.

In addition to these two standard classifiers, the DIPIX software provides two minor, fast, but less general classifiers which are a fast maximum likelihood classifier for four feature files, separating up to 16 classes, and an instantaneous parallelepiped classifier which classifies only data that exist in the video memory separating them from 2 to 16 classes. These two fast classifiers are useful preliminary methods which can be applied before making use of the standard classifiers.

6.3.1 Unsupervised classification

This method involves the recognition of certain types of reflectance values on the data set, and identifies areas with similar reflectance values. Separation of classes depends on the skill of the analyst and the harmony of the data set; in other words the computer uses an algorithm to choose a certain class for a certain range of data numbers, then the analyst must change the scale to enable the computer to separate data into useful and recognisable classes. Unsupervised classification can use an algorithm to examine a large number of unknown pixels, and cluster them according to their natural spectral groupings. The cover types to be specified as classes within a scene are not known 'a priori', and the analyst must compare classified data with some form of reference data (e.g. existing maps or ground truth obtained by field work) to determine the identity and

informational value of the spectral classes. In a case where there is a lack of appropriate ground truth, or the surface features of the scene are not well defined, unsupervised classification is the best way to classify an image. In general circumstances the application of this method can also be helpful to further classification of an image.

This method was applied in the study area but it was not very successful due to the extensive relief and the presence of shadows, sunfacing slopes and poorly illuminated surfaces. However, it gave some useful information about the nature of remote areas. Plate 6.14 shows an unsupervised classification in the study area.

6.3.2 Supervised Classification

In supervised classification the identities of the cover types of interest are already known for small training areas within an image from field work, pre-existing maps or other data . The first step is to locate within an image those areas of interest which are to be classified in the same class. The second step is to calculate the statistical parameters of each set of training areas and store these as a signature file in the computer memory. Each class has its own characteristic multivariate parameters. Every unknown pixel outside the training areas will be assigned to a known class on the basis of its multispectral properties, unless it lies further than a user-specified distance from all classes.

If there are some unclassified pixels left on the scene the analyst can decide whether to choose a separate class for them, or absorb them into the other classes. A certain fraction of unknown pixels will be misclassified, especially for those classes with overlapping variances. The classification must therefore be checked

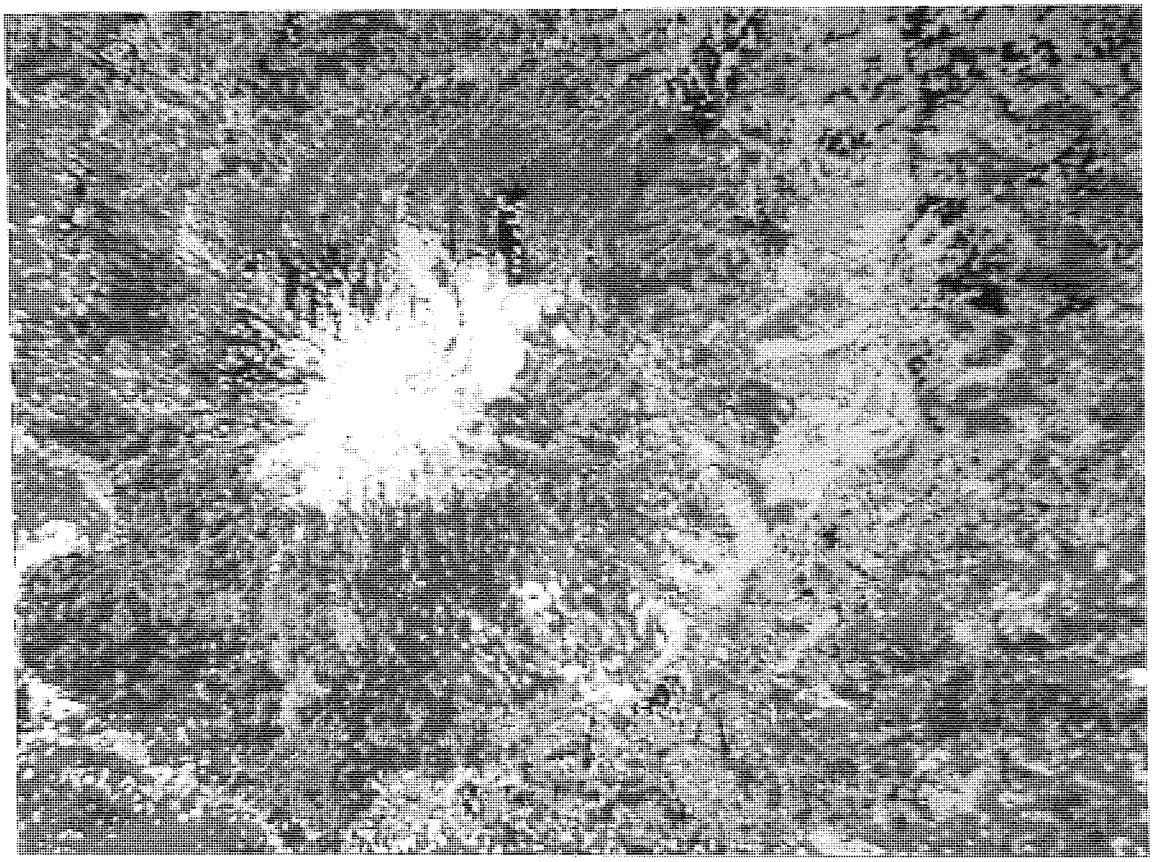

Plate 6.14 Unsupervised classification.

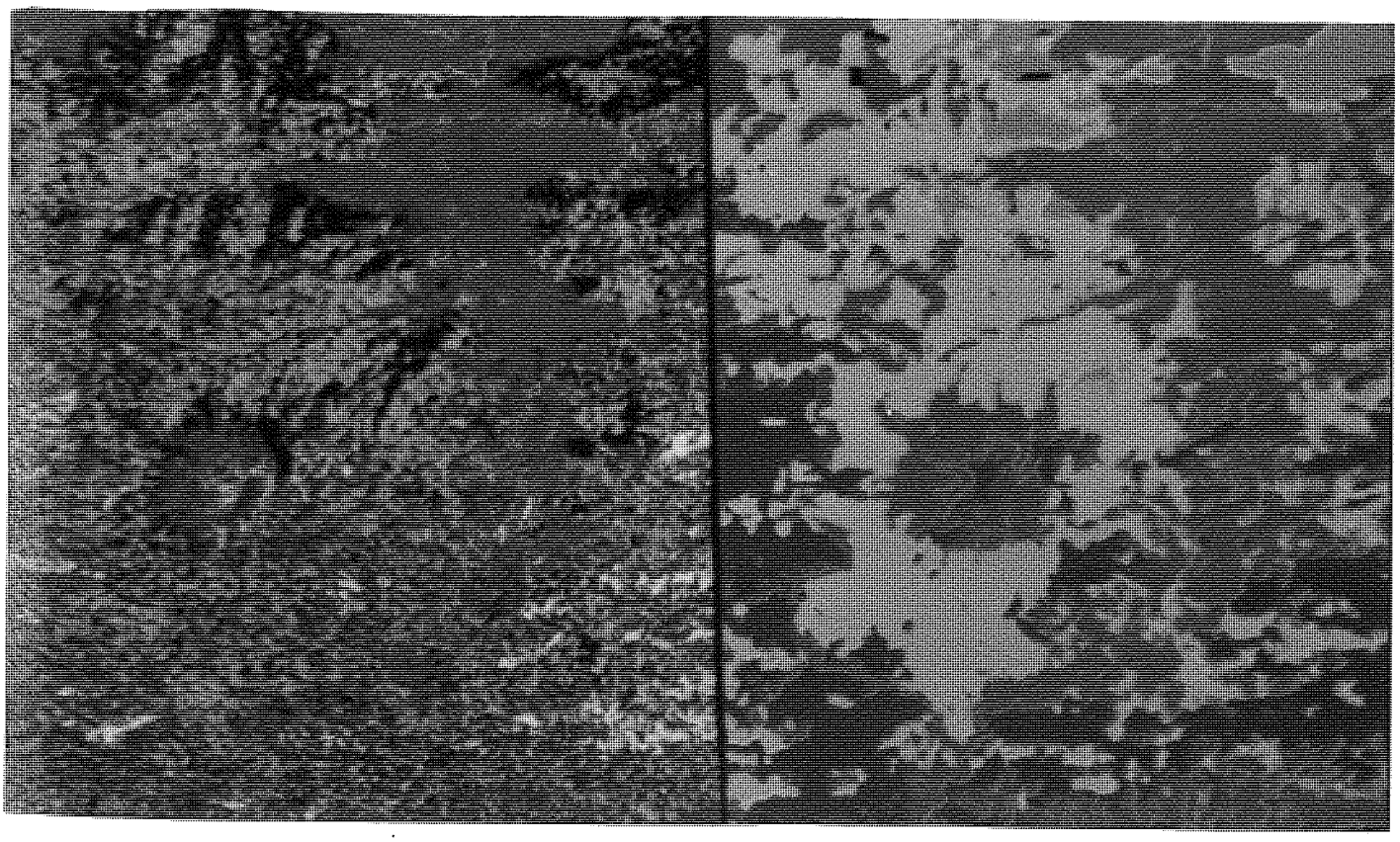

(a) (b)

Plate 6.15 Smoothed supervised classification. a) Supervised classification of September image. b) Smoothed version of (a) which is more useful for mapping. The colours correspond : orange = lava flow, red = screes and unstable areas, blue = pale limestone green = lower jurassics (Shemshak formation) and purple = vegetation cover. There are misclassified areas such as top of the volcano which is classified as lower jurassics.

against available ground truth to pick out misclassified areas. By combining certain classes, and wiping out small misclassified areas by applying smoothing methods (e.g. task "CU" on the DIPIX), the classificationcan be improved(Plate 6.15). If all the relevant classes within the scene are properly specified, and both scene and training areas are reasonably homogeneous, the accuracy of a supervised classification can be quite high, particularly for vegetation types in multitemporal images.

6.4 CONCLUSION

Image processesing techniques as described in this chapter were used to correct and enhance the images selected for this research. The resultant images were all improved for visual interpretation through the techniques applied . Radiometric correction eliminated noise and haze, leaving a harmonic and fluent image : whereas geometrical correction enabled superimposition of existing data with the images to quantify matching or missmatching of the imagery with this data. Addition of two or more spectral bands enhanced tectonic features, while subtraction highlighted vegetation cover as well as differences between certain rock types.

The vegetation index improved delineation of vegetated areas, but some dark shadows were misclassified as vegetation. On the basis of this research it seems better to use subtraction as a method to discriminate vegetation cover, rather than the vegetation index. However, the lower part of the vegetation index histogram proved to be useful in revealing details of unstable areas with a disturbed surface (mixed pixels). Unstable areas have mixed surface characteristics with a lack of homogenous vegetation cover, resulting

in varied pixel values in all four bands. Application of the vegetation index stretched low values of the histogram and revealed any disparity between the unstable areas and the stable vegetated areas.

The combination of several principal components to form a colour composite image can enhace and sharpen the visual effect. The best results were achieved when three sets of addition of two bands (7+6, 6+5 and 5+4) were combined as a colour composite (Plate 6.16). As can be seen in this plate more details are shown than by any conventional colour composite.

Several combinations of single bands from images taken at different dates (all registered with each other) were examined. In addition several principal component transformations were carried out and compared against ground data obtained from field work, available maps and other information. The extensive relief of the study area and the size of ground cell resolution were the two main major factors which prevented the best possible results being obtained. The most promising approach was the use of a combination of ground data and Landsat MSS imagery (results could be further improved by adding images with smaller resolution, for example Spot imagery which will be available in early 1986). This technique could be used in the primary study of areas of Iran and to prepare a low-cost 1:250,000 scale map of the whole country. However, field work is essential for any remote sensing study in order to select the best training areas to distinguish different spectral signatures and to obtain the best possible classification.

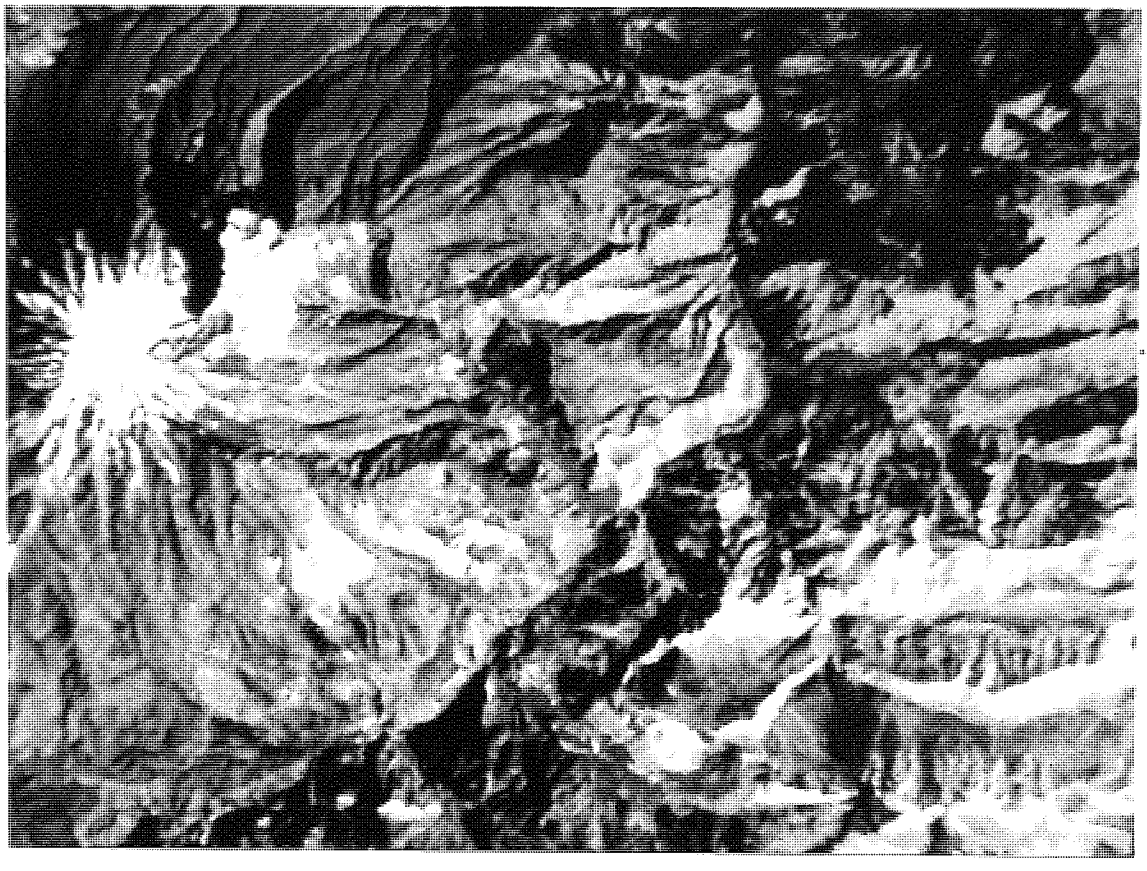

Plate 6.16 Colour composite of the additions of two bands. This image is constructed from (B7+B6)in red, (B6+B5) in green and (B5+B4) in blue from September image. As can be seen this image is more enhanced than conventional colour composites.

CHAPTER 7

DATA ANALYSIS CARRIED OUT WITH ASTON UNIVERSITY FACILITIES

7.1 INTRODUCTION

Initial analysis and image processing of the CCT scenes on a DIPIX Image Processing System yielded a large amount of information on the geology of the study area as a whole. Access to an image processing system to perform the analysis of remotely sensed data is desirable for most investigators. However, the high cost of image processing time is an element which limits computer use. The costs of image analysis are much reduced by carrying out statistical analysis on a non-image processing computer. Aston University has good computer facilities, able to perform a range of statistical manipulations. In addition there is no time limit on access to these facilities. These advantages justified an attempt to develop a primary method of data analysis, involving the writing of some simple programs. The programs allowed several small subscenes of MSS images to be produced in a digital format, and subsequently displayed using the appropriate software. As a follow up exercise it was decided to select suitable subscenes from along the road and process these further in order to gain detailed information.

At first, 26 subscenes from the July '77 image and 27 subscenes from the September '72 image were chosen for detailed interpretation. Several statistical manipulations were carried out on the data extracted from these subscenes, with fairly good results (see Appendix A). However, it became apparent after developing the analytical

methods that it would be worthwhile operating on a new, fully corrected data set free from geometric distortion, radiometric striping and atmospheric effects, since these interfered with processing and subsequent analysis.

After applying geometric and radiometric corrections, resampling at 50 x 50 metres, registering all 4 multitemporal images together on the Dipix, 35 subscenes (each of 40 x 40 pixels) were chosen along the road for further investigation (Plate 7.1).

Thirty-five subscenes consisting of 9 bands were taken from the September 72, July 77 and April 78 images; Band 6 was ignored in all cases. The pixel values for these three subscenes were stored on a computer tape in the format shown in Figure 7.1.

September 72			July 77			April 78		
BAND 7	BAND 5	BAND 4	BAND 7	BAND 5	BAND 4	BAND 7	BAND 5	BAND 4
1600 rows x 9 columns								
(= 40 x 40 image in 9 bands)								
37	51	58	35	44	53	37	45	38
38	52	62	35	52	59	37	45	36
40	55	64	35	52	59	40	48	41
39	56	66	32	49	59	43	50	45
.	.	.	.	.	.	.	.	.
.	.	.	.	.	.	.	.	.

Figure 7.1 An example of the tape format used for processing on the Harris H500

This tape was loaded onto the Harris H500 computer at the University of Aston Computer Centre and the data processed. The processing fell into 2 categories:

1. Visual display and manipulation
2. Statistical analysis

7.2 VISUAL DISPLAY AND MANIPULATION

The programming at Aston followed three avenues all involving single band display:

1. Display of image on a 16 colour Sigma Colour Graphics terminal attached to the Harris H500.
2. Display of image on an Apple microcomputer, after downloading information from the Harris H500 via the Apple, onto floppy discs.
3. Display of image in the form of a grey map on a Dot Matrix printer.

7.2.1 Display of Image on Sigma Colour Graphics Terminal

The programs available were developed to test the viability of using the Sigma/Harris for image processing. Therefore, they are fairly crude and at present are limited to the following:

1. CCT LOAD Loads a CCT scene from tape onto hard disc storage. The general outline of the program is shown in Appendix B. The program takes data from the tape and produces 5 files:

   CCT TEXT : Contains the tape directory data - an example is contained in Appendix B.

   CCT SAMP : Contains a sampled overview of the scene (a sampling of one band).

   CCT BND1, CCT BND2 and CCT BND3 :

   Together these make up a colour composite of a segment of the scene. Each of the files holds the data for a band.

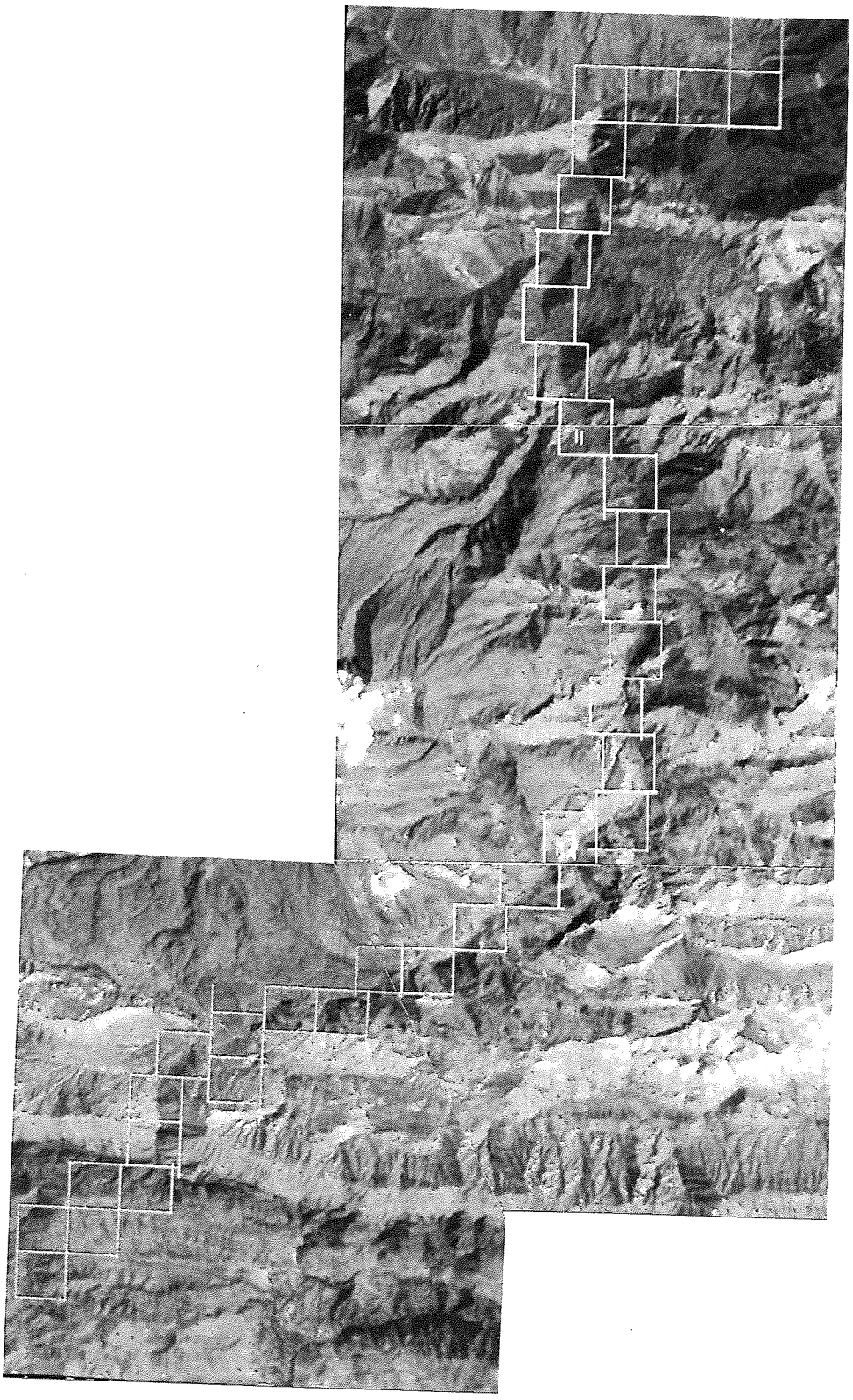

Plate 7.1 Location of selected subscenes along the road.

devise a suitable method for producing the composite, mainly due to the Sigma being limited to a maximum of 16 colours on the screen at any one time.

Summary

A simple display system was developed using the Harris and Sigma. However, the system was not entirely successful for number of reasons: tape loading is awkward to arrange, only parts of scenes can be stored; each scene takes around 20 minutes to display. In addition any processing on the scene takes considerable time as array processing is not possible. It therefore seems that if the system is to be developed further on the Harris and Sigma, it should only be used as a last resort when purpose designed image processing equipment is unavailable.

7.2.2 Image Display on the Apple II Microcomputer

Initially data extracted from the small subscenes (40 x 40 pixels) were read into the Harris H500 computer using a columnar format (see para. 7.1). A program (CONVERT) was applied to change the data to a (40 x 40) format (see Appendix B).

The Apple II microcomputer in addition to working as a microcomputer, can, in a certain mode, be used as a terminal for the Aston University Harris H500. However, whilst the Apple is being used as a terminal, the operator cannot under normal cicumstances use Apple II commands without first disconnecting from the Harris. To have access to the Apple and the Harris simultaneously a program (SERIAL) was written (see Appendix B). This program enables the user to access the Harris H500, and transfer data files or programs from the main frame to the Apple or vice versa. These files can be stored on a

floppy disc, the link with the Harris system cut, and processing continued on the Apple II microcomputer.

On receiving the subscene data in 40 x 40 pixel format on the Apple II another basic program (PLOTFILE) was applied to display these data in low resolution using the graphics mode of the Apple II (see Appendix B). This display is actually colour density slicing and enables the user to choose a slicing scale to provide a fairly good colour image on the Apple monitor, which is sharper than that on the Sigma.

Due to the format of the Apple monitor which is rectangular (250 x 140 mm) it was difficult to produce a square display of pixels without image distortion (Plate 7.2). It was therefore necessary to write a program to give each a pixel square shape, particularly in the second set of data (see para. 7.1). A basic program (DISPLAY) was written using the high resolution graphics mode of the Apple II although the number of colours was restricted to six (Plate 7.3).

Density slicing apart, the Apple II microcomputer is of little use for serious image processing due to lack of capabilities and capacity. The only real use is in connection with the Harris H500 from which data can be accessed, recorded on floppy disc and then displayed on the colour monitor using the Apple II graphics mode. Even this display requires scale alterations.

7.2.3 Grey Maps

The aim of this section was to make a comparison of processed images with ground truth . A set of aerial photographs along the Haraz Road were printed at a scale of 1:20,000. Other field data required a set of subscenes extracted from satellite images and these

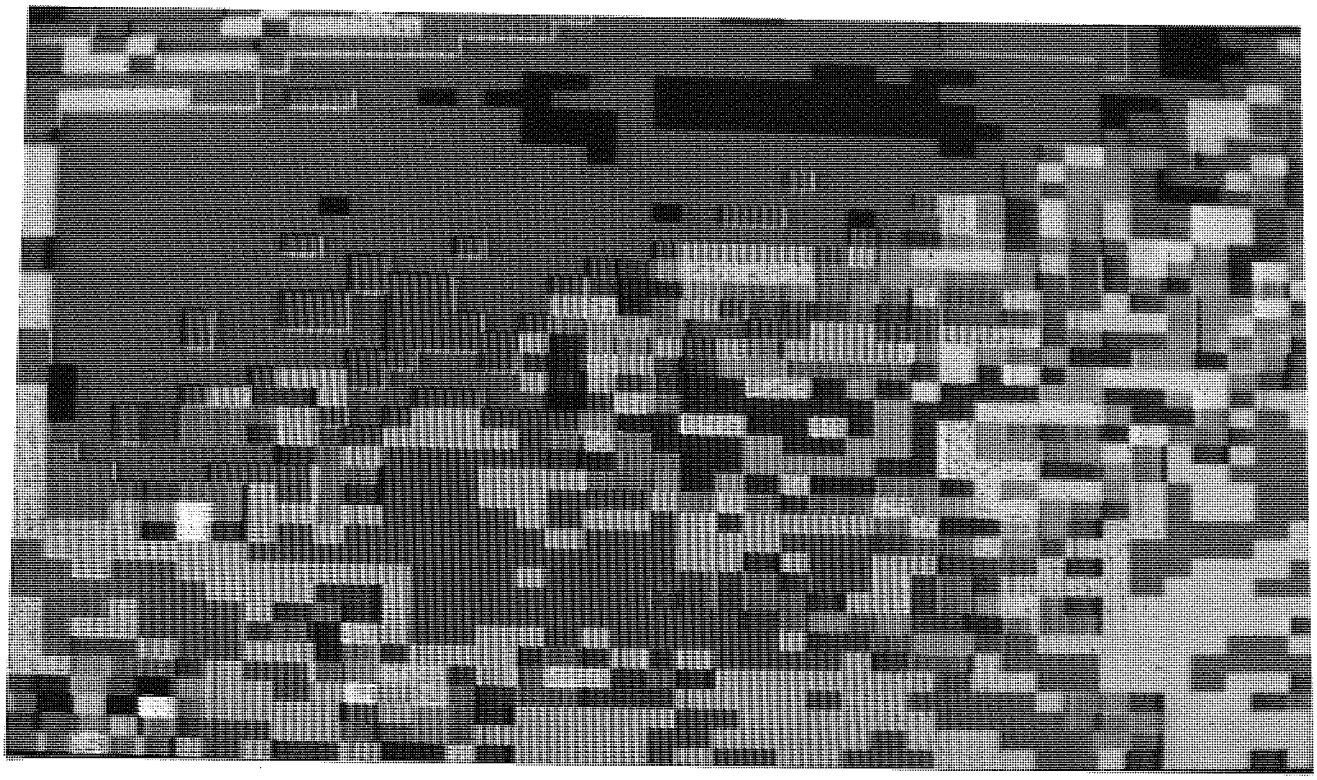

Plate 7.2 A distorted subscene on Apple II monitor.

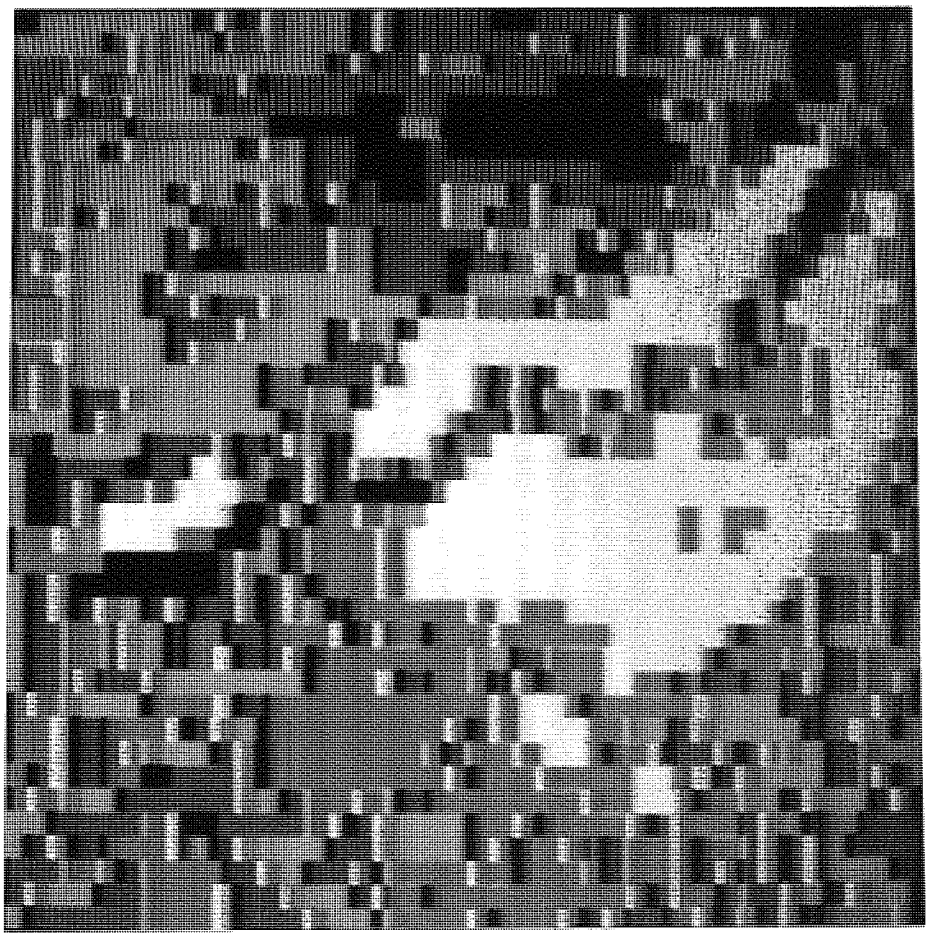

Plate 7.3 A correct format subscene on the Apple II monitor. The 40 by 40 pixels subscene showing Shangoldeh area in km 58.

were also printed at a scale of 1:20,000. Subscenes of 40 x 40 pixels, corrected and resampled at 50 x 50 m, were employed to print a series of grey maps. A variable grey scale ranging from 0 to 99 was chosen with eight levels of grey available for the pixels. Although it was possible to print the grey map in a square format, it was not possible due to restrictions on the printer, to print them at the correct scale. Forty by forty pixels measure 67 mm length and depth, and this gives a grey map at a scale of 1:33,500. To overcome this limitation a program (SCALEUP) was provided to take each pixel and generate it twice in a line and twice in a column. Consequently scale up 40 x 40 to 80 x 80 repeating each pixel twice. Thus the size of the print becomes 134 mm. By reducing this grey map in the photocopying machine to 100 mm square, a scale of 1:20,000 was achieved. Figure 7.2 shows a Greymap of a subscene located on km. 58.

Because of skew, the satellite image format is not square but appears as a parallelogram with a skew angle of approximately 3^{o} 34' west of south (Figure 7.2). Therefore a program (SKEW) was written to reform the plot to match the parallelogram shape of the NASA hard copy format (see Appendix B for greymaps). This program is applicable to the first data set which is not geometrically corrected.

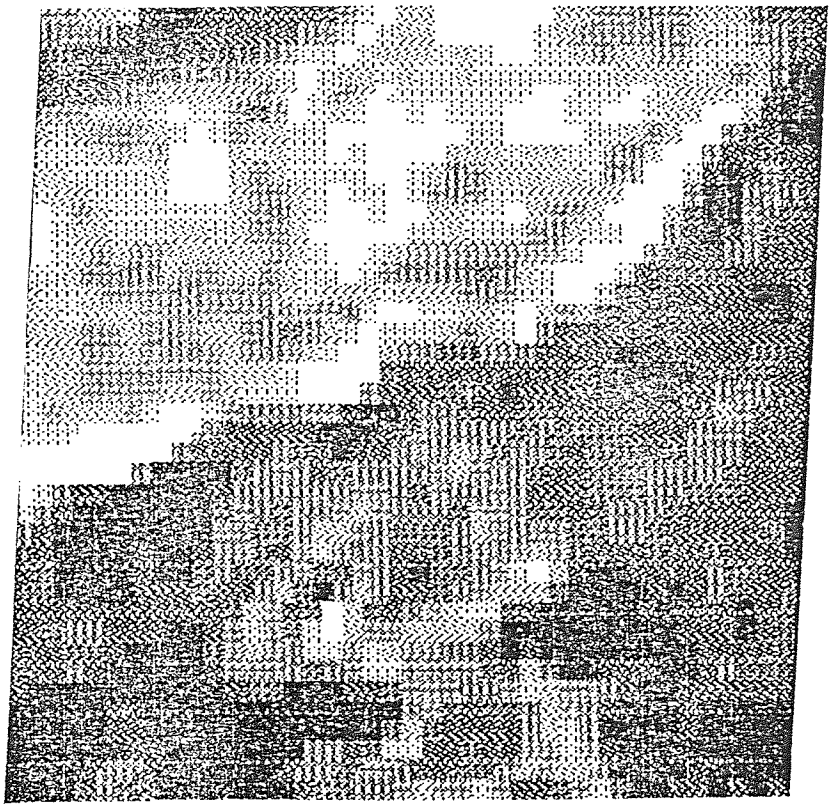

Figure 7.2 A skewed subscene in greymap format.

7.3 STATISTICAL ANALYSIS OF MSS DATA

7.3.1 Introduction

It is important in statistical analysis of image data that atmospheric effects, particularly haze, must be eliminated otherwise the results of the analysis will be badly degraded. A correction to the histogram was therefore applied to free all data from haze. Several different types of image analysis were then carried out on the basis of their brightness values to discriminate land features. The task was complicated by extensive terrain relief causing deep shadows and highly illuminated sunfacing slopes. Dark shales in the lower Jurassic rocks have reflectance properties similar to slightly

shadowed areas, whereas the light coloured upper Jurassic limestone and pale Cretaceous limestone reflect light as strongly as the well illuminated sunfacing slopes.

Statistical manipulations were carried out on the 35 subscenes of 40 by 40 pixels along the road stored on the Harris H500 computer at Aston University. The package employed for this task, MINITAB, enables the user to process data interactively. Different bands were plotted against each other to find standard deviation, mean, correlation coefficient and regression line. Addition, subtraction and division were also applied using this package. These operations are described in greater detail below.

7.3.2 Addition

This package enables the user to add two spectral bands to each other, pixel by pixel to investigate more details. The operation was applied in order to add data values of two bands and highlight obscure points such as slightly shadowed areas. It was necessary to apply some offset after the addition process in order to set the data within the correct range. The addition of two bands of an image revealed more information in this method because it widened the range of spectrum, but it was very useful in the image processing system in revealing tectonic linear features.

7.3.3 Subtraction

Subtraction of different bands proved to be useful for MSS image data processing, particularly when applied to multi-temporal images. The differences between juxtaposed images allow the investigator to see changes between the two acquisition dates. An offset was applied

to raise the greatest negative integer to zero. Figure 7.3 shows a subtracted subscene in a greymap format.

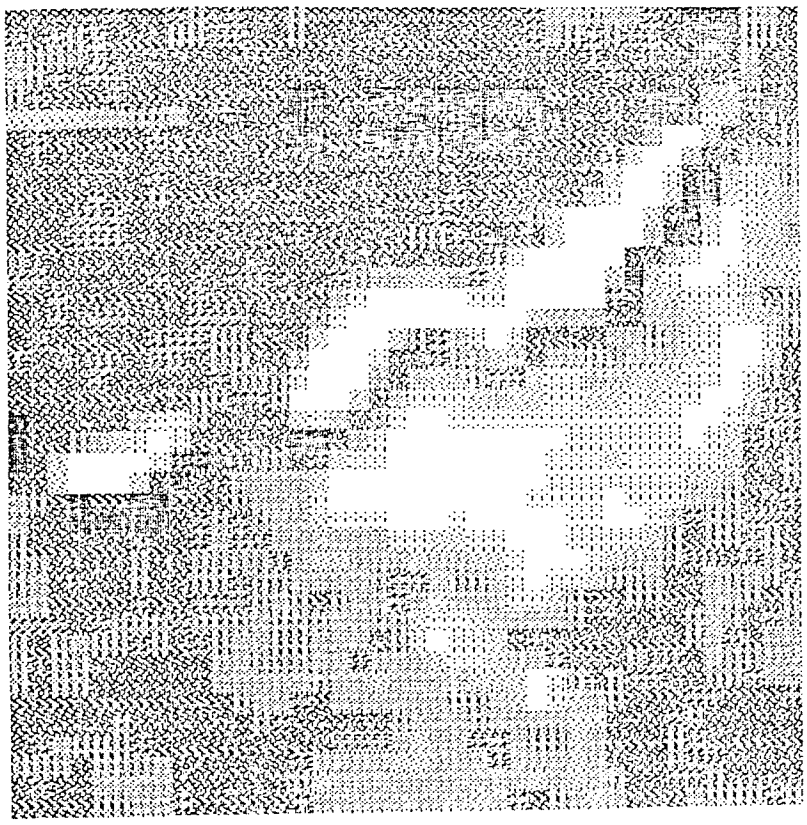

Figure 7.3 Subtraction of (B7-B5) of subscene no. 18.

7.3.4 Division

This task is similar to ratioing in digital image processing, but offset and gain must also be applied manually. Running this task using the MINITAB package is difficult and time consuming, whereas it is relatively easy using the Dipix because of the software facilities available on the DIPIX machine. The task was nevertheless performed using MINITAB to fully examine the methodology of image analysis on non-specialist equipment. Figure 7.4 shows a ratio of band 7/band 5 in a greymap format.

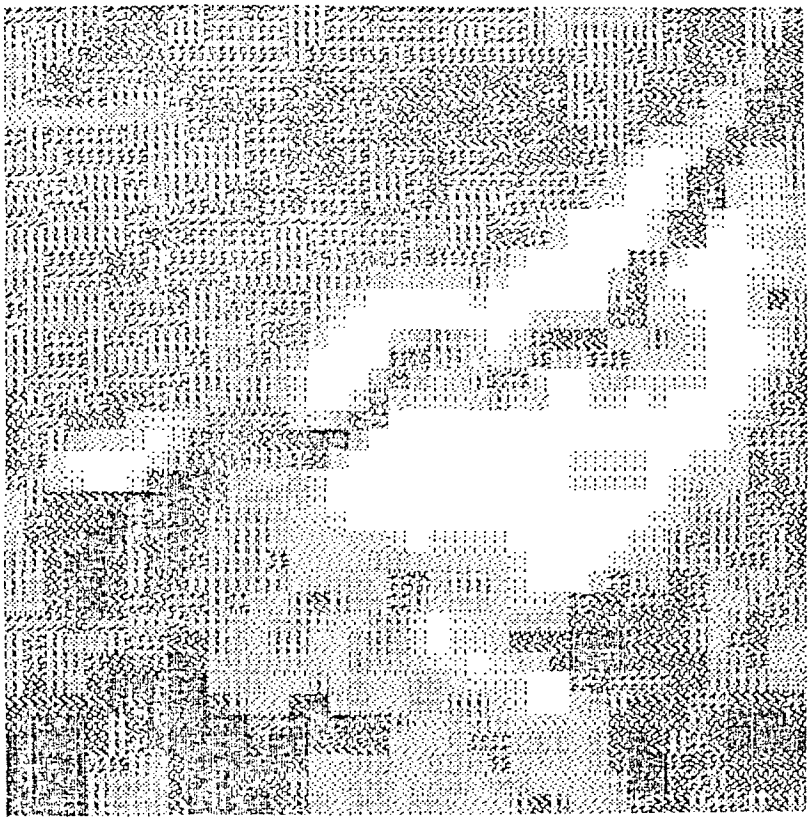

Figure 7.4 A ratio (B7/B5) image of subscene no. 18.

7.3.5 Scatter Diagram

This task plots the spectral reflectance of two or more bands against each other and is the key operation preceeding digital image classification. Most of the spectral bands were plotted against one

another and evaluated. Some combinations of spectral bands were also examined (Figure 7.5). To interpret the resultant clusters, selected training areas were plotted at a similar scale. Comparison between clusters of training areas and subscenes did lead to certain distinct categories and cover types (see Appendix A). However, the majority of categories overlapped and this prevented optimum results being achieved. All scatter diagrams showed a high degree of correlation between spectral bands 4 and 5 (Table 7.1). Separation of categories into clusters was dependent on the size of the standard deviation, (shown in Table 7.2). Due to the narrow range of spectral bands and because of the nature of the terrain, standard deviations were not very large; this prevented the isolation of different categories among the scatter diagram clusters. Additionally the minimum, maximum and mean of each spectral band in the training areas were obtained to improve separation of the clusters. Correlation coefficients and regression lines for two or more spectral bands were applied to provide improved understanding of principal component routines in the digital image processing systems.

Table 7.3 shows that for any subscene containing dense vegetation, the correlation coefficients of band 7 with band 5 and also of band 7 with band 4 are less than for subscenes which are not covered by vegetation. This is due to the low reflectance of vegetation in bands 4 and 5 and its high reflectance in band 7. Due to the low pixel values of shadow in all three bands, subscenes which contain shadow and are free of vegetation, are highly correlated between bands. The correlation coefficients of these subscenes on the three bands, are higher than 90%. The variation in the correlation coefficients is independent of the variation in standard deviations. However, the variation of standard deviation corresponds to the

variation of ground features within each subscene. For example in subscene No. 18, highly illuminated areas on sunfacing slopes, plus the considerable amount of vegetation cover, result in broad standard deviations for bands 4 and 5. Conversely in band 7 the high pixel values of vegetation means that the standard deviation is lower than for other bands. Because of the similarity of reflectance of ground features in bands 4 and 5 the correlation coefficients between these two bands are high.

High correlation coefficients between spectral bands makes classification of zones within the study area a difficult task. The easiest data to analysis is that which exhibits low correlation and broad standard deviation between spectral bands. Where this is the case, the investigator can manipulate the data to extract more information. Where data is highly correlated between bands, no further detail can be obtained by manipulation.

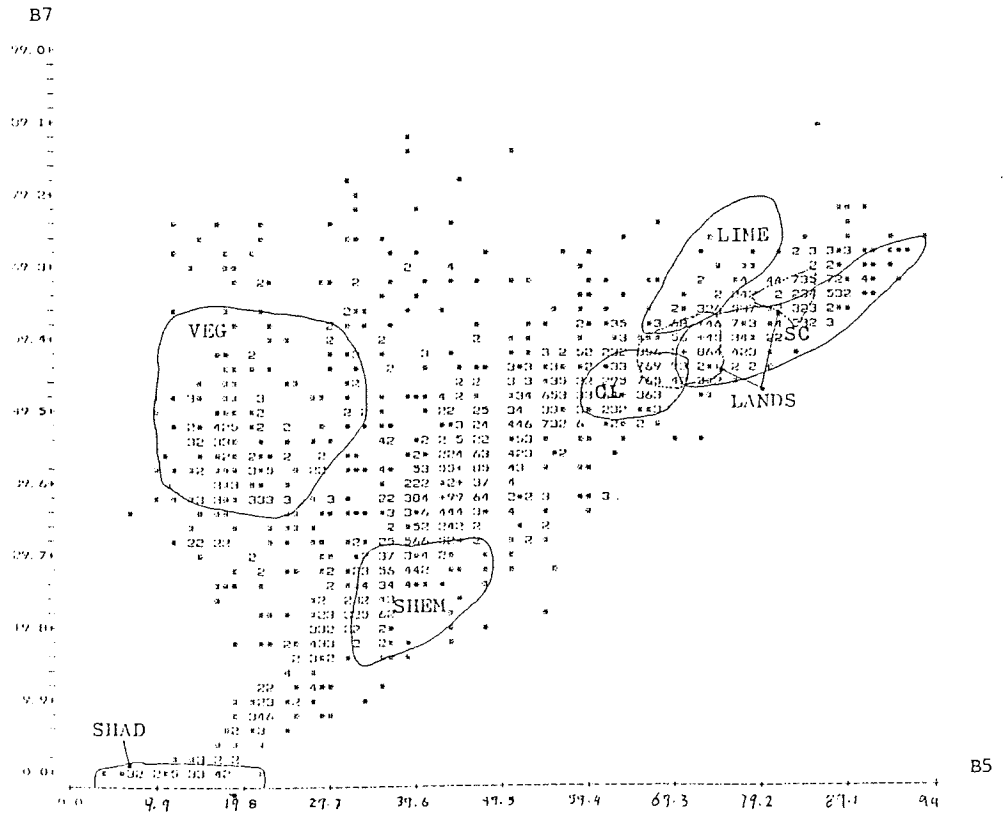

Figure 7.5 Scatter diagram of subscene no. 18. The diagram was plotted band 7 against band 5 showing separation of some features (see section 8.3 for dedails)

Subsc. no.	4 September 1972			13 July 1977			28 Aril 1978		
	7&5	7&4	5&4	7&5	7&4	5&4	7&5	7&4	5&4
1	0.62	0.59	0,96	0.65	0.61	0.94	0.70	0.68	0.94
2	0.29	0.33	0.97	0.13	0.01	0.97	0.03	0.12	0.97
3	0.68	0.68	0.93	0.66	0.65	0.91	0.54	0.54	0.95
4	0.91	0.90	0.96	0.88	0.79	0.92	0.88	0.83	0.97
5	0.95	0.93	0.97	0.94	0.93	0.96	0.95	0.94	0.98
6	0.98	0.97	0.99	0.97	0.96	0.99	0.98	0.97	0.99
7	0.96	0.94	0.98	0.95	0.92	0.97	0.94	0.92	0.98
8	0.85	0.82	0.97	0.79	0.75	0.95	0.86	0.84	0.97
9	0.94	0.91	0.97	0.95	0.91	0.96	0.93	0.91	0.97
10	0.65	0.69	0.98	0.71	0.72	0.97	0.84	0.85	0.98
11	0.95	0.93	0.97	0.95	0.93	0.96	0.94	0.93	0.97
12	0.84	0.81	0.95	0.84	0.83	0.96	0.85	0.83	0.97
13	0.76	0.74	0.93	0.77	0.75	0.92	0.80	0.78	0.96
14	0.87	0.85	0.98	0.82	0.80	0.96	0.87	0.86	0.98
15	0.97	0.95	0.98	0.97	0.95	0.98	0.96	0.95	0.99
16	0.93	0.91	0.98	0.92	0.90	0.96	0.89	0.89	0.98
17	0.87	0.87	0.98	0.84	0.84	0.98	0.87	0.85	0.98
18	0.68	0.69	0.98	0.50	0.50	0.97	0.56	0.59	0.99
19	0.70	0.71	0.99	0.54	0.53	0.97	0.61	0.63	0.98
20	0.52	0.54	0.97	0.44	0.41	0.95	0.44	0.43	0.98
21	0.50	0.50	0.97	0.38	0.40	0.92	0.49	0.51	0.98
22	0.77	0.75	0.96	0.70	0.65	0.96	0.76	0.74	0.98
23	0.67	0.62	0.92	0.68	0.61	0.94	0.67	0.64	0.94
24	0.92	0.86	0.95	0.79	0.71	0.93	0.85	0.82	0.97
25	0.87	0.79	0.95	0.74	0.70	0.95	0.83	0.79	0.97
26	0.72	0.66	0.96	0.50	0.45	0.95	0.66	0.63	0.97
27	0.88	0.80	0.93	0.64	0.49	0.89	0.71	0.68	0.97
28	0.57	0.56	0.96	0.07	0.03	0.94	0.40	0.38	0.96
29	0.86	0.84	0.97	0.73	0.69	0.95	0.82	0.82	0.96
30	0.93	0.91	0.96	0.90	0.87	0.97	0.79	0.75	0.97
31	0.93	0.88	0.95	0.82	0.76	0.90	0.92	0.93	0.98
32	0.90	0.83	0.94	0.52	0.35	0.87	0.90	0.94	0.97
33	0.71	0.63	0.86	0.63	0.56	0.88	0.43	0.40	0.92
34	0.88	0.84	0.95	0.82	0.78	0.93	0.88	0.84	0.95
35	0.33	0.36	0.95	0.24	0.26	0.93	0.57	0.60	0.93

Table 7.1 Correlation coefficients of spectral bands in the three images. Highly correlated pixel values in all three spectral bands of all three images specially in bands 4 and 5 makes interpretation and data processing task very difficult.

sub. No.	4 September 72						13 July 77						28 April 78					
	B7		B5		B4		B7		B5		B4		B7		B5		B4	
	M.	S.	M.	S.	M.	S.	M.	S.	M.	S.	M.	S.	M.	S.	M.	S.	M.	S.
1	28	10	36	10	39	11	22	8	29	10	35	11	34	10	29	11	24	9
2	20	12	23	12	25	12	22	12	20	11	25	11	34	15	17	12	16	8
3	21	9	33	8	34	8	19	8	28	8	33	7	29	9	26	9	21	7
4	23	12	43	12	40	13	22	8	37	9	43	10	29	10	35	10	28	12
5	28	13	46	13	50	13	27	11	44	12	51	12	33	12	42	15	34	11
6	20	21	36	23	38	24	22	18	37	21	42	22	24	20	32	26	25	26
7	18	15	35	14	37	14	20	13	35	13	40	13	24	14	32	15	25	11
8	18	13	35	13	38	13	20	11	36	11	42	11	23	12	31	14	26	10
9	17	10	36	10	38	11	20	10	36	11	41	11	23	10	31	12	25	10
10	22	17	35	14	37	14	23	15	35	14	40	14	25	15	31	16	25	12
11	23	13	39	13	41	13	41	12	26	13	44	13	28	12	36	13	29	10
12	23	12	37	10	39	10	24	11	36	11	42	11	27	11	33	12	27	9
13	21	11	34	9	36	9	23	10	35	9	40	9	26	10	32	10	26	8
14	38	17	44	17	45	16	37	14	44	15	47	14	38	14	40	17	31	12
15	33	21	44	20	45	21	34	16	45	18	49	17	33	18	40	21	32	15
16	44	20	51	17	41	17	41	16	50	16	53	15	41	17	46	19	36	13
17	40	18	52	20	53	20	41	16	52	21	56	20	40	15	47	21	37	15
18	45	17	49	21	49	21	47	11	50	18	53	16	45	13	46	21	35	14
19	54	19	59	20	60	20	49	14	56	18	60	17	49	16	53	20	41	15
20	49	13	52	14	54	14	46	9	52	13	55	12	46	12	49	16	38	11
21	51	15	48	13	49	14	49	12	46	13	50	12	48	14	45	14	36	10
22	41	17	44	14	44	14	42	13	43	12	47	11	40	15	41	15	32	11
23	45	11	45	9	44	8	45	10	43	10	46	10	43	9	44	10	33	7
24	39	16	42	12	41	12	46	12	44	11	47	10	39	13	42	15	33	12
25	43	14	46	11	45	11	45	13	44	12	47	11	38	12	41	13	32	10
26	51	11	47	11	46	11	51	10	42	10	45	12	41	10	37	13	28	9
27	50	11	51	10	48	11	57	10	51	10	51	9	48	11	49	17	37	14
28	54	12	49	11	46	11	59	11	42	12	45	12	50	12	39	12	30	9
29	57	16	59	16	56	16	60	15	58	16	58	15	52	16	57	22	44	20
30	52	19	55	16	53	16	49	16	52	15	53	13	46	17	48	18	37	13
31	40	13	46	10	42	8	44	11	46	8	47	7	41	18	51	22	40	22
32	46	12	49	11	43	10	49	9	49	8	48	7	63	23	76	23	66	28
33	58	8	60	6	52	6	52	9	54	8	51	6	47	8	47	8	33	5
34	45	12	51	11	44	9	40	10	45	10	44	8	36	10	40	10	28	7
35	46	13	47	12	43	11	41	10	44	11	44	10	38	10	37	10	27	7

Table 7.2 Mean and standard deviation of spectral bands in the three images. Data was deliberately stretched in the region of 0-100. Low standard deviation means the ground features within that subscene are homogeneous. Highly illuminated areas and vegetation cover engaging a part of a subscene is the reason whythere is a high standard deviation in that subscene.

sub. No.	Band 7				Band 5				Band4				Correlation between bands		
	minimum	maximum	mean	standard deviation	minimum	maximum	mean	standard deviation	minimum	maximum	mean	standard deviation	7&5	7&4	5&4
1	0	56	28	10.04	6	61	36	10.22	4	70	39	10.78	0.62	0.59	0.96
2	0	60	20	11.85	1	56	23	12.48	2	62	25	12.42	0.29	0.33	0.97
3	2	59	21	8.57	12	67	33	8.22	16	66	34	7.96	0.68	0.68	0.93
4	0	60	23	12.16	6	70	43	12.29	4	74	40	13.25	0.91	0.90	0.96
5	0	77	28	13.22	10	99	46	13.73	8	99	50	13.19	0.95	0.93	0.97
6	0	69	20	20.07	3	87	36	22.85	6	93	38	24.32	0.98	0.97	0.99
7	0	64	18	14.59	4	78	35	13.86	6	82	37	13.71	0.96	0.94	0.98
8	0	57	18	12.63	8	74	35	12.89	10	80	38	12.94	0.85	0.82	0.97
9	0	52	17	9.75	11	73	36	10.42	8	74	38	10.59	0.94	0.91	0.97
10	0	92	22	17.22	4	78	35	13.89	8	82	37	13.94	0.65	0.69	0.98
11	0	71	23	13.09	6	87	39	12.35	6	91	41	12.76	0.95	0.93	0.97
12	0	61	23	11.78	12	80	37	10.37	14	78	39	10.02	0.84	0.81	0.95
13	0	62	21	10.69	10	69	34	8.86	12	66	36	8.92	0.76	0.74	0.93
14	0	93	38	17.47	12	95	44	16.51	10	97	45	15.84	0.87	0.85	0.98
15	0	87	33	21.32	3	96	44	19.59	6	99	45	20.51	0.97	0.95	0.98
16	0	85	44	20.01	4	89	51	17.29	6	95	41	17.30	0.93	0.91	0.98
17	0	92	40	18.08	11	99	52	20.42	12	99	53	20.46	0.87	0.87	0.98
18	0	88	45	17.10	4	98	49	20.83	4	99	49	20.90	0.68	0.69	0.98
19	0	99	54	19.49	10	99	59	20.34	12	99	60	20.23	0.70	0.71	0.99
20	4	96	49	12.63	7	94	52	13.94	10	99	54	14.24	0.52	0.54	0.97
21	7	94	51	15.42	17	88	48	13.43	21	89	49	13.57	0.50	0.50	0.97
22	0	81	41	17.16	7	85	44	14.17	6	91	44	14.48	0.77	0.75	0.96
23	4	88	45	11.00	15	88	45	9.17	17	93	44	8.11	0.67	0.62	0.92
24	0	84	39	15.77	0	80	42	12.26	0	80	41	12.15	0.92	0.86	0.95
25	0	75	43	13.81	12	80	46	10.83	8	85	45	10.97	0.87	0.79	0.95
26	0	99	51	10.79	15	99	47	10.84	11	99	46	11.15	0.72	0.66	0.96
27	7	99	50	11.18	23	99	51	10.24	19	99	48	10.74	0.88	0.80	0.93
28	17	81	54	11.94	21	79	49	11.37	19	83	46	11.08	0.57	0.56	0.96
29	11	95	57	15.85	27	99	59	15.72	25	95	56	15.94	0.86	0.84	0.97
30	0	95	52	19.29	15	89	55	15.80	15	85	53	15.64	0.93	0.91	0.96
31	3	73	40	12.61	19	73	46	9.57	15	67	42	8.18	0.93	0.88	0.95
32	5	77	46	11.94	23	77	49	11.03	19	73	43	9.99	0.90	0.83	0.94
33	23	83	58	8.16	19	85	60	6.27	21	77	52	5.66	0.71	0.63	0.86
34	13	75	45	12.33	23	81	51	11.31	19	71	44	9.20	0.88	0.84	0.95
35	11	87	46	12.61	13	77	47	12.45	15	73	43	10.67	0.33	0.36	0.95

Table 7.3 Characteristics of pixel values of 35 subscenes in the September image. Columns 2, 3, 6, 7, 10 and 11 show minimum and maximum of pixel values after stretching 0-100, columns 4, 8 and 12 are mean values of all 1600 pixel in every subscene and columns 5, 9 and 13 are standard deviations of the data. Columns 14, 15 and 16 are correlation between three bands of the image.

7.3.6 Summary

Statistical manipulation of Landsat MSS data can be a useful guide to digital image processing. Interpretation of subtraction of two spectral bands can create good separation between scatter diagrams, whereas addition can intensify the data density to allow extraction of information through the application of principal component analysis in digital image processing.

7.4 CONCLUSION

The image processing and data analysis described in this chapter was undertaken to find an optimum means of manipulating the data for detailed study. All the computer facilities at Aston Universiy were employed, and the maximum capacity of the available software available was utilised. Comparison of the greymaps with ground truth showed that these analyses can be useful in recognising ground features and even in correcting entire maps. Statistical analysis of the data helps the investigator to understand the concepts of data manipulation and to save expensive time on image processing facilities. By performing statistical analysis the user can decide which kind of processing is most appropriate for the data being studied.

Since this work was carried out the University of Aston has bought a number of Tektronix terminals which can be connected to the Harris and the VAX computers. These are capable of colour display and enable the user to produce colour printouts of the displayed images. For subsequent research it will be more convenient and fruitful to use these new devices to carry out the image analysis operation described in this chapter. Some examples are shown in chapter 8 to demonstrate the capabilities of these facilities.

CHAPTER 8

DISCRIMINATION OF LITHOLOGIES, UNSTABLE SLOPES AND TECTONIC FEATURES

8.1 INTRODUCTION

Processed digital images of the study area obtained on four different dates (see App.A) showed scope for distinguishing between land cover categories. Several types of processing and display techniques have been examined and the results are outlined and evaluated in this chapter.

The relatively small size of the unstable areas in the Haraz Valley and extremes of relief in the area, impose considerable limitations on the utilisation of MSS data. As mentioned in chapter 7, a new and original package for image display was developed at Aston University for providing cheap and detailed analysis of chosen image subscenes.

Interactive image processing of the data was performed mainly on the DIPIX computer at the Open University and the GEMS system at Silsoe College. The lack of an image processing system at Aston was a limitation which prompted work on developing an in-house package.

8.2 HARDCOPY

Two false colour composites (FCCs) of the study area, (scale 1:250,000) were purchased from NASA. The first, taken in April 1975 (Plate 8.1) shows mainly snow cover of the highlands; while the other, (Plate 8.2) which was taken in September 1972, reveals more information on the land cover of the highland area. In addition, positives and negatives of single bands, plus colour transparancies of both images were obtained.

8.2.1 Black and White Prints From 70mm Transparencies

Black and white negatives of single bands can be printed at various scales. Prints of differing tones were produced from these single band negatives by various combinations of aperture and exposure time. The resultant photographs were viewed stereoscopically to help in the detection of topography and drainage systems. A map was prepared of the main drainage patterns in the study area to give a better understanding of the topography. For a fuller interpretation of Landsat imagery, it is necessary to identify the location of slopes. By devising a slope map of the area, it was possible to estimate the degree of illumination. As with aerial photography, in highly shadowed areas, MSS imagery can only provide very limited information. Thus the investigator has to extrapolate the extent of ground features in shadow by comparison with those in illuminated areas. This limitation can be overcome by using other sorts of imagery, such as Radar or thermal infrared, to enable the interpreter to extract true data from shadowed areas.

8.2.2 Colour Additive Viewer

A colour additive viewer was employed to print hardcopies from 70 mm positives at the National Remote Sensing Centre in Farnborough (NRSC). The machine consists of three enlargers which are illuminated by the three primary light colours, green, blue and red or by the three complementary colours, cyan, yellow and magenta. The density of colours is adjastable to allow for colour balance of the output print. The enlargers are also adjustable for zooming in on specific areas of the image. Several different FCCs at 1:1000000 scale were produced for primary image interpretation, giving a good understanding of the

different band concept. Significantly detailed changes in the multitemporal imagery could be detected by careful manipulation of the colour additive viewer. In addition, the instrument can produce positives and negatives for use in diazo processing.

8.2.3 False Colour Composites

False colour composites are constructed by combining three bands, 4, 5 and 7 (1,2 and 4 in Landsat 4 and 5) using the complementary colours, Cyan, Yellow and Magenta respectively. By use of the Electron Beam the imagery has been corrected for pitch, yaw, spacecraft instabilities, scanning mirror fluctuations and Earth rotation. These products can be obtained from NASA and NOAA at a scale of 1:250,000 or less. The primary interpretation of the image was carried out visually using only the two FCCs from NASA (Plates 8.1 and 8.2). The results of interpretation showed certain differences with existing geology and topographic maps. These maps were combined, or copied from existing air photo based maps, by consultant engineers involved with the Haraz Road construction. Only the 1:250,000 scale topographic map prepared in 1971 showed an acceptable level of accuracy.

8.2.3.1 Vegetation

Without access to computer facilities, and relying totally on the use of two colour composite images, interpretation accuracy proved to be good but somewhat limited. Nevertheless the use of overlays produced from a topographic map of the same scale as the images (1:250,000), has revealed areas of known vegetative cover which in turn have been employed as control areas from which other areas have been identified.

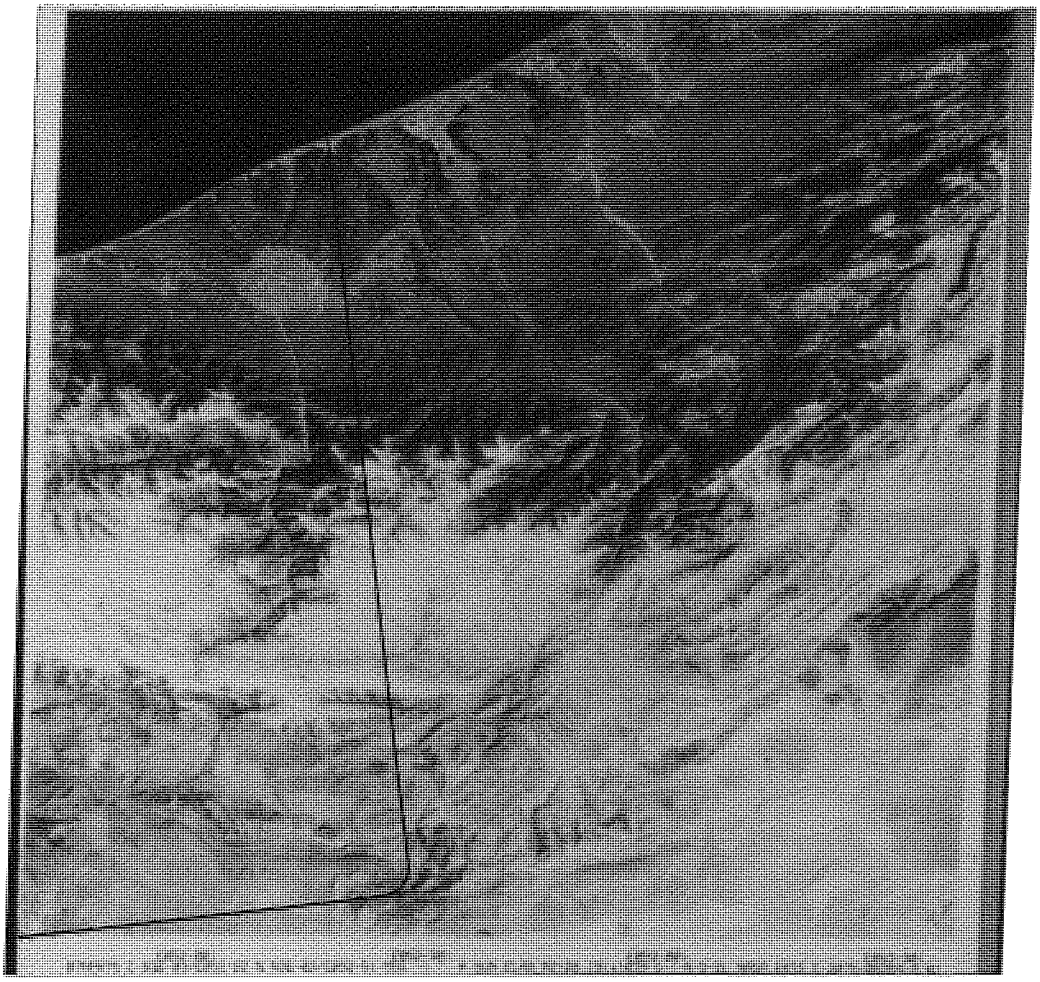

Plate 8.1 False colour composite of N. Iran, 7 April 1975. The study area is located northeast part of the scene. Scale 1:2,000,000.

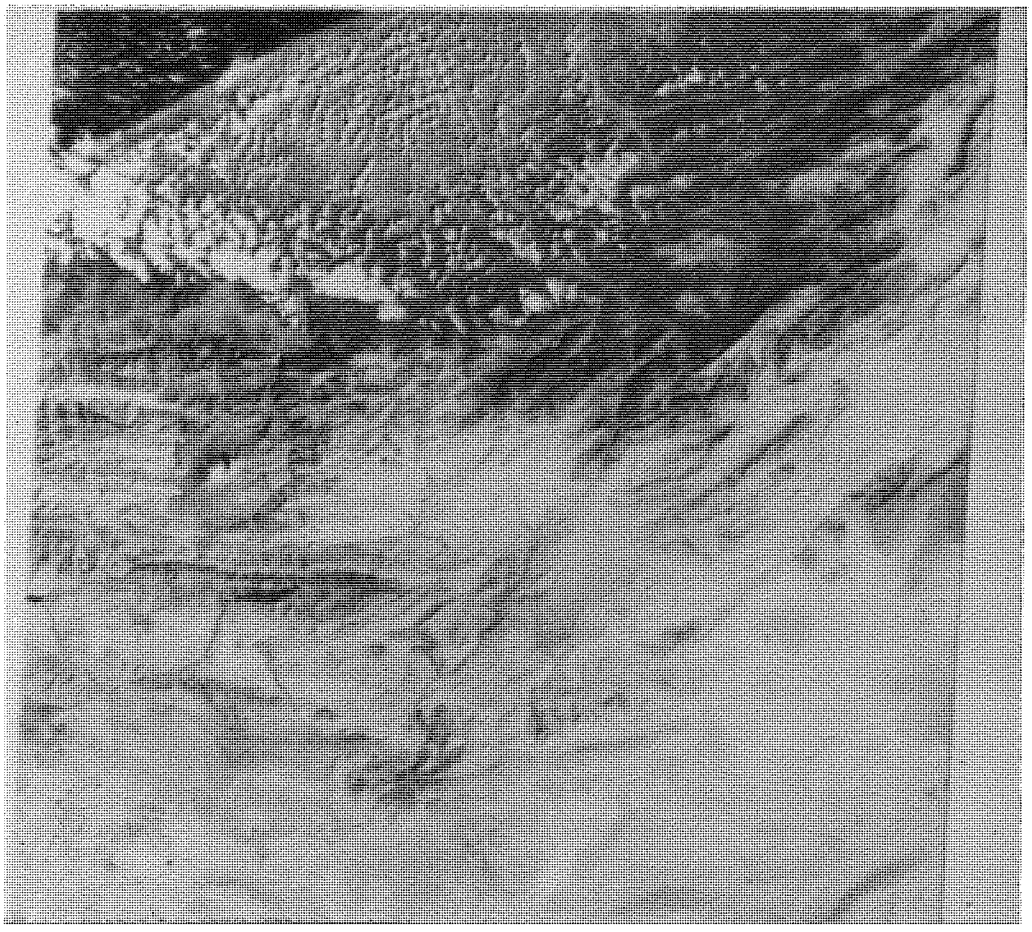

Plate 8.2 False colour composite of N. Iran, 4 september 1972. Scale 1:2,000,000.

Having only visual data (the two images) all data supplied must be utilised; such as the identification of topography. Rice and forestry, for example, are two areas that may appear identical in radiance levels of one band. However, if the particular area is mountainous then the likelihood of the area containing rice fields is minimal. Other data supplied by the image such as drainage, the possible recognition of soil type and accessibility, may not at first be apparent.

Having two images taken in September and April respectively is of great importance for interpretation and boundary delineation. As vegetative cover varies with the season of the year rice does not show up on the April image which allows delineation of the bordering forested area. Using the September image it is possible to complete the boundary for rice as it is fully grown and shows up clearly in band 7.

8.2.3.2 Forested Areas

Land cover contrasts are important in the delineation of any boundaries. Computer methods have been devised to enhance and increase contrasts. As a result delineation of boundaries is made simpler and these methods offer a more scientific and accurate approach.

As the southern limit of the forest is found to occur in the mountains, delineation of the boundary using the April image is not possible because the mountains are covered in snow. The September image does produce a good contrast between the forest and the bordering land cover (bare rock, soil). The forest boundary

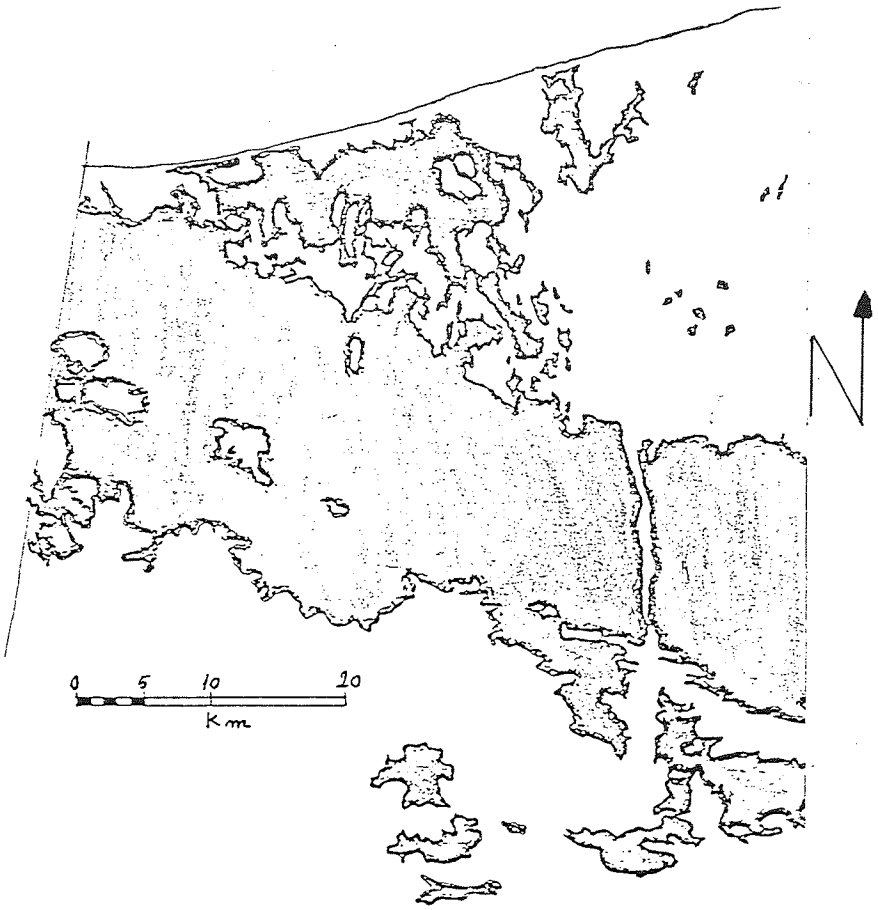

(a)

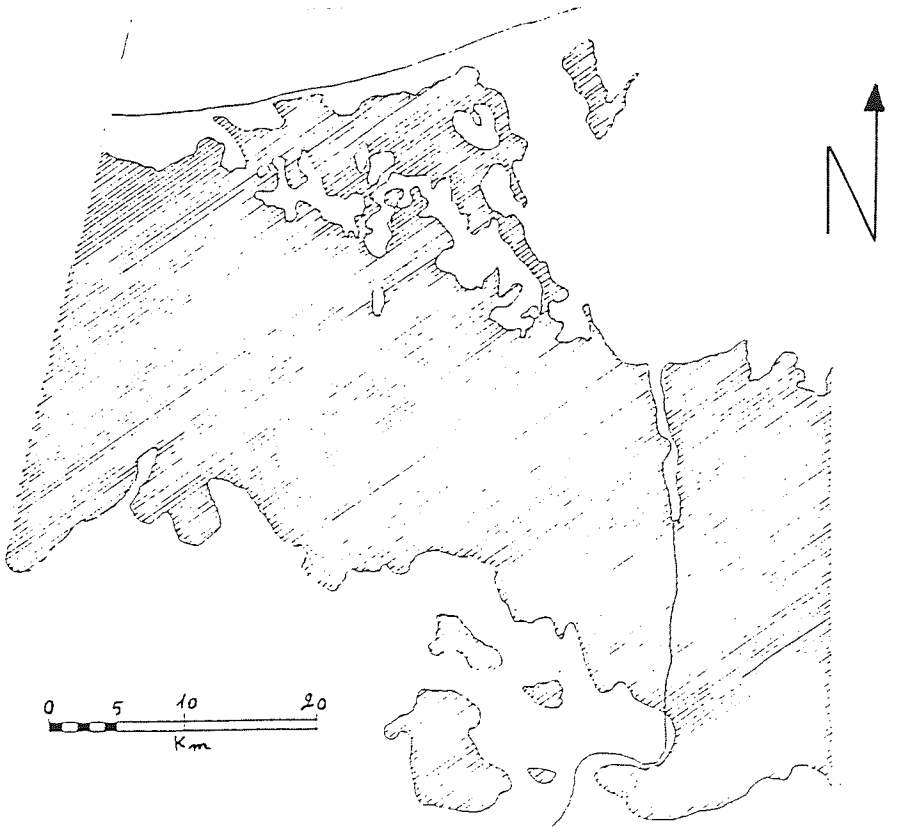

(b)

Figure 8.1 Forest area. a) Forest area derived form topographical map, b) forest area derived from the two Landsat MSS images.

delineation in the September image corresponds well with the overlay. The forest belt (Figures 8.1a and 8.1b) running approximately east-west, can be identified in both images and the topographical map.

The northern boundary of the forest borders mainly rice fields. Rice fields are sown in March-April in a significant depth of water. The water predominates the April image in all bands and hence a good contrast occurs with the forest's in band 7. Although the boundary delineation in these images correspond successfully with the overlay (Figures 8.1a and 8.1b) there are some small exceptions (Table 8.1). The rice fields appear to have extended into the forest (as delineated by the overlay) suggesting that some forest has been cleared for more rice fields.

The northern boundary can be delineated using the September image but using visual methods only may cause difficulites. In September the rice is mature and has a high band 7 characteristic which corresponds with the band 7 reflectance of coniferous forests.

The overlay Figure 8.1a, is derived from the topographical map, and Figure 8.1b, is drawn from the two images. Comparison of these two Figures indicates an area of forest in the southwest region of the image. The images show no corresponding associated with forest in this area. Both the overlays are produced from data compiled at approximately the same time, (the April image was taken five years after the topographical map was made) hence date differential as an answer to this anomally is unlikely, especially when the area of forest in question is large. The time to clear the forest would exceed the maximum time differential possible between the data compilations. The only conclusion which can be drawn is the

replantation of forest which was carried out by Government in this period of time.

Table 8.1 indicates correlation between the map and the two images at the same scale. The foresty areas measure 15% more than that on the map. The data derived from the images missmatch 6% and overmatch 21% comparing with the map.

8.2.3.3 Cultivated Areas

The greatest source of information for cultivated areas came from the contrasts between the two images. As crops are seasonal vegetation, April and September are good times for images to be recorded. April is generally the season when the sowing of crops takes place while September is the season for their harvesting. Therefore April has virtually no band 7 radiance values and the July image the colour composite of which was not available has potentially the greatest, thus producing the largest possible contrast. However, the September image shows better contrast.

Using printed images, discrimination between crop types is very difficult, with the exception of rice. As mentioned previously the growing periods are approximately the same and as a result information would have to be employed based on topography and drainage combined with crop characteristics. Unfortunately no ground truths, other than the topographic map were available. The referenced control indicated on the topographic map was for 'cultivated areas' and thus discrimination of crop types was not possible(Figure 8.2). This emphasises the importance of ground truths have in image interpretation of land cover.

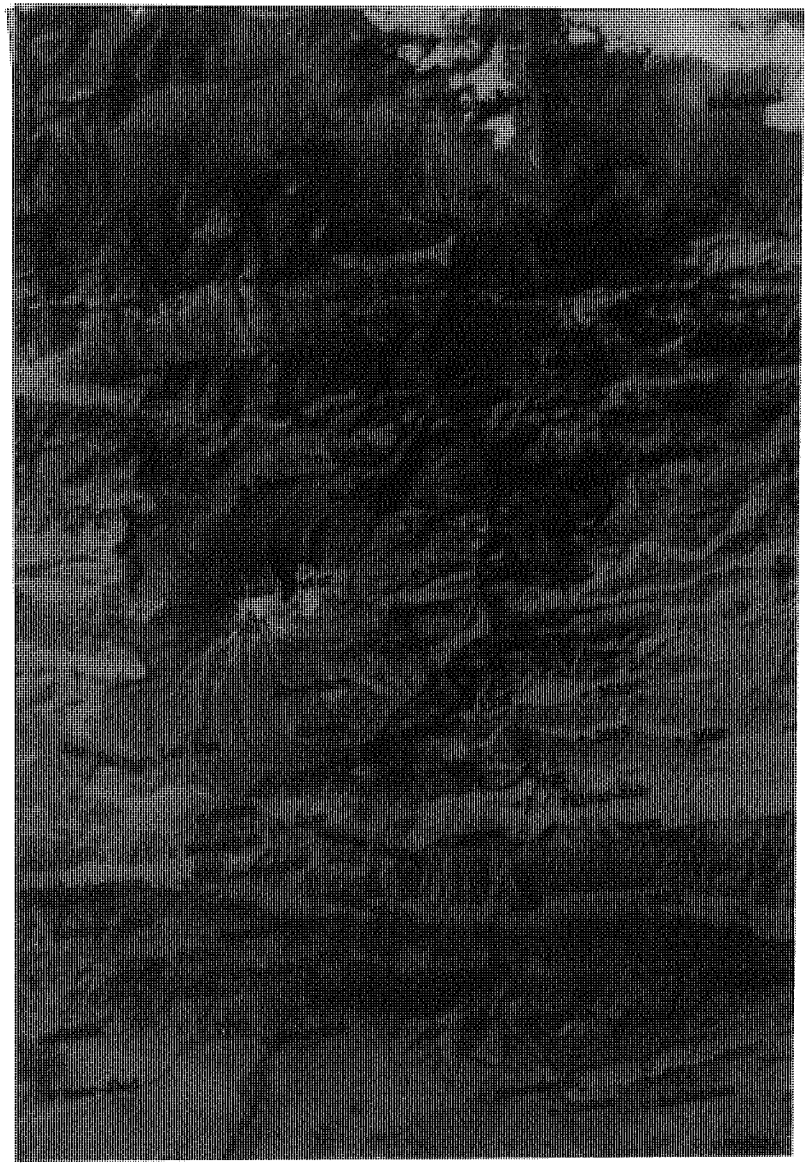

Plate 8.3 Settlements. Location of settlements superimposed on the Landsat MSS image.

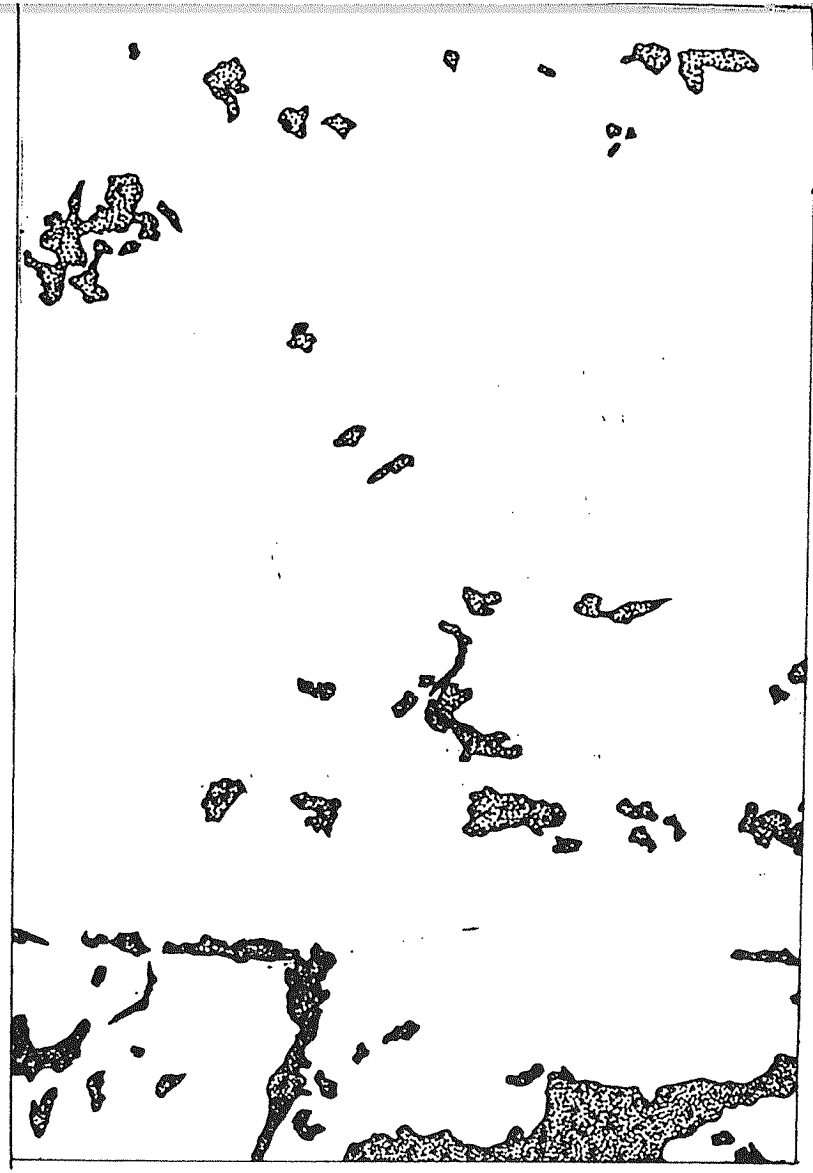

Figure 8.2 Cultivated areas. derived from topgraphical map.

In delineating the boundaries of crops, consideration had to be given to the surrounding land cover. The reason being the delineation of boundaries is made easier when effective contrast exists with the bordering land. Hence for the cultivated areas in the forested regions of Northern Iran, the most suitable image to use is the April one as the crops are very young and vegetative cover is minimal. Therefore bare soil predominates showing up clearly in band 5.

Also in the April image, areas of cultivation in the snow covered mountain region cannot be successfully interpreted and as a result delineation is not possible.

On the September image cultivated areas in the mountains are not easily distinguishable, as in band 7 there are traces of red strewn all over the mountains. As this is the case the visual delineation of boundaries is made difficult.

In the region south of the mountains the overlay of crop boundaries does not correspond with any featured boundary of the image. This may be due to an outdated form of crop rotation and could be overcome by using multidate images which should allow the correlation of boundaries to occur. Other reasons may be poor yield leading to a clear image on band 5 or short growing time with the crop having been shown after April and harvested before September.

For a better comparison all settlements situated in the study area where naturally represent orchards and cultivated areas were teken on overlay from topographical map and superimposed to images. The result of this comparison as shown in (Plate 8.3) proves significant coincidence.

8.2.3.4 Rice Fields

As mentioned previously, the rice fields in April are dominated by water. Thus as a result all rice fields bordered by forests are most easily delineated in April (Figure 8.3b).

Varying species of crop are also intermingled in the rice fields. In the September image the band 7 characteristics of rice and the intermingled crops appear visually similar. Hence boundary delineation in the September image is difficult. In April the rice fields covered in water are predominant, visually, in bands 4 and 5. The intermingled crops are, in the April image, predominately high reflectence in band 5 (bare soil) contrasting well with the water.

As the April image produces the best contrasts and because cloud cover exists in the September image, only the April image was employed. Boundary delineation was found to correspond very well apart from small areas which have been discussed previously in forestry delineation. Figure 8.3a is drawn from the topographical map and quantitative comparison between that and Figure 8.3b is shown in Table 8.1. As can be seen in Table 8.1 identification of rice fields from the images measures 7% less than that on the map which has been prepared by field controlled survey using aerial photographs. The images mismatch 10% in correlation by map, whereas they overmatch 5%.

8.2.3.5 Geology

Simple visual interpretation does not reveal much information about the geology of the area under study. Different types of rock can be delineated from the changes in tone and colour, but they cannot be characterised. Because of gradual change in tone, from one rock

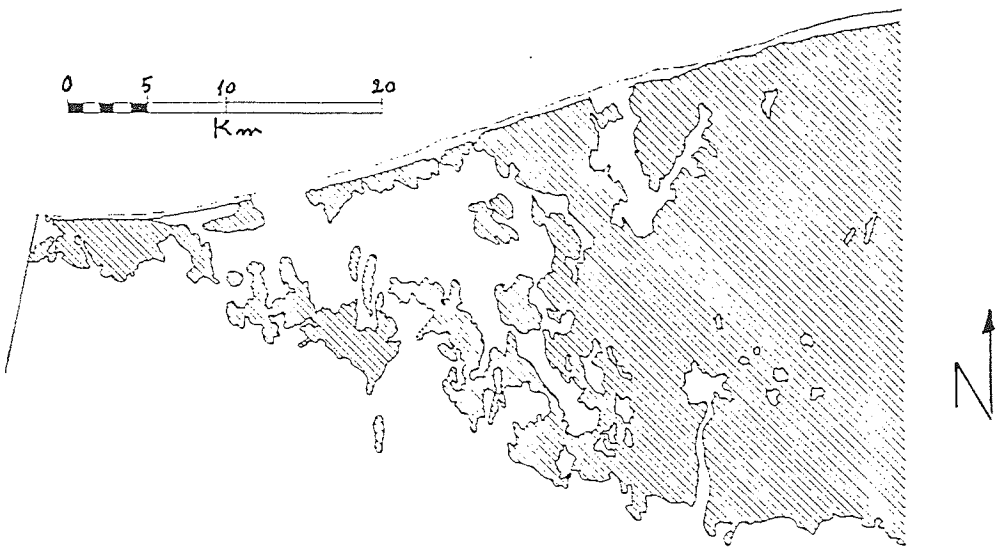

(a)

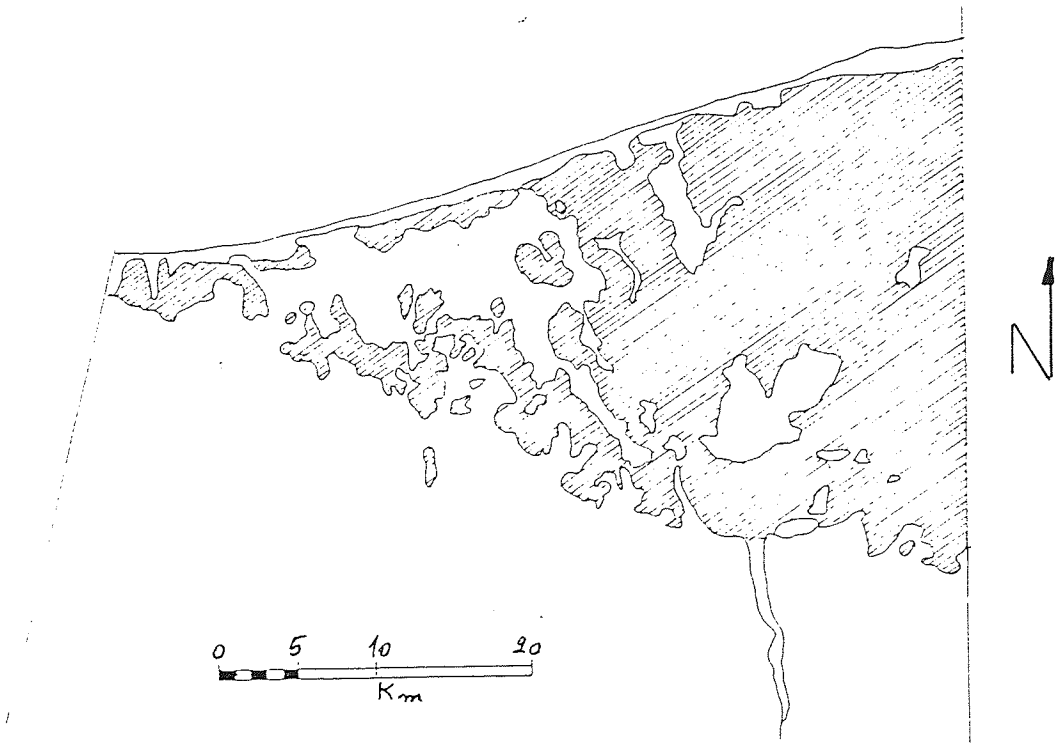

(b)

Figure 8.3 Rice fields overlay. a) Rice fields drawn by overlaying from the topographical map which located on vicinity of the Caspian Sea. b) Rice fields derived from the two MSS FCCs.

type to another, no distinct boundaries can be drawn between different outcrops of rock. With the aid of the geological map of this area it was possible to distinguish areas of Jurassic coal and outcrops of limestone. The Desert region in the South east portion of the image was delineated most easily.

Relying on tonal changes to aid interpretation can be misleading, especially in the presence of shadows. Both Jurassic coal and some of the shadows exhibit similar tones in the false colour composite. Relying on colour can also be misleading, especially if more than one image of the same area is used. This was highlighted by the images used in the interpretation. The colour presentation of the April image is much bolder than the September image. Therefore similar features are displayed in different colours in the two images.

In areas where there is extensive snow cover very little information about underlying rock is obtained. Similarly areas of extensive vegetation cover reveal very little information about the underlying rock. However, it is sometimes possible to predict the type of soil from vegetation. This is because some types of vegetation have affinity for particular types of soil. Physical features such as drainage patterns and shapes of valleys are good indicators of rock types, hence geomorphology of area can be distinguished using this method.

8.2.3.6 Drainage

As the effective image ground cell resolution (in terms of the smallest adjacent ground feature which can be distinguished from each other) of the Landsat image is approximately 79 m on the MSS image, severe limitations would be expected in the visual interpretation of

the drainage pattern. The reason may be that the size of the small water bodies (rivers and streams) which are much smaller than the minimum resolution. Fortunately this is not the case and delineation of these features is possible if they possess reflectance which contrasts sharply with their surroundings. This is supported by a remarkable similarity between the drainage pattern overlay (ground truth) and the false colour composites (Landsat images) utilised in the visual interpretation. Comparing the ground truth with the satellite image (Figures 8.4a and 8.4b) shows more drainage pattern (apart from waterfullness) can be delineated from MSS images than from the topographical map at same scale.

8.2.3.6.1 Ambiguities In Interpretation

To avoid misinterpretation of data acquired by satellite, consideration should be given to ambiguities occurring in the image. Therefore, to enhance interpretation, reliable information concerning the ground truth is essential. The main sources of error which could result in misinterpretation are misprinting, cloud shadows and damage to the image. Cloud shadows, can be easily misinterpreted as water bodies such as lakes and reservoirs. As the scale of the image is very small (1:250,000) the effect of false interpretation is greatly exaggerated. Errors due to misprinting are rare and ambiguities resulting from damage to the image (ink marks, etc) can be easily avoided if the image is handled with care. Finally, misinterpretation resulting from cloud shadows can be effectively avoided if methodical procedure is adopted during interpretion. The best strategy is to first choose the satellite image which has least cloud cover obstructing the area under study. The next step is to correctly identify all the shadows associated with the clouds (the shape of

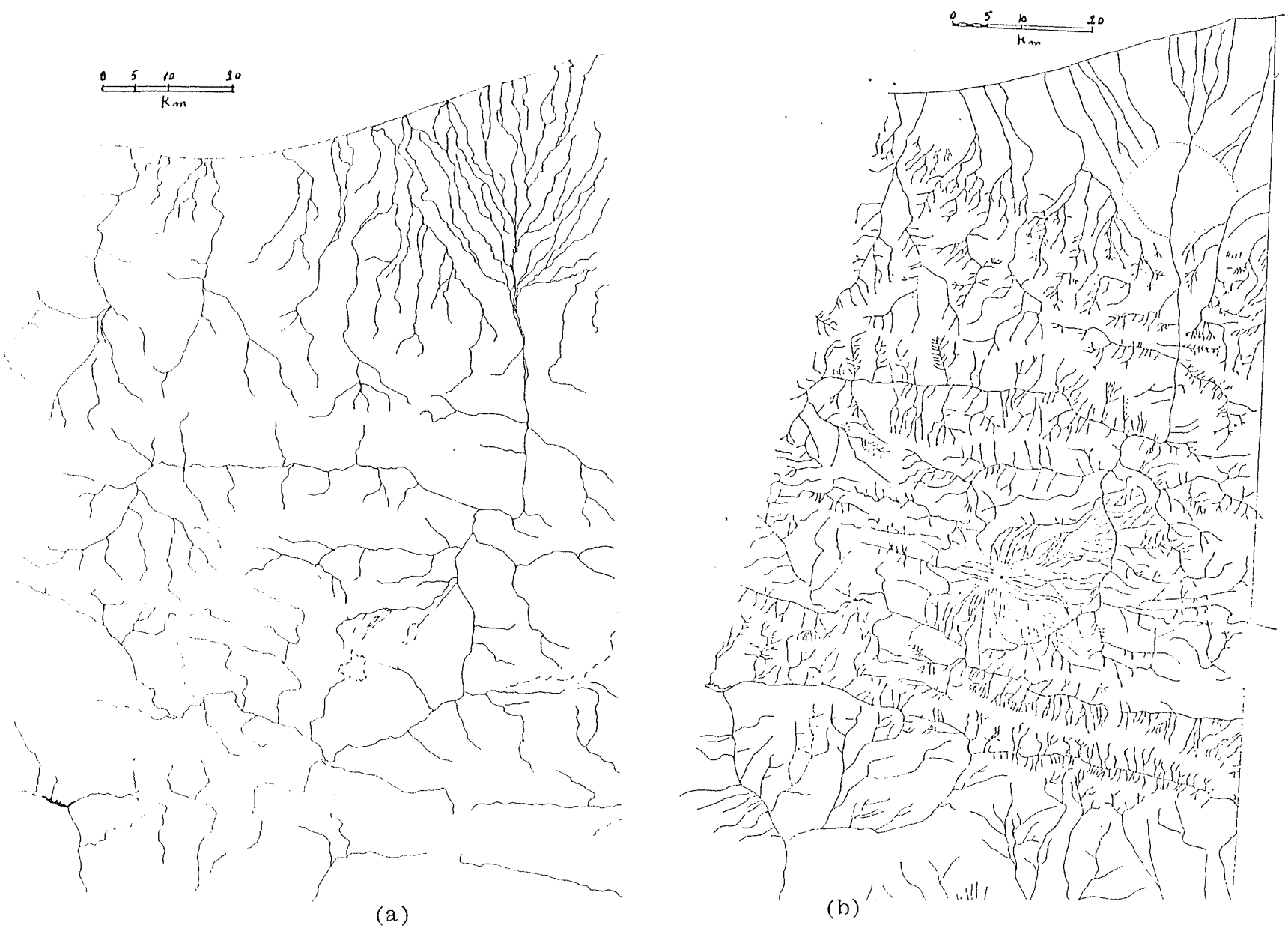

Figure 8.4 Drainage pattern. a) Derived from the topographical map.
b) Derived from Landsat at same area as (a).

shadow is the same as the parent cloud). Once all the cloud shadows have been identified the image can then be used for delineating water bodies. It must also be noted that the detection of clouds against a background of snow cover can be very difficult because of the similarity in their reflectance.

8.2.3.6.2 Catchment Areas

Initially the catchment areas (ground truths) were identified by using the contour overlay (Figure 8.5) prepared from the topographical map. Boundaries of the catchment area are defined by the ridge crests. The area enclosed between the two or more ridges is defined as the catchment for the water courses originating from within that area. Catchment area boundaries show up remarkably well on the image. Identification of ridges is aided by shadow effects and/or snow peaks. All major ridges were identified with relative ease using simple visual interpretation. Once the catchment areas have been identified they can be utilised in extrapolating the line of a river, especially in the upper reaches.

8.2.3.6.3 Drainage Pattern

Drainage is probably the most important indicator of terrain features which have been formed by natural processes. Analysis of drainage pattern can give a great deal of information concerning the parent rock and soil materials since they both influence the amount of runoff and the way in which water drains from a given surface.

In the vicinity of Mount Damavand the type of drainage pattern, obtained from the September image is shown in Figure 8.6a. This pattern is formed by streams that radiate outwards from a central area

Figure 8.5 Contour map. Derived from the topographical map. The north most of the region borded the Caspian sea which is 25 m below sea level.

as is typical of volcanoes and domes. Small streams cannot be delineated successfully as the resolution of the image is 79 m. However the drainage pattern delineated from the September image compares favourably with the overlay (ground truth). The April image does not provide much information about the drainage pattern in this area because of extensive snow cover. In the drainage pattern coarse texture and wide spacing of main streams indicates that there is relatively little runoff. This suggests the presence of permeable bedrock and a lack of stored water.

The drainage pattern dominant in the intermediate region of the river is shown in Figure 8.6b. This pattern consists of the main streams flowing in one dominating direction with tributaries joining the main stream at right angles. Both images can be utilised to provide information about the drainage in this area. Therefore a more the information from the two images.

In the northern region no distinct drainage pattern can be obtained when each image is interpreted separately. Main drainage channels (rivers, streams) can be delineated from the September image and the marshy area shows up quite distinctly in the April image. By combining the information obtained from each image a drainage pattern of the form shown in Figure 8.6c is obtained. Drainage pattern of this type is typical of flood plain and delta areas.

Table 8.1 shows correlation between the map and the images at the same scale which was compared in three parts of the area. In the Northern part covered by forest, including the Caspian plain, discrimination of drainage patern shows 36% improvement in the images. However, 107% improvement in the Central region covering moutainous accurate picture of the drainage pattern can be obtained by combining

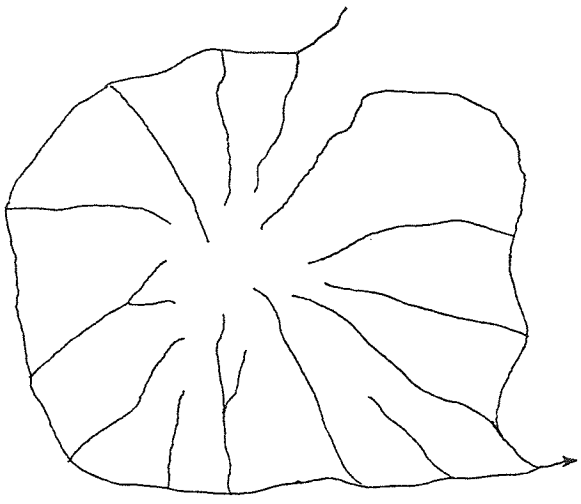

(a)

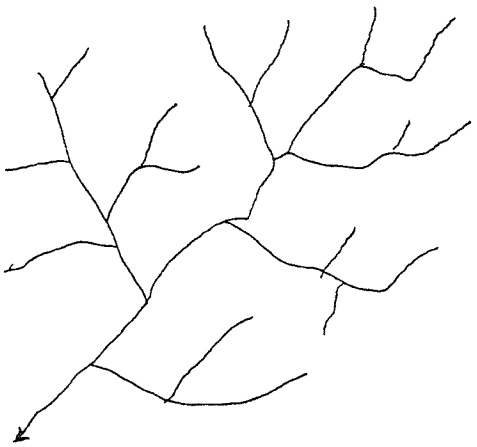

(b)

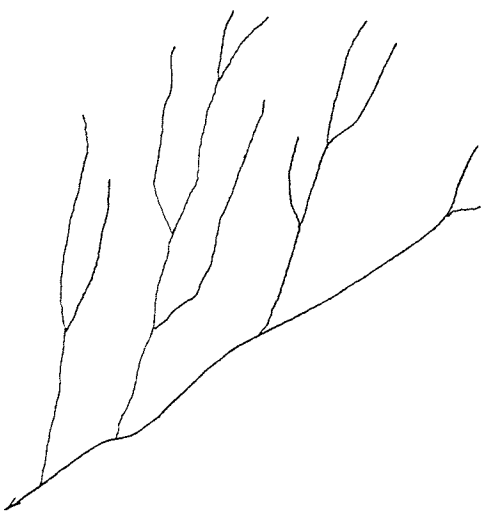

(c)

Figure 8.6 Typical drainage pattern. a) Radial drainage pattern around Mt. Damavand. b) Rectangular drainage pattern in the intermidiate area. c) Parallel drainage pattern Look like in the delta area. (after Way, 1973).

terrain, whereas the Southern part consisting of arid land and relatively moderate topography, there was only 13% improvement.

aera	data source		discrepancy with map		mismatched		under match	
	images	map	amount	ratio	amount	ratio	amount	ratio
Forest (km^2)	1622	1406	+216	+15%	81	6%	302	21%
Rice Field (km^2)	670	720	-50	-7%	74	10%	33	5%
Drainage : (km)								
A) North	1455	1067	388	+36%			388	36%
B) Centre	2332	1125	1207	+107%			1207	107%
C) South	1137	1006	131	+13%			131	13%

Table 8.1 Quantitative data evaluation of the images against the map. Comparison of primary visual information on the two images with the data derived from the topographical map at the same scale.

Note: Mismatched and overmatch are resulted from misregistration of the image with the map whereas discrepancy corresponding to amount of the areas on the image with the map.

8.2.3.6.4 Mapping The Course Of The River (main drainage channel)

It is almost impossible to delineate the river (main stream) and small streams which feed the river in the upper reaches. However if there is good reflectance contrast between the line of rivers or streams and their surroundings, delineation is made possible. This is true where the underlying rock has been exposed by erosion, resulting in contrast between the path of the river and the surrounding rock which shows up as bright streaky lines on the image. The path of the river in the upper reaches can also be extrapolated with the aid of

physical features such as ridges and valleys. These features are distinguished, on the satellite image, by shadow effects. Most of the information about the river is obtained from the September image. However little information is obtained from the April image due to extensive snow cover in the mountainous region.

The path of the river in the intermediate portion (altitude 300 m - upper boundary of forested area) can be delineated with the aid of physical features particularly using April image. In this region the valleys begin to widen out and the ridge crests are no longer sharp thus making their lines difficult to interpret. This tendancy was overcome using a packet stereoscope to view the F.C.C. However, the river swells due to feeding by snow melts in April, and thus the river is clearly visible on the image. Therefore the size of the river and its reflectance contrast is sufficient for its delineation from the April image.

As the river progresses downstream it broadens and is delineated with relative ease. In April, due to the large amounts of water used in rice fields, it is difficult to distinguish the path of the river from surrounding water. This is because March/April time is the beginning of the rice planting season and it is essential to have plenty of water for a good rice crop. In September rice fields are covered with vegetation (fully grown rice) and there is good contrast between the rice plants (vegetation) and the rivers, allowing the path of the river to be clearly seen. However, cloud cover prevents very clear distinction of the river path in teh September image.

8.2.3.7 Conclusion

Land use on the Caspian Sea plain could be distinguished using the two multidate FCCs. Rice fields appear dark and sharply contrasting in the April imagery, whereas in the September image during the growing season they are indistinguishable from adjacent tea plantations and woodlands. Likewise forest due to high biomass reflectivity in band 7 appear red in both images but in September seems the forest cover to have expanded (top left corner plate 8.2). High altitude settlements frequently characterized by a surounding agricultural/ Orchard belt, are obscured in the April image, whereas they show up sharply in the September image. However, due to the nature of small fields, cultivated areas are not distinguishable in both images, only orchards can be assumed as a sign of adjacent settlements. This also makes it difficult to locate cultivated areas within forestry areas. Temporary vegetation which appears pale red and subdued in the September image is obsent in the early spring (April) imge. Cloud cover in September and snow cover in April are the two main limitations to interpretation of the FCC images.

The data (Figure 8.7) extracted from the topographical map of the area has been quantified (Table 8.1). A small forestry area (bottom left corner on Figure 8.7) is not detectable in both images and it can said after examinining other sources that there is no forest in that location. Another significant discrepancy between the images and the topographical map is drainage pattern discrimination. As can be seen in Figures 8.4a and 8.4b the drainage pattern derived from the two images shows far more detail than the topographical map at the same scale.

Bearing these comparisons in mind it is clear thet multidate false colour composite images taken at the begining of all four seasons can be a useful tool in any primary study in arid and semi arid areas. False colour composites produced by Electron Beams which are skewed to the Earth rotation and geometrically corrected provide efficient overall data for a broad area with information on vegetation cover, water bodies, morphology and tectonic features. This information is appropriate for first look in the initial phase of a study.

8.2.4 Line Printer Grey Maps

Grey maps of 35 subscenes along the Haraz Road were plotted at Aston University. As was mentioned in chapter 7, a lack of conventional image processing facilities, necessitated the development of a special software package. Eight grey levels from black to white were employed to demonstrate the variety of reflectivity values existing within the subscenes. After plotting the 35 subscenes, a mosaic map of the whole area was prepared and compared against the ground truth. The comparison clearly showed the inadequacy of MSS imagery in both shadowed and some highly illuminated areas. These grey maps or density sliced plots revealed distortion in both the aerial photography and those maps constructed from aerial photography. Extensive topographical relief prevents obtaining reliable result by this method, and to obtain better output it is recommended to apply this method in areas with only moderate topography. Despite their shortcomings the grey maps are useful for interpreting the details in small areas.

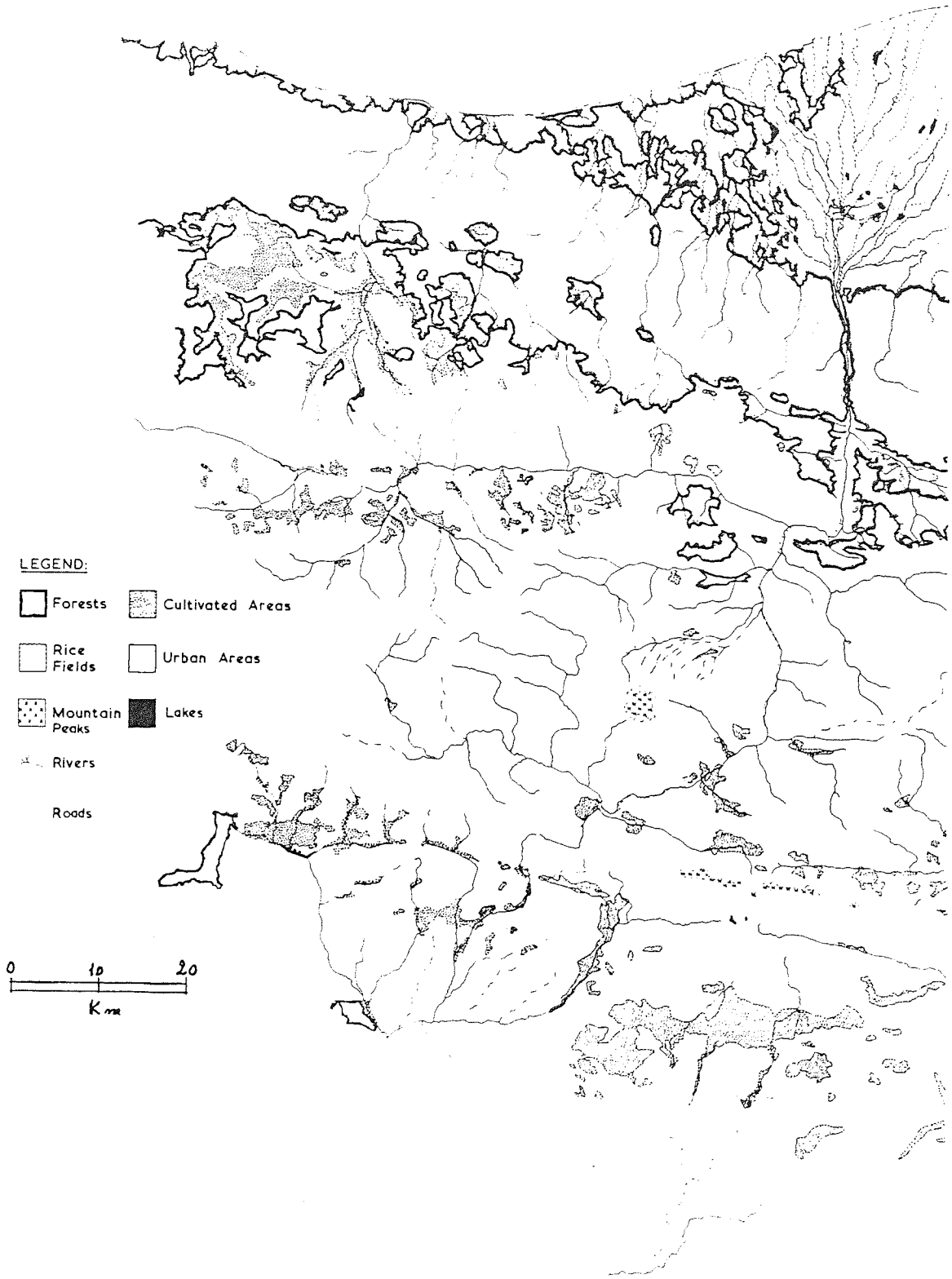

Figure 8.7 Topographic data of the study area. Derived from topographic map.

8.2.5 Colour Prints From The 'TEKTRONIX' Ink Jet Colour Plotter

" Tekronix " terminals recently connected to a VAX mini computer,(July 84), have an ink jet colour plotter facility. A FORTRAN program was developed to enable plotting of the subscenes in eight colours. The software program is similar to that for the grey maps mentioned above but it has the advantage of colour which enables easier interpretation and greater freedom in selecting the scale of the plot.

The package developed can perform mathematical manipulation of the data to produce a variety of combinations viz: additions, subtractions, ratios, and vegetation index/formulae etc. and plots the output data in the form of a histogram. These statistical analyses have been applied to the majority of the subscenes particularly on Nos. 17, 18, 26 and 27. Subscenes 26 and 27 are located near Pulur, and geologically consist of unstable slopes of lavas. Subscene 18 consists of the Shangoldeh landslide with further instabilities in area 17 immediately to the north.

8.2.5.1 Evaluation Of The MSS Data In Comparison With Ground Truths

In the following section each of the four subscenes listed above are described separately. Subscene number 18 (obtained by plotting single bands and combinations of bands after comparing them with ground truths) are outlined first.

In processing subscene 18, plots of single bands in eight colours (black to white) were found to be most acceptable to the human eye. However, due to low values of vegetation in band 5 and higher values of them in band 7, different combinations of the bands showed further

improvement in the identification of ground features. Subtraction of the two bands (B7-B5) showed clearly the boundaries of ground vegetation (Figure 8.8). The high reflectivities of screes and bare soil in both bands 7 and 5 when they were combined in vegetation index (B7-B5/B7+ B5) caused low values in the resultant image (Figure 8.9). Hence all unvegetated areas appeared dark in the vegetation index. By stretching the lower part of histogram representing bare soil and screes, unstable areas with naturally disturbed surfaces could be identified (figure 8.10).

The results of the different combinations were compared against the ground truths at same the scale (1:23,000). The outcome is shown in Table 8.2 comparing results of different combinations of different bands and the ground truths derived from existing maps of the study area.

As can be seen from the eight different combinations in Table 8.2, the best results are obtained after subtraction which allows discrimination of vegetation covered areas (units 1, 2, 3 and 4). The worst combination appears to result from addition of the bands, which provides no basis for significant discrimination of the vegetated areas.

The vegetation index, shown in Table 8.2 and Figure 8.9 highlights vegetated areas, but some areas of dark shadow are also classified in the vegetation class. Hence the use of the vegetation index in unknown areas produces imperfect results. Despite the recommendation of many Remote Sensing texts that a vegetation index should be used as a tool to distinguish vegetated areas in the Landsat MSS images, it seems, on the basis of this research that the best results are obtained by subtracting band 5 from band 7 (B7-B5).

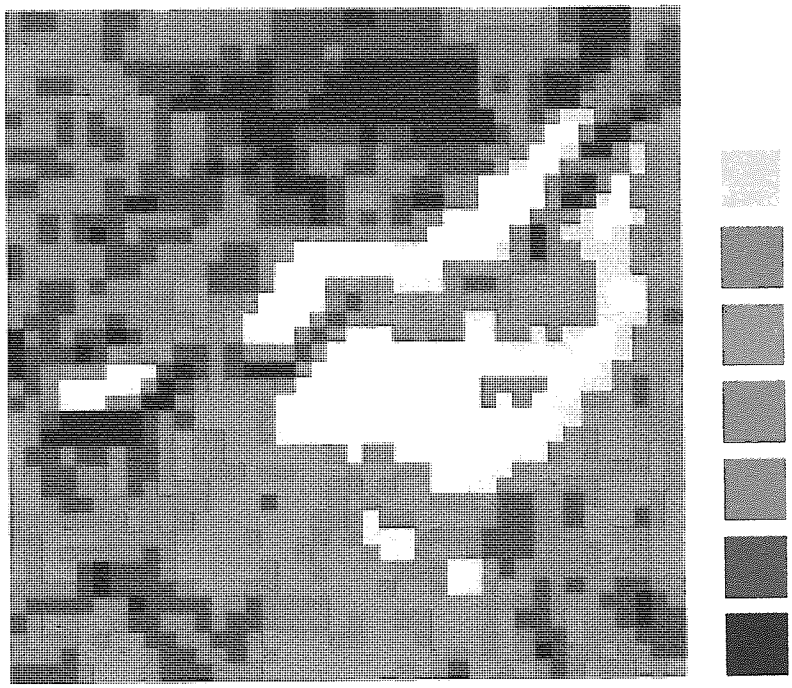

Figure 8.8 Subtraction of band 5 from band 7 of the September image. White and yellow colours representing vegetated areas. Scale 1:23,000

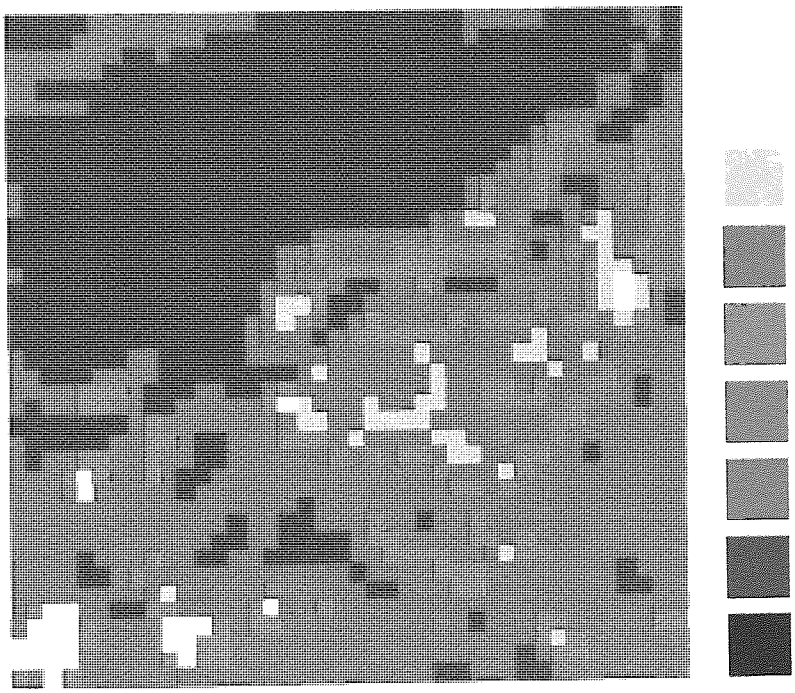

Figure 8.9 Vegetation Index (B7-B5/B7+B5) of the September image. The lowest values represent sunfacing unvegetated areas, while high values correspond to shadow and vegetation. scale 1:23,000

Subtraction of band 4 from band 7 (B7-B4) in both September and July images (figure 8.11) resulted in over classification in three vegetated areas and under classification in one area located on the west facing slope of the Valley (Table 8.2). The shadow is responssible for misclassification in the number 3 vegetated area whereas mixed pixels of high reflection of vegetation in boundaries are responsible for over classification.

Where band 5 was subtracted from band 7 (B7-B5), two sunfaced vegetated areas (units 1 and 2) were found to match the base map (Figures 8.8 and 8.11) whereas two low illuminated areas (units 3 and 4) mismatched (Table 8.2 and Figure 8.12).

Additions of different bands in each of the September and July images revealed no more information in this case. Only by the additions of both band 5 and band 7 (B7+B5) and band 7 and band 4 (B7+B4) does there seem to be slight improvement in landslide discrimination which show positive error in both areas (Table 8.2). It should be mentioned here that addition of two bands in image processing systems in a vast area showed a better result in linear features recognition.

In addition to conventional image procesing techniques, the use of either a vegetation index or subtraction can assist the interpreter in the identification of unstable areas between bare soil and in the classification of vegetated areas. Both procedures should be performed after applying radiometric correction to the MSS image. Without haze removal any mathemtical manipulation on the data will not reveal an acceptable result.

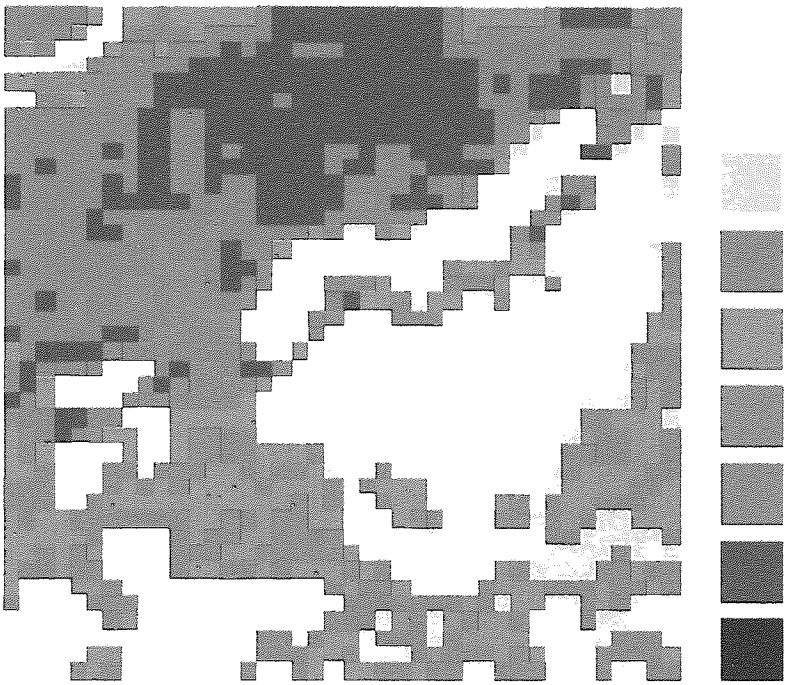

Figure 8.10 Different stretch of VI (Figure 8.9). Scree, the lowest values (black) and landslide located between scree and vegetated area can be delineated in this plot. Scale 1:23,000

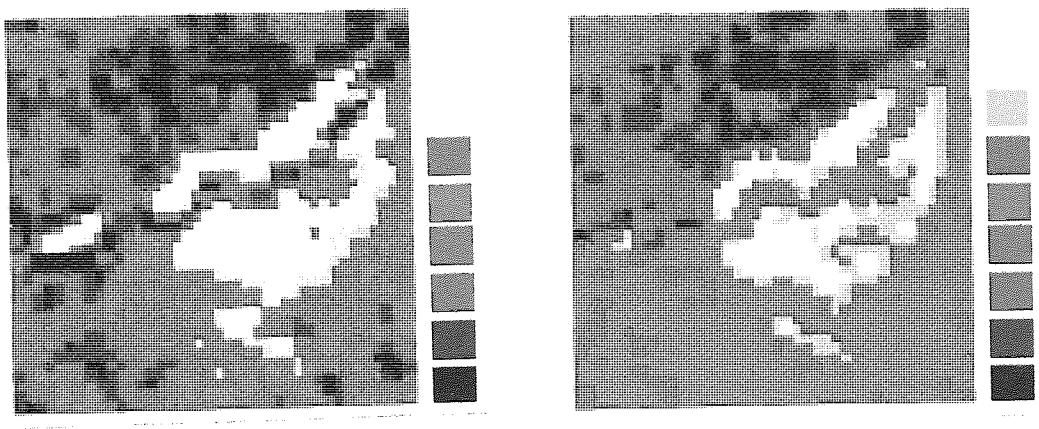

(a) (b)

Figure 8.11 subtractions of bands 4 and 5 from band 7 in the September and July images. a) subtraction of band 4 from band 7 of the September image (high values, white and yellow, correspond to vegetation). b) subtraction of band 4 from band 7 of the July image (also high values represent vegetation). scale 1:40,000

area	veg.1 plain Alfalfa farms		veg.2 sunfacing farms/orchards		veg.3 poorly illuminated orchards		veg.4 poorly illuminated wood lands		sunfacing landslide	
combination of MSS bands	measurement square metre	% match	measurement square metre	% match	measurement square metre	% match	measurement square metre	% match	measurement square metre	% match
map	18750		134375		306250		16000		53000	
Sept. 1972										
B7-B4	22500	120	150000	112	230000	75	20000	125		
B7-B5	20000	107	145000	108	185000	60	7500	47		
VI	12500	67	142500	106	485000	158	30000	187		
B7+B4									72500	137
B7+B5									90000	170
July 1977										
B7-B5	7500	40	182500	136	445000	145	30000	187		
VI	2500	13	135000	100	440000	144	25000	156		

Table 8.2 Quantification of vegetation and landslide. A comparison of unsupervised classification of MSS data with ground truth.

Note: In the vegetation index of the September image 185,000 square metre of shadowed areas were classified as vegetation and in the vegetation index of the July image 145,000 square metre of shadow were misclassified as vegetation (see Fig 8.8 for details of selected features).

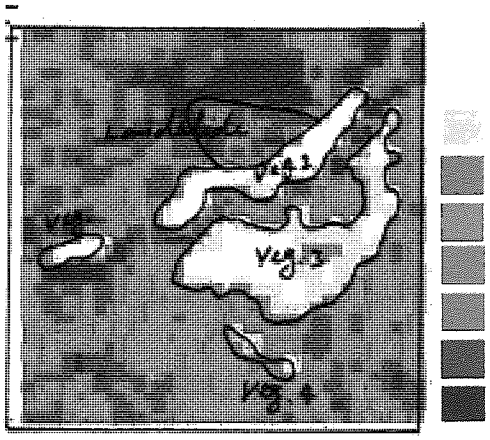

Legend:
1- Veg. 1-Plain Alfalfa farms.
2- Veg. 2-Sunfacing farms and orchards.
3- Veg. 3-Poorly illuminated orchrds.
4- Veg. 4-poorly illuminated wood lands.
5- Sunfacing landslide.

Figure 8.12 Location of Table 8.2 categories.

8.3 CLASSIFICATION METHOD FOR THE LANDSAT MSS DATA

The results of the evaluation of the MSS data (shown in Table 8.2) were not very satisfactory. Various manipulation techniques were explored in order to find an appropriate method of classifying the MSS data. Several combinations of techniques were applied and the results examined. The method which yielded optimum results is described below.

8.3.1 Methodology

A sample of 35 subscenes along the Haraz road was used to develop a classification method. The most dominant features observed across a majority of the subscenes were chosen for classification. The features comprised:

1- (VEG) Vegetation: orchards and farms

2- (SC) Scree: sunfacing steep slopes, usually slumps resulting from landslides.

3- (CL) Coarse lava: poorly vegetated quaternary volcanic conglomerate mixed with volcanic tuffs.

4- (LIME) Light limestone

5- (SHEM) Shemshak formation: dark coaly lower Jurassics

6- (LANDS) Landslide: unstable grounds

7- (SHAD) Shadow

By combining data acquired by field work with existing maps, a geological map of the Haraz Valley was compiled at a scale of 1:23,000. Subscenes were then plotted at the same scale and superimposed on the map. Several appropriate training areas, containing the seven features listed above, were selected from the map and were superimposed on the plots of the subscenes. The pixel values of each of the selected areas were transferred to separate data files.

The files contained bands 4, 5 and 7 of the three images of 4 September 1972, 13 July 1977 and 28 April 1978 for the seven selected categories.

To simplify the training area data sets, the mean and standard deviation of the data were calculated, and only pixels falling within the range of three standard deviations (mean, plus and minus 1.5 standard deviations) were reselected. The pixels selected by this sieving procedure were more homogenous than before, and were less biased by outlying values.

Images of the training areas were examined using the simplified sets of data for each of 3 bands. Various combinations of bands were also examined employing the same gains and offsets which were used for subscene No. 18 (because intention was classification of this subscene as an example). The combinations were: addition of band 7 with band 5 (B7+B5), band 7 with band 4 (B7+B4), subtraction of band 5 from band 7 (B7-B5), band 4 from band 7 (B7-B4) and the vegetation index (B7-B5/B7+B5). Means and standard deviations were calculated and histograms plotted for each of the newly derived data sets corresponding to each of the 8 combinations of bands. Table 8.3 shows the range of pixel values for each seven classes

According to Table 8.3 dark shadow and lower Jurassics can be distinguished in band 7. In bands 5 and 4, lower Jurassics can also be delineated in the middle part of the histogram, while vegetation and shadow coincide in lower part of the histogram, preventing definitive classification. Subtraction of band 5 from band 7 (B7-B5) and band 4 from band 7 (B7-B4) separates vegetation and limestone in the upper and middle part of the histogram respectively, while the other features tend to overlap.

	B 7	B 5	B 4	B7+B5	B7-B5	VI	B7+B4	B7-B4
				VEGETATION				
mean	48.30	20.29	22.07	39.78	61.01	15.66	39.39	59.24
SD	6.51	5.88	5.87	5.57	7.89	2.67	5.29	8.14
mean+,- 1.5 SD	39-58	11-29	13-31	34-52	50-70	11-21	32-48	50-70
				SCREE				
mean	64.41	85.97	86.16	87.16	11.45	1.29	84.31	11.26
SD	4.34	5.76	6.15	5.67	3.03	0.56	2.23	3.97
mean+,- 1.5 SD	58-71	77-95	77-95	76-96	7-14	1-2	76-92	6-16
				COARSE LAVA				
mean	54.23	65.37	64.54	69.41	21.87	3.19	66.58	22.69
SD	2.30	3.00	3.08	2.68	2.83	0.51	2.23	3.66
Mean+,- 1.5 SD	51-58	61-70	60-69	66-74	18-27	3-4	63-69	19-26
				LIMESTONE				
mean	69.53	72.19	72.47	82.22	30.34	3.68	79.57	30.06
SD	4.53	3.91	4.40	4.62	2.71	0.47	4.65	3.53
mean+,- 1.5 SD	63-76	66-78	66-79	76-91	27-36	3-4	72-87	24-35
				LOWER JURASSICS				
mean	23.71	40.05	41.36	36.96	16.66	4.62	36.41	15.35
SD	3.92	4.54	4.80	4.45	3.74	1.28	4.19	4.65
mean+,- 1.5 SD	18-30	33-47	34-49	31-45	12-24	3-7	31-41	10-24
				LANDSLIDE				
mean	62.28	75.91	77.13	80.16	19.38	2.41	78.00	18.16
SD	4.56	6.44	4.76	6.03	4.00	0.71	4.89	3.39
mean+,- 1.5 SD	55-69	66-86	70-84	72-87	15-24	2-3	72-85	13-21
				SHADOW				
mean	0.00	14.31	15.50	8.31	18.67	27.60	8.90	17.50
SD	0.00	4.37	4.76	2.52	4.37	19.48	2.66	4.76
mean+,- 1.5 SD	0.00	0-18	0-19	5-13	12-26	10-50	6-14	8-24

Table 8.3 Characteristics of the training areas. Mean, standard deviation and range of each band or combination are recorded under the name of each selected features of the training areas.

Addition of band 7 to band 5 reveals more detail and permits shadow and coarse lava to be classified across the range of the histogram. However, other features still tend to coincide on the upper

and middle part of the histogram. As was pointed out previously, shadow and vegetation overlap in the vegetation index for most of the upper range of the histogram, whilst landslide and scree (usually associated with each other on the ground) can be delineated from the lower part of the data range. The vegetaion index therefore appears to be less suitable for classifying vegetation in a mountainous region (such as the study area) than for a plain terrain where there is such little or no shadow. Table 8.4 shows the results achieved using the approach described above with all seven classes classified using three spectral bands together with the classifications obtained by the five combination of the three bands.

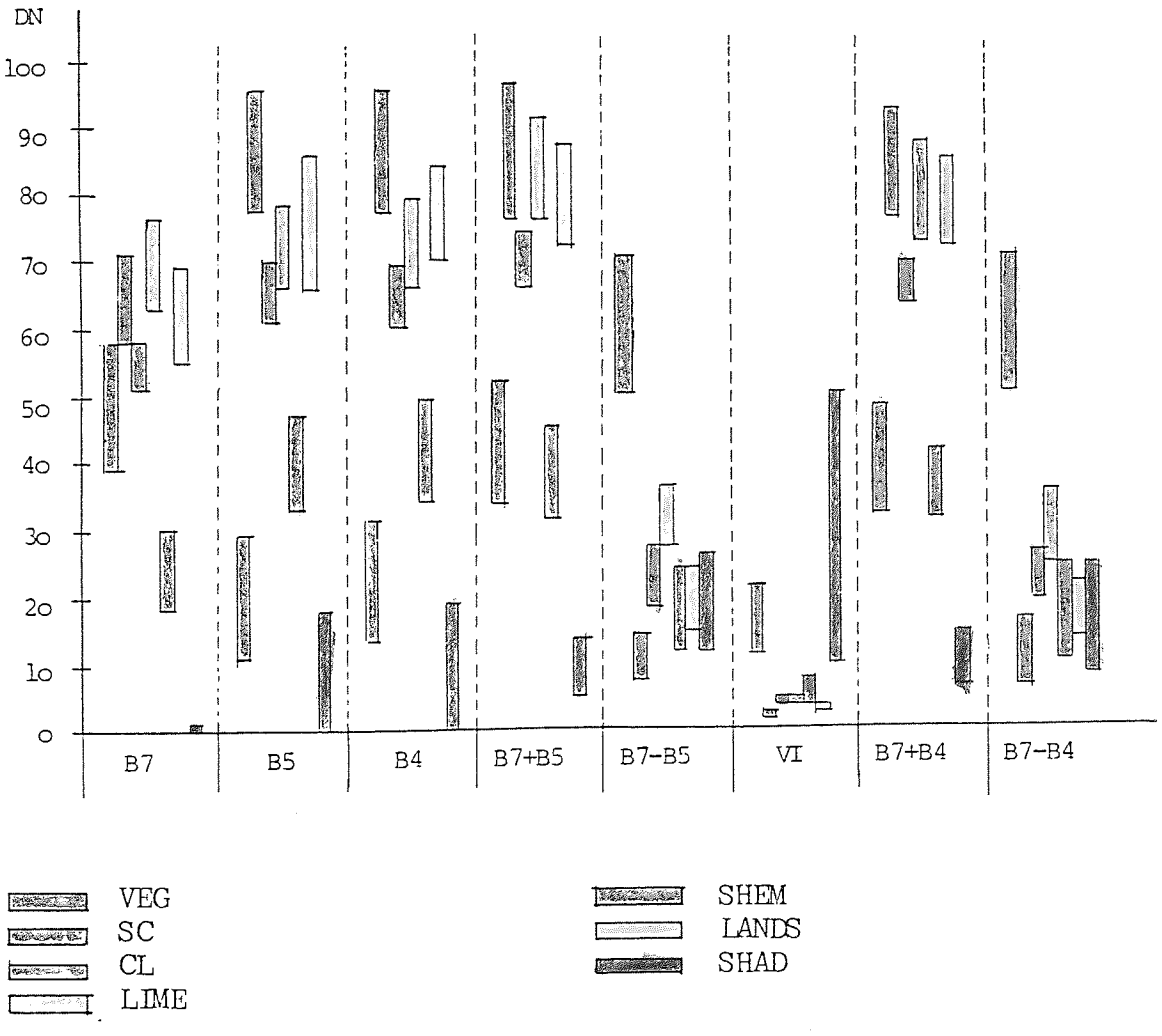

Figure 8.13 Diagram of separation of categories using different combinations of Landsat MSS bands.

MSS band combination	seperated features (and their values
band 7	SHAD (0-1) and SHEM (18-30)
band 5	SHEM (33-47)
band 4	SHEM (34-49)
band 7 + band 5	SHAD (5-13) and CL(66-74)
band 7 - band 5	SC (7-14), LIME (27-36) and VEG (50-70)
Vgetation Index	SC (1-2) and LANDS (2-3)
band 7 + band 4	SHAD (6-14) and CL (63-69)
band 7 - band 4	LIME (24-35) and VEG (50-70)

Table 8.4 Feature separation using Landsat MSS band combinations

A detailed study of each of the features listed in Tables 8.3 and 8.4 provides a useful insight into the nature of image processing. For example one can see how, for all three bands, low pixel values in shadowed areas produce a very high range of values on the vegetation index. While in the vegetated areas a moderate response of the spectral signatures in the three bands gives moderately high values using the same combination.

Taken as a package, the various combinations of bands used in this research provide a comprehensive and concise method of classification. Each band/combination of bands yields additional, unique information on at least one of the seven features. The number of bands/combinations of bands used represents the smallest number that will allow all the features to be properly classified. The classification procedure is illustrated diagramatically in Figure 8.14.

As a general point, this section has demonstrated that without an understanding of how an image processing system works, the use of sophisticated computer equipment to analyse images will produce spurious results. A thorough understanding of the principles underlying image processing is therefore essential, in order to both choose the appropriate computer routines and to usefully interpret the results.

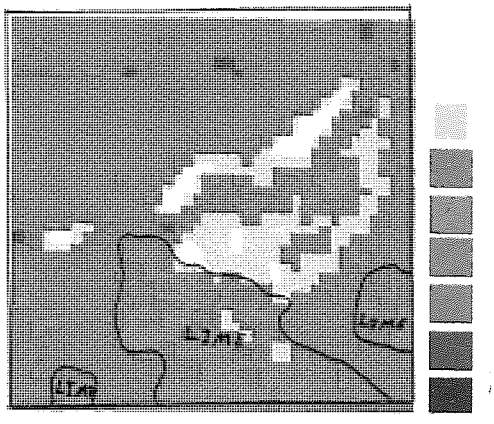

(a)

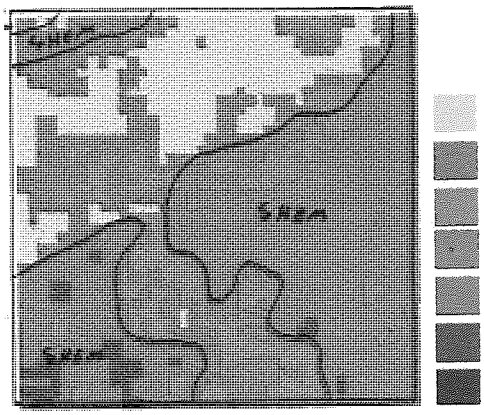

(b)

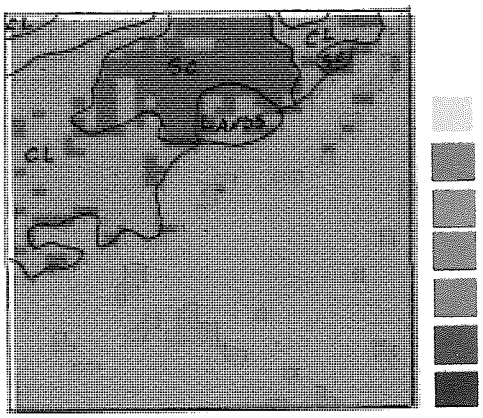

(c)

(d)

Figure 8.14 Classification of the subcene No. 18. a) Subtraction of band 5 from band 7 showing vegetation in white and yellow and limestone in blue. b) Addition of band 5 with band 7 indicating lower Jurassics in red and coarse lava in green. c) Vegetation Index classifying scree in purple and coarse lava plus landslide in red. d) A classification of the subscene derived from the all three combinations (a,b and c). Shaded areas indicate unclassified or misclassified regions within the subscene.

8.4 LIMITATIONS

During this study the main aim was to search for a method to locate unstable areas in mountainous region. Several limitations of MSS data for this kind of discrimination were revealed. The main shortcoming was the size of the ground cell resolution (79x79 m). A second limitation in this particular area was the shadow effects of the dramatic relief. The other limitations can be listed as vegetation cover, and atmospheric effects.

8.4.1 Ground Cell Resolution

The smallest picture element (pixel) in MSS imagery is 79 x 79 m. Due to the technical characteristics of the equipment on boardthe Landsat satellite, an overlap occurs along the latitudinal scan lines. This makes each pixel 79 m long in N - S direction and 57 m in E - W direction and prevents features smaller than 79 m from being distinguished (except for very highly reflective features such as water bodies and disturbed construction sites).

Despite the narrowness of the roads and channels, these can be detected on the MSS images. However, the high reflectivity of small areas of disturbed land, combined with the reflectivity of surrounding features produces a mixed pixel response and makes interpretation difficult.

8.4.2 Topographic and Atmospheric Effects

Topographically the study area is one of the most uneven in the country. The slopes are extremely steep and altitude varies from 200 m to 5670 m within a few tens of kilometers. The time of data

collection (10 am) gives rise to long shadows which due to the relief obscure a large proportion of the image, making discrimination of features very defficult or even impossible. This problem is exaggerated during classification of the image. A major problem is that shadow is often wrongly classified with low reflective features, particularly with the poorly reflecting coaly layers of the Shemshak formation.

General haze effects on the imagery were eliminated by use of conventional image processing techniques. However, an effective method for enhancing the suppressed detail of heavily shadowed valley sides, incorporates a " mirror type principle " which accentuates the subtle differences of shadow areas according to their degree of contrast with brighter adjacent slopes. At the present time software for this process is not commercially available.

8.5 CONCLUSION

This chapter has described how the Processing of Landsat MSS data using the VAX computer and the Tektronix Ink Jet Plotter, and subsequent comparison of the results in hard copy format with ground truths, can achieve a considerable improvement over conventional image processing methods in terms of delineation. Small subscenes (40x40 pixels) were manually processed and plotted in single bands or combinations of different bands. The technique demonstrated that even Landsat MSS data can be used to classify the geological features at a small scale.

Overall, the study showed that the vegetation index is not a suitable tool for use over an extensive area of relief for the

delineation of vegetation. The main reason is that the index tends to classify shadows as vegetation, leading to errors in the final result. However, the lower values in the vegetation index histogram proved useful for the identification of landslides and screes which are hazardous to the Haraz Road. Table 8.2 shows a quantitative analysis of the capability of different combinations of the bands for an unsupervised vegetation classification.

Supervised classification was carried out by selecting certain training areas and using their pixel values to classify the subscenes (Table 8.3). The separation of different features is shown in Figure 8.13 which enables the investigator to carry out a supervised classification of the area. As can be seen in Table 8.4 each combination is most suitable for the classification of one specific feature. As result the subscene was classified employing three combinations as shown in Figure 8.14. By this method only a small portion of the subscene was misclassified or was not classified. Ground cell resolution and topographic effects were two major difficulties in obtaining optimum results.

The method devised can be used for classification of a bigger area, even an entire scene of a Landsat image. Vegetation which appears on Landsat MSS imagery can be classified more accurately than by conventional classification techniques. Some geological features were located very precisely, for example landslides and screes which generally cannot be observed on a false colour composite were also delineated (see Figure 8.14).

CHAPTER 9

CONCLUSION

The Haraz road in North Iran forms a major line of communication between Tehran and the Caspian Sea, and for most of its length it traverses the Alborz mountains. Because of the combination of geology, soil, land cover and steep slopes there are problems in keeping the road open for traffic. The combination of these adverse environmental factors have created large areas of slope instability along the roadway. This results in considerable hazards to the traveller and very high costs in maintenance (mostly cosmetic) and repair work.

With the increase in traffic these dangers and costs continue to grow each year, and it became clear that there was urgent need for a more extensive and rigorous study of slope instability along this motorway. The problem was to identify and evaluate a cost-effective method of gathering information about the geology, land cover and slope condition which could provide useful data for those concerned with the maintenance and management of the Haraz road.

The main aim of this research project is to critically evaluate existing remote sensing materials, aerial photography and satellite imagery, to identify the extent to which remotely sensed data might provide useful information.

With this aim in view a search was made to identify and acquire any relevant aerial photography and satellite imagery that covered the study area. A very limited amount of aerial photography was found to be available, and four Landsat (4 bands) scenes were acquired as CCTs,

two of which were produced as colour composites at a scale of 1:250,000. These together with maps of topography and geology, and some field investigation, provided the data sources for study and evaluation.

One job was to carry out a series of digital image processing tasks to improve the image and assist in multiband, multidate, correction and enhancement of the original data. For these tasks dedicated image processing equipment belonging to other organisations was used.

A variety of image processing techniques were used to correct and enhance the images derived from the Landsat MSS Computer Compatible Tapes. Geometric and radiometric corrections were carried out and various bands were put together to highlight certain features.

These tasks were carried out using a variety of dedicated image processing systems (GEMS, DIPIX, DIAD and IDP3000) provided by other organisations.

A simple unsupervised classification of the major geological types and vegetation was attempted, and the result compared visually with the •ground truths•. This comparison revealed cosiderable errors of identification which were due mainly to relief and shadow.

Whilst some improvements in accuracy were noted with a supervised classification, the results were still unsatisfactory. It was found that using band subtraction gave better vegetation discrimination than using the vegetation index. The most promising result was in using a combination of ground truth and MSS data.

Attention was then directed to the compilation of a number of subscenes of 40 x 40 pixels which together covered the entire road area. Three Landsat images each of 3 bands were used as the data set, and the nine sets of data were compared for all 35 subscenes. With so many data sets it was possible to identify those which yielded the best results for differentiating shadow and vegetation.

Statistical analysis of the data enables the investigator to understand the concepts of data manipulation and helps him to decide the kind of processing most relevent to his data and his needs.

The third stage was to use only visual methods of compilation and comparison. Two false colour composite images were used together to produce land cover and drainage maps which were then compared with the ground truth maps. This comparison was in terms of both the areal extent and location of each land cover type and drainage pattern recorded. This quantitative comparison yielded some very useful information and will serve as a guide to other workers in this particular area. Extending this visual comparison four subscenes were selected and used in various combinations to produce grey scale and colour digital maps.

A package was developed which allowed considerable manipulation of the data and the production of a great variety of maps. These various digital map outputs were compared with the ground truth and revealed a number of very useful results, particularly in respect of identifying areas of slope instability.

It is evident from the results of this study, that the use of Landsat MSS data to identify areas of slope instability is associated with numerous problems. In particular are those concerned with shadow

and poor resolution of the Landsat MSS imagery. However, a lot of interesting and new information has been discovered with the experience of this study, particularly in the development of various methods of data handling and identifying the problems of working on this specific topic.

This study has laid the foundations for further work and the next logical step is to carry out similar work using the newly developed and developing remote sensing systems of Landsat TM, Space Shuttle and SPOT data.

REFERENCES

Allenbach, P., 1966. Geologie und petrographie des Damavand und seiner umgebung (Zentral Elborz), Iran. Mitt. Gelo. Inst. ETH und Universitat Zurich, N. F. 63. Geological Survey of Iran, Report No. 17. 1970, 153 p.

Ambraseys, N. N. and Melville, C. P., 1982. A history of Persian earthquakes. Cambridge Earth Sceince Series, 219 p.

Assereto, R., 1963. The Paleozoic formations in Central Elborz (Iran). (Preliminary Note), Riv. Ital. Paleont. Vol. 69/4, pp. 503-543.

Assereto, R. 1966. i) The Jurassic Shemshak Formation in Central Elborz (Iran). Riv. Ital. Paleont. Strat. Vol. 72/4., pp. 1133-1177.

Bagchi, A. K. 1983. Generation of the Snowline. Jour. American Society of Photogrammetry, Vol. 49 No. 11, pp. 1679-1689.

Bailey, E. B., Jones, R. C. B. and Asfia, S., 1948. Notes on the geology of the Elburz Mountains, north-east of Tehran, Iran. Quart. Journ. Geol. Soc., London. 104/1.

Bailey, E. B. and Stevens, R., 1960. Selective staining of K-Feldspar and plagioclase on rock slabs and thin sections. The American mineralogist, Vol. 45/9-10.

Beaven, P. J., 1984. A Microcomputer based image processing. Presented in RSS workshop, Reading Univasity, U.K. 12 April 1984.

Benny, A. H., 1980. Coastal definition using Landsat data. Journal of British Remote Sensing Society. Vol. 1/3 pp. 255-260.

Bout, P. and Derruau, M. 1961. Le Demavend. Centre Nat. Rech. Scientif. centre de Doc. Cartogr. et Geogr. Mem. et Doc. vol. 8.

Burton, A. N., 1970. The influence of tectonics on the geotechnical properties of calabrian rocks and the mapping of slope instability using aerial photographs. Quar. Jour. Engng Geol. Vol. 2, pp. 237-254.

Carr, J. R. and Gloss, C. E., 1983. Signature extension versus retraining for multispectral classification of surface mines in arid regions. Jour. American Society of photogrammetry, Vol. 49 No. 8, pp. 1193-1199.

Cartier, E. G., 1971. Die Geologie des unteren Chalus Tals Zentral-Alborz/Iran. Diss. Zurich.

Cazabat, C., 1982. Recommendations for remote sensing in a new country. TRRL Supplementary Report No. 690, pp. 122-124.

Christa, E., 1940. Ueber Kristallisation in magmatischen geosteinen Persiens. Min. Petr. Mitt. Vol. 51.

Davies, T. P., Carter, P. G., Mills, D. A. C. and West, G., 1981. Kielder aqueduct tunnels-predicted and actual geology. TRRL Supplementary Report No. 676, 26 p.

Dellenbach, J., 1964. Contributions a l etude geologique de la region situee a l est de Tehran (Iran). Diss. Strasbourg.

Denegre, J., 1982. Different methods of image processing for essistance in interpretation. TRRL Supplementary Report 690, pp. 125-132.

Derruau, M. 1959. Sur la morphologie du Demavend. Bull. Ass. Geogr. Francais, pp. 284-285.

Fantini Sestini, N., 1965. i) The geology of the upper Djadjerud and Lar valleys (north Iran).
ii) Paleontology. Bryozoans, brachiopods and molluscs from Ruteh Limestone (Permian). Riv. Ital. Paleot. Strat. Vol 71/1 pp. 13-108.

Fischer, W. A. ed., 1975. History of remote sensing. Manual of Remote Sensing first edition. Vol. 1, pp. 27-50.

Glaus, M., 1964. Tria und Oberperm im Zentralen Elburz (Persien). Eclogae Geol. Helv. Vol. 57/2.

Hoek, E. and Bray, J. W., 1974. Rock slope engineering. Institution of Mining and Metallurgy, 309 p.

Imhoff, M. L., Petersen, G. W., Sykes, S. G. and Irons, J. R., 1982. Digital overlay of cartographic information on Landsat MSS data for soil surveys. Jour. American Society of Photogrammetry, Vol. 48 No. 8, pp. 1337-1343.

Jeremine, E., 1942. Sur quelques roches du Demavend (Perse). C. R. hebd. des seances de l'Ac. des Sc., 215 p.

Krinsley, D. B., 1976. Lake flactuations in the Shiraz and Neyriz Playas of Iran. ERTS-1 A New Window On Our Planet. U.S. Geolo. Surv. Proff. Paper. Williams, R. S. and Carter, W. D. eds., pp. 143-149.

Landsat Data Users Handbook, 1979. Revised edition, U S Geological Survey, Arlington VA.

Landsat Data Users Handbook, 1984. U S G S, National Oceanic and Atmospheric Administration, Alexandria, V A.

Lorenz, C., 1964. Die Geologie des oberen karaj-Tales (Zentral-Elburz), Iran. Diss. Zurich.

Markhov, A. V., 1962. Probable structure and nature of the formations on the reverse side of the Moon according to photometric measurments of Lunar photographs. " The Moon" I. A. U. Symposium 14, Newyork Academic Press. Kopal, Z. and Mikhailov, Z. K. eds., pp. 39-44.

Maruyasu, T., Onishi, S. and Nishimura, T., 1982. Study of tidal vortices at the naruto strait through multi level remote sensing. Preceeding of International Symposium of Society for Phtogrammetry and Remote Sensing, Toulouse. Vol. 1, pp. 735-744.

Moore, P., 1982. The unfolding universe. Published by Book Club Associates, London, 256 p.

NASA Reference Publication 1078, 1982. The Landsat Tutorial Workbook, Basic of Satallite Remote Sensing, ed Short, N. M., 553 p.

NRSC and Macauley Institute, 1983. A case study of iceberg movement in Greenland.

Ochanda, N. and Hepp, H., 1982. Monitoring recent changes in extent of natural forests in Keneya using Remote Sensing techniques. Preceeding of International Symposium of Society for Photogrammetry and Remote Sensing, Toulouse. Vol. 1, pp. 489-496.

Ovcinnikow, A., 1930. Outline of the geology of the Damavand region. Bull. Naturalistes Moscou, sect. geol., 8/4.

Price, C. J., 1982. Satellite orbital dynamics and observation strategies in support of agricultural applications. Joun. American Society of Photogrammetry, Vol. 48 No. 10, pp. 1603-1613.

Riviere, A., 1934. Contribution a l'etude Geologique de l'Elbourz (Perse). Rev. Geogr. Phys. et Geol. Dyn., 7.

Rothery, D. A., 1982. The evolution of the Wuqbah block and applications of remote sensing in the Oman Ophiolite. Open University Ph.D. thesis, 414 p.

Rothery, D. A., 1984. Interactive processing of satellite images for geological interpetation: An unpublished case study.

Scherillo, A. 1935. Descrizione di alcune lave del Demavend (Persia). Per. Min. 6.

Seegmiller, B. L., 1979. Twin Buttes Pit slope failure, Arizona, U.S.A.. Rockslides and Avalanches, Development in Geotechnical Engineering. Vol. 14B. Voight, B. ed., pp. 651-666.

Shih, E. H. H. and Schowengerdt, R. A., 1983. Classification of arid geomorphic surfaces using Landsat spectral and textural features. Jour. American Society of Photogrammetry, Vol. 49 No. 3, pp. 337-347.

Shoemaker, E. M. and Hackman, R. J., 1962. Stratigraphic basis for a Lunar time scale. " The Moon " I. A. U. Symposium 14, Newyork Academic Press. Kopal, Z. and Mikhailov, Z. K. eds., pp. 289-300.

Smit, G. S., 1980. Use of Landsat imagesry for forest management mapping; a study of " Kobernausserwald " in Austria. Congress of the International Society for Photogrametry, Hamburg. Vol. 23, Part B8, pp. 863-873.

Stahl, A. F., 1897. Zur geologie von Persien, geognostische beschreibug von Nord-und zentral Persien. Peterman's Mitt., Erganzungsband 26, 122 p.

Stahl, A. F., 1911. " Persien " Handbuch der regionalen geologie 5. Abt. 6 Heidelberg.

Steiger, R., 1966. Die geologie der west Firuzkuh area (Zentral Elburz, Iran). Mitt. Geol. Inst. ETH und Univ. Zurich. N. F. 68.

Stepanov, D. L., Golshani, F. and Stocklin, J., 1969. Upper Permian and Permian Triassic boundary in north Iran. Geological Survey of Iran, Report No. 12.

Stocklin, J., Ruttner, A. and Nabavi, M., 1964. New data on the lower Paleozoic and Precambrian of north Iran. Geological Survey of Iran, Report No. 1.

Stocklin, J., Nabavi, M. and Samimi, M., 1965. Geology and mineral resources of the Soltanieh Mountains (northwes Iran). Geological Survey of Iran, Report No. 2.

Stocklin, J., 1968. Structural history and tectonics of Iran. A review. Bull. Amer. Assoc. Petroleum Geol. 52/7, 1229.

Sussli, P. E., 1976. The geology of the lower Haraz Valley area, Central Alborz, Iran. Geological Survey of Iran, Report No. 38, 116 p.

Tietze, E., 1878. " Der Vulkan Damavand in Persian." Jahrb. D. k. k. Geol. Reichsanst. 28.

Ulaby, F. T., Dobson, C., Stiles, J., Moore, R. K. and Holtzman, J., 1982. A simulation study of siol moisture estimation by a space SAR. Jour. American Society of Photogrammetry, Vol. 48 No. 4, pp. 645-660.

Varnes, D. J., 1958. Landslide type and processes. Highway Research Board, Special Report 29, Committe on Landslide Investigations, Washington D.C. . Edwin B. Eckel. ed., pp. 20-47.

Wahlestrom, E. E., 1974. Dams, Dam Foundations. Developments in Geotechnical Engineering. Vol. 6.

Way, D. S., 1973. Terrain Analysis: a guide to site selection using Aerial Photographic interpretation, 392 p.

Zaruba, Q. and Mencl, V. 1969. Landslides and their control. Published by Elsveier in English 1976.

BIBLOGRAPHY

Anderson, D. T and Misra, K. S., 1983. Structural mapping of Precambrian rocks blow Paleozoic and Quaternary sedimentary material using spectral and geophysical remote sensing techniques in the Canadian shield. Pro. 17th International Symposium on Remote Sensing of Environment, Vol. 2, pp. 697-701.

Anderson, J. E., 1985. The use of Landsat-4 MSS digital data in temporal data sets and the evaluation of scene-to-scene registration accuracy. Jour. American Society of Photogrammetry Vol. 51 No. 4, pp. 457-462.

ii) Geological map of upper Djadjrud and Lar valleys (Central Elborz, Iran), Scale 1:50000 with explanatory notes. Geolo. Inst. Univ. Milano, Ser. G. Publ., 232 p.

Beaumont, T. E. and Beaven, P. J., 1977. The use of satellite imagery for highway engineering in overseas countries. TRRL Supplementary Report No. 279, U. K. 16p.

Beaumont, T. E., 1978. Remote sensing for transport planning and highway engineering in developing countries. TRRL Supplementary Report No. 433, 10 p.

Beaumont, T. E., 1979. Remote sensing for the location and mapping of engineering construction materials in developing countries. Qua. Journal of Engng. Geol. Vol. 12, pp. 147-158.

Bell, F. G., 1980. Engineering Geology and Geotechnics. 497 p.

Boyd, J. M., Hinds, D. V., Moy, D. and Rogers, O., 1973. Two simple dvices for monitoring movements in rock slopes. Q. Jour. Engng. Geol. Vol. 6., pp. 295-302.

Caron, R. H., 1975. Evaluation of full-scene registered ERTS MSS imagery using a multitemporal/multispectral bayes supervised classifier. Remote Sensing of Earth Resources. Shahrokhi, F., ed. Vol. 4., pp. 783-806.

Dick, O. B., 1982. Remote sensing for transport planning and highway engineering. TRRL Supplementary Report No. 690, pp. 96-110.

Ehlers, M., 1985. The effects of image noise on digital correlation probability. Jour. American Society of Photogrammetry, Vol. 51 No. 3, pp. 357-365.

Eidenshink, J. C., 1985. Detection of leaks in buried rural water pipelines using thermal infrared images. jour. American Society of Photogrammetry, Vol. 51 No. 5, pp. 561-564.

Forster, B. C., 1985. Principle and rotated component analysis of urban surface reflctances. Jour. American Society of Photogrammery, Vol. 51 NO. 4, 475-477.

Franklin, J. A. and Denton, P. E., 1973. The monitoring of rock slopes. Q. Jour. Engng. Geol. Vol. 6, pp. 259-286.

Fukue, K., Shimoda, H. and Sakata, T., 1981. Complete lineament extraction with the aid of shadow free Landsat image. 7th International Syposium Machine Processing of Remotely Sensed Data, Purdue Univ., pp. 94-111.

Gould, J. P. and Dunicliffe, C. J., 1971. Accuracy of field deformation measurements. Proc. 4th Panamerican Conf. Soil Mech. Found. Engng., Vol. 1, pp. 212-366.

Heath, W., Parsley, L. L. and Dowling, J. W. F., 1978. Terrestrial photogrammetric surveys of unstable terrain in Colombia. TRRL Laboratory Report No. 816, 39 p.

John, K. W., 1968. Graphical stability analysis of slopes in jointed rock. Jour. Soil Mech. and Found. Div., Proe. ASCE Vol. 94/SM2, pp. 497-526.

John, K. W., 1970. Engineering analyses of three dimentional stability problems utilizing the reference hemisphere. Second International Congr. Int. Soc. Rock Mech., pp. 7-16.

Kenneth, J. Hsu., 1978. Observations on Landslides and relevance to modern interpretation. Rockslides and Avalanches, Vol. 14A, Voight, B. ed., pp. 71-93.

Khorram. S. and Cheshire, H. M., 1985. Remote sensing of water quality in the Neuse River eastury, North Carolina. Jour. American Society of Photogrammetry, Vol. 51 No. 3, pp. 329-341.

Knepper, D. H. and Raines, G. L., 1985. Determining stretch parameters for lithologic discrimination on Landsat MSS band-ratio images. Jour. American Society of Photogrammetry Vol. 51, No. 1, pp 63-67.

Lawrence, C. J., 1982. The use of Landsat imagery as a basis for materials inventories and terrain maps. TRRL Supplementary Report No. 690, pp. 117-121.

Liu, J. K., Wu, C. M. and Chuang, M. Y., 1983. Relations between lineaments, joint patterns, seismicity, and tectonic stresses in Taiwan island. 17th intenational Symposium on Remote Sensing of Environment, Michigan, pp. 687-696.

Londe, P., Vigier, G. and Vormeringer, R., 1969. Stability of rock slopes, a three dimentional study. Jour. Soil Mech. and Found. Dvi., Proc. ASCE, Vol. 95/SM1, pp. 235-262.

Malacamp, J., 1982. The use of remote sensing from space in a track rehabilitation project in Upper Volta. TRRL Supplementary Report no. 690, pp. 111-116.

Matheson, G. D., 1983. Rock stability assessment in preliminary site investigations-graphical methods. TRRL Laboratoey Report No. 1039, 30 p.

Moore, R. F. and Simpson, C. J., 1983. Image analysis - a new aid in morphotectonic studies. 17th International Symposium on Remote Sensing of Environment, Michigan. Vol. 3, pp. 991-996.

Nabavi, M., 1977. Seismic activities of Iran in 1971-1976. Jounal of the " Earth and Space " University of Tehran, pp. 38-86.

Nelson, R., 1985. Reducing Landsat MSS scene variability. Jour. American Society of Photogametry, Vol. 51 No. 5, pp. 583-593.

Planhol. X., 1968. Geography of settlements, in Camb. Hist. Iran, 409 p.

Planika, A. and Nosel, L., 1970. Terrestrial photogrammetry in measurement of defoemations of rockfill dams. Proc. 10th Int. Cong. Large Dams, Montreal, Vol. 6, pp 207-215.

Rifman, S. S., Monuki, A. T. and Shortwell, C. P., 1979. Multi-sensor Landsat MSS registration. 13th International Symposium on Remote Sensing of Environment, Vol. 1, pp. 245-258.

Ritchie, A. M., 1958. Recognition and identification of landslides. Landslides and Engineering Practice. Washington, D.C.. Eckel, E. B.. ed., pp. 48-68.

Ritchie, A. M., 1963. The evaluation of rock fall and its control. Highway Res. Rec., Vol. 17, pp. 13-28.

Root, A. W., 1958. Prevention of landslides. Landslide and Engineering Practice. Report No. 29, Washington D.C.. Eckel, E. B. ed., pp. 131-149.

Rothery, D. A. and Drury, S. A., 1984. The neotectonics of the Tibetan plateau. techtonics, Vol. 3/1, pp. 19-26.

Savage, R. J., 1973. Soil and rock slope instrumentation. Q. Jour. Engng. Geol., Vol. 6, pp. 287-294.

Schowengerdt, R. A., 1983. An optimized cubic interpolator for image resampling. 17th international Symposium on Remote Sensing of Environment, Vol. 3, pp. 1291-1299.

Shazly, E. M., Abdel Hady, M. A. and Kassas, I. A., 1983. Regional geological investigation of Wadi el Allaqi area, southern Egypt, from the interpretation of Landsat imagery. Pro. 17th International Symposium on Remote Sensing of Environment, Vol. 2, pp. 703-713.

Simard, R., 1983. Digital stereo enhancement of Landsat MSS data. proc. 17th International Symposium on Remote Sensing of Environment, Vol. 3, pp. 1275-1281.

Steven, M. D., Moncrieff, J. B. and Mather, P. M., 1984. Atmospheric attenuation and scattering determined from multiheight multispectral scanner imagery. Int. Journal of Remote Sensing, Vol. 5, N0. 4, pp. 733-747.

Stewart, M. and Celis, A. C., 1976. The use of geophysics in landslide studies. TRRL Laboratory Report No. 703, 13p.

Swanson, L. W., 1984. The development of geometric satellite triangulation and field operations. Jour. American Soceity of Photogrammetry, Vol. 50 No. 9, pp. 1333-1340.

Toombs, A. F., McCaul, C. and Symons I. F., 1982. Ground movements caused by deep trench construction in an urban area. TRRL Reprt No. 1040, 8p.

Verdin, J. P., 1985. Monitoring water quality conditions in a large wstern reservoir with Landsat imagery. Jour. American Society of Phtogrammetry, Vol. 51 No. 3, pp. 343-353.

Wahlstrom, E. E., 1973. Tunneling in Rock. Developments in Geotechnical Engineerimg. Vol. 3, 250 p.

Wyatt, C. L. and Trivedi, M. M., 1985. Measurement techniques for spectral characterzation for Remote Sensing. Jour. American Society of Photogrammetry, Vol. 51 No. 2, pp. 245-251.

Appendix A

APPENDIX A

XV INTERNATIONAL CONGRESS OF PHOTOGRAMMETRY AND REMOTE SENSING

RIO DE JANEIRO BRAZIL

17 - 29 JUNE 1984

SLOPE STABILITY IN MOUNTAINOUS ROADS IN IRAN.

A CASE FOR REMOTE SENSING?

Hassan Taherkia
Research Graduate
University of Aston, U.K.

Dr J A Morton
Department of Geological Sciences
University of Aston, U.K.

Dr W G Collins
Department of Civil Engineering
University of Aston, U.K.

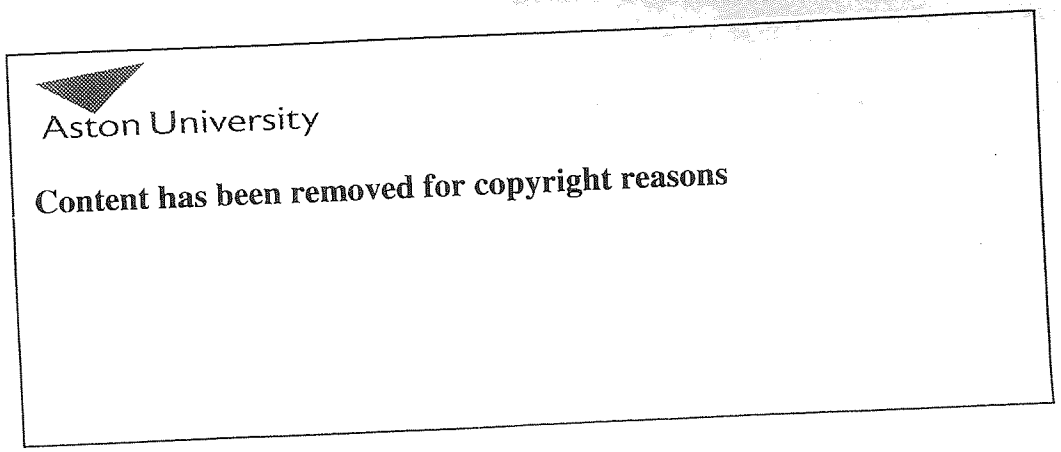
Aston University
Content has been removed for copyright reasons

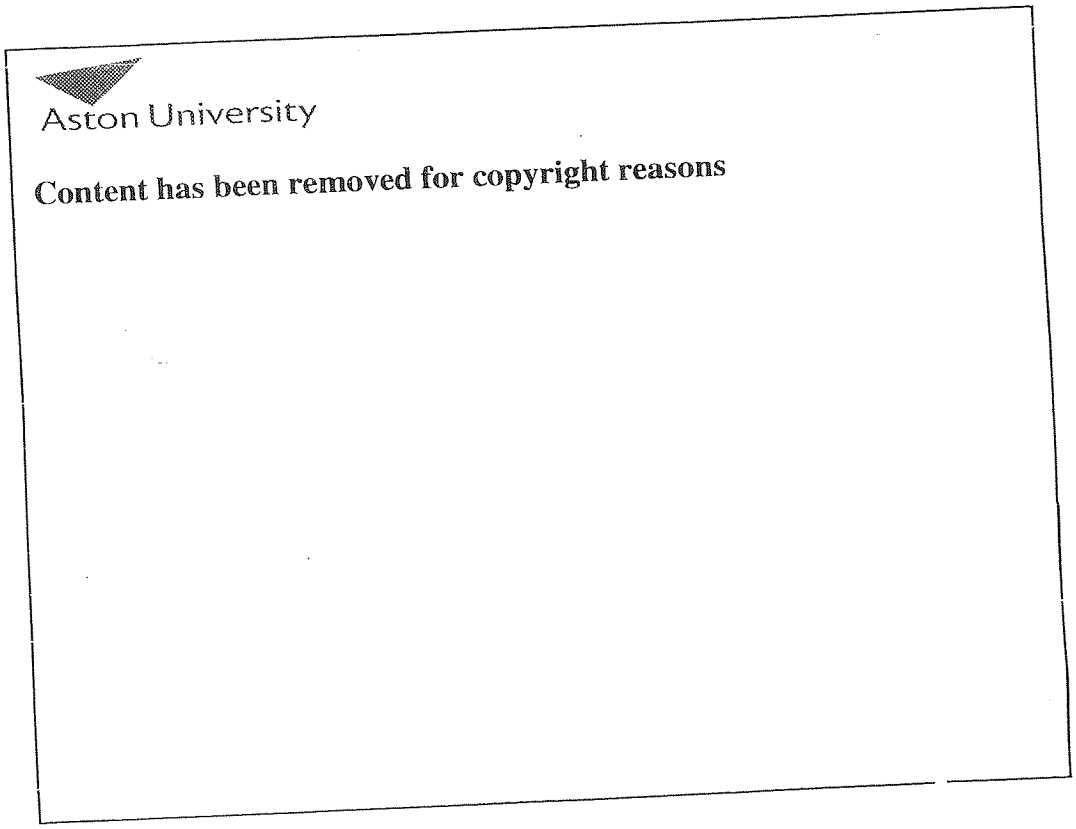
Aston University
Content has been removed for copyright reasons

Figure 1. Location of Study Area.

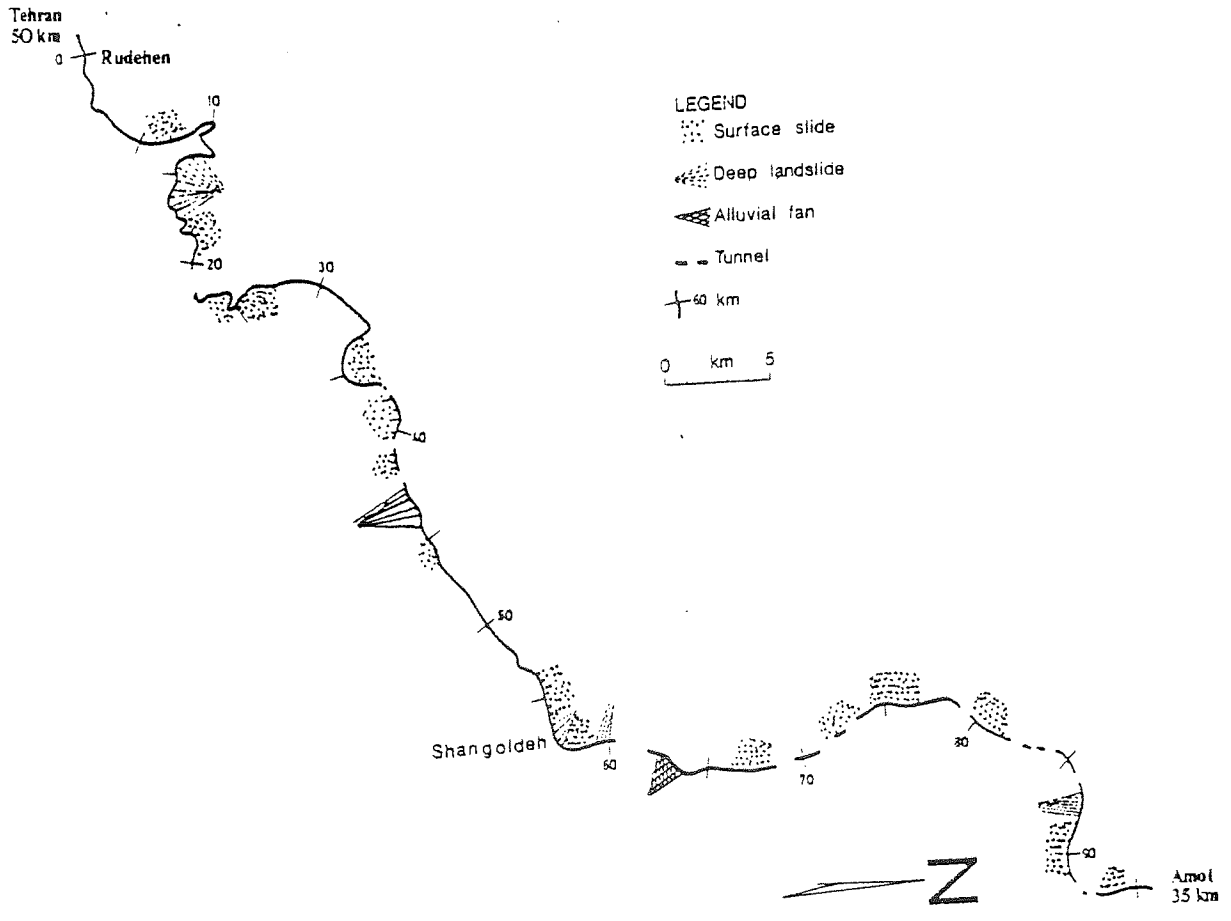

Figure 2. Details of the Haraz Road.

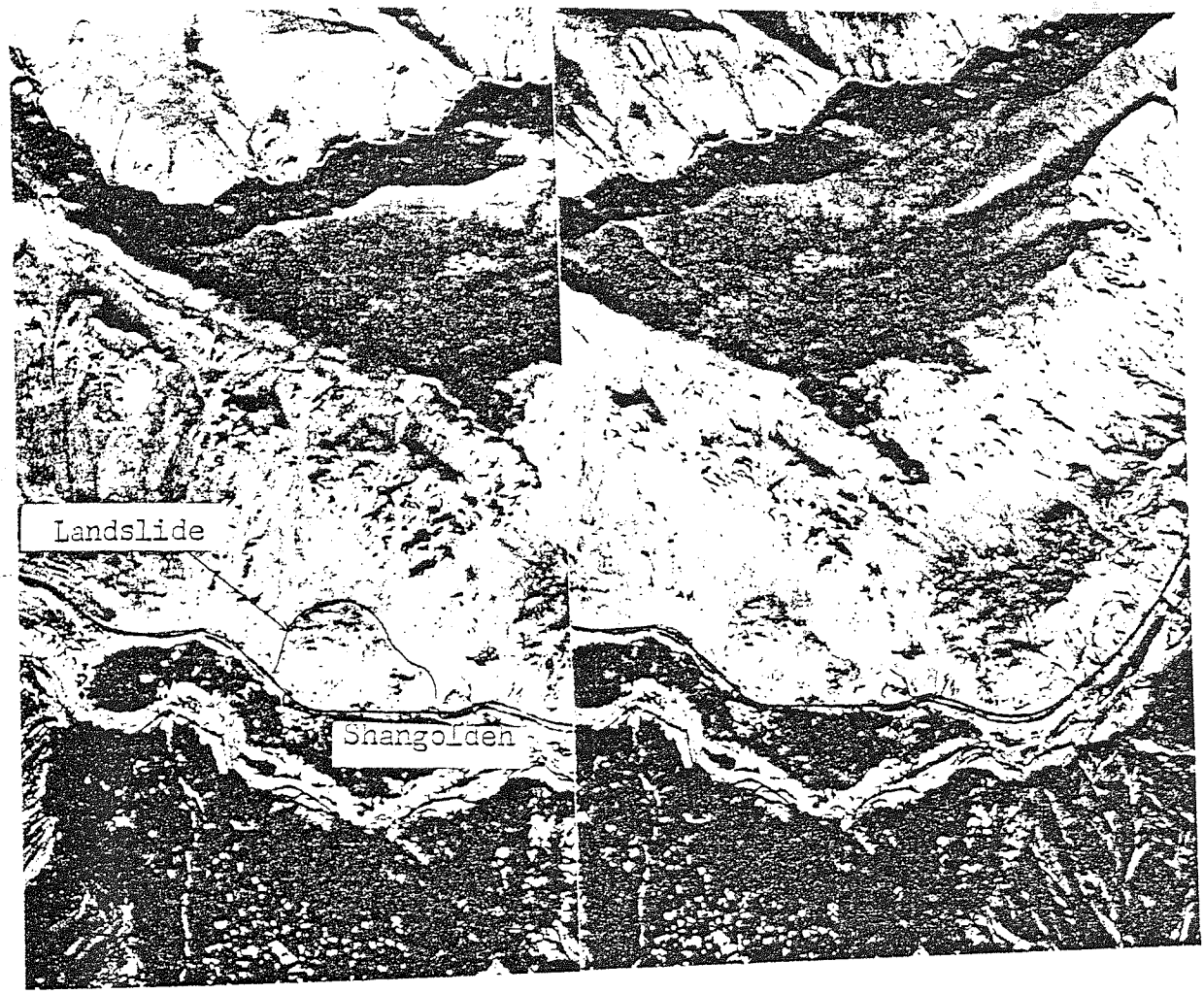

Figure 3. Stereo pair of aerial photographs of Shangoldeh. The landslide is shown in the bottom left corner.

No	Symbol	Description
1	Js	Lower Jurassic sediments: dark shale, sandstone, coal and plant remains
2	Kv	Cretaceous volcanics: basic lavas and pyroclastics
3	F	Forest and dense vegetation
4	Jl	Upper Jurassic: well bedded cherty limestone
5	Lt	Quaternary lavas: mainly trachyandesite
6	K2	Cretaceous sediments: biogenic cherty limestone
7	Td	Recent terrace deposits: sand and gravels

Table 1. Description of Training Areas Selected.

Training areas		Band 4		Band 5		Band 6		Band 7	
Code	Size in pixels	Mean	S.D.	Mean	S.D.	Mean	S.D.	Mean	S.D.
1 - Js	108	41.6	3.9	41.4	6.0	39.6	6.0	34.0	7.2
2 - Kv	36	37.4	2.7	35.8	3.8	33.3	4.3	27.5	5.2
3 - F	36	23.4	2.0	15.9	1.8	34.9	5.6	41.2	8.7
4 - Jl	108	53.1	8.8	59.1	11.9	56	10.9	49.1	11.3
5 - Lt	72	43.0	4.9	47.4	6.1	49.4	6.0	46.3	6.5
6 - K2	36	54.2	6.9	58.8	9.7	54.3	9.7	43.5	9.5
7 - Td	72	47.0	6.3	48.5	9.5	44.0	8.7	35.9	8.3

Table 2. Average Pixel Values for training areas (see Figure 4.)

Training areas		Band 5 - Band 4		Band 6 - Band 4		Band 7 - Band 4		Band 6 - Band 5		Band 7 - Band 5		Band 7 - Band 6	
Code	Size in pixels	Mean	S.D.	Mean	S.D	Mean	S.D.	Mean	S.D	Mean	S.D.	Mean	S.D.
1 - Js	108	-0.20	3.9	-1.98	4.8	-7.59	6.5	-1.79	4.4	-7.40	7.1	-5.61	5.3
2 - Kv	36	-1.62	2.8	-4.14	3.8	-9.93	5.3	-2.51	3.7	-8.3	5.4	-5.79	4.8
3 - F	36	-7.47	2	11.5	6.2	17.83	9.7	18.97	6.2	25.31	9.4	6.33	5.6
4 - Jl	108	6.0	5.7	2.85	6.3	-4.0	9.8	-3.16	4.8	-10.0	9.7	-6.85	8.5
5 - Lt	72	4.40	3.4	6.35	3.9	3.29	5.9	1.94	4.4	-1.11	5.2	3.05	6.3
6 - K2	36	4.58	4.3	0.08	4.9	-10.72	6.2	-4.50	3.8	-15.31	6.7	-10.81	5.1
7 - Td	72	1.44	4.5	-2.97	4.8	-11.17	6.1	-4.42	3.9	-12.61	6.6	-8.19	5.3

Table 3. Subtraction Pixel Values for training areas (see Figure 5.)

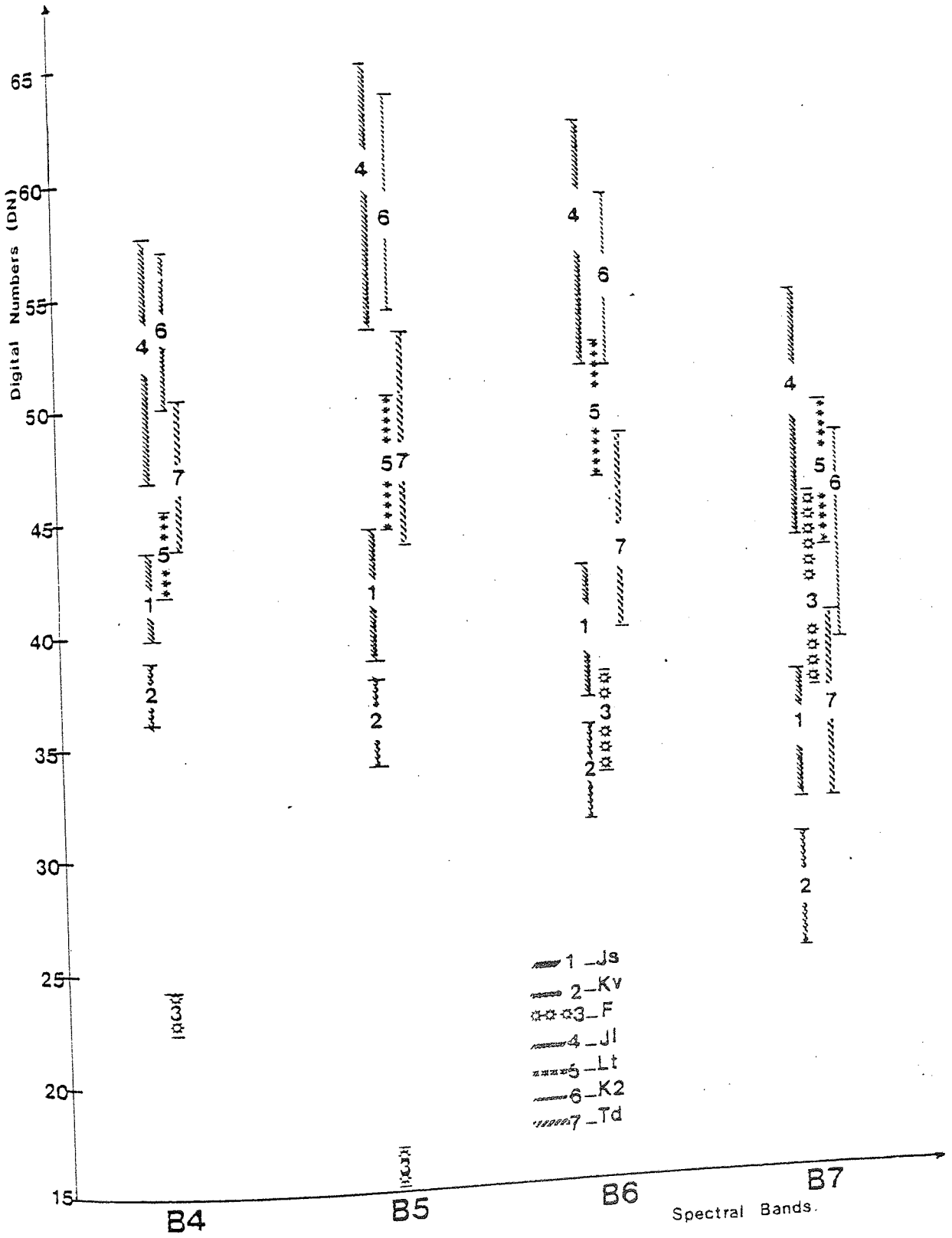

Figure 4. Pixel Values. Digital numbers are shown, with their standard deviations, for the seven chosen categories.

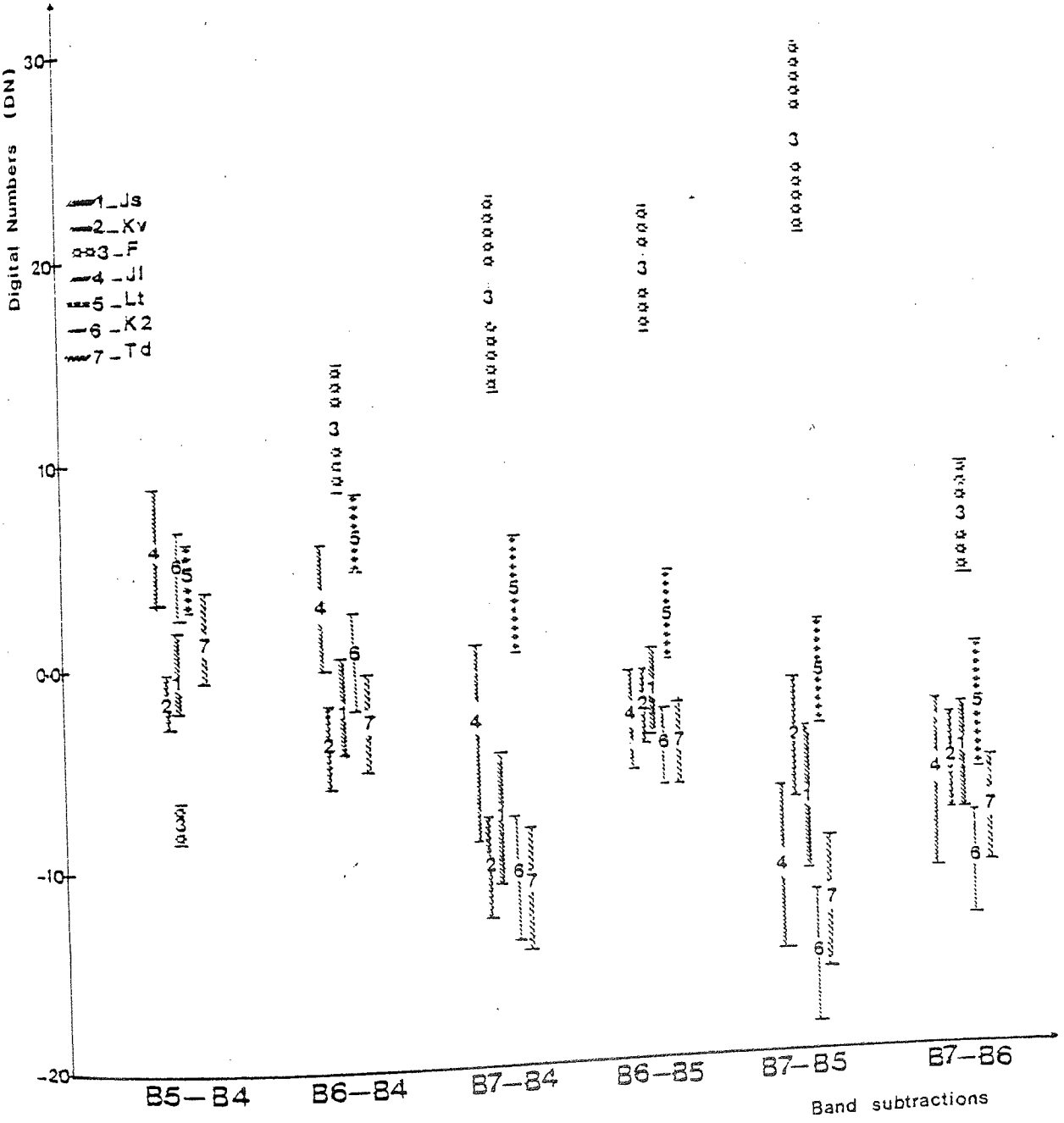

Figure 5. Subtractions of pixel values. Digital values for seven chosen categories.

Appendix B

```
1         INTEGER *3 COUNT, IOSTAT
2 C
3         INTEGER *1 BUF1(5388)
4         INTEGER *3 BUF3(1796), BSIZE
5         LOGICAL MSS, BIL, RBV, GEOCOR
6         COMMON /LAND/ BUF1, BSIZE, MSS, BIL, RBV, GEOCOR
7         EQUIVALENCE (BUF1(1),BUF3(1))
8 C
9 C
10         BSIZE=1796
11 100    BUFFER IN (10, BUF3, S, BSIZE, IOSTAT, COUNT)
12         CALL STATUS(10)
13 C
14         WRITE(12,234)(BUF3(I), I=4,8)
15 234    FORMAT(5A3)
16         WRITE(12,400)
17         WRITE(12,500) COUNT, IOSTAT, BUF1(6)
18         IF (IOSTAT.EQ.4) GO TO 200
19 C
20         IF (BUF1(6).EQ.9)
21           CALL CCT011
22         ELSE IF (BUF1(6).EQ.18)
23           CALL CCT022
24         ELSE IF (BUF1(6).EQ.36)
25           CALL CCT044
26         ELSE IF (BUF1(6).EQ.219)
27           CALL CCT333
28         ELSE IF (BUF1(6).EQ.237)
29           CALL CCT355
30         ELSE IF (BUF1(6).EQ.246)
31           CALL CCT366
32         ELSE
33           WRITE(12,999)
34         END IF
35 C
36         GO TO 100
37 C
38 200    WRITE(12,300)
39         WRITE(12,400)
40         STOP
41 C
42 300    FORMAT(' *** END-OF-TAPE ENCOUNTERED ***')
43 400    FORMAT(' ##################################################')
44 500    FORMAT(' BLOCK SIZE ',I5,'    STATUS ',I1,'    BYTE SIX ',I3)
45 999    FORMAT(' UNRECOGNISED RECORD TYPE CODE ********************')
46         END
47         SUBROUTINE CCT011
48 CCCCCCCCCCCCCCCCCCCCCCCCCCCCCCCCCCCCCCCCCCCCCCCCCCCCCCCCCCCCCCCC
49 CCCC
50 CCCC   TAPE DIRECTORY DECODING (03/11/82)
51 CCCC
52 CCCCCCCCCCCCCCCCCCCCCCCCCCCCCCCCCCCCCCCCCCCCCCCCCCCCCCCCCCCCCCCC
53         INTEGER *1 LGT1(3)
54         INTEGER *3 LGT2
55         EQUIVALENCE (LGT1(1),LGT2)
56 C
57         INTEGER *1 BUF1(5388)
58         INTEGER *3 BUF3(1796), BSIZE
59         LOGICAL MSS, BIL, RBV, GEOCOR
60         COMMON /LAND/ BUF1, BSIZE, MSS, BIL, RBV, GEOCOR
61         EQUIVALENCE (BUF1(1),BUF3(1))
62 C
63         WRITE(12,1000)
64         IF (BUF1(30).NE.237) WRITE(12,1010)
65         WRITE(12,1001) BUF1(7),BUF1(8),BUF1(9),BUF1(10),BUF1(11)
```

```
66          IF (BUF1(9).EQ.'M')
67            WRITE(12,1002)
68            MSS=.TRUE.
69            IF (BUF1(31).EQ.0)
70              WRITE(12,1003)
71            ELSE
72              WRITE(12,1004)
73            END IF
74          ELSE IF (BUF1(9).EQ.'R')
75            WRITE(12,1005)
76            MSS=.FALSE.
77          END IF
78          IF (BUF1(34).EQ.'C')
79            GEOCOR = .TRUE.
80            WRITE(12,1006)
81          ELSE IF (BUF1(34).EQ.'U')
82            GEOCOR = .FALSE.
83            WRITE(12,1007)
84          ELSE IF (BUF1(34).EQ.' ')
85            WRITE(12,1008)
86          ELSE
87            WRITE(12,1009)
88          END IF
89          RBV = .NOT. MSS
90          LGT1(2)=BUF1(32)
91          LGT1(3)=BUF1(33)
92          WRITE(12,1011) LGT2
93          BSIZE=LGT2/3
94          WRITE(12,1012) (BUF1(I),I=35,52)
95          RETURN
96  1000    FORMAT(' TAPE DIRECTORY')
97  1001    FORMAT(' MISSION-',2A1,'  SENSOR TYPE-',1A1,'  TAPE TYPE-',2A1)
98  1002    FORMAT(' MULTISPECTRAL SCANNER SYSTEM (MSS) FORMAT')
99  1003    FORMAT(' BAND SEQUENTIAL (BSQ) FORMAT')
100 1004    FORMAT(' BAND INTERLEAVED BY LINE (BIL) FORMAT')
101 1005    FORMAT(' RETURN-BEAM VIDICON (RBV) FORMAT')
102 1006    FORMAT(' GEOMETRICALLY CORRECTED DATA (SOURCE HDT)')
103 1007    FORMAT(' GEOMETRICALLY UN-CORRECTED DATA (SOURCE HDT)')
104 1008    FORMAT(' SOURCE HDT N/A')
105 1009    FORMAT(' SOURCE HDT NOT RECOGNISED*******************')
106 1010    FORMAT(' ******* THIS CCT WAS NOT GENERATED BY EDIPS ! *****')
107 1011    FORMAT(' SIZE OF FOLLOWING RECORDS = ',I5)
108 1012    FORMAT(' SCENE ID:  ',18A1)
109         END
110         SUBROUTINE CCT022
111 CCCCCCCCCCCCCCCCCCCCCCCCCCCCCCCCCCCCCCCCCCCCCCCCCCCCCCCCCCCCCCCC
112 CCCC
113 CCCC    HEADER RECORD
114 CCCC
115 CCCCCCCCCCCCCCCCCCCCCCCCCCCCCCCCCCCCCCCCCCCCCCCCCCCCCCCCCCCCCCCC
116         INTEGER *1 BUF1(5388)
117         INTEGER *3 BUF3(1796), BSIZE
118         LOGICAL MSS, BIL, RBV, GEOCOR
119         COMMON /LAND/ BUF1, BSIZE, MSS, BIL, RBV, GEOCOR
120         EQUIVALENCE (BUF1(1),BUF3(1))
121 C
122         WRITE(12,2000)
123 2000    FORMAT(' HEADER')
124         RETURN
125         END
126         SUBROUTINE CCT044
127 CCCCCCCCCCCCCCCCCCCCCCCCCCCCCCCCCCCCCCCCCCCCCCCCCCCCCCCCCCCCCCCC
128 CCCC
129 CCCC    ANCILLARY RECORD
130 CCCC
131 CCCCCCCCCCCCCCCCCCCCCCCCCCCCCCCCCCCCCCCCCCCCCCCCCCCCCCCCCCCCCCCC
```

```
      INTEGER *1 BUF1(5388)
      INTEGER *3 BUF3(1796), BSIZE
      LOGICAL MSS, BIL, RBV, GEOCOR
      COMMON /LAND/ BUF1, BSIZE, MSS, BIL, RBV, GEOCOR
      EQUIVALENCE (BUF1(1),BUF3(1))
C
      WRITE(12,3000)
3000  FORMAT(' ANCILLARY')
      RETURN
      END
      SUBROUTINE CCT333
CCCCCCCCCCCCCCCCCCCCCCCCCCCCCCCCCCCCCCCCCCCCCCCCCCCCCCCCCCCCCCCCCC
CCCC
CCCC   ANNOTATION RECORD DECODING
CCCC
CCCCCCCCCCCCCCCCCCCCCCCCCCCCCCCCCCCCCCCCCCCCCCCCCCCCCCCCCCCCCCCCCC
      INTEGER *1 BUF1(5388)
      INTEGER *3 BUF3(1796), BSIZE
      LOGICAL MSS, BIL, RBV, GEOCOR
      COMMON /LAND/ BUF1, BSIZE, MSS, BIL, RBV, GEOCOR
      EQUIVALENCE (BUF1(1),BUF3(1))
C
      WRITE(12,4000)
      WRITE(12,4001) (BUF1(I), I=7,14)
      WRITE(12,4002) (BUF1(I), I=15,31)
      IF (BUF1(32).EQ.'D')
        WRITE(12,4003) (BUF1(I), I=33,35),(BUF1(I), I=37,39)
      ELSE IF (BUF1(32).EQ.'A')
        WRITE(12,4004) (BUF1(I), I=33,35),(BUF1(I), I=37,39)
      ELSE
        WRITE(12,4005)
      END IF
      WRITE(12,4006) (BUF1(I), I=41,57)
      IF (RBV)
        WRITE(12,4007) (BUF1(I), I=63,64)
        IF (BUF1(65).EQ.'I') WRITE(12,4008)
        IF (BUF1(65).EQ.'O') WRITE(12,4009)
      END IF
      IF (BUF1(66).EQ.'D')
        WRITE(12,4010)
      ELSE IF (BUF1(66).EQ.'R')
        WRITE(12,4011)
      ELSE
        WRITE(12,4012)
      END IF
      WRITE(12,4013) (BUF1(I), I=68,81)
      WRITE(12,4014) BUF1(82)
      IF (BUF1(83).EQ.'1')
        WRITE(12,4015)
      ELSE IF (BUF1(83).EQ.'2')
        WRITE(12,4016)
      ELSE IF (BUF1(83).EQ.'3')
        WRITE(12,4017)
      ELSE
        WRITE(12,4018)
      END IF
      WRITE(12,4019) BUF1(84)
      IF (BUF1(86).EQ.'C')
        WRITE(12,4020)
      ELSE IF (BUF1(86).EQ.'N')
        WRITE(12,4021)
      ELSE
        WRITE(12,4022)
      END IF
      IF (BUF1(92).EQ.'1')
        WRITE(12,4023)
```

```
198         ELSE IF (BUF1(92).EQ.'2')
199           WRITE(12,4024)
200         ELSE
201           WRITE(12,4025)
202         END IF
203         WRITE(12,4026) (BUF1(I), I=94,106)
204         WRITE(12,4027) (BUF1(I), I=107,121)
205         RETURN
206 4000    FORMAT(' ANNOTATION')
207 4001    FORMAT(' EXPOSURE DATE ',8A1)
208 4002    FORMAT(' FORMAT CENTRE ',17A1)
209 4003    FORMAT(' DESCENDING ACQUISITION - PATH ',3A1,' ROW ',3A1)
210 4004    FORMAT(' ASCENDING ACQUISITION - PATH ',3A1,' ROW ',3A1)
211 4005    FORMAT(' NOMINAL PATH-ROW IDENTIFIER UNRECOGNISED *****')
212 4006    FORMAT(' NOMINAL LATITUDE AND LONGITUDE ',17A1)
213 4007    FORMAT(' RBV SHUTTER DURATION CODE - ',2A1)
214 4008    FORMAT(' APERTURE CORRECTION IN')
215 4009    FORMAT(' APERTURE CORRECTION OUT')
216 4010    FORMAT(' DIRECT TRANSMISSION')
217 4011    FORMAT(' TRANSMITTED VIA WBUT RECORDER')
218 4012    FORMAT(' TRANSMISSION CODE NOT RECOGNISED ******')
219 4013    FORMAT(' SUN ANGLES - ',15A1)
220 4014    FORMAT(' TYPE OF CORRECTION APPLIED - ',1A1)
221 4015    FORMAT(' SCALE 185KM X 185KM')
222 4016    FORMAT(' SCALE 99KM X 99KM')
223 4017    FORMAT(' SCALE 185KM X 170KM')
224 4018    FORMAT(' UNRECOGNISED SCALE CODE **********')
225 4019    FORMAT(' PROJECTION CODE - ',1A1)
226 4020    FORMAT(' CUBIC CONVOLUTION RESAMPLING APPLIED')
227 4021    FORMAT(' NEAREST NEIGHBOUR RESAMPLING APPLIED')
228 4022    FORMAT(' RESAMPLING CODE NOT RECOGNISED******')
229 4023    FORMAT(' LINEAR MODE TRANSMISSION')
230 4024    FORMAT(' COMPRESSED MODE TRANSMISSION')
231 4025    FORMAT(' TRANSMISSION MODE UNRECOGNISED ******')
232 4026    FORMAT(' AGENCY/PROJECT - ',13A1)
233 4027    FORMAT(' FRAME ID - ',15A1)
234         END
235         SUBROUTINE CCT355
236 CCCCCCCCCCCCCCCCCCCCCCCCCCCCCCCCCCCCCCCCCCCCCCCCCCCCCCCCCCCCCCCC
237 CCCC
238 CCCC    IMAGE DATA DECODING
239 CCCC
240 CCCCCCCCCCCCCCCCCCCCCCCCCCCCCCCCCCCCCCCCCCCCCCCCCCCCCCCCCCCCCCCC
241         INTEGER INDEX, REC, COUNT, IOSTAT
242 C
243         INTEGER *1 BUF1(5388)
244         INTEGER *3 BUF3(1796), BSIZE
245         LOGICAL MSS, BIL, RBV, GEOCOR
246         COMMON /LAND/ BUF1, BSIZE, MSS, BIL, RBV, GEOCOR
247         EQUIVALENCE (BUF1(1),BUF3(1))
248 C
249         WRITE(12,5000)
250 C
251          BUFFER IN (10, BUF3, S, BSIZE, IOSTAT, COUNT)
252          CALL STATUS(10)
253          BUFFER IN (10, BUF3, S, BSIZE, IOSTAT, COUNT)
254          CALL STATUS(10)
255          DO 5555 REC=1,512
256            BUFFER IN (10, BUF3, S, BSIZE, IOSTAT, COUNT)
257            CALL STATUS(10)
258            BUFFER IN (10, BUF3, S, BSIZE, IOSTAT, COUNT)
259            CALL STATUS(10)
260            DO 6000 INDEX=1,3584,224
261 6000        WRITE(13,5002) (BUF1(I), I=INDEX, INDEX+223,7)
262            BUFFER IN (10, BUF3, S, BSIZE, IOSTAT, COUNT)
```

```
263             CALL STATUS(10)
264             DO 6004 IDUMP=1,9
265               BUFFER IN (10, BUF3, S, BSIZE, IOSTAT, COUNT)
266 6004          CALL STATUS(10)
267 5555        CONTINUE
268           RETURN
269 5000      FORMAT(' IMAGE DATA')
270 5001      FORMAT(64A1)
271 5002       FORMAT(32I4)
272           END
273           SUBROUTINE CCT366
274 C
275           INTEGER *1 BUF1(5388)
276           INTEGER *3 BUF3(1796), BSIZE
277           LOGICAL MSS, BIL, RBV, GEOCOR
278           COMMON /LAND/ BUF1, BSIZE, MSS, BIL, RBV, GEOCOR
279           EQUIVALENCE (BUF1(1),BUF3(1))
280 C
281           WRITE(12,6000)
282 6000      FORMAT(' TRAILER')
283           RETURN
284           END
EOF..
```

```
1          INTEGER *1 BUF1(3585)
2          INTEGER *3 BUF3(1195), IOSTAT
3          EQUIVALENCE (BUF1, BUF3)
4
5  100     BUFFER IN (10,BUF3,S,1195,IOSTAT)
6          CALL STATUS(10)
7          GO TO (200,100,800), IOSTAT - 1
8  200     IF (BUF1(6) .EQ. 237) GO TO 300
9          GO TO 100
10
11 300      BUFFER IN (10,BUF3,S,1195,IOSTAT)
12          CALL STATUS(10)
13          GO TO (400,800,800), IOSTAT - 1
14
15 400       DO 500 J=1,3584,224
16 500          WRITE(12,5000) (BUF1(I), I=J,J+224,7)
17          X = 0
18
19 600      BUFFER IN(10,BUF3,S,1195,IOSTAT)
20          CALL STATUS(10)
21          GO TO (700,800,800), IOSTAT - 1
22 700      X = X + 1
23          IF (X .EQ. 32)
24             GO TO 400
25          ENDIF
26          GO TO 600
27
28 800      WRITE(11,6000)
29          STOP
30
31 5000     FORMAT(32I4)
32 6000     FORMAT('*** END OF TAPE ENCOUNTERED ***')
33          END
EOF..
```

```
1 CP811490212
2  ##########################################################
3  BLOCK SIZE   120    STATUS 2    BYTE SIX   9
4  TAPE DIRECTORY
5  MISSION-L2  SENSOR TYPE-M  TAPE TYPE-CP
6  MULTISPECTRAL SCANNER SYSTEM (MSS) FORMAT
7  BAND INTERLEAVED BY LINE (BIL) FORMAT
8  GEOMETRICALLY CORRECTED DATA (SOURCE HDT)
9  SIZE OF FOLLOWING RECORDS =  3596
10  SCENE ID: 2159206572 D181058
11 592065720 D1810
12  ##########################################################
13  BLOCK SIZE  1198    STATUS 2    BYTE SIX  18
14  HEADER
15 UN79 C NO2-54/E
16  ##########################################################
17  BLOCK SIZE  1198    STATUS 2    BYTE SIX 219
18  ANNOTATION
19  EXPOSURE DATE 02JUN79
20  FORMAT CENTRE C NO2-54/E036-55
21  DESCENDING ACQUISITION - PATH 181 ROW 058
22  NOMINAL LATITUDE AND LONGITUDE N NO2-53/E037-01
23  TRANSMITTED VIA WBUT RECORDER
24  SUN ANGLES - SUN EL48 A059
25  TYPE OF CORRECTION APPLIED - S
26  SCALE 185KM X 170KM
27  PROJECTION CODE - H
28  CUBIC CONVOLUTION RESAMPLING APPLIED
29  COMPRESSED MODE TRANSMISSION
30  AGENCY/PROJECT - NASA LANDSAT
31  FRAME ID - E-21592-06572-4
32  ##########################################################
33  BLOCK SIZE  1198    STATUS 2    BYTE SIX 237
34  IMAGE DATA
```

```
1 PROGRAM NODDY(INPUT,INFILE(LFN=10),OUTPUT,OUTFILE(LFN=12));
2 VAR   INFILE,OUTFILE:TEXT;
3       X,Y,C,F,S,N,N1:INTEGER;
4       TOT:ARRAY[0..127]OF INTEGER;
5
6       PROCEDURE INUM;
7       BEGIN
8       READ(INFILE,N);TOT[N]:=TOT[N]+1
9       END;
10
11       PROCEDURE S1;
12       VAR Z:INTEGER;
13       BEGIN
14       FOR Z:=1 TO F
15        DO INUM;
16       WRITE(OUTFILE,N:3);
17       FOR Z:=(F+1) TO C
18        DO INUM
19       END;
20
21 BEGIN
22 FOR X:=0 TO 127 DO TOT[X]:=0;
23 WRITELN(OUTPUT,'HOW MANY COLUMNS ARE THERE IN THE FILE?');
24 READLN(INPUT,C);
25 WRITELN(OUTPUT,'WHICH COLUMN DO YOU WISH TO CONVERT?');
26 READLN(INPUT,F);
27 FOR X:=1 TO 40
28  DO BEGIN
29      FOR Y:=1 TO 40
30       DO S1;
31       WRITELN(OUTFILE);
32      END;
33 WRITELN(OUTPUT,'FINISHED')
34 END.
EOF..
```

```
1 PROGRAM HCOPY(INPUT,INFILE(LFN=10),OUTFILE(LFN=12),OUTPUT);
2 VAR   IMAGEW, IMAGED, PLOTW, PLOTD, WCOORD, DCOORD, SUBW, SUBD,
3          WIDTH, DEPTH, A, B, N, RANGE, ENDLINE: INTEGER;
4       INFILE, OUTFILE: TEXT;
5       SCALE: ARRAY[1..8] OF INTEGER;
6       C: CHAR;
7 VALUEXXX SCALE = (10,20,30,40,50,60,70,80);
8
9       { ---------------------- }
10
11       PROCEDURE DENSITYSCALE;
12       VAR    X: INTEGER;
13       BEGIN
14       WRITELN(OUTPUT,'Do you wish to use the default density scale? (Y or N)');
15       READLN(INPUT,C);
16       IF C <> 'Y'
17       THEN BEGIN
18            WRITELN(OUTPUT,'Type in 8 numbers defining the bounds of the scale');
19            WRITELN(OUTPUT,'eg: typing  15 25 35 45 55 65 75 128  will give a');
20            WRITELN(OUTPUT,'scale <0-14> <15-24> <25-34> <35-44> ......');
21            WRITELN(OUTPUT,'(NOTE: The example above is the default scale)');
22            WRITELN(OUTPUT);
23            FOR X:=1 TO 8
24             DO  READ(INPUT, SCALE[X])
25            END
26       END;
27
28       { ---------------------- }
29
30       PROCEDURE PLOTSYMBOL;
31       VAR  X: INTEGER;
32            FIN: BOOLEAN;
33       BEGIN
34       FIN:=FALSE;
35       X:=1;
36       REPEAT
37            IF N > SCALE[X]
38            THEN X:= X + 1
39            ELSE BEGIN
40                 WRITE(OUTFILE,X:1);
41                 X:= 8;   FIN:=TRUE
42                 END;
43       UNTIL X = 8;
44       IF NOT FIN
45       THEN BEGIN
46            WRITE(OUTFILE,'8');
47            END
48       END;
49
50       { ---------------------- }
51
52       PROCEDURE PLOTLINE;
53       VAR  A, B: INTEGER;
54       BEGIN
55       FOR A:=1 TO WIDTH
56        DO  BEGIN
57               READ(INFILE,N);
58            PLOTSYMBOL
59            END;
60       WRITELN(OUTFILE);
61       END;
62
63       { ---------------------- }
64
65 BEGIN
66 RESET(INFILE);
67 REWRITE(OUTFILE);
68 WIDTH:=80; DEPTH:=80;
69       WRITELN(OUTFILE,WIDTH:3,'x',DEPTH:3);
70       DENSITYSCALE;
71       WRITELN(OUTPUT,'Please wait a few moments');
72 FOR A:=1 TO DEPTH
73  DO  PLOTLINE;
74 END.
```

GRAF

```
 1 PROGRAM GRAF(INPUT(LFN=10),OUTPUT(LFN=12));
 2 TYPE PTYPE= ^NODE;
 3      NODE= RECORD
 4                C: CHAR;
 5                NEXT: PTYPE
 6            END;
 7 VAR  A,B,W,D: INTEGER;
 8      P, LISTHEAD: PTYPE;
 9      C: CHAR;
10       GRAPHICS: ARRAY[1..8,1..4] OF INTEGER;
11 VALUEXXX  GRAPHICS = (   0, 34,  0,  0,      34,  0,  8,  0,
12                         65,  0, 34,  0,      34,  0, 85,  0,
13                         73, 20, 65, 20,      85, 42, 85, 34,
14                         85, 62, 85, 62,     127,127,127,127   );
15
16      PROCEDURE PLOTLINE;
17      VAR  A,B,L,N: INTEGER;
18
19
20      BEGIN
21      FOR L:=1 TO 8
22       DO  BEGIN
23           IF L > 4 THEN A:=(9-L) ELSE A:=L;
24           WRITE(CHR(0),CHR(0),CHR(0));
25           P:=LISTHEAD;
26           FOR B:=0 TO W
27            DO  BEGIN
28                CASE P^.C OF
29                 ' ': WRITE(CHR(GRAPHICS[1,A]));
30                 'o': WRITE(CHR(GRAPHICS[2,A]));
31                 '-': WRITE(CHR(GRAPHICS[3,A]));
32                 '+': WRITE(CHR(GRAPHICS[4,A]));
33                 'x': WRITE(CHR(GRAPHICS[5,A]));
34                 '*': WRITE(CHR(GRAPHICS[6,A]));
35                 '@': WRITE(CHR(GRAPHICS[7,A]));
36                 '#': WRITE(CHR(GRAPHICS[8,A]))
37                END;
38                P:=P^.NEXT
39                END;
40           WRITELN(CHR(0))
41           END;
42      WRITELN
43      END;
44
45 BEGIN
46 FOR A:=1 TO 9
47  DO  READ(C);
48 READLN(W,C,D);  READLN;
49 FOR A:=1 TO 4
50  DO  BEGIN
51      WRITE(CHR(0));
52      FOR B:=1 TO 8
53       DO  WRITE(CHR(0),CHR(GRAPHICS[B,A]),CHR(0));
54      WRITELN(CHR(0),CHR(0));
55      END;
56 FOR A:=4 DOWNTO 1
57  DO  BEGIN
58      WRITE(CHR(0));
59      FOR B:=1 TO 8
60       DO  WRITE(CHR(0),CHR(GRAPHICS[B,A]),CHR(0));
61      WRITELN(CHR(0),CHR(0));
62      END;
63 FOR A:=1 TO 8 DO WRITELN;
64 NEW(LISTHEAD);
65 READ(C,C);
66 P:=LISTHEAD; READ(P^.C);
67 FOR A:=1 TO W
68  DO  BEGIN
69      NEW(P^.NEXT);
70      P:=P^.NEXT;  READ(P^.C)
71      END;
72 P^.NEXT:=NIL;
73 PLOTLINE; READLN;
74 FOR A:=2 TO D
75  DO  BEGIN
76      READ(C,C);
77      P:=LISTHEAD;
78      FOR B:=0 TO W
79       DO  BEGIN
80           READ(P^.C);
81           P:=P^.NEXT
82           END;
83      PLOTLINE; READLN
84      END
85 END.
EOF.
```

```
 1          INTEGER *1 BUF1(129), L(258), GX(4, 8), COUNT
 2          INTEGER *3 BUF3(43), PIXELS, LINES, IOSTAT
 3          EQUIVALENCE (BUF1, BUF3)
 4          DATA ((GX(I,J), I=1,4), J=1,2)/15,15,15,15,   11,14,7,13/
 5          DATA ((GX(I,J), I=1,4), J=3,4)/10,7,14,5,     9,10,5,9/
 6          DATA ((GX(I,J), I=1,4), J=5,6)/5,8,1,10,      2,8,1,4/
 7          DATA ((GX(I,J), I=1,4), J=7,8)/ 2,0,8,2,      0,0,0,0/
 8          DATA BUF3/43*0/
 9
10           COUNT = 0
11           READ(10, 5000) (PIXELS, LINES)
12           PIXELS = PIXELS + 1
13           DO 100 I=1, LINES
14              READ(10, 5001) (L(X), X=2, PIXELS)
15              DO 100 J=1, 4
16                 DO 101 K=2, PIXELS/2 + 1
17 101                BUF1(K)=GX(J,L(K*2-2))*16 + GX(J,L(K*2-1))
18                 BUFFER OUT (12, BUF3, B, 43, IOSTAT)
19                 COUNT = COUNT + 1
20                 CALL STATUS(12)
21                 IF (COUNT .EQ. 5)
22                    COUNT = 0
23                    N = J - 2
24                    IF (N .LT. 1)
25                      N = 4 - N
26                    ENDIF
27                    DO 102 K = 2, PIXELS/2 + 1
28 102                BUF1(K)=GX(N,L(K*2-2))*16 + GX(N,L(K*2-1))
29                    BUFFER OUT (12, BUF3, B, 43, IOSTAT)
30                    CALL STATUS(12)
31                 ENDIF
32 100             CONTINUE
33 5000    FORMAT (1I3, 1X, 1I3)
34 5001    FORMAT (128I1)
35         END
EOF..
```

HCOPY-Y

```
1          INTEGER *1 BUF1(258), GX(4, 8), COUNT
2          INTEGER *3 BUF3(86), IW, ID, PW, PD, WCO, DCO, SUBW, SUBD
3          INTEGER *3 WIDTH, DEPTH, X, Y, L(257), BOUND(9)
4          EQUIVALENCE (BUF1, BUF3)
5          DATA ((GX(I, J), I=1, 4), J=1, 4)/0, 0, 0, 0, 2, 0, 8, 2, 2, 8, 1, 4, 5, 8, 1, 10/
6          DATA ((GX(I, J), I=1, 4), J=5, 7)/5, 10, 5, 10, 10, 7, 14, 5, 11, 14, 7, 13/
7          DATA (GX(I, 8), I=1, 4)/15, 15, 15, 15/
8          DATA BOUND/15, 25, 35, 45, 55, 65, 75, 128, 0/
9          DATA BUF3/86*0/
10
11          WRITE(11, 7000)
12          WRITE(11, 7001)
13          WRITE(11, 7002)
14          WRITE(11, 7003)
15          WRITE(11, 7004)
16          READ(11, ) (IW, ID, PW, PD, WCO, DCO, SUBW, SUBD)
17          IF ((WCO + PW) .GT. IW)
18             WIDTH = (IW - WCO)
19          ELSE
20             WIDTH = PW
21          ENDIF
22          IF ((DCO + PD) .GT. ID)
23             DEPTH = (ID - DCO)
24          ELSE
25             DEPTH = PD
26          ENDIF
27
28          DO 100 X=2, DCO
29 100      READ(10, )
30          DO 300 Y=1, DEPTH, SUBD
31             READ(10, ) (L(I), I=2, IW+1)
32             C = 0
33             DO 200 X= WCO, WIDTH, SUBW
34                C = C + 1
35                IF (L(X) .LT. BOUND(1))
36                   L(C) = 1
37                ELSE IF (L(X) .LT. BOUND(2))
38                   L(C) = 2
39                ELSE IF (L(X) .LT. BOUND(3))
40                   L(C) = 3
41                ELSE IF (L(X) .LT. BOUND(4))
42                   L(C) = 4
43                ELSE IF (L(X) .LT. BOUND(5))
44                   L(C) = 5
45                ELSE IF (L(X) .LT. BOUND(6))
46                   L(C) = 6
47                ELSE IF (L(X) .LT. BOUND(7))
48                   L(C) = 7
49                ELSE IF (L(X) .LT. BOUND(8))
50                   L(C) = 8
51                ENDIF
52 200          CONTINUE
53
54          COUNT = 0
55          DO 300 J=1, 4
56             DO 301 K=2, WIDTH/2 + 2
57 301             BUF1(K)=GX(J, L(2*K-2))*16+GX(J, L(2*K-1))
58             BUFFER OUT (12, BUF3, B, 86, IOSTAT)
59             COUNT = COUNT + 1
60             CALL STATUS(12)
61             IF (COUNT .EQ. 5)
62                COUNT = 0
63                BUFFER OUT (12, BUF3, B, 86, IOSTAT)
64                CALL STATUS(12)
65             ENDIF
66 300          CONTINUE
67
68          STOP
69 7000     FORMAT(32X, 'GREY MAP PLOTS')
70 7001     FORMAT('Hassan Taherkia. ', 50X, 'July, 1983. ')
71 7002     FORMAT(//'Please input the following : '/)
72 7003     FORMAT('<Image Width, Depth> <Plot Width, Depth>'/)
73 7004     FORMAT(5X, '<Starting Coords> and <Subsample Factors>'/)
74          END
```

SKEW

```
 1 PROGRAM SKEW (INPUT(LFN=10),OUTPUT(LFN=12));
 2 VAR X,Y,Z,A,COUNT: INTEGER;
 3
 4 BEGIN
 5 FOR X:=1 TO 6
 6  DO  BEGIN
 7       FOR Y:=1 TO 5 DO WRITELN('O');
 8       FOR Y:=1 TO 80
 9        DO  BEGIN
10             READ(A);
11             WRITELN(A)
12             END;
13       END;
14 COUNT:=4;
15 FOR X:=7 TO 80
16  DO  BEGIN
17       FOR A:=1 TO COUNT
18        DO WRITELN('O');
19       FOR Y:=1 TO 80
20        DO  BEGIN
21             READ(A);
22             WRITELN(A)
23             END;
24       FOR A:=COUNT TO 4
25        DO WRITELN('O');
26       IF ((X-24) MOD 17)=0 THEN COUNT:=COUNT-1
27       END
28 END.
EOF..
```

SCALEUP

```
 1 PROGRAM NODDY(INPUT(LFN=10),OUTPUT(LFN=12));
 2 VAR X,Y,Z: INTEGER;
 3     N:ARRAY[1..40,1..40] OF INTEGER;
 4 BEGIN
 5 FOR X:=1 TO 40 DO FOR Y:=1 TO 40 DO READ(N[X,Y]);
 6 FOR X:=1 TO 40
 7  DO BEGIN
 8     FOR Z:=1 TO 2
 9     DO BEGIN
10          FOR Y:=1 TO 40
11           DO WRITELN(N[X,Y],N[X,Y]);
12          END
13      END
14 END.
EOF..
```

```
1            $MS
2            $FR 5 6 7
3          $JE.P !DMMY
4 !DMMY      $IF (.NUL(&1)) $JUMP !NOFILE
5            $AS  7=&1
6            $JE 2100 !NOTT
7            $JE  2300 !NOTT
8            $PR Fortran .. Compilation starting
9            FO.&0 &1
10            $JE.P 4008 !COMPF
11            $JE.P !OTHER
12            $PR Compilation successful
13            $JS 3799AA*COMPILE !VUPARS
14            $ME
15 !VUPARS    $FR 6
16            $VU.RN
17            AL S+0
18            SP S+50
19            MO NX
20            LIB *GINO-F *LIBERY
21            BEGIN
22            $JE.P !OTHER2
23            $PR Vulcanization successful .. Type XE to run the program
24            $AS 6=LO
25            $WI 6
26            $JS
27 !NOFILE    $PR No program file has been given
28            $ME
29 !COMPF     $PR Fortran Fatal Errors ... Compilation failed.
30            $ME
31            $ME
32 !OTHER     $PR Compilation abandoned due to system error .. seek advice
33            $ME
34 !NOTT      $PR File &1 does not exist or is private to another user
35            $ME
36 !OTHER2    $PR Vulcanization failed .. seek advice
37            $ME.E
EOF..
```

```
1  PROGRAM HCOPY(INPUT,INFILE(LFN=10),OUTFILE(LFN=12),OUTPUT);
2  VAR   IMAGEW, IMAGED, PLOTW, PLOTD, WCOORD, DCOORD, SUBW, SUBD,
3           WIDTH, DEPTH, A, B, N, RANGE, ENDLINE: INTEGER;
4        INFILE, OUTFILE: TEXT;
5        SCALE: ARRAY[1..8] OF INTEGER;
6        C: CHAR;
7  VALUEXXX SCALE = (10,20,30,40,50,60,70,80);
8
9        { ---------------------- }
10
11       PROCEDURE DENSITYSCALE;
12       VAR    X: INTEGER;
13       BEGIN
14       WRITELN(OUTPUT,'Do you wish to use the default density scale? (Y or N)');
15       READLN(INPUT,C);
16       IF C <> 'Y'
17       THEN BEGIN
18            WRITELN(OUTPUT,'Type in 8 numbers defining the bounds of the scale');
19            WRITELN(OUTPUT,'eg: typing  15 25 35 45 55 65 75 128  will give a');
20            WRITELN(OUTPUT,'scale <0-14> <15-24> <25-34> <35-44> ......');
21            WRITELN(OUTPUT,'(NOTE: The example above is the default scale)');
22            WRITELN(OUTPUT);
23            FOR X:=1 TO 8
24             DO  READ(INPUT, SCALE[X])
25            END
26       END;
27
28       { ---------------------- }
29
30       PROCEDURE SKIP(LIMIT: INTEGER);
31       VAR X: INTEGER;
32       BEGIN
33       FOR X:=1 TO LIMIT
34        DO  READ(INFILE,N);
35       END;
36
37       { ---------------------- }
38
39       PROCEDURE PLOTSYMBOL;
40       VAR   X: INTEGER;
41             FIN: BOOLEAN;
42       BEGIN
43       FIN:=FALSE;
44       X:=1;
45       REPEAT
46            IF N > SCALE[X]
47            THEN X:= X + 1
48            ELSE BEGIN
49                 WRITE(OUTFILE,X:1);
50                 X:= 8;   FIN:=TRUE
51                 END;
52       UNTIL X = 9;
53       IF NOT FIN
54       THEN BEGIN
55            WRITE(OUTFILE,'9');
56            END
57       END;
58
59       { ---------------------- }
60
61       PROCEDURE PLOTLINE;
62       VAR   A, B: INTEGER;
63       BEGIN
64       FOR A:=0 TO WCOORD
65        DO  READ(INFILE,N);
66       PLOTSYMBOL;
67       FOR A:=2 TO WIDTH
68        DO  BEGIN
69            FOR B:=1 TO SUBW
70             DO  READ(INFILE,N);
71            PLOTSYMBOL
72            END;
73       WRITELN(OUTFILE);
74       SKIP(ENDLINE)
75       END;
76
77       { ---------------------- }
78
79 BEGIN
80 RESET(INFILE);
81 REWRITE(OUTFILE);
82 WRITELN(OUTPUT); WRITELN(OUTPUT,'Please type in the following :');
83 WRITELN(OUTPUT);
84 WRITE(OUTPUT,'<IMAGE WIDTH+DEPTH> <PLOT WIDTH+DEPTH> <START CO-ORDs>');
85 WRITELN(OUTPUT,' <SUBSAMPLE FACTORS>'); WRITELN(OUTPUT);
86 READLN(INPUT, IMAGEW,IMAGED,PLOTW,PLOTD,WCOORD,DCOORD,SUBW,SUBD);
87 WRITELN(OUTPUT);
88 IF (WCOORD > IMAGEW) OR (DCOORD > IMAGED)
89 THEN WRITELN(OUTPUT,'*** STARTING COORDINATES OUT OF IMAGE RANGE ***')
90 ELSE BEGIN
91       IF (WCOORD + PLOTW * SUBW) > IMAGEW
92       THEN WIDTH:= (IMAGEW - WCOORD) DIV SUBW
93       ELSE WIDTH:= PLOTW;
94       IF (DCOORD + PLOTD * SUBD) > IMAGED
95       THEN DEPTH:= (IMAGED - DCOORD) DIV SUBD
96       ELSE DEPTH:= PLOTD;
97       ENDLINE:=IMAGEW - WCOORD - WIDTH * SUBW - 1;
98       WRITELN(OUTFILE,WIDTH:3,'i',DEPTH:3);
99       DENSITYSCALE;
100       WRITELN(OUTPUT,'Please wait a few moments');
101       FOR A:=1 TO DCOORD
102        DO  SKIP(IMAGEW);
103       PLOTLINE;
104       FOR A:=2 TO DEPTH
105        DO  BEGIN
106            FOR B:=2 TO SUBD
107             DO SKIP(IMAGEW);
108            PLOTLINE
109            END;
110       END
111 END.
```

```
]LOAD SERIAL
]LIST

10  HOME
20 D$ =  CHR$ (4):TERM = 4096
30  PRINT "TERMINAL PROGRAM FOR T
     HE APPLE ][+"
40  PRINT D$;"BLOAD SERIAL.OBJ"
50  PRINT D$;"NOMON C,I,O"
60  ONERR  GOTO 1000
70  PRINT "CTRL-B     BREAK"
80  PRINT "CTRL-C     CATALOG"
90  PRINT "CTRL-R     RECEIVE FILE
     "
100  PRINT "CTRL-T     TRANSMIT FI
     LE"
110  PRINT "CTRL-X     FINISH"
120  PRINT "CTRL-K     RESET CARD"
130  PRINT "WHEN RECEIVING OR TRA
     NSMITTING A FILE"
140  PRINT "CTRL-Z WILL CLOSE FIL
     E AND RETURN TO"
150  PRINT "TERMINAL MODE"
160  CALL TERM
170  PRINT : PRINT D$;"CLOSE";
180  PRINT "STOP"
190  END
1000  PRINT : PRINT D$;"CLOSE"
1010  PRINT "SYSTEM ERROR NUMBER
     "; PEEK (222)
1020  PRINT "(SEE MANUAL FOR EXPL
     ANATION)"
1030  POKE 216,0
1040  GOTO 60
```

```
]LOAD PLOTFILE
]LIST

10  HOME : PRINT "IMAGE PROCESSIN
    G "
20  INPUT "FILENAME ";FI$
30  PRINT  CHR$ (4);"OPEN ";FI$
40  PRINT  CHR$ (4);"READ ";FI$
50  REM  INSERT ERROR HANDLER HER
    E
60  DIM A(39,39)
70  FOR J = 0 TO 39: FOR I = 0 TO
    39
80  GOSUB 500:A(J,I) = X
90  NEXT I,J
100  PRINT
110  PRINT  CHR$ (4);"CLOSE ";FI$

120  PRINT "ALL DATA READ"
130  INPUT "COLOUR SCALE ";SC: GR

140  FOR J = 0 TO 39: FOR I = 0 TO
     39
145 K = 39 - J
146 L = 39 - I
150  COLOR=  INT (A(L,K) / SC)
160  PLOT K,L
170  NEXT I,J
180  VTAB 22
190  PRINT "SCALE FACTOR ";SC
200  PRINT "PRESS ANY KEY FOR OPT
     IONS"
210  GET A$
220  TEXT : HOME
230  PRINT "OPTIONS"
240  PRINT
250  PRINT "1. READ NEW FILE"
260  PRINT "2. CHANGE SCALE"
270  PRINT "   ELSE END"
280  GET A$



290  IF  VAL (A$) = 1 THEN  RUN
300  IF  VAL (A$) = 2 THEN 130
310  END
500 X = 0:
510  GET A$
520  IF A$ = " " OR A$ =  CHR$ (1
     3) GOTO 510
530 X =  VAL (A$)
540  GET A$
550  IF A$ = " " OR A$ =  CHR$ (1
     3) THEN  RETURN
560 X = X * 10 +  VAL (A$)
570  RETURN
1000  PRINT
1010  INVERSE
1020  PRINT "ERROR NUMBER ", PEEK
     (222)
1030  END
```

```
]LOAD HPLOTFILE
]LIST

5  LOMEM: 16384
10  HOME : PRINT "IMAGE PROCESSIN
    G "
20  INPUT "FILENAME ";FI$
30  PRINT  CHR$ (4);"OPEN ";FI$
40  PRINT  CHR$ (4);"READ ";FI$
50  REM  INSERT ERROR HANDLER HER
    E
60  DIM A(39,39)
70  FOR J = 0 TO 39: FOR I = 0 TO
    39
80  GOSUB 350:A(J,I) = X
90  NEXT I,J
100  PRINT
110  PRINT  CHR$ (4);"CLOSE ";FI$

120  PRINT "ALL DATA READ"
130  INPUT "COLOUR SCALE ";SC
140  HGR
150  FOR J = 156 TO 0 STEP  - 4
160  FOR I = 156 TO 0 STEP  - 4
170  HCOLOR= A(J / 4,I / 4) / SC
180  FOR M = 0 TO 3: FOR N = 0 TO
    3
190  HPLOT J + M,160 - I - N
200  NEXT N,M,I,J
210  VTAB 22
220  PRINT "SCALE FACTOR ";SC
230  PRINT "PRESS ANY KEY FOR OPT
    IONS"
240  GET A$
250  TEXT : HOME
260  PRINT "OPTIONS"
270  PRINT
280  PRINT "1. READ NEW FILE"

290  PRINT "2. CHANGE SCALE"
300  PRINT "   ELSE END"
310  GET A$
320  IF  VAL (A$) = 1 THEN RUN
330  IF  VAL (A$) = 2 THEN 130
340  END
350 X = 0:
360  GET A$: IF  ASC (A$) <  = 32
     THEN 360
370 X = X * 10 +  VAL (A$)
380  GET A$: IF  ASC (A$) > 32 THEN
    370
390  RETURN
```

```
]LIST

10  LOMEM: 16384:OF = 60
20  TEXT : HOME
30  PRINT "IMAGE DISPLAY"
40  DIM C(5):C(0) = 0:C(1) = 1:C(
    2) = 2:C(3) = 5:C(4) = 6:C(5
    ) = 7
50  DIM A(39,39),BN(6):BN(0) = 0:
    BN(6) = 99
60  INPUT "ENTER DATA FILENAME";F
    I$
70  PRINT  CHR$ (4);"OPEN";FI$
80  PRINT  CHR$ (4);"READ";FI$
90  FOR J = 0 TO 39: FOR I = 0 TO
    39
100  GOSUB 510:A(J,I) = X
105  NEXT I,J
106  PRINT
110  PRINT  CHR$ (4);"CLOSE";FI$
120  PRINT "ALL DATA READ"
130  FOR I = 1 TO 5
140 BN(I) = I * 99 / 6
150  NEXT I
160  PRINT "DO YOU WANT THE DEFAU
    LT VALUES ?";
170  GET A$
180  IF A$ <  > "Y" AND A$ <  > "
    N" THEN  GOTO 170
185  PRINT A$
190  IF A$ = "Y" THEN 280
200  PRINT "FOR EACH NUMBER ENTER
     BAND LIMIT"
210  FOR I = 1 TO 5
220  INPUT BN(I)
230  IF BN(I) < BN(I - 1) THEN  PRINT
    "MUST BE BIGGER THAN LOWER B
    AND": GOTO 220
250  IF BN(I) > 99 THEN  PRINT "S
    OME DATA BIGGER THAN RANGE":
     GOTO 220
270  NEXT I
280  HGR
290  FOR J = 39 TO 0 STEP  - 1
300  FOR I = 39 TO 0 STEP  - 1
310 X = A(J,I):L = 0
320  FOR K = 1 TO 6
330  IF X < BN(K) THEN L = K - 1:
    K = 6:
340  NEXT K
350  HCOLOR= C(L)
360 X = OF + I * 4:Y = 3 + 4 * J
370  HPLOT X,Y TO X + 3,Y
380  HPLOT X,Y - 1 TO X + 3,Y - 1

390  HPLOT X,Y - 2 TO X + 3,Y - 2

400  HPLOT X,Y - 3 TO X + 3,Y - 3

410  NEXT I,J
420  VTAB 22
430  PRINT "OPTIONS"
440  PRINT "1. CHANGE BANDS 2. RE
    AD NEW FILE"
450  PRINT "3. END PROGRAM"
460  GET A$:A =  VAL (A$): IF A <
    1 OR A > 3 THEN 460
470  ON A GOTO 160,400,490
480  RUN
490  TEXT
500  END
510 X = 0
520  GET A$: IF  ASC (A$) <  = 32
     THEN 520
530 X = X * 10 +  VAL (A$)
540  GET A$: IF  ASC (A$) > 32 THEN
    530
550  RETURN
560  END
```

```
1 $MS
2 $PR
3   $PR  ------------------------- GREYMAP -------------------------
4   $PR                           ===+===
5 $PR  HASSAN TAHERKIA                                    July, 1983
6 $PR
7 $PR   &     GREYMAP is a package to produce grey maps of pixel values
8 $PR  on a PRINTRONIX Printer.  The pixel values can be read either
9 $PR  from a file of integer values or off an EROS CCT containing a
10 $PR  LANDSAT image.  Documentation will be available soon.
11 !ASFIL $PR   OWhat is the name of the file containing the pixel values? (Q to Quit)
12 $SR. SRI #FLN
13 $IF (#FLN = Q) $JU !GMEND
14 $JU !SCALE
15 $AS 10=#FLN 12=89
16 $JE !FERR
17 !COMP 3799AA*X-HCOPY
18 !PRNTR $PR At what printer do you want the map to be plotted?
19 $SR. SRI #FLN
20 $AS 10=89 12=: #FLN
21 $JE !PERR
22  3799AA*X-GRAF
23 $FR ALL
24 $PR
25 $PR Do you wish to plot any more Grey Maps? (Y or N)
26 $SR. SRI #FLN
27 $IF (#FLN = Y) $JU !ASFIL
28 !GMEND $PR    &              ---------- GREYMAP ENDS ----------
29 $ME
30 !FERR $PR The data file is invalid in some way ... try again
31 $JU !ASFIL
32 !PERR $PR The Printer is invalid in some way ... Printers available are:
33 $PR <6 - Computer Room> <7 - User Area> <8 - Room 418, Main Building>
34 $JU !PRNTR
35 !SCALE $AS 10=#FLN 12=87
36 $JE !FERR
37 X-SCALE
38 $AS 10=87 12=88
39 X-SKEW
40 $AS 10=88 12=89
41 $JU !COMP
EOF..
```

```
      PROGRAM PIXELMAP
      CHARACTER CHAR*2,REPLY*1,FILE*10
      REAL SPACE,SIZE
      INTEGER BAND,WIDTH,VALUE(40),NB,RANGE(17)
      LOGICAL FLAG
      COMMON /BK2/NB,RANGE,CHAR,REPLY
      CHAR='N'
      PRINT*,'-----------------------------------PLOT',
     G    '-----------------------------------'
      PRINT*,'                                        ========= '
      PRINT*,' '
      PRINT*,' '
      PRINT*,'HASSAN TAHERKIA                                    ',
     G   '                        JULY 1984'
      PRINT*,' '
      PRINT*,' '
      PRINT*,'Pixelmap is a package to create colour or grey',
     G    ' maps on a TEKTRONIX(4113a)'
      PRINT*,'terminal. The data is read from a file of ',
     G    'integer values.'
      PRINT*,'N.B the FILE NAME MUST BE TEN CHARACTERS LONG.'
      PRINT*,' '
      PRINT*,' '
      PRINT*,'-----------------------------------------',
     G    '-----------------------------------'
      PRINT*,' '
      PRINT*,' '
      PRINT*,'Default settings are equally spaced density ',
     G    'slices with a choice of either '
      PRINT*,'8 or 16 colours. If you chose not to have ',
     G    'default ranges you will be asked'
      PRINT*,'to enter your own values.'
      print*,' '
      PRINT*,'Please enter your file name.'
12    FORMAT(1A10)
      READ(*,12) FILE
      OPEN(UNIT=10,NAME=FILE,STATUS='OLD')
      print*,'How many colours do you require?'
      ACCEPT*,NB
      IF (NB.EQ.8.OR.NB.EQ.16) THEN
       CALL AUTO
      ELSE
       CALL DEFRAN
      ENDIF
      PRINT*,' '
      PRINT*,'PLEASE ENTER THE SCALE'
      ACCEPT*,UN
      PRINT*,' '
      PRINT*,'Do you want Colours or Grey levels(C/G)?'
      READ(*,24) CHAR
      CALL GINO
      CALL T4113

      CALL SCALE2(UN,UN*10/9.8)
      CALL SHIFT2(248.0,157.0)
      CALL RGBDEF(0,1.0,1.0,1.0)
24    FORMAT(1A1)
      CALL LINCOL(0)
      CALL PICCLE
      IF (CHAR.EQ.'C'.OR.CHAR.EQ.'c') THEN
       CALL ASGCOL
      ELSE
       CALL ASGREY
      ENDIF
```

```
      DO 100 J=1,40
      READ(10,*)(VALUE(I),I=1,40)
      DO 200 I=1,40
      DO 45 L=1,NB
      IF (VALUE(I).LT.(RANGE(L)+1).AND.VALUE(I).GT.RANGE(L-1)) THEN
       BAND=L
      ENDIF
45    CONTINUE

      X1=REAL(I*6.0-6.0)
      Y1=REAL(240-J*6.0)
      X2=REAL(I*6.0)
      Y2=REAL(240-J*6.0+6.0)
      CALL LINCOL(BAND)
      DO 50 X=0,6.0,1.0
      CALL MOVTO2(X1+X,Y1+X)
      CALL LINTO2(X1+X,Y2-X)
      CALL LINTO2(X2-X,Y2-X)
      CALL LINTO2(X2-X,Y1+X)
      CALL LINTO2(X1+X,Y1+X)
50    CONTINUE
200   CONTINUE
100   CONTINUE
      SPACE=240/(4*NB-1)
      SIZE=3*SPACE
      DO 300 K=1,NB
      CALL LINCOL(K)
      DX=0.0
      DO 400 DY=0,SIZE,0.5
      CALL MOVTO2(255+DX,4*SPACE*(K-1)+DY)
      CALL LINTO2(255+DX,4*SPACE*(K-1)+SIZE-DY)
      CALL LINTO2(275-DX,4*SPACE*(K-1)+SIZE-DY)
      CALL LINTO2(275-DX,4*SPACE*(K-1)+DY)
      CALL LINTO2(255+DX,4*SPACE*(K-1)+DY)
      DX=DX+0.5
400   CONTINUE
300   CONTINUE
      CALL LINCOL(1)
      CALL MOVTO2(10.0,270.0)
      CALL CHASTR(FILE)

      PAUSE
      CALL DEVEND
      END
      SUBROUTINE ASGREY
      COMMON /BK2/NB
      CALL RGBDEF(1,0.0,0.0,0.0,0.0)
      CALL RGBDEF(NB,1.0,1.0,1.0)
      D=REAL(NB)
      DO 600 I=2,NB-1
      X=REAL(I)
      C=X/D
      CALL RGBDEF(I,C,C,C)
600   CONTINUE
      RETURN
      END
      SUBROUTINE AUTO
      INTEGER RANGE(17)
      COMMON /BK2/NB,RANGE,REPLY
23    FORMAT(1A1)
      CHARACTER REPLY*1
      PRINT*,'The Default Settings are;'
      IF (NB.EQ.8) THEN
```

```
      PRINT*,'(0-11),(12-23),(24-35),(36-47),(48-59)'
      PRINT*,'(60-71),(72-83),(84-99)'
     ELSE
      PRINT*,'(0-5),(6-11),(12-17),(18-23),(24-29),(30-35),'
      PRINT*,'(36-41),(42-47),(36-41),(42-47)'
      PRINT*,'(48-53),(54-59),(60-65),(66-71),(72-77),'
      PRINT*,'(78-83),(84-89),(90-99)'
     ENDIF
     PRINT*,'DO YOU WANT THESE DEFAULT SETTINGS?(Y/N)'
     READ(*,23) REPLY
     IF (REPLY.EQ.'Y') THEN
      CALL ARANGE
     ELSE
      CALL DEFRAN
     ENDIF
     RETURN
     END
     SUBROUTINE DEFRAN
     INTEGER RANGE(17)
     COMMON /BK2/NB,RANGE
     PRINT*,'Enter ranges as following:(0-19),(20-29)'
     PRINT*,' would be 19 then 40 etc.'
     DO 250 I=1,NB
     ACCEPT*,RANGE(I)
250  CONTINUE
     RETURN
     END
     SUBROUTINE ARANGE
     INTEGER RANGE(17)
     COMMON /BK2/NB,RANGE
     IF (NB.EQ.8) THEN
      N=12
     ELSE
      N=6
     ENDIF
     DO 350 I=1,NB-1
     RANGE(I)=I*N-1
350  CONTINUE
     RANGE(NB)=99
     RETURN
     END
     SUBROUTINE ASGCOL
     INTEGER NB
     COMMON /BK2/NB
     CALL RGBDEF(1,0.0,0.0,0.0)
     CALL RGBDEF(2,0.0,0.0,1.0)
     CALL RGBDEF(NB,1.0,1.0,1.0)
     IF (NB.LE.8.AND.NB.GE.6) THEN
      CALL RGBDEF(3,0.75,0.0,0.88)
     ENDIF
     IF (NB.GE.4.AND.NB.LE.6) THEN
      CALL RGBDEF(NB-1,0.0,1.0,0.0)
     ENDIF
     IF (NB.EQ.5.OR.NB.EQ.6) THEN
      CALL RGBDEF(NB-2,1.0,0.0,0.0)
     ENDIF
     IF (NB.EQ.7.OR.NB.EQ.8) THEN
      CALL RGBDEF(NB-1,1.0,1.0,0.0)
      CALL RGBDEF(NB-2,0.0,1.0,0.0)
     ENDIF
     IF (NB.EQ.8) THEN
      CALL RGBDEF(5,0.1,0.9,1.0)
      CALL RGBDEF(4,1.0,0.0,0.0)
```



```
     ENDIF
     RETURN
     END
```